Developement of microtechnologies for 3D cell culture to study prostate acini formation and carcinogenesis

Monika Elzbieta Dolega

UNIVERSITÉ DE GRENOBLE

THÈSE

Pour obtenir le grade de

DOCTEUR DE L'UNIVERSITÉ DE GRENOBLE

Spécialité : **Biotechnologie, Instrumentation, Signal**

Arrêté ministériel : 7 août 2006

Présentée par

Monika Elzbieta DOLEGA

Thèse dirigée par Dr. Nathalie PICOLLET-D'HAHAN

préparée au sein du LBGE/**BIOMICS** du CEA/DSV/iRTSV
dans **l'École Doctorale Ingénierie Pour La Santé, La Cognition et l'Environnement**

Development of microtechnologies for 3D cell culture to study prostate acini formation and carcinogenesis

Thèse soutenue publiquement le **17 Octobre 2014,**
devant le jury composé de:

Pr Magnus Karl Magnusson
Professor, University of Island, Island (Président)
Pr Séverine Le Gac
Professor, University of Twente, Netherlands (Rapporteur)
Dr Matthias Nees
PhD, VTT, Technical Research Center of Finland, Finland (Rapporteur)
Dr Joanne Young
PhD, CYTOO Grenoble, France (Examinateur)
Dr Nathalie Picollet-D'hahan
PhD, CEA Grenoble, France (Directeur de thèse)
Dr Xavier Gidrol
PhD, CEA Grenoble, France (Invité)

Université Joseph Fourier / Université Pierre Mendès France / Université Stendhal / Université de Savoie / Grenoble INP

Acknowledgments

I would never have achieved what I've achieved without the people with whom I have worked and studied. Therefore, I would like to thank all professors, especially Prof. Holyst, Prof. Garstecki, Prof. Opallo, Dr. Luboradzki, Prof. Waluk and Prof. Kutner, from my University and Institute of Physical Chemistry of Polish Academy of Sciences in Warsaw, for their passionate lectures, conferences, organized internships and discussions. Without their passion, science would never have become a passion of mine.

For this PhD thesis, I have changed scientific direction over 180 degrees, from Physical Chemistry into Biology. At first I would like to thank Xavier Gidrol and Nathalie Picollet-D'hahan who have kindly welcomed me in their BIOMICS lab and allowed me to work in this real biological scientific environment. It was very stimulating and motivating to discover and learn every day new biological facts. I will never forget the first steps and excitement of seeing just a simply stained cellular nucleus. Thank you for this opportunity and your patience! Further, I am grateful to Nathalie also for the perfect professional and personal relations during these three years. I appreciate all the advice, help, optimism and commitment in the perfect organization of the work within our small "3D group". Thank you!

I would like to acknowledge all of those, who patiently advised me and answered my very simple biological questions in the everyday manner during the first several months.

I would like to thank Cédric Allier for this inspiring collaboration, who introduced me to the recently rapidly developing lensfree systems. Additionally, and more personally, I would like to acknowledge Cédric Allier for the atmosphere during work which gave me a lot of pleasure and satisfaction. Merci!

This work could never have been performed without help of our lab technicians who continuously cultivated cells and served with a helpful hand; thank you Fred, Nathalie B. and Sophie.

I would like to say thank you for all the proofreaders of the manuscript; Delphine, Vincent, Ruth, and Eric. Thank you!

My successful accommodation in France would never have been possible without my very best friend Fabien Abeille. Thank you for your help in administrative obstacles, interesting discussions, collaboration and friendship.

Nastya, thanks for all those long evenings and weekends in the lab!

Thanks to Jonathan, Eric, Delphine, Fred, Nathalie, Nastya, and Ruth for all the soiree en ville or hiking in mountains!

Na koniec, ale jako najważniejszym, dziękuję mojej kochanej rodzinie, bez której nie byłoby mnie tu gdzie jestem. Kochanemu Mężowi dziękuję za wsparcie, pomoc i wytrwałość, szczególnie w czasie powstawania tej pracy.

Motivations and Context

Biomics is a team of the "Large Scale Biology" research unit which research programs are strongly oriented towards functional genomics approaches and biomarker discovery. Biomics is specialized in developing RNAi-screening-based strategies with a targeted application in prostate cancer research. More specifically the scientists use a system biology approach to systematically analyze the phenotypic consequences of genetic perturbations (High throughput and high content RNA interfering-based screens) and microenvironmental perturbations (micro pattern of extracellular matrix, 3D microcultures, etc…).

With prostate cancer as model, the strategy is to use the potential of microtechnologies to address the following issue: What are the genetic and microenvironmental determinants that control the proliferation/differentiation balance and carcinogenesis? Also, the aim is to investigate new candidates/targets for cancer treatment through RNAi-based screening assays.

Microfabricated systems offer the opportunity to grow cells under conditions that maintain normal 3D environmental cues and to perform HT parallelized assays. The motivation of this PhD work was to combine 3D cell cultures with cutting-edge technologies to address issues in cancer research and to better understand the cell/tissue function under normal and pathological situations. To do so, the implementation of conventional 3D cell culture methodology, the development of useful models for drug discovery in oncology, and the development of new tools to better control and standardize 3D models were required in the lab.

List of publications

Presented in this thesis:

- **Label-free analysis of prostate acini by lens free imaging**

  Dolega, M.E., C. Allier, S. Vinjimore Kesavan, S. Gerbaud, F. Kermarrec, P. Marcoux, J.M. Dinten, X. Gidrol, and N. Picollet-D'Hahan.
  2013, *Biosens Bioelectron*. 49c:176-183.

- **Facile Bench-top fabrication of enclosed Circular Michrochannels Provides 3D Confined Structure for Growth of Prostate Epithelial Cells**

  Dolega, M.E., J. Wagh, S. Gerbaud, F. Kermarrec, J.-P. Alcaraz, D.K. Martin, X. Gidrol, and N. Picollet-D'hahan.
  2014, *PloS one*, 9:e99416-e99416

- **Controlled 3D culture in Matrigel-droplet microfluidics shows that acinar development relies on autocrine signaling**

  Dolega M.E., Abeille, F., Picollet-D'hahan, N., Gidrol, X., submitted 2014

Other:

- **The modulation of attachment, growth and morphology of cancerous prostate cells by polyelectrolyte nanofilms**

  Picollet-D'hahan, N., S. Gerbaud, F. Kermarrec, J.-P. Alcaraz, P. Obeid, R. Bhajun, L. Guyon, E. Sulpice, P. Cinquin, M.E. Dolega, J. Wagh, X. Gidrol, and D.K. Martin.
  2013, *Biomaterials*. 34:10099-10108

- **Continuous microcarrier-based cell culture in a benchtop microfluidic bioreactor**

  Abeille, F., F. Mittler, P. Obeid, M. Huet, F. Kermarrec, M.E. Dolega, F. Navarro, P. Pouteau, B. Icard, X. Gidrol, V. Agache, and N. Picollet-D'hahan.
  2014, *Lab on a chip*. 14:3510-3518

Conferences

Results described in this thesis have been presented on the following conferences:

- 2014 – **Atelier Inserm – The third dimension bridges the gap between cell culture and live tissue** , Bordeaux, France

  Oral presentation "Droplet microfluidics for 3D epithelial cell culture"

- 2014 - **Lab-on-chip European Congress**, Berlin, Germany

  Best Poster Award "3D culture in beads – a microfluidic approach for high throughput screens"

- 2014 - **Nano&Microenvironment for cell biology,** Grenoble, France

  Best Poster Award "3D culture in beads – a microfluidic approach for high throughput screens"

- 2013 - **Screening and Functional Analysis of 3D Models,** MIT, Boston, USA

  Best Poster Award "Droplet microfluidics for 3D epithelial cell culture"

- 2013 – **GIRC International Congress**, I'AB, Grenoble, France

  Poster: "3D culture in beads – a microfluidic approach for high throughput screens"

- 2013 - **Cellules et Toxiques en 3D: La vision du future**, Chatney – Malabry, France

  Oral presentation: "Droplet microfluidics for 3D epithelial cell culture"

- 2013 - **1st ERC BIOMIM meeting: At the Frontier between Materials and Biology**, Grenoble, France

  Oral presentation: "Epithelial 3D cell culture – a microfluidic approach"

- 2013 - **Lab-on-chip European Congress**, Barcelona, Spain

  Best Poster Award "3D culture in beads – a microfluidic approach for high throughput screens"

- 2013 - **1st Symposium of the Cancer Research Center of Lyon**, Lyon, France

  Poster: "3D culture in beads – a microfluidic approach for high throughput screens"

Contents

1. General Introduction

Our understanding of the function, formation and homeostasis of tissues originates from two dimensional models (2D). Also 2D-based studies have greatly contributed to the fundamentals of cancer biology. The reason why 2D cell culture models are readily applied is due to the simplicity in preparation, the well-controlled culture conditions, which sustain proliferation for most cell types, and facile microscopic analysis. However, a plastic petri-dish does not recapitulate the real tissue environment which is organized in three dimensions (3D). The cell-cell and cell-ECM (extracellular matrix) interactions present in native tissue are very limited in 2D culture. Furthermore, the inadequacy of current 2D models is well reflected in the poor outcome of drug development and approval processes. The third dimension provides better external mechanical inputs, and cell adhesion, which dramatically affects integrin ligation, cell contraction, and as a consequence, influences intracellular signaling. Therefore, there is an increasing need to elaborate new 3D reductionist *in vitro* models that will better recapitulate *in vivo* conditions. The relevance of 3D culture strategies is further detailed in **Chapter 2**. Since most of the tumors originate in glandular tissue, Chapter 2 also introduces fundamental information on epithelial morphogenesis *in vivo* and *in vitro*.

One of the well accepted forms of 3D tumor models are multicellular aggregates called spheroids, where a small aggregate of cells grow free of foreign materials. Spheroids have found extensive application in drug screening and toxicology assays by reflecting accurately the 3D cellular organization, diffusion limits within the tissue, and necrotic core that is characteristic of tumors. Furthermore, from a technical point of view, spheroids are cellular masses that are constrained by imposed conditions to aggregate from a solution of single cells. Additionally aggregation occurs in the absence of ECM and thus studies on the effect of ECM proteins and eventual remodeling during carcinogenesis are consequently limited. In conclusion, spheroids can serve as a model for pharmacological assays on mature tumors but may not necessarily be suitable to the modeling of tumor initiation and carcinogenesis.

The acinus, a spherically organized and polarized* cellular structure containing lumen, is the functional unit of glandular epithelial tissues. Acini are further interconnected with polarized tubules through which secreted fluids are transported. As opposed to spheroid culture, epithelial cells are cultured within a gel composed of ECM where acini are formed. These functional structures are broadly used to study development of glandular tissue *in vitro* but also to model tumor initiation and progression. Spheroid models with a necrotic core in

* Certain proteins are locally organized within each cell. For example E-cadherins are localized specifically to the baso-lateral membrane while integrins, only to the basal membrane

general imitate properties of already formed tumors. The 3D culture of epithelial cells, which organize into acini, enables research on tumor formation. Cancer of epithelial tissues is indeed reflected in the loss of the polarity and filling up of lumens. To date, drug evaluation is often assessed by tumor spheroid growth and invasion. A new opportunity would be to use polarity and lumen formation as an output of the treatment (drugs, siRNA etc.). However to effectively do so, high-throughput and high-content 3D analytical tools capable of recording changes in cellular polarity and organization are required. In addition to these proposed screening approaches, 3D culture is a relevant model to study genetic and microenvironment determinants, which are known to play an important role in acini morphogenesis and homeostasis.

With the aim of i) addressing fundamental issues in prostate cancer, and ii) performing RNAi (RNA interference) screens in a more physiologically relevant (as compared to 2D) context, I have developed innovative tools based on microsystems suited for intermediate high-throughput analysis of a large amount of 3D objects. The objectives of this thesis are listed in **Chapter 3**.

Coherent with the focus of BIOMICS laboratory on the prostate cancer, the RWPE1 cell line has been introduced to model acini formation and to study genetic determinants important in acini homeostasis. The results on implantation (optimization of the protocol) and characterization (immunofluorescence) of 3D RWPE1 culture within the ECM gel (Matrigel) are presented in **Chapter 4**.

Conventional 3D cultures, however, often lack reproducibility, a factor critical to any screening approach. Considerable heterogeneity in the shape, size and developmental stage of 3D structures during culture has been observed. Implementation of automatic analysis which requires the use of confocal microscopy (including time-lapse acquisitions) is further impeded by the tendency of structures to merge, overlap or to grow at different focal planes. Furthermore, recovery of cells from Matrigel is difficult as well as retrieving of proteins and RNA from the sample. To overcome these limitations and to provide homogenous growth of acini in a controlled environment, I developed a droplet microfluidic encapsulation technology. Microfluidics provides a high level of control over flow conditions by manipulation of liquids within micrometer-scale channels. As a consequence a reproducible formation of Matrigel droplets containing a single cell has been achieved. Moreover, each encapsulated cell has exactly the same environment, therefore, problems of aggregation and merging have been effectively eliminated. Furthermore, it is possible to study morphogenesis starting from single cells. Microfluidic techniques provide a solution for a high-throughput analysis by using flow-based analysis of fluorescent biomarkers for proliferation, differentiation etc... Results that I have generated using a microfluidics approach concerning the optimization, characterization

and ultimately, the biological applications of this microfluidic approach are presented in **Chapter 5**.

The process of glandular tissue formation is not limited only to acini formation but also it consist stage of tubulogenesis. The importance of studying the organization of cells into tubules relies on the fact that these structures transport secreted liquids, the analysis of which can potentially help to identify new biomarkers in prostate cancer. However, studying tubulogenesis *in vitro* has been limited to only several cell models, and access to the secretions has not yet been possible. Therefore, in order to study cellular tubule-like organization in 3D, I developed a technique to generate circular microfluidic channels to mimic the ductal environments. **Chapter 6** describes the fabrication methods and biological characterization of cells grown within a constrained tubular environment.

Live observations of tubulogenesis *in vitro* are limited by the small field of view (typically smaller than 1 mm^2) of traditionally-used microscopic techniques. As a consequence, only a restricted number of structures can be observed during acquisition, thus rare events occurring during tubulogenesis process can be missed. Therefore, in collaboration with CEA-Leti, we developed lens-free systems specifically with the intent to observe a large field of view, so as to record a more global and inclusive view of the dynamics of acini and tubule morphogenesis. We demonstrate that application of lens-free video microscopy to 3D culture of developing acini reveals never before-detected *in vitro* self-seeding-like collective cell migration during branching morphogenesis. **Chapter 7** presents the results on the influence of the microenvironment on cell phenotype and time-lapse observations of these phenotypic changes during branching-like processes.

Furthermore, due to the lack of lenses, obtained images during lens-free acquisition are in fact light diffraction patterns of observed objects. We have observed that spheroids in 3D Matrigel cell culture differ drastically from acini in obtained holographic patterns. This observation served to develop a lens free system to distinguish spheroids from acini containing lumen. Therefore, the lens-free label-free system we have developed facilitates screening for environmental factors that affect epithelial tubulogenesis. Development and implementation of the lens-free system for label-free analysis of acini is described in **Chapter 7**.

2. Literature Review

2.1 Epithelium *in vivo*

Evolutionarily, epithelia are the most representative polarized tissues in metazoa – 60 % of mammalian cells are epithelial or epithelial-derived (Alberts *et al.*, 2002). Also, the most fundamental type of cell organization in animal kingdom is that of epithelia. Although epithelial tissues exhibit a wide variety of morphology, they serve in general to form a coherent barrier and divide organism into topologically and physiologically distinct species. Epithelial tissues can be composed of multilayers of cells as the stratified squamous epithelium of skin or a one cell thick form as in the case of simple epithelia (Figure 2-1). The shape of the cell might differ drastically from cylindrical, through cuboidal to pavimental. Also considering the role of the cell one can find cells than only serve as a mechanical barrier or cells that have a specific biochemical function (i.e., secretion of hormones as in prostate or absorption of nutrients as in intestine) or serve as signal receptors (e.g., photoreceptors in eyes and ciliated cells in ears).

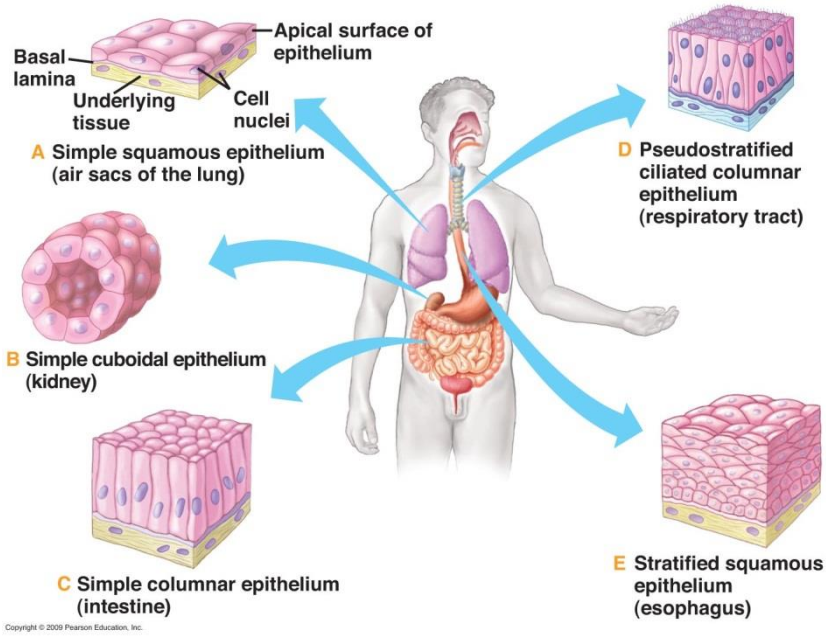

Figure 2-1 Schematic representation of types of epithelial tissue throughout the human body. Source: Inc © 2009 Pearson Eduction

Some epithelia cover the outside of the organism while others line internal organs. Despite all the differences, there are features shared by epithelial tissues. In general, an epithelial layer presents two specific surfaces i) an **apical surface** that is in contact with air or an aqueous liquid, and ii) a **basal surface** that is in direct contact with a very thin layer of an extracellular matrix (**ECM;** the role of ECM is further discussed in Chapters 2.3) and rests on another type

of tissue (in most cases connective tissue) to which it is attached. The presence of two chemically distinctive sites of an epithelium brings a particular and essential polarity to a single cell. The apico-basal polarization is responsible for the directional transportation of materials. The epithelium and thus also polarity are maintained mainly by presence of cell-junctions (Datta *et al.*, 2011).

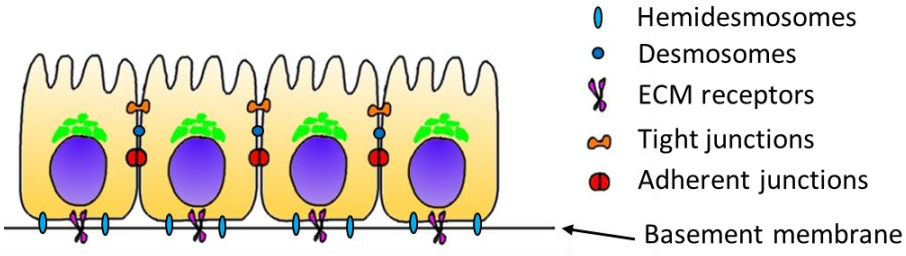

Figure 2-2 Each cell of the epithelium has a microvilli-reach apical surface, a lateral membrane that faces the neighboring cells, and basal membrane connected directly through hemidesmosomes to a basement membrane (BM). Between cells, various cell-cell junctions are established including desmosomes, tight junctions, adherent junctions, and gap junctions (not shown in here). Tight junctions play the main role in keeping tissue homeostasis.

Cell junctions between epithelial cells can be classified on the basis of their function and are characterized by specific membrane proteins. In vertebrate epithelia, the major types of intercellular junctions are (Figure 2-2):

- Gap junctions – permit transportation and passage of the small molecules and cytosolic molecules in between the neighboring cells
- Tight junctions – indispensable for establishing and maintaining the physical barrier characteristic for epithelial tissue
- Adherent junctions – modulate the tissue integrity through association of actin filaments
- Desmosomes – similarly as adherent junctions modulate the tissue integrity but through organization of intermediate filaments
- Hemidesmosomes – establish junction between cell and ECM

While tight junctions are characteristic and exist only in epithelium, other types of junctions under modified forms exist in non-epithelial tissues.

Adherent junctions and desmosomes rely on the family of transmembrane proteins called **cadherins.** A single cadherin molecule of the plasma membrane of one cell is attached directly with the corresponding identical molecule from the neighboring cell. Presence of Ca^{2+} in an extracellular medium is necessary for the proper establishment of cadherin junctions. On the level of adherent junctions, each molecule of cadherin is fixed in the cytoplasm of the cell and further connected to actin filaments. Due to adherent junctions the network of actin

filaments is interconnected through the whole epithelium. This network of actin is potentially contractile and it gives the epithelium flexibility to change the shape into a great extent. This flexibility plays a key role in embryonic development.

2.1.1 Prostatic glandular epithelium

Analysis of development *in vivo* resulted in a great deal of information, concerning growth factors, receptors, signaling pathways and transcriptome factors that control the most fundamental properties as location, differentiation and shape of tubular organs (Hogan and Kolodziej, 2002). Significant information about the process of development was provided by observing of much simpler organisms like in the case of formation of trachea in *Drosophila* (Affolter *et al.*, 2003; Lubarsky and Krasnow, 2003). Many important developmental pathways that were discovered in *Drosophila* or worms have been conserved throughout the evolution and found equally significant in vertebrate systems.

The development of glandular tissue *in vivo* differs depending on organs type. In mouse model prostatic buds first arise in the endoderm anterior urogenital sinus epithelium and invade the underlying mesenchyme to undergo multiple rounds of branching events and canalization, leading to the pseudostratified structure of the prostate epithelium. In mammary glands lumen formation is secondary to the branching, while in lung embryonic development both processes are associated (Affolter *et al.*, 2003).

One structural and functional unit: the Acinus

Glandular epithelial organs are typically formed of two building blocks, cysts and tubules (schematic representation Figure 2-3 and histological image Figure 2-4). Both cysts and tubules are enclosing lumens, with the former being formed by spherically organized cells and the latter by cylindrically organized cells. Cysts in dependence of their occurrence are called also *acini* in prostate and mammary gland, *alveoli* in the lung and *follicles* in the thyroid.

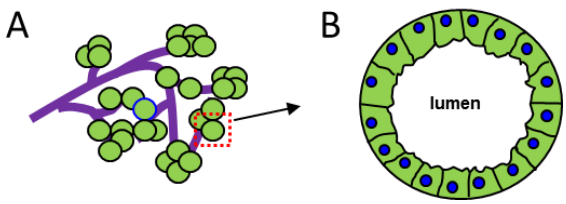

Figure 2-3 Schematic representation of glandular epithelium *in vivo*. A) Glandular tissues are composed of polarized tubules (violet) terminated with acini. B) Acini are spherically organized cellular structures that enclose lumen and are situated at the end of tubules. These functional units of glandular tissue are responsible for secretions.

Apart of forming lumen, acini are also polarized. Similarly as described before for a monolayer of epithelium, cells of acini organize to enclose lumen, and each particular cell follows a certain polarity. As a consequence basal and luminal cells can be distinguished (Figure 2-4).

The main function of prostate is to produce seminal fluid. The prostatic glandular epithelium is composed of three different types of cells: luminal secretory, basal and neuroendocrine. Compared to other glandular tissues, in prostate there are fewer basal cells (Figure 2-4). One of their functions is to secrete components of the basement membrane. The luminal cells secrete the prostate specific antigen (PSA), components of prostatic fluid, and beside that they express the androgen receptor. The stroma around prostatic cells contains fibroblast, smooth muscle cells, endothelial cells, dendritic cells and nerves. This complex environment affects the prostate mainly by paracrine signals (i.e., production of growth factors) coming from the androgen responsive stromal cells (Chung, 1995).

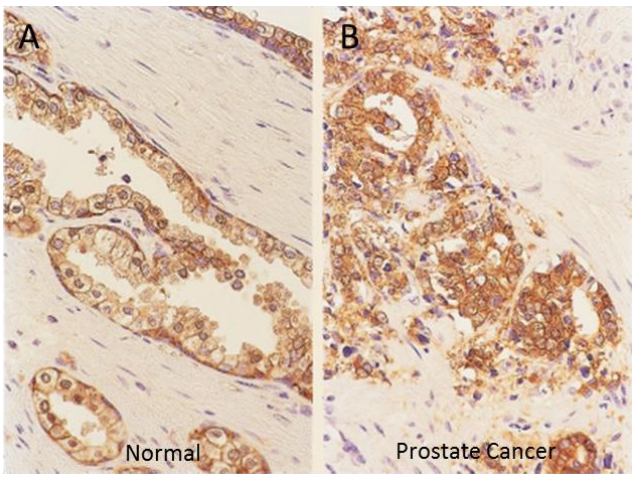

Figure 2-4 Prostate histology from a normal (A) and cancer prostate tissue (B). Sections were stained with E-cadherin, a marker for adherent junction. Prostate cancer reflects in the disruption of the epithelial organization and filling lumens. Note in A that basal cells do not form a uniform layer. Source: (Feldman and Feldman, 2001)

Stages of development in vivo

Prostate gland is an endodermal structure and originates from the urogenital sinus (UGS). The continuous process of prostate development can be divided into four separate stages composed of determination, initiation or budding, branching morphogenesis, and pubertal maturation (Figure 2-5). Determination is the stage before any visual evidence of prostate formation and involves expression of molecular signals that specify the prostatic cell fate. The first evidence of phenotypic prostate development starts when the epithelial cells from UGS form outgrowths or buds that penetrate into the surrounding UGS mesenchyme. In human, the prostate develops during the second and third trimester and is completed at the time of birth

(Lowsley, 1912). Studying the processes of development in human is often technically difficult or impossible due to ethical reasons. We are therefore, forced to use animal models which to some extent are perfectly fulfilling the physiological environment, however, their development might differ drastically from that of humans. The prostate development in rodents takes its major stages after the birth. The initial outgrowth occurs between 16,5-17,5 fetal days (f16,5-f17,5) in a 19 days gestation strain (Sugimura *et al.*, 1986) while in the rat it occurs at 18,5-19,5 in a 21 day gestation strain (Hayashi *et al.*, 1991). At birth, the rodent prostate lobes are composed primarily of unbranched, solid elongating buds (or ducts) and subsequent stage of outgrowth and patterning takes place postnatally. Branching morphogenesis starts when elongating UGS epithelial buds contact the prostate mesenchymal pads which initiate establishment of secondary, tertiary and further branch points (Timms *et al.*, 1994). Morphogenesis of the prostate in rodents is completed between postnatal days 15 and 30, and the final growth and maturation occurs during puberty with the increased levels of circulating androgens. Epithelial and mesenchymal cell differentiation is coordinated with branching morphogenesis and occurs during later days of branching (Hayward *et al.*, 1996a; Hayward *et al.*, 1996b; Prins and Birch, 1995). Differentiation relies on the formation of distinctive basal and luminal layers along with lumenization of the solid epithelial cords.

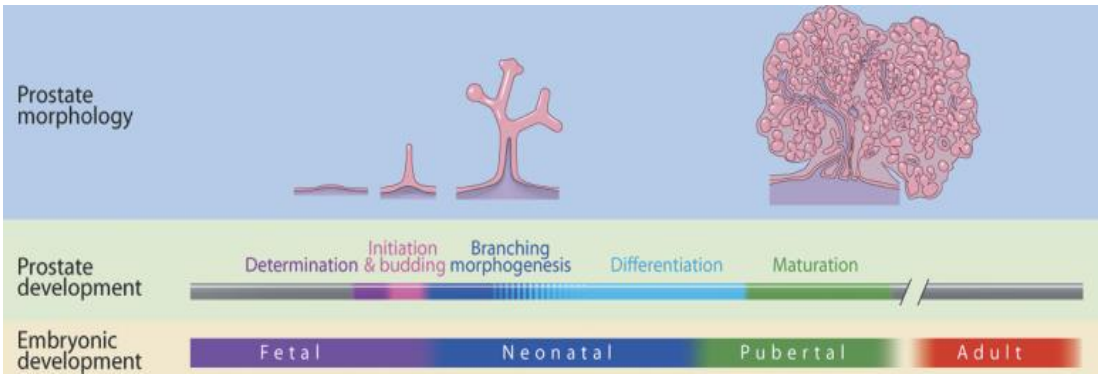

Figure 2-5 Rat prostate developmental stages and corresponding timeline. Source: (Prins and Putz, 2008)

The concept that the development of prostate depends and is regulated by androgens has been proven with several approaches. For example, anti-androgen administration in rodents during fetal period results in inhibition of prostate development (Price, 1936). However, the result of inhibition is highly dependent on the period of development. Organ cultures of UGS explants from male mice were retrieved at different time of the development; at day f12 before fetal testes produce testosterone (day f14) and at day f15. It has been shown that the extent of inhibition depends strictly on timing of androgen ablation in relation to the budding process. USG extracted before initiation of budding (day f12) did not produce prostatic buds even after 6-7 days of culture without androgens. Conversely, USG explants removed at day f15 initiated buds when cultured for 6 days in the absence of androgens (Cunha, 1973;

Lasnitzki and Mizuno, 1977). The same results were obtained in study performed on rats (Lasnitzki and Mizuno, 1977). Taken together these findings indicate the androgens are causal factor to induce the process of budding (the number of buds and their length during initiation), however, it can continue to a large degree in the absence of testosterone. Interestingly, as mentioned, branching morphogenesis can occur in the absence of androgens, the final organization, growth and differentiation are only followed upon addition of exogenous testosterone(Lipschutz *et al.*, 1997).

Action of Androgens

Androgens are the main regulators of development in prostate. To simplify, androgens have a direct influence on the ratio of proliferating to dying cells. No wonder that the first stages of prostate cancer use the same pathways to induce proliferation in already differentiated environment.

Testosterone is the main circulating androgen and is secreted principally by the testes. Testosterone circulates in blood where it is tightly bound to albumin and sex-hormone-binding globulin (SHBG) of human blood plasma with a small fraction of unbound form in the serum. Testosterone enters prostatic cells only when it is in the free form and is converted in ~90% to dihydrotestosterone (DHT) by the enzyme 5α-reductase (5RD5A2) (Figure 2-6). Compared to testosterone, DHT has the fivefold higher affinity for androgen receptor. The AR belongs to the family of steroid-thyroid-retinoid nuclear receptors (Quigley *et al.*, 1995). It contains three major domains: an aminoterminal activating domain♣, a carboxy-terminal ligand and a DNA binding domain comprising two zinc fingers♦. Androgen receptor functions as other nuclear receptors where in the basal state it is bound to heat-shock protein that prevents DNA binding. Upon binding with androgen, AR undergoes conformational changes reflected in dissociation from the heat-shock protein and subsequent phosphorylation (ref 6 from nature review). This conformational change facilitates the formation of AR homodimer complexes and binding to androgen-response elements in the promoter regions of target genes (Brinkmann *et al.*, 1999). Presence of co-activators (ARA70) facilitates or prevents, depending on the function, AR-complex to interact with the general transcription apparatus (GTA) (McKenna *et al.*, 1999). In response to activation of target genes increased growth, survival and PSA production are observed. As it will be described below, detection of levels of PSA is used in prostate cancer diagnosis.

♣ Region of steroid hormone receptors that enhances target gene transcription.

♦ Protein module in which conserved cysteine or histidine residues coordinate a zinc atom. Some zinc-finger regions bind specific DNA sequences; others are involved in protein–protein interactions.

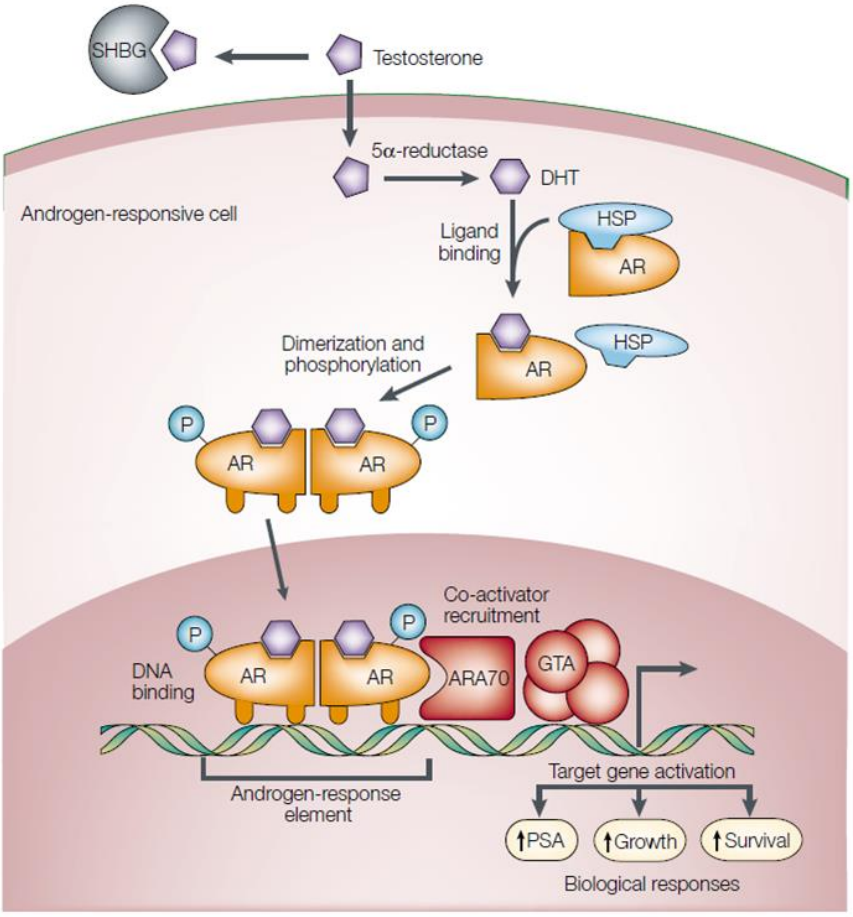

Figure 2-6 Path from circulating testosterone to androgen-response and PSA secretion. Source: (Feldman and Feldman, 2001)

2.1.2 Prostate cancer

According to the National Institute of Cancer in the United States, prostate cancer is the most common form of cancer in men and after lung cancer is the second leading cause of death in USA (Greenlee *et al.*, 2000). A lifetime's risk for man to develop prostate cancer is one to seven. Interestingly, among all risk factors, age and race are the most important (Miller *et al.*, 2006).

Initially grown tumor is androgen-dependent which facilitates the treatment. Already 30 years ago, Huggins has reported androgen ablation by orchiectomy♣ as a treatment that causes regression of tumors (Huggins, 1967). Recently, androgen ablation maintains as a main and the most effective therapeutic treatment of hormone-sensitive prostate cancer (Eisenberger *et al.*, 1998). However, developed tumors eventually become androgen-independent, followed by progression and metastasis. It is still unknown what primarily triggers the development of androgen-independent prostate cancer (AIPC). What is known, as for most types of cancer, early diagnosis gives the highest survival rate (Figure 2-7).

♣ Orchiectomy – surgical removal of the testes

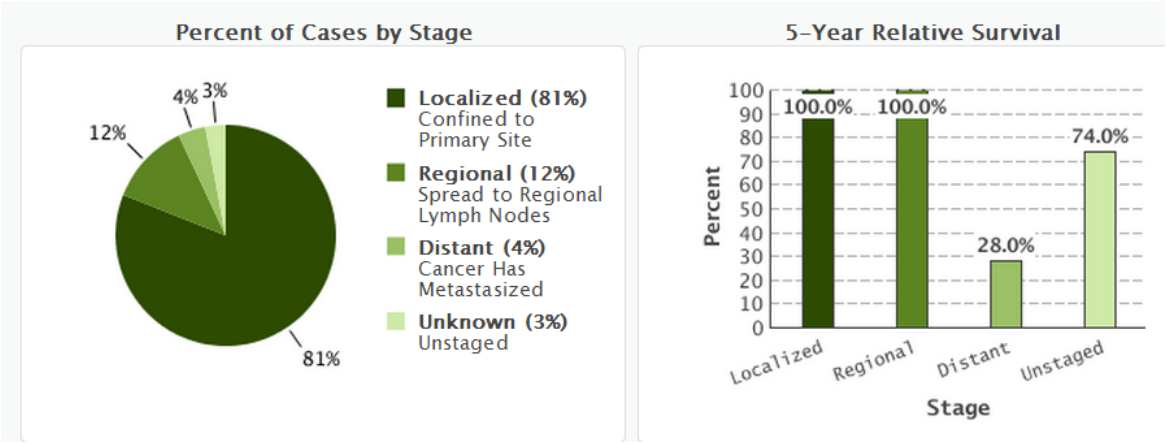

Figure 2-7 Percent of cases and 5-year relative survival by stage at diagnosis for prostate cancer. Source: SEER 18 2004-2010, All Races, Males by SEER Summary Stage 2000

Prostate cancer diagnosis – PSA controversy

As has been shown androgen action stimulates the cells during development of prostate by increased proliferation, survival and secretion of PSA. The same cell response is characteristic for prostate cancer which was a basis to use PSA as a diagnosis marker.

PSA is androgen regulated serine protease which is produced primarily by luminal epithelial cells. Its role is to cleave semenogelin♦ I and II in the seminal coagulum (Lilja *et al.*, 1987). PSA is secreted as an inactive 244-aminoacid proenzyme (proPSA) that is activated by cleavage of seven N-terminal amino acids. Secreted PSA is rapidly bound by protease inhibitors although some fraction of PSA circulates in an unbounded form, comprising around 10 % to 30 % of total PSA. It consistently expressed in prostate cancer, although the levels of expression are lower than in normal prostate (Magklara *et al.*, 2000; Pretlow *et al.*, 1991). Studies performed in 1990s confirmed that tests on concentration of PSA in serum can serve for prostate cancer diagnosis (Catalona *et al.*, 1991; Labrie *et al.*, 1992) and overpower digital rectal examination used at that time. To increase the sensitivity of the test, later, diagnosis relied on calculating the ratio of free to total PSA, which is lower in many patients with prostate cancer. However, today, it is controversial whether the test is reliable and beneficial or socially harmful due to high false-positive and false-negative results. The United States Preventive Services Task Force has analyzed the data from two big trials on prostate cancer performed in the USA and Europe and revealed striking results (Figure 2-8) (Moyer, 2012).

Based on the results there is only 0 to 1 patient among 1000 would avoid prostate cancer while 100 to 120 would have a false-positive result. This data illustrate the problem of the prostate cancer diagnosis. **Therefore, new and more specific biomarkers are necessary to increase the survival rate.**

♦ Semenogelin – proteins that mediate gel formation in semen

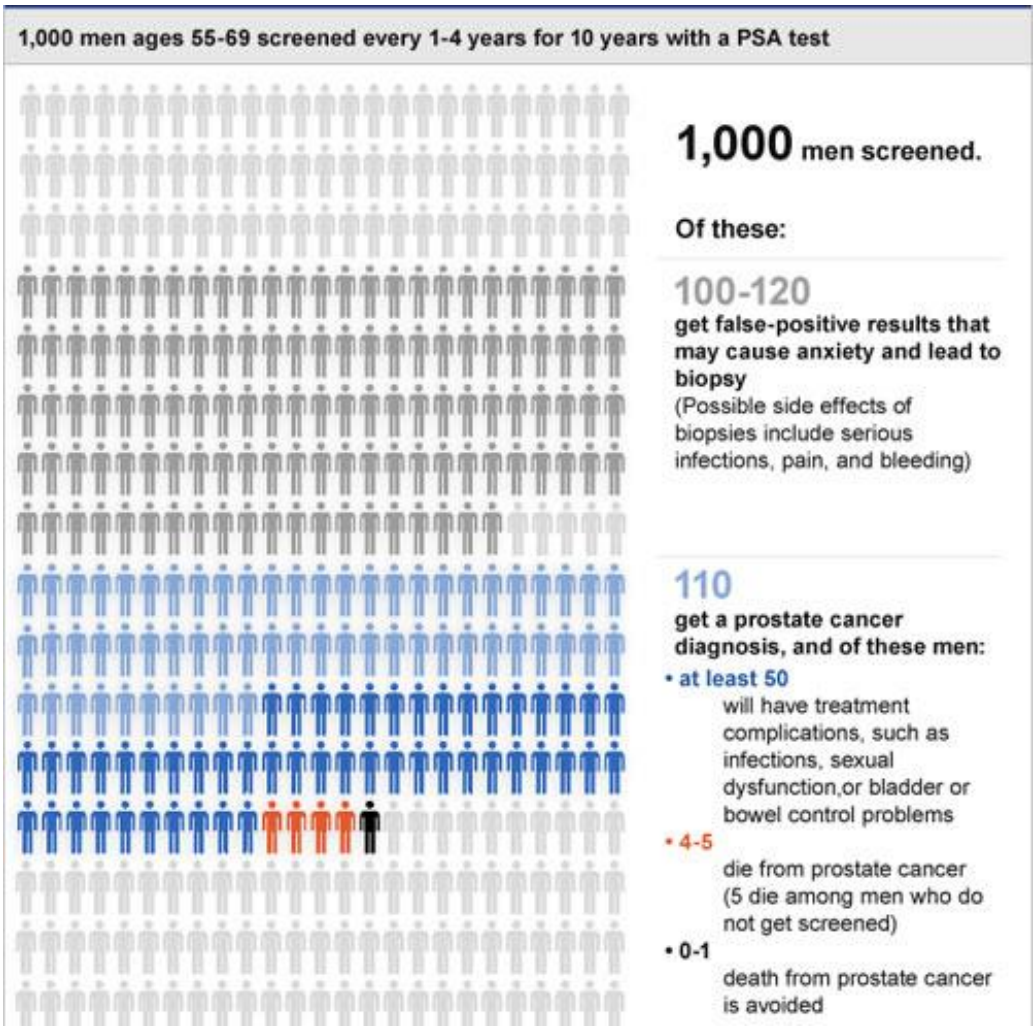

Figure 2-8 Benefits and harms of PSA screening for prostate cancer. Source: National Cancer Institute at the National Institutes for Health, USA; http://www.cancer.gov/

Hallmark of cancer - Loss of polarized organization

PSA as a diagnostic marker presents a high false-negative or false-positive results. Therefore, diagnosis further comprises prostate biopsies which are used to investigate cellular organization of the prostatic tissue. A hallmark of cancer is the loss of polarity which is reflected by the disorganization within the acini (schematic representation Figure 2-9 and histology observation Figure 2-4). The process can occur even from a single cell whose phenotype differs drastically from differentiated epithelial cells (Leung and Brugge, 2012). Uncontrolled proliferation leads to filling the luminal space with cells to finally develop a tumor, solid aberrant masses. At this stage basal and luminal cells are undistinguishable since they co-express basal and luminal markers (for example Keratin 5 and Keratin 8) (Frank and Miranti, 2013) .

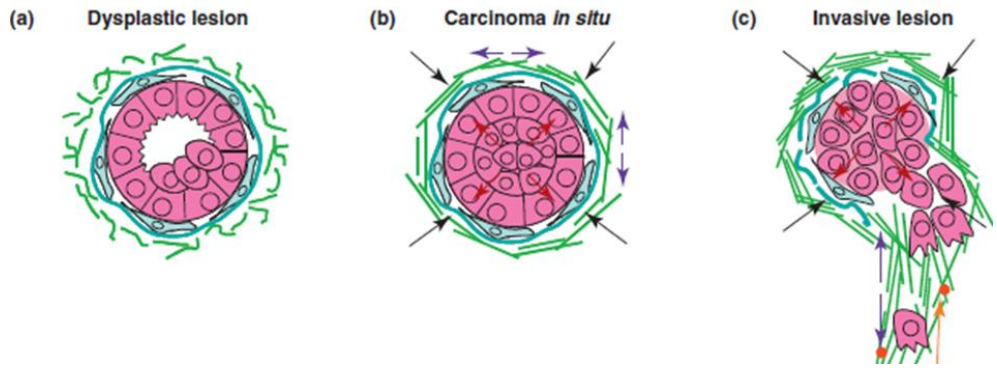

Figure 2-9 Process of tumor development. A) In dysplastic lesions, cells lose polarity and proliferate into the luminal space. **B)** In carcinoma *in situ* lesions, lumen is filled with tumor cells. Volume expansion and resistance from ECM leads to increased forces between tumor and stromal matrix. Simultaneously, remodeling of ECM occurs leading to increased ECM and tissue stiffness. **C)** In invasive lesions, tumor cells break the BM barrier and invade into the interstitial ECM. Source: (Yu *et al.*, 2011)

Conclusions

Fighting cancer requires perfect understanding of the changes that cause uncontrolled proliferation, dedifferentation that in first stages is reflected by filling up of acinar lumens. Better understanding can be achieved by reductionist cell culture models. However, standard 2D cultures do not recapitulate functions and the three dimensional cellular organization within glandular tissues. High potential lies in 3D cell culture which proved to provide more physiological environment for cells to develop into fully polarized acini with lumens. With available models discovery of new biomarkers (to overcome limitations of PSA diagnosis) is hampered by the analysis limitations, and thus difficulties occur when performing high-throughput screens and drug assays in 3D. Therefore, with the advances in cell culture biology, 3D culture is awaiting for the technology to meet the requirements for efficient high throughput screening tools. These needs include facilitation of analysis providing structural and functional information of acini but also means for high-throughput and reproducible 3D cell culture preparation.

2.2 Epithelial cell culture *in vitro*

The potential to find new strategies in cancer treatment, not only for prostate, lies in designing experiments based on human cell models within the well-controlled environment (mechanical, chemical and cell-cell signals) combined with high throughput analysis. Experiments performed in such a reductionist environment can bring us closer to understand processes that control the initial acquisition of cells polarity and epithelial organ formation. Also, drug or RNAi (RNA interference) screens could be successfully executed to reveal new important actors in cancer disease.

2.2.1 Limitations of animal models

Animal models recapitulate only some of the aspects of human responses. A good example is a high number of pathogens that are specific to humans (i.e., hepatitis C) which causes the failure of new drugs tested clinically due to the liver toxicity that has not been observed in animal models (Sivaraman *et al.*, 2005). Researchers try to overcome this problem by transplanting human cells into mice (Katoh *et al.*, 2005; Kuperwasser *et al.*, 2004), however, these models are challenging and expensive to be adopted for routine experiments.

Moreover, important variances in telomerase* regulation between rodents and humans (Rangarajan *et al.*, 2004) raised doubts regarding the relevance of transgenic and inducible mouse cancer models. The uncertainty of xenografts lies in the incompatibilities of certain cytokines. Therefore, opportunity to develop *in vitro* tissue models that are based on human cells provides a potential bridge over the gap between animal models (but also between 2D cultures) and humans to better understand the basic mechanisms that govern human disease.

2.2.2 Limitations of 2D models

Tissues and organs are multicellular structures organized three dimensionally (3D). However, to date our understanding of the function, formation or pathology relied on two dimensional models (2D). Even though the 2D culture does not recapitulate environment by which cell is surrounded *in vivo*, this model of culture has produced many important insights into fundamentals of cell biology.

The interest to use cell culture techniques relies on the simplicity of such models where cells are exposed to a far more limited number of cues compared to *in vivo*. Epithelial cells when cultured on flat plastic dishes recapitulates to some point polarized monolayers of epithelial sheets and can be used for toxicology assays (Suuronen *et al.*, 2005) as they mimic the responses of real tissues to drugs and certain toxins. However, the polarity (which will be

* Telomerase – an enzyme in a eukaryote that adds DNA sequence to the 3' end of DNA strands. Its role is to repairs the telomeres of the chromosomes so that they do not become progressively shorter during successive rounds of chromosome replication.

discussed later) and cell orientation is forced by the artificial support, which brings a powerful external cue for placement of the basal membrane. When mammary epithelial cells are cultured in traditional 2D conditions, they fail to differentiate, even in the presence of prolactogenic hormones (Barcelloshoff *et al.*, 1989). After development of techniques and biomaterials which serve to incorporate cells in 3D, now we know that morphology, cell-cell, cell matrix interactions and finally differentiation differ drastically from those growing on flat plastic substrates (Cukierman *et al.*, 2002; Nelson and Bissell, 2006).

2.2.3 Transition from 2D into 3D

Most cells, though, require cues from a truly 3D environment. *In vivo*, this environment is a bundled meshwork of extracellular collagens, proteoglycans, adhesion proteins, and at the same time, it contains soluble signals like growth factors cytokines and chemokines. By definition Extracellular matrix (ECM) encompasses these components (Aumailley and Gayraud, 1998; Streuli, 1999) and by alterations governs basic processes of i.e., morphogenesis, development, and regeneration. In a simplified way, a biological response of cells to the ECM is based on multiple cell interactions with different components of the ECM that induce signals trough surface receptors, which are further integrated through intracellular pathways to finally regulate gene expression and influence the phenotype. Therefore, the cell fate and function depends on several biophysical and biochemical factors that can be divided into i) physical signals originating from the ECM structure-building components (collagens, laminins, fibronectins etc.), ii) soluble signals (growth factors, cytokines etc.), and iii) signals that originate from cell-cell interactions (Figure 2-10). The interaction between the cell and ECM is mediated by two types of integrin-dependent junctions – focal adhesions, which are linked to actin cytoskeleton and hemidesmosomes, which are linked to intermediate filaments of the cell. The large family of integrin receptors (18 alpha and 8 beta subunits) plays a crucial role in physical linkage to the ECM and signal transduction (Campbell and Humphries, 2011).

The complexity of ECM and the interaction between particular components defines unique matrices (Czyz and Wobus, 2001). Within one organism, different tissues are surrounded by ECM that vary considerably in the amount and type of specific components (Streuli, 1999). Therefore, importance of ECM has been studied extensively *in vivo* on mice using gene targeting approach (Gustafsson and Fassler, 2000). In certain cases, when a particular ECM component gene was missing, mice died or presented phenotype changed by inappropriate signaling during early development. For example, mice lacking gene that encodes laminin gamma1[♣] failed to synthetize and organize a basement membrane (BM) and died at embryonic stage (Gustafsson and Fassler, 2000).

[♣] Laminin gamma 1 – necessary in initial matrix scaffolding processes

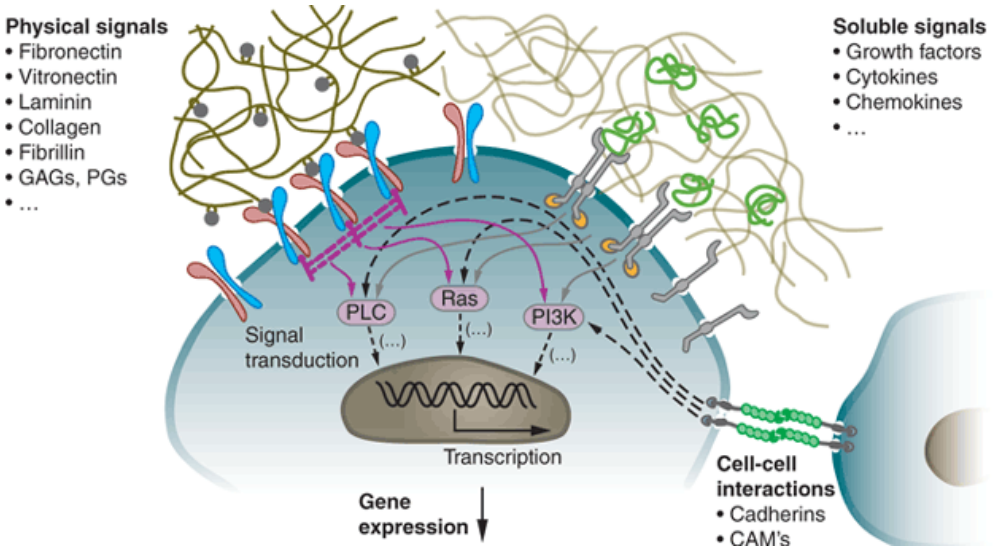

Figure 2-10 Cell fate *in vivo* is governed by multiple cues including soluble signals, physical and mechanicals signals and signals resulting from the cell-cell interaction. Source: (Lutolf and Hubbell, 2005)

In conclusion strengths of 3D culture include:

- More physiological (than in 2D culture) cell morphology and signaling,
- Ability to rapidly verify hypotheses without need to use animal models,
- Facile observations and image acquisitions compared to animal models,
- Relatively low total cost

However, among the drawbacks one have to include:

- ability to mimic *in vivo* tissue conditions varies upon the cell model and culture conditions (small differences in culture media composition my drastically change the phenotype and cell fate, i.e., additions of Human Growth Factor (HGF) induces branching morphogenesis (Zegers *et al.*, 2003)
- lack of vasculature and signals that *in vivo* originate from surrounding cells short-term cell culture conditions (usually samples are maintained no longer than 3 weeks) limits observation of long-term processes that occur *in vivo*

2.3 Recapitulating glandular-like structures in 3D cultures

2.3.1 Matrigel, a magic mixture

As has been shown above, the ECM sends various signals to cells to control their function, proliferation and survival. The complexity of ECM has hampered for years 3D cultures *in vitro* due to the lack of appropriate matrices that would recreate the natural environment. The discovery, (Orkin *et al.*, 1977), that a particular type of mouse tumor forms rapidly abundant ECM, brought the possibility to obtain large quantities of natural basement membrane (BM). Today, known as EHS extract (after J.Engelbreth-Holm and R. Swarm who highly contributed to the discovery) or under commercial name Matrigel, it is irreplaceable and indispensable product in 3D culture experiments. Matrigel is composed of laminin, collagen IV, perlecan (heparin sulfate proteoglycan) and nidogen (known also as entactin). Because it is naturally obtained it consists also of proteases, growth factors (i.e., Tgf ß, FGF, EGF, PDGF, IGF) and other proteins. The assembly of BM proceeds by polymerization of two separate networks. The first, of collagen IV, is covalently stabilized (Timpl *et al.*, 1981; Yurchenco and Ruben, 1988), while the second of laminin, forms a non-covalent, calcium-dependent network (Yurchenco and Cheng, 1993). This complex, but necessary composition of Matrigel, promotes *in vitro* differentiation of cell lines and primary cells and also of tissue explants (Kleinman and Martin, 2005).

Recent studies based on mass spectrometry revealed that apart the main listed components, signals for over 1000 other proteins were detected (Hughes *et al.*, 2010). Since Matrigel is naturally derived, lot-to-lot variations appear and bring controversy weather the results obtained within this ECM can be reliable and well reproducible (Vukicevic *et al.*, 1992). To limit these variations, it is generally advised to perform all experiments within the scientific project on the same lot of Matrigel.

2.3.2 Cell culture on Matrigel

Matrigel forms a hydrogel upon particular conditions; it is in a liquid, pre-polymerized form below 8°C and polymerizes at temperature higher than 10°C and maintains a form of a gel at physiological temperature of 37°C. These properties force special precaution in preparation of a BM substrate for cell culture; during manipulation Matrigel has to be kept on ice and pipette tips need to be cooled down.

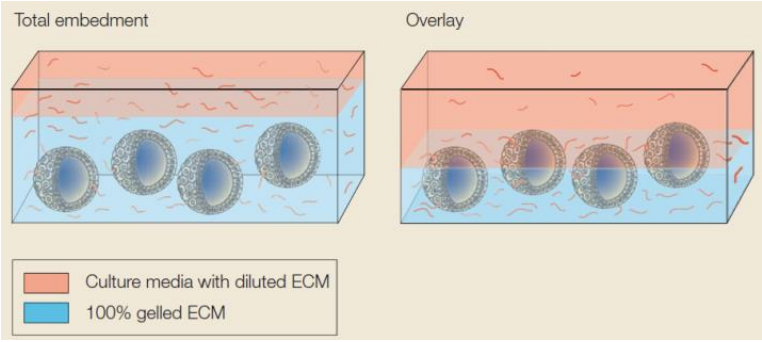

Figure 2-11 3D epithelial cell culture can be performed according to two different protocol; embedded when cells are fully surrounded by Matrigel and top-coat (or overlay) when cells are seeded on the compliant layer of Matrigel. Source: (Debnath and Brugge, 2005)

In 3D cultures epithelial cells proliferate to form growth-arrested acini that are characterized by polarized cells enclosing the hollow lumen (Debnath *et al.*, 2003; Petersen *et al.*, 1992). Typically to induce growth of acini, 3D culture of epithelial cells relies on either mixing single cells with the gel before the polymerization (Embedded conditions) so that the cells are fully surrounded, or on seeding the cells on the layer of polymerized gel and addition of diluted Matrigel into the culture media (*top-coat* conditions) (Figure 2-11). While the first protocol enables homogenous conditions in the ECM-cell interactions the second facilitates the microscopic analysis as all structures are cultivated on the same plane.

2.3.3 Acini morphogenesis and lumen formation

3D culture techniques described above brought insights into development and homeostasis of epithelial tissue. Established cell lines (i.e., MCF10-A as a breast cell model, MDCK as a kidney model, RWPE1 as a prostate model) when cultured in Matrigel or collagen I form acini through different stages (Figure 2-12). Initially, cells seeded in 3D culture are isolated. They proliferate and form clusters surrounded by ECM. Depending on the origin and polarity of the initial aggregate, lumen formation can occur by cavitation or hollowing. In the cavitation model, two distinctive cell populations occur; i) polarized outer layer of cells that maintains ECM-cell contacts, and ii) non-polarized cells that fill up the inner space of 3D structures. Another step is based on apoptosis of these inner cells that leads to lumen formation (Debnath *et al.*, 2002). The hollowing process is based on the vacuolar exocytosis and does not require any apoptosis for the lumen formation.

For many models *in vitro*, but also observed *in vivo* (Mailleux *et al.*, 2008), apoptosis is a key step in the lumen formation process. It has been shown that this process is significantly delayed, both *in vivo* and *in vitro*, when overexpressed BCL-2 (anti-apoptotic protein) (Debnath *et al.*, 2002; Humphreys *et al.*, 1996). Additionally, growth and survival of epithelial cells is regulated by integrin-mediated contact with ECM and cells that detach from ECM undergo apoptosis (specifically called anoiksis) (Frisch and Francis, 1994). It is suspected that

resistance to this apoptotic process can play a role in the early stage of cancer which is reflected by luminal filling.

Besides ECM-cell interactions, also cell-cell signaling (mainly through cadherins) governs lumen formation. Experiments, on CEACAM 1, (cell-cell adhesion protein; carcinoembryonic antigen-related cell adhesion molecule) identified it as a lumen formation regulator. Inhibition in non-malignant epithelial cells *in vitro* prevents lumen formation, while expression in malignant cells induces luminal development (Kirshner *et al.*, 2003).

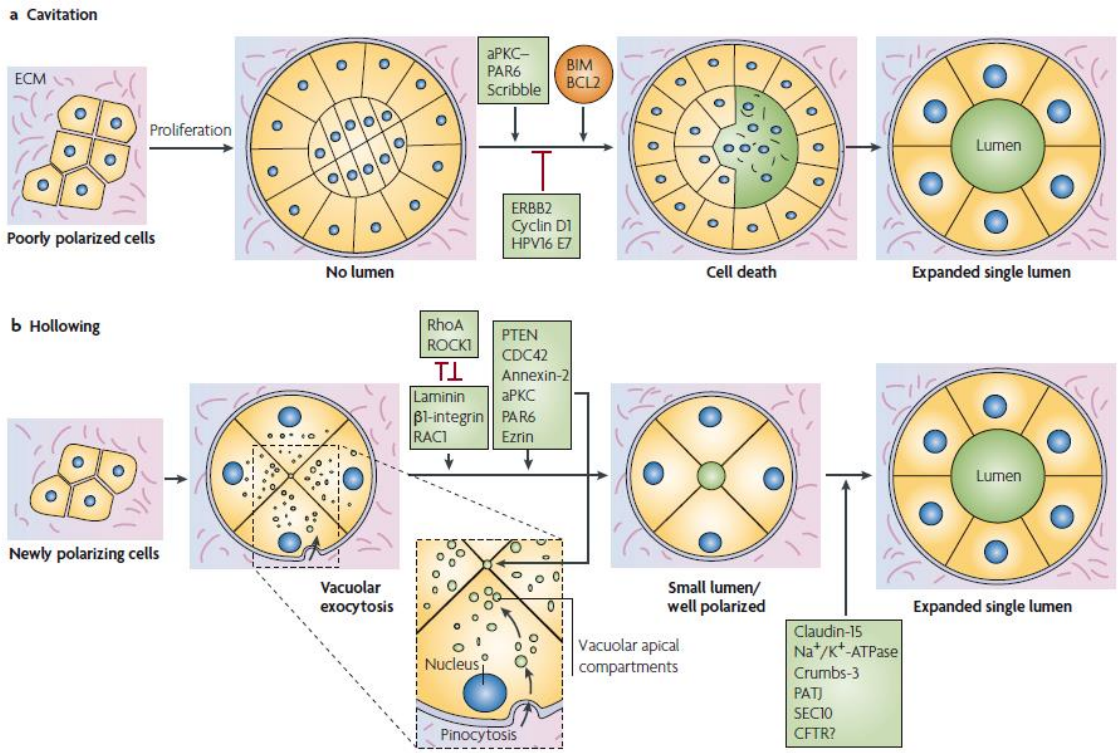

Figure 2-12 The process of acinus formation occurs either by cavitation which is associated with apoptosis of luminal cells or by hollowing by vacuolar exocytosis. Source: (Bryant and Mostov, 2008)

These results together indicate that lumen formation is a complex process governed by signals that originate from the environment. Because, cells are surrounded by ECM, and are in direct contact with neighboring cells, the signaling that induces lumen formation has to be considered as a complex signaling that originates from different cues. For example inhibition of anoiksis that is responsible for lumen clearing only delays the lumen formation but finally does not prevent it.

Epithelial cells need apical and basal polarity to carry out crucial vectorial transport functions. Each cell in fully developed acini has three distinctive surfaces: apical directed towards lumen, basal that adheres to ECM, and lateral that adheres to neighboring cells. Work in Drosophila and other systems indicated that formation of these three surfaces depends on

particular groups of proteins that work in hierarchy (Lecuit and Wieschaus, 2002). These conserved protein complexes distribute asymmetrically in cells and promote the expansion of the membrane they are associated with. First, the Par complex (Par3/Par6/aPKC) defines the apical surface. Subsequently, downstream of Par complex, the Crumbs complex (Crumbs/Std1 also known as PALS1/PATJ) (Bilder *et al.*, 2003; Tepass, 2012) promotes further development of apical membrane. The Scribble complex (Scribble/DLG a discs large homolog/LGL a Lethal giant larvae) (Bilder *et al.*, 2000) plays role in establishing the basolateral identity.

Orientation of polarity

Formation of epithelial tissue requires cells to organize themselves in 3D into acini or tubules to enclose lumens. It is necessary that each single cell of this multicellular construct establishes the three surfaces. In 3D, as mentioned before, cells define and develop the apical surface that is directed towards the lumen. In the artificial environment of 2D culture, where cells are seeded on plastic flat surfaces, this orientation is provided and forced by the external cue that specifies the basal membrane. Moreover, intriguing questions remain without answer; what links stages of lumen formation and polarity establishment? Is lumen formation process dependent on polarity, or inverse? Can lumen exist without polarity? The distinction between polarization and its orientation has been studied in simple models of chemotactism, but has not been addressed in epithelial cell culture extensively yet. Though, it has been shown that the establishment of polarity can be separated from the orientation of that polarity (O'Brien *et al.*, 2002).

2.3.4 Tubulogenesis *in vitro*

The development of metazoan organs begins with a single epithelial layer. As has been described in chapter 2, epithelial cells form sheets or layer of cells which are characterized by tight connections between cells, maintained by various cell-cell junctions with particular importance of adherens junctions (Yap *et al.*, 1997). Such configuration along with established apico-basal polarity ensures that epithelial cells can only migrate within the epithelial-layer (along the basal surface) and not into an extracellular matrix (ECM). The presence of mesenchymal cells along with epithelial cells in early embryos has been observed for a long time, but the distinct program of the conversion of epithelial cells into mesenchymal cells has been introduced in 80s under the name “epithelial-to-mesenchymal” (EMT) transition (Greenburg and Hay, 1982; Greenburg and Hay, 1986). It is accepted that epithelial branching morphogenesis presents characteristic properties of EMT process described by migrative cells, which lose their polarity and cell-cell junctions. During embryonic development the EMT program has been observed for instance in mesoderm formation (Viebahn *et al.*, 1995), neural crest development (Duband and Thiery, 1987), and cardiac valve formation (Bolender and Markwald, 1979). Interestingly the EMT process can be reversible by mesenchymal-to-epithelial (MET) transition, for instance, in developing kidney (Davies, 1996). The resulting

cellular motility recognized in EMT presents common properties with carcinoma progression and metastasis except that these processes in general do not undergo MET as compared to development. Attributing EMT as a mechanism of metastasis is still controversial due to limitations of human tumors observation in time and space.

Despite, much has been discovered in the field of epithelial development and branching morphogenesis, little is known about *i)* what controls branching process initiation, *ii)* what is the role of the ECM, *iii)* how tubes are formed, *iv)* what controls their diameter and remodeling , and *v)* what are cues that control ending of the development program.

The ECM has long been recognized as providing morphogenetic signals during glandular tissue morphogenesis (Wicha *et al.*, 1980). For example, composition of ECM changes during morphogenesis of the gland and is different within the duct as compared to the terminal end buds (Silberstein and Daniel, 1982). Moreover, branching morphogenesis is dependent not only on the presence of the specific components of ECM but also on their amount (Silberstein *et al.*, 1990; Wicha *et al.*, 1980). Adhesion to the basal lamina controls, through integrin signaling, apical secretion, proliferation and apoptosis (Parry *et al.*, 1987). Invading cancers appear to reactivate pathways of development and, as observed, tissues that apply collective cell migration during morphogenesis will organize similarly during neoplastic progression (Christiansen and Rajasekaran, 2006; Friedl *et al.*, 2004). Therefore, better understanding of morphogenesis can lead to a progress in development of new cancer therapies. A major challenge today is to distinguish the relative contributions of specific genetic and microenvironmental changes during branching morphogenesis *in vivo* and *in vitro.*

The 3D MDCK system is to date the best characterized *in vitro* tubulogenesis model. MDCK cells in 3D culture on collagen I form polarized cysts (acini) but upon treatment with HGF (hepatocyte growth factor) they generate tubules (Pollack *et al.*, 1998). Process of tubule formation in this model can be described by following stages. First, some cells from the polarized cyst form long extensions (similar to pseudopodia) to the environment. Second, cells undergo division and subsequently migrate to the ECM to form “chains” of cells still connected to the initial cyst. At this stage, cells lose their apico-basal polarity. Moreover, cells at the end of the chain highly resemble form of migrating fibroblasts or mesenchymal cells (Yu *et al.*, 2003). After formation of a cellular chain, cells undergo further division to form cords which are 2-3 cells thick. The apico-basal polarity is re-established through formation of small lumens which further enlarge and merge to form a continuous lumen between the polarized cyst and tubule. These observations suggest that branching morphogenesis progresses through EMT process (O'Brien *et al.*, 2002), which is followed by the polarity re-establishment.

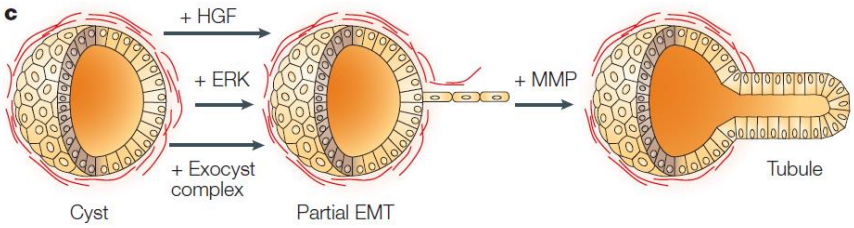

Figure 2-13 Hepatocyte growth factor (HGF) induces the formation of branched tubules in MDCK cells grown in collagen I gels

2.3.5 Loss of polarity in cancer

3D cultures provide a context in which cellular genes that induce phenotypic alteration can be identified and mechanism responsible for these phenotypic changes can be studied. Phenotypic alterations similar to those associated with tumor progression are reflected for instance, in cellular organization, proliferation, and apoptosis. Similarly as *in vivo*, a hallmark of most glandular epithelial tumors is the absence of a hollow lumen associated with the loss of polarity. To date, answer to questions on how cells generate lumens during morphogenesis and what mechanisms are used during tumorigenesis require further investigation. Studies in 3D cultures have defined a number of mechanisms and molecular regulators that contribute to these processes. Phenotypic changes include for example outgrowth of the structures, high affinity for aggregation, and transformation into spheroids (tumor-like solid aberrant masses) (Figure 2-14).

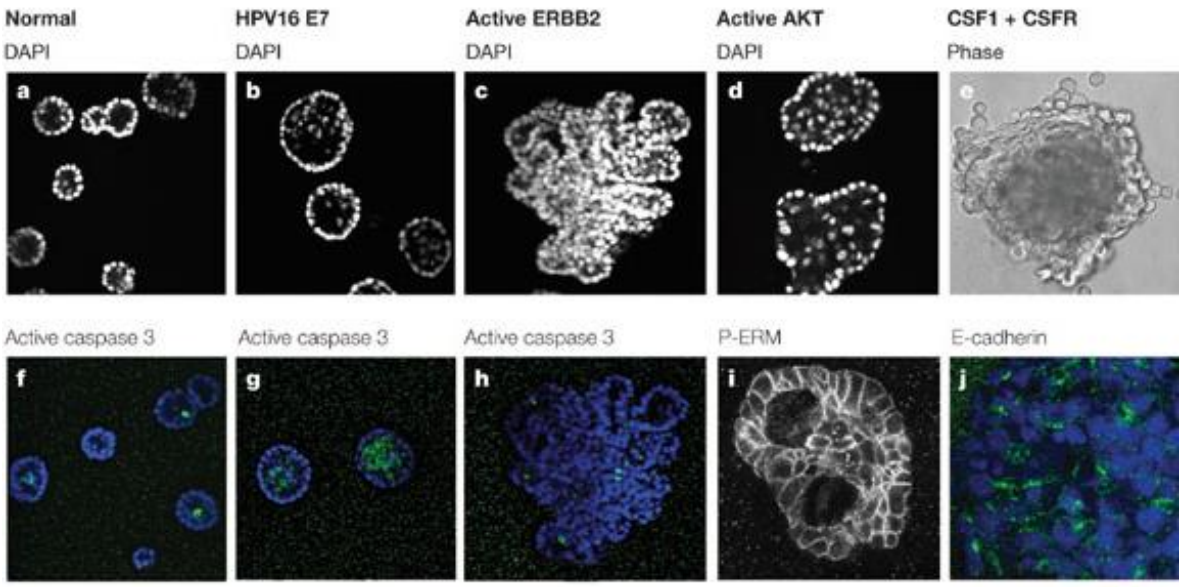

Figure 2-14 The examination of oncogenes and activated growth factor receptors in MCF-10A cells grown in 3D culture. Source: (Debnath and Brugge, 2005)

2.4 Limitations of current 3D approaches for screening approaches

Insofar as the relative formation of acini *versus* spheroids can be used as a cancer model, today researchers are blocked by technical limitations of Matrigel culture in identifying new oncogenes or biomarkers. These are related to analysis, which aims in discrimination between acini and spheroids. In details the limitations will be simply explained on the example of Figure 2-15.

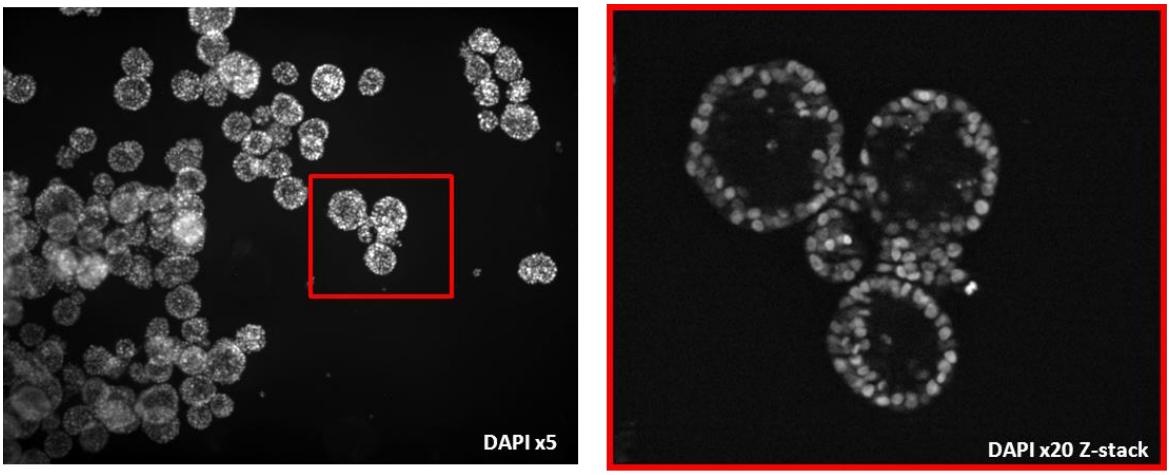

Figure 2-15 Growth of RWPE1 prostatic epithelial cells in Matrigel. Cells are stained with Hoechst to indicate nuclei. On the left an overview of the 3D culture with low magnification objective. Image on right presents higher magnification of the regions of interest (in the red frame) taken with Z-stack module. It reveals the presence of lumen.

- **Environmental limitations**

3D cell culture is based on using Matrigel or Collagen (in dependence of the cell line) to grow cells into acini. The gel itself constitutes a physical (and possibly a chemical) barrier that limits diffusion and thus prevents using standard laboratory techniques practiced daily on 2D cultures (e.g., limited efficiency in transfection has been observed in BIOMICS laboratory). Cells, when grown in Matrigel, are immobilized and are difficult to recover (for RNA or protein extraction) without interfering the 3D organization of acini or spheroids.

Furthermore, Matrigel and the protocol itself limit also the control over environment conditions. The distance between growing structures, the size of the environment, possible constraint and the rigidity cannot be controlled in standard 3D cell culture. Still, little is known how force can regulate the cell fate and tissue phenotype. Recent reports indicate the importance of mechanical cues by showing that cancer is associated with tissue stiffening (up to several kPa's). Unfortunately, Matrigel has a very limited range of rigidity (expressed in Pa)

and can be controlled only by the concentration of proteins, and thus its rigidity falls around 400 Pa when in undiluted form.

- **Analysis limitations**

Cells when seed are randomly positioned on the gel which results in merging or overlapping of the structures (Figure 2-15), which limits application of an automatized acquisition. Because the most important information is weather 3D structures contain lumen, which indicates the correct phenotype of acini, or form filled solid spheroids, it is necessary to perform labeling of cells and to use confocal microscopy to retrieve details of the cellular organization in 3D. Furthermore, for quantitative data analysis and hence statistical analysis, a large amount images of objects need to be collected which is further more difficult with the relatively small field of view of traditional microscopes. Similarly, small field of view during time-lapse microscopy combined with a Z-stack acquisition (4D) can be a limitation since rare events might not be detected. Such types of acquisitions are also time consuming, need human assistance and are difficult to be automated (properties of Z-acquisition need to be adjusted manually) due to the environmental limitation listed above. Therefore, available today analytical tools are not sufficiently powerful for high-throughput and high-content analysis. Additionally, the population of acini is heterogeneous and structures develop at different pace. Therefore, analysis of development stages can be hampered.

2.5 Conclusions

Studies on development, morphogenesis and carcinogenesis were performed for years on animal models, which only to some extent recapitulate physiology of humans. Because most human cancers arise from a highly organized and polarized epithelial tissue, new and relevant models are required to further study cues that initiate formation and metastasis of cancers. As well, in the general interest, is to identify new biomarkers for early diagnosis which in most cases promise a high rate of survival. Of particular is prostate cancer which to date lacks appropriate and non-invasive diagnostic tests. Recently used is a blood test of PSA marker that rises up the questions whether it is more beneficial or harmful due to the high false-negative and false-positive results.

A primary approach to study cellular processes is to culture cells *in vitro*. 3D epithelial cell culture recapitulates numerous features of epithelial glandular tissues *in vivo*, including development of acini with hollow lumen that form a basement membrane and maintain apico-basal polarity. Acini formation in 3D culture serves as a model to study morphogenesis, but also carcinogenesis by observation of proliferation of cells within the lumen which can be directly correlated with the first stage of cancer observed *in vivo*. Known cancer genes give changes in the phenotypes observed in 3D culture that resemble well the histopathology observed in cancers *in vivo*. Therefore, with the development of methods to knock-out particular genes of human genome (for example using siRNA approach or viral transfections) 3D cell culture can contribute to identification of new oncogenes.

However, epithelial 3D cell culture in Matrigel raises difficulties in performing studies with a high throughput analysis. These are associated with the limitation of confocal microscopy, including time-consuming acquisitions, need for human assistance and small field of view. Development of new approach for high-throughput and high-content analysis promises to bring new insights in *in vitro* epithelial development and carcinogenesis.

3. Thesis objectives

This thesis aims to find the technological improvement for 3D cell culture. There are two main areas of particular interest that in future can bring more fundamental information about epithelial development and carcinogenesis.

The main two questions are as follows:

1) How to bring high-throughput and high-content analysis into the 3D cell culture?

Since filling up of lumen of acinar structures is a hallmark of cancer, *in vitro* studies are based on manipulation of genes and environmental cues in order to determine factors responsible for the transformation of acini into spheroids. Therefore, a high-throughput preparation and analysis of 3D culture is required to perform those studies efficiently.

Chapter 5 introduces droplet microfluidic systems used for cell encapsulation in a controlled Matrigel environment. This approach allows using high-throughput flow-based methods (large-particle Fluorescently Activated Cell Sorter) to study phenotypes in 3D culture. The analysis is based on the detection of fluorescent markers which can serve to determine the phenotypic alterations (proliferation, apoptosis, differentiation etc.).

In order to go further in 3D analysis and to determine presence of lumen within the structures without need for labeling, lens free imaging systems were applied to 3D epithelial cell culture (collaboration with Dr. Cedric Allier, CEA-Leci). **Chapter 7.2** presents development of the lens-free imaging system for automatic high-throughput imagining and analysis of population of acini and spheroid within the 3D epithelial cell culture. Furthermore, these lens free imaging systems have been successfully used for time-lapse observation (**Chapter 7.3**). With the advantageous large field of view a rare dynamic phenotypes were detected.

2) How to bring higher control over the environment?

Requirements for higher control over environment include i) control over cell number, ii) spatial constraint by controlling the shape and the size of the environment, and iii) control over rigidity of the environment.

The fine control provided by the microfluidics approach makes it possible to regulate both the microenvironment and bead size such that morphogenetic analysis at the single cell level can be applied with greater reproducibility than has been previously possible in standard 3D culture systems. Since the formation of acini can proceed through two different mechanisms (hollowing or cavitation), encapsulation of a single cell per bead leads to a homogenous acini formation. Furthermore, microfluidic technology described in **Chapter 5**, allows isolating a single bead with a single cell to show that an acinus can be initiated without signals from neighboring cells.

Chapter 6 presents the development of a microfluidic circular-shape channels fabrication process in order to observe tubule-like organization of epithelial cells within these channels. These results served as a preliminary concept for the on-chip analysis of epithelial secretions.

Additionally, a change in the composition of the Matrigel has been observed upon modification of the standard 3D cell culture protocol. A heterogeneous transfer of proteins from Matrigel into solution has been observed. Alteration of the environment cause repeatable occurrence of branching-like process of normally non-migrative epithelial cells. Results on the effect of the Matrigel composition on the epithelial phenotype are presented in **Chapter 7.3**.

Preliminary results on the control of the rigidity of the environment are presented in **Chapter 9.1** (Supplementary results).

4. Implementation and optimization of prostate 3D cell culture

As described in the introduction, various epithelial cells types when cultured in Matrigel recapitulate their form and function in 3D culture. This chapter describes culture requirements of the model RWPE1 cells, which undergo acinar morphogenesis when culture on Matrigel. The aim of these experiments was to determine conditions upon which a homogenous culture of acini was obtained. My work relied on implementation and optimization of RWPE1 cell culture in Matrigel environment by *i)* establishing a protocol of Matrigel deposition, *ii)* studying influence of Matrigel concentration and culture media composition on development, and *iii)* characterizing growth and assessment of acini polarity.

Key findings

- RWPE-1 Prostate epithelial cells form acini when cultured in Matrigel
- RWPE-1 3D culture does not show growth-arrest
- Development of an acinus is highly dynamic process
- Structures at early stages development (day 0-day 3) are not polarized
- Only top-coat protocol induces polarized acini
- Development of acini follows both types of mechanisms; cavitation and hollowing

4.1 Introduction

In vitro epithelial cell models have provided valuable insights into development and tissue homeostasis. Among numerous non-transformed cells lines which undergo acinar morphogenesis, two have received much attention. The breast epithelial cell line MCF10-A when grown in Matrigel serves to recapitulate some aspects of mammary morphogenesis *in vivo*. It has been used to understand the mechanism of lumen formation based on cavitation (Debnath *et al.*, 2002) or to understand the purpose of dynamic rotational movement during acinus formation (Wang *et al.*, 2013). The second MDCK (Madin-Darby canine kidney) cell line, has been broadly used to study polarity, membrane trafficking and cell adhesion, but most of all it serves as a model of tubulogenesis and branching upon stimulation with HGF (hepatocyte growth factor) (Zegers *et al.*, 2003). There are similarities between these two models but there are also differences. One of many, but very important, is the difference in the extracellular matrix that is used to cultivate cells. MCF10-A grow successfully in laminin-rich Matrigel cultures, while MDCK cells are cultured within the collagen-1 matrices, which suggests different type of ECM-cell signaling for these two cell lines.

3D epithelial cell culture of prostatic cells received much less attention in literature. The reason might be a result of important difficulties to establish prostatic cell lines (van Bokhoven *et al.*, 2003). Currently various cell lines exist which differ considerably in the 2D and 3D phenotype and the level of malignancy and the site of the metastasis (Harma *et al.*, 2010). For fundamental research on cancer formation in prostate, three *in vitro* model cell lines were used extensively: i) LnCap, androgen responsive cells, from the lymph node metastasis (Horoszewicz *et al.*, 1983), ii) DU-145, insensitive for hormone stimulation, from the brain metastasis (Stone *et al.*, 1978), and iii) PC3, initiated from a bone metastasis of a grade IV prostatic adenocarcinoma (Kaighn *et al.*, 1979). Interestingly, some of the cancerous cell lines when plated in 3D culture recapitulate the proper organization and expression of specific luminal markers (Harma *et al.*, 2010). Such unexpected phenotype in 3D culture on Matrigel shows how important is the context, the environment that directly influences the phenotype.

In 1991, another prostate immortalized cell line has been introduced under the name RWPE-1 (Bello *et al.*, 1997; Webber *et al.*, 1997). RWPE1 were immortalized with Human Papilloma Virus (HPV) in order to retain growth and differentiation of characteristic for their normal cells of origin. As a cell line, it presents characteristic for luminal cells markers of cytokeratin 8 and 18. Furthermore, when plated in 3D culture, they form acinar structures enclosing lumen. RWPE1 cells are interesting as a model to study development and eventually transformation into cancer upon genetic alterations due to the androgen responsiveness and PSA secretion (Bello *et al.*, 1997). In parallel, a family of RWPE1-originated cell line has been created. RWPE2 cells which are the result of transformation of RWPE1 with vi-K-Ras, were developed to obtain malignant characteristics. Later RWPE1 derivatives with the increasing

properties of invasiveness were created (WPE-NA22, WPE-NB14, WPE-NB11, and WPE-NB26). Availability of prostatic cell lines with normal phenotypes and as a reference cancerous phenotypes can serve to study changes in gene expression upon environment alteration or various treatments.

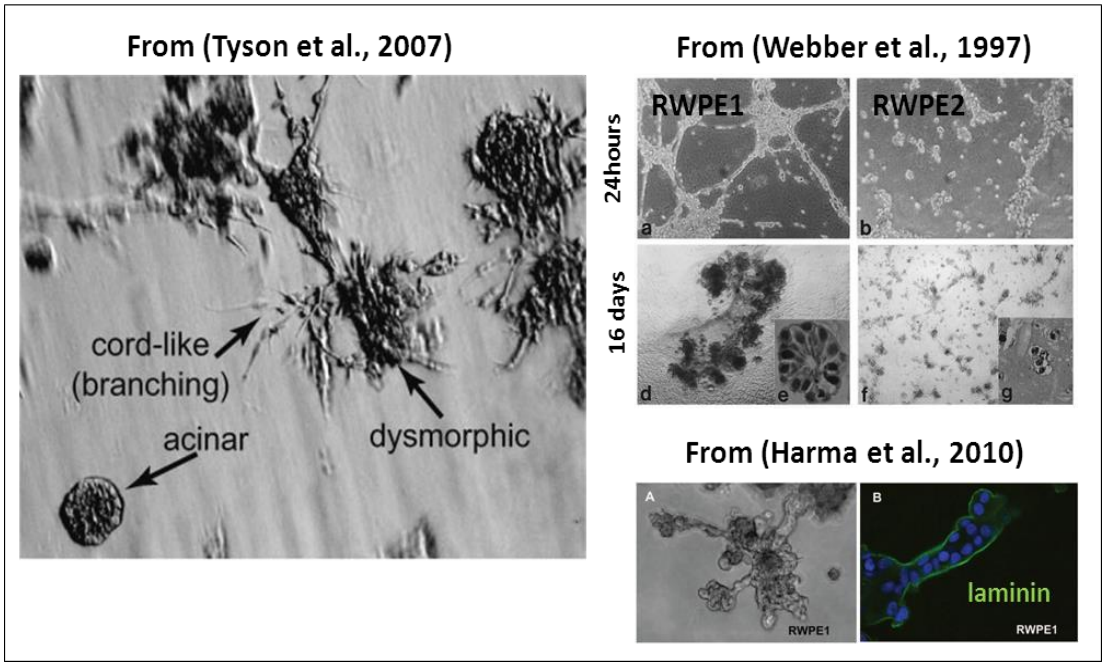

Figure 4-1 The organization of RWPE1 cells grown in 3D culture in Matrigel indicates the heterogeneity of phenotypes. Source: modified from reports indicated within the Figure

In this study we have used RWPE1 cells to observe acinar development. However, available protocols presented complex 3D phenotype of acini associated with branches or amorphous structures (Bello *et al.*, 1997; Harma *et al.*, 2010; Tyson *et al.*, 2007). Often, the differences in media composition were striking including presence/absence of serum or diluted Matrigel in the culture medium. Those differences have directly input on the morphology of 3D structures in 3D.

I have tested various protocols in order to stabilize the 3D cell culture conditions to obtain a robust protocol in Biomics laboratory. My aim was to clearly control culture conditions promoting either single acini or branched-structures. Assays on lumen formation and subsequent immunostaining were performed to reveal presence of basal, apical and baso-lateral membrane.

4.2 Results

4.2.1 Optimization of culture media composition

According to existing reports RWPE1 cells are routinely cultured in KSFM culture medium. It is a culture medium from Life Technologies that has been prepared specially to cultivate keratinocytes and epithelial cells. Within the kit, two additional components are supplied; epidermal growth factor (EGF) and Bovine Pituitary Extract (BPE). While the function in culture of recombinant human EGF is well known, the exact composition of BPE remains indefinite. Additionally, for other epithelial 3D models culture medium is supplemented with a diluted Matrigel (a top-coat layer in range of 2%v/v to 10% v/v) and fatal bovine serum. Therefore, following parameters were optimized for RWPE1 cells in 3D culture:

- Matrigel concentration – diluted or not diluted – has been varied after discussion with Dr. Bello-DeOccampo who suggested advantageous diluting Matrigel layer
- Presence/absence of the top-coat layer
- Culture medium composition
- Concentration of cells per cm^2
- *Top-coat* protocol/ embedded protocol

The starting conditions were retrieved from the report that introduced RWPE-1 cell line. Limiting the number of factors in 3D culture can be beneficial due to the high complexity of the environment. Therefore, initial experiments discriminated i) importance of the concentration of Matrigel in the bottom layer (the more concentrated the more rigid), and ii) the cell seeding concentration.

- **Influence on Matrigel concentration**

Cells on the non-diluted Matrigel formed branching and occasionally spherical structures, despite the cell seeding number (Figure 4-2A). Dilution of Matrigel to 6 mg/ml favored spherical organization of cells and branching was rare (Figure 4-2B). Presence of diluted Matrigel in the culture medium had a spectacular influence on the formation of acini with a well visible lumen (even with phase contrast microscopy). With the 10% Matrigel (0,9 mg/ml of Matrigel) in top-coat medium 3D structures grew into well organized and spherical acini (Figure 4-2C).

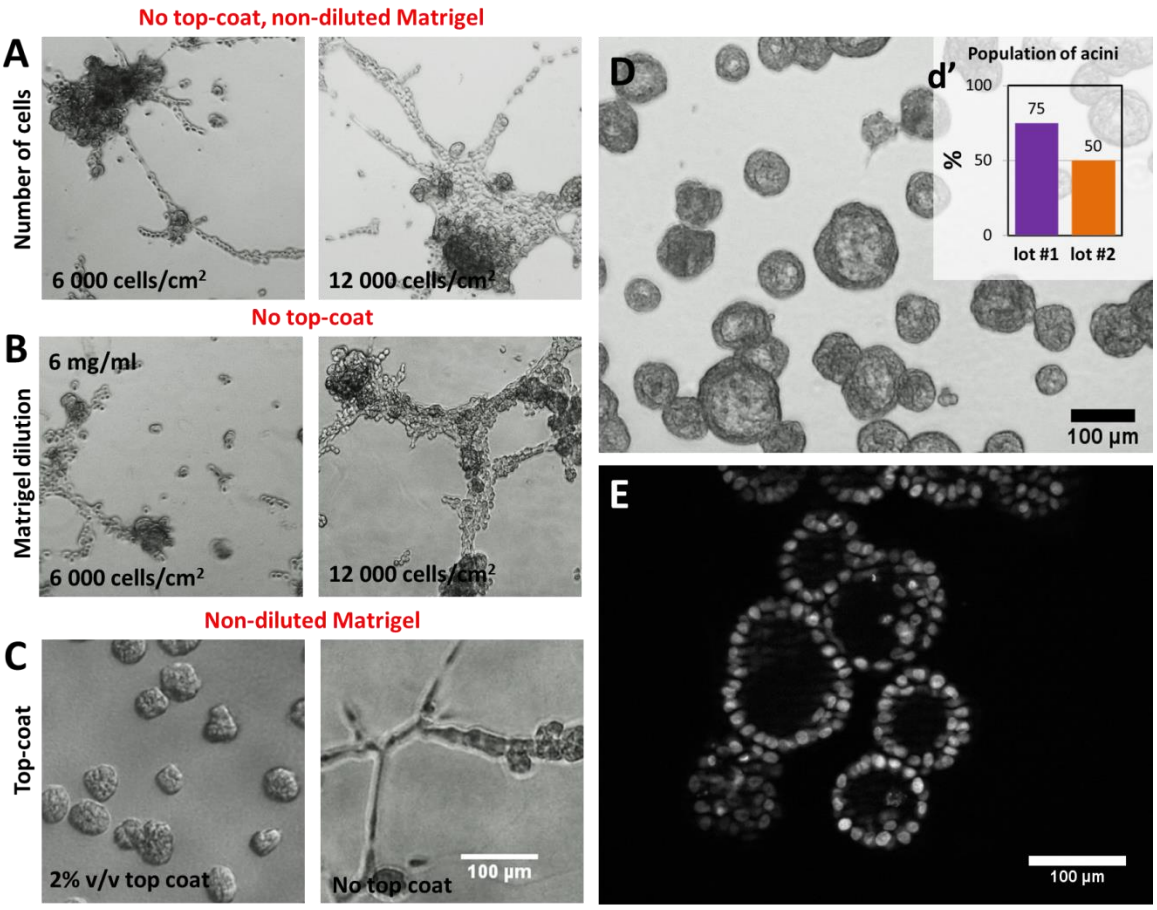

Figure 4-2 Optimization of cell culture conditions of RWPE1 cells in 3D culture. Various parameters including presence of top-coat, dilution of matrigel and culture medium composition were optimized.
(**A**) Fixed parameters: No top-coat, non-diluted Matrigel (9 mg/ml), KSFM with 2% FBS, 50 ng/ml EGF; Observed parameters: cell seeding number. Upon these conditions cells created aggregates with frequent branching despite the cell seeding concentration.
(**B**) Fixed parameters: No top-coat, diluted Matrigel (6 mg/ml), KSFM with 2% FBS, 50 ng/ml EGF; Observed parameters: Matrigel dilution. Upon these conditions cell continued to form aggregates with frequent branching.
(**C**) Fixed parameters: non-diluted Matrigel (9 mg/ml), KSFM with 2% FBS, 50 ng/ml EGF; Observed parameters: presence of top-coat (2%, ~0,2 mg/ml). A crucial factor was the presence of the diluted matrigel in the culture medium. As the result of the optimization a top-coat protocol of 10% matrigel v/v (0,9 mg/ml of Matrigel), 50ng/ml EGF and 2% v/v fatal bovine serum were used for the successful 3D culture (**D** and **E**). **d'** presents % of acini within the 3D cell culture with two different lots of Matrigel. Population of acini has been calculated on 30 structures (of diameter ~100 µm) per each condition.

- **Influence of culture medium components**

The composition of culture medium, including EGF and BPE which are supplied within the KSFM kit was examined. Taking into consideration other reports on RWPE1 cells (Bello *et al.*, 1997; Tyson *et al.*, 2007), and well established protocols for MCF10-A cells, BPE has been replaced by 2% serum in the culture medium and the concentration of EGF was adjusted at 50 ng/ml. Afterwards, the concentration of matrigel in culture medium has been increased to 10% (~ 0,9 mg/ml) due to more stable top-coat layer that otherwise has the tendency to be removed

during the culture medium exchange. According to these conditions, developed 3D structures presented lumen and round shape as visible by phase contrast microscopy (Figure 4-2D 7 days). Lumen formation is clearly indicated by the organization of nuclei as visualized by confocal microscopy (Figure 4-2E). Depending on the lot of the Matrigel, established protocol gives in average ~62% of structures containing lumen (Figure 4-2d').

- **Influence of cell seeding density**

In the initial tested conditions the difference resulting from the cell seeding concentration was negligible. However, with the elaborated protocol in the final conditions the initial number of cells had influence on the later output of the culture; if concentration was insufficient (1500 cells/cm^2) cells grew slowly and in contrary with the high cell concentration (12 000 cells/cm^2) lumen formation has been observed earlier than in the optimized conditions of 6000 cells/cm^2 (Figure 4-3). Additionally, with the high concentration of cells it is necessary to consider the risk of structures overlapping and merging which in result hinders microscopic acquisitions and analysis.

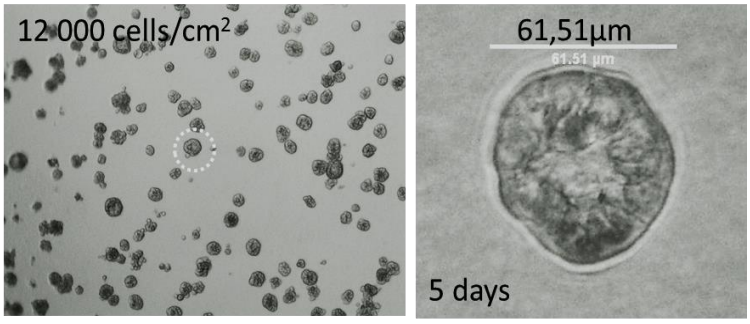

Figure 4-3 Influence of the cell seeding number of on the time of the lumen formation. Cells were cultivated under top-coat conditions (0,9 mg/ml in culture medium) with KSFM medium containing EGF (50 ng/ml) and FBS (2% v/v) conditions. The concentration of Matrigel layer was 9 mg/ml. In standard condition cell seeding number has been set to 6000 cell/cm^2 to limit structures' overlapping and margining.

- ***Top-coat versus* embedded**

As has been mentioned in the introductory chapter two strategies to cultivate cells in 3D exist. *Top-coat* protocol is simple in preparation and seeded cells grow on the same plane of the Matrigel layer. Such strategy facilitates observation and microscopic acquisitions, however, in this orientation cells sense anisotropic conditions which can influence establishment of the apico-basal polarity. On the other hand, embedded protocol provides homogenous conditions, as cells grow within the gel, but the preparation and further analysis is more difficult.

Both protocols were used to culture RWPE1 cells. The top-coat protocol was executed as described above and two conditions for embedded protocol were tested (diluted to 6 mg/ml and non-diluted at 9 mg/ml). Due to the much increased number of cells per well when compared

with top-coat protocol, the frequency of exchange of culture media had to be increased (each day instead of each 2nd day) otherwise cells have much lower rate of growth than expected (Figure 4-4A). After optimization of culture media supply (Figure 4-4C, Figure 4-4D) structures grew more rapidly and became bigger when embedded in diluted Matrigel. The average size of cells grown in 9 mg/ml Matrigel is 81.32 µm and 109.9 µm in 6 mg/ml Matrigel. These results follow the logic that more compliant matrices are easier to be transformed by growing cells.

Due to the difficulties in preparation and analysis of embedded cells, a *top-coat* protocol was chosen to optimize and observe morphogenesis and development of prostatic acini on the example of RWPE1 cell model.

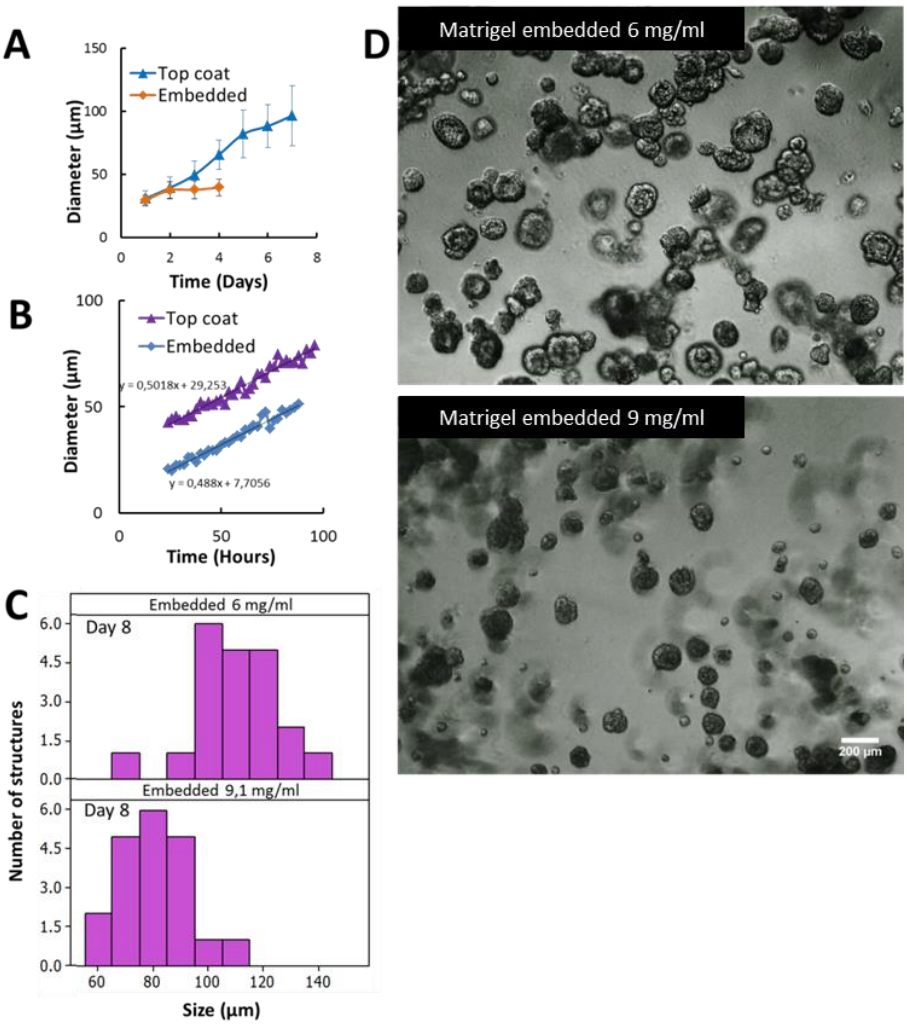

Figure 4-4 Growth of 3D structures according to embedded and top-coat protocol. A) Rate of growth during 7 days with equal frequency (every 2nd day) of culture medium refreshment. Embedded culture requires change of culture media every day otherwise, the culture does not proceed. **B**) rate of growth measured at the beginning of the acini formation for embedded and *top-coat* culture shows alike rate of growth in both cases. **C)** Influence of the matrigel concentration on the average size of structures grown in embedded conditions. Two concentrations were tested 6mg/ml and 9 mg/ml). **D**) Phase contrast microscopy of embedded structures grown in matrigel of varied concentration.

4.2.2 Rate of growth and lumen formation

Ideally, the development of an acinus *in vitro* covers initial stage of proliferation, followed by polarization of cells and subsequent apoptosis of luminal cells and finishes by differentiation. In other words after acinus formation cells exit cell cycle into G0 phase and do not proliferate any more. In reality immortalized cell lines can obey this rule and even though they form lumen, it does not indicate the differentiation. The indirect way to observe the stability is to measure in time size of growing acini.

As has been shown in point 1.2.1, embedded conditions limit the growth of 3D structures compared to *top-coat* protocol. Figure 4-4B presents results of time-lapsee microscopy that started 20 hours after seeding cells in 3D culture. Diameter was evaluated at each time point. Rate of growth was comparable which is indicated by the linear trendline (for *top-coat* 0,51 and 0,48 for embedded) however, the starting point for both structures is different and might result from more important constraint in embedded conditions that delay the first cellular division.

Growth of acini was observed over 17 days with phase contrast techniques so that to have the high field of view to compare numerous structures at once. For each day around 25-30 pictures were taken and combined together into an image (Figure 4-5). Because RWPE1 form lumen around day 7, if the structures stabilized it would happen within the chosen period of observation. However, in majority of cases, acini (even with a visible lumen) continued to grow while only few have stabilized in size (Figure 4-6). Stabilized structures had an average size of 83 µm while other grew up to 230 µm. Non-linear growth can be explained by the refreshment of culture media each 2nd day. Also, a tendency of structures to overlap or merge in the later stages of culture has been observed. Because the size of structures changes visibly, high viability of culture can be assumed over a period of 17 days.

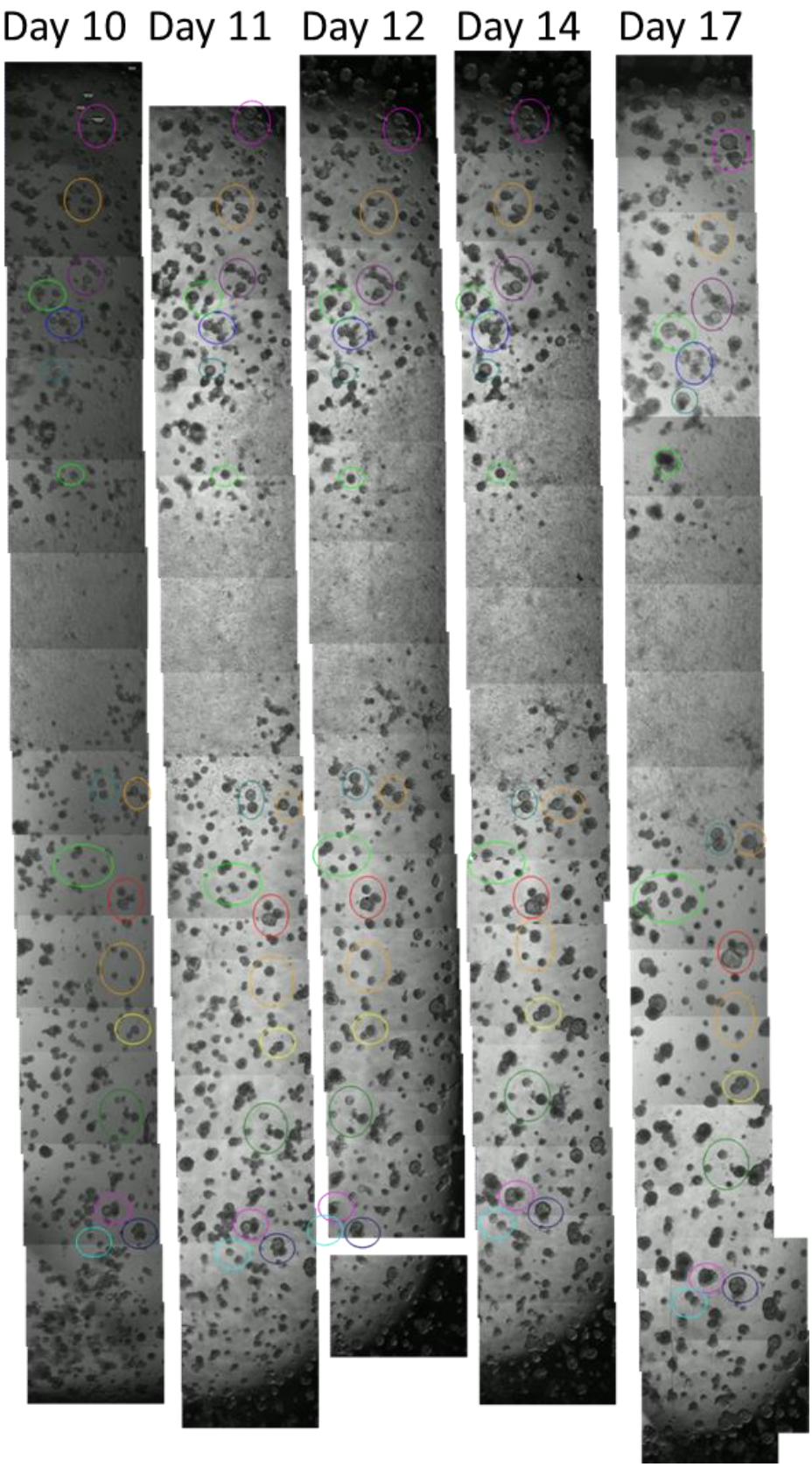

Figure 4-5 Large-field long-term observation of growth of 3D structures in top-coat conditions. In colorous circles structures that were recognized and analyzed.

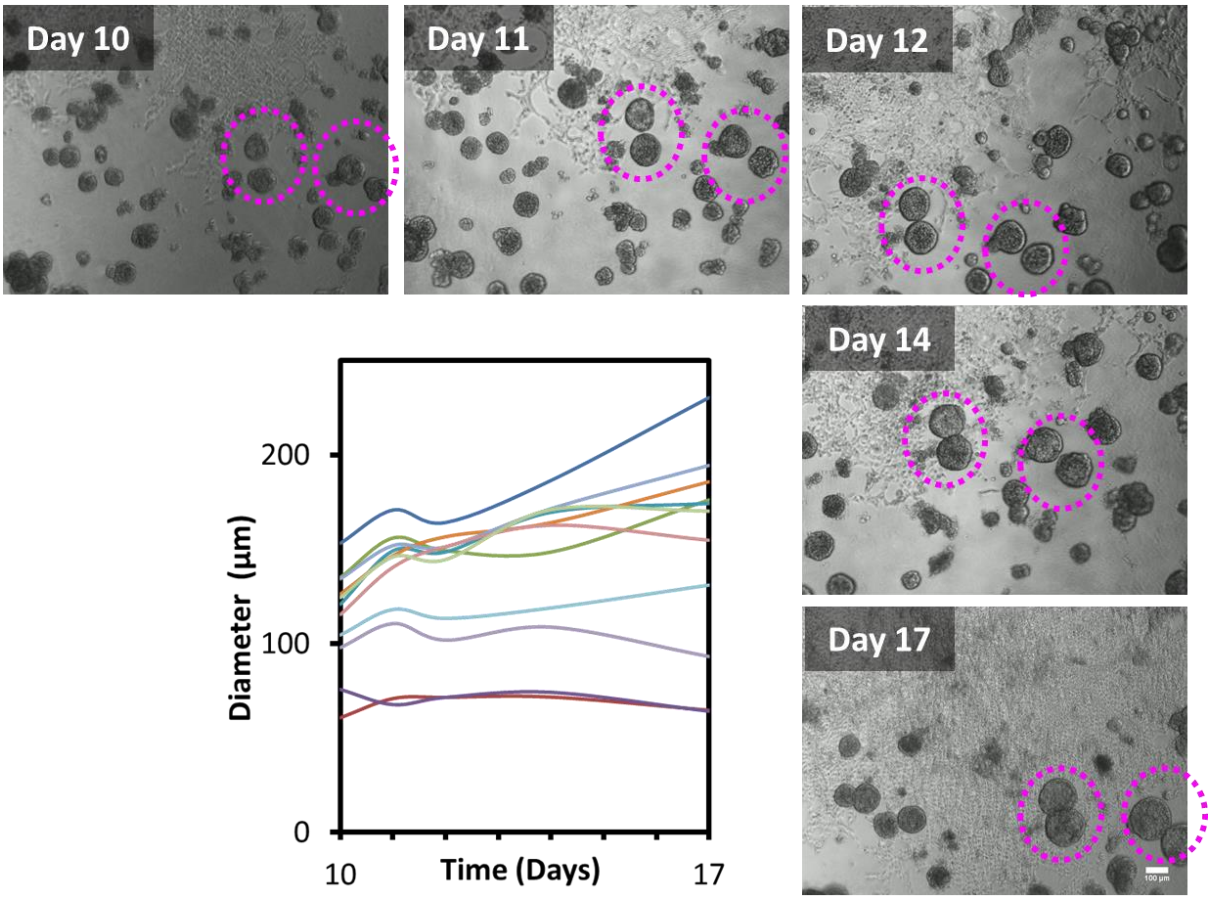

Figure 4-6 Analysis of the growth of structures between 10 and 17 days. Phase contrast images visualize a small region of the total field observed presented in Figure 3-5. Circles show analyzed structures. Graph presents the change of diameter in time for various acini indicating the heterogeneity of the culture. Scale bar 100 µm.

4.2.3 Dynamic phenotype – rotational movement

The growth and formation of an acinus is a highly dynamic process. With the first division cells undergo rotational and coherent movement around their axis (Figure 4-7). The direction of rotation changes and is random. The effect of rotation has been observed in tissue development in Drosophila (Viktorinova and Dahmann, 2013), but also in breast epithelial cells. Forming acini continue to rotate and in case of MCF10A cells (breast epithelial cell line) they stop after around ~5 days (Wang *et al.*, 2013) while RWPE1 after ~8 days. The general role of the rotation for acini formation has been discovered and covers the importance of ECM deposition around the forming structures (Wang *et al.*, 2013). Although stop of rotation can be associated with differentiation, it has been observed for RWPE1 cells that rotational arrest is temporal and lasts in average 20 hours and is followed by contraction in size and continuation in rotation (Figure 4-8). Such behavior has been verified for both protocols (embedded and *top-coat*) and the mechanism behind it remains unknown.

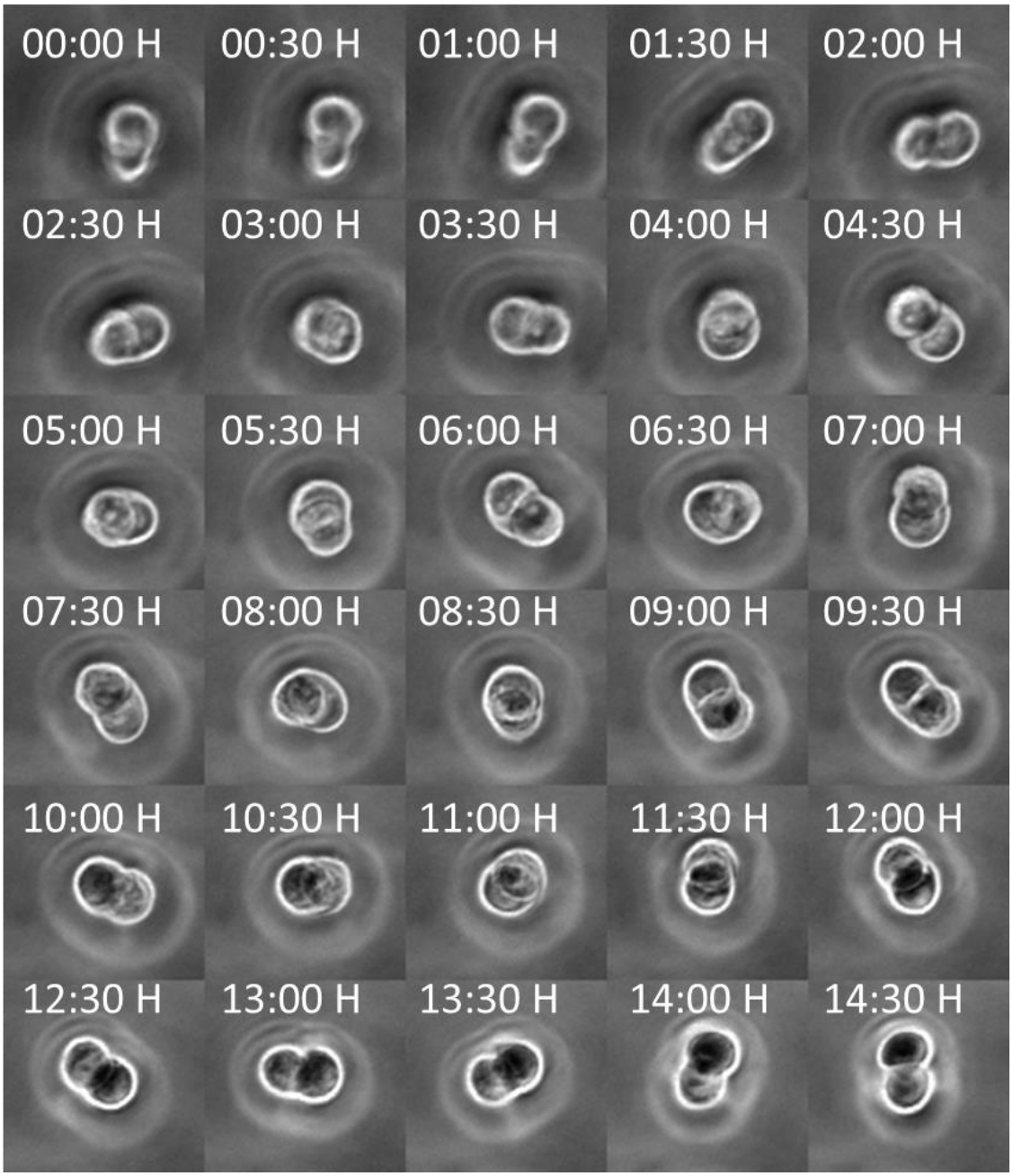

Figure 4-7 Visualization of the rotation movement associated with the growth and formation of an acinus. Here, in order to facilitate the observation, rotational movement has been shown on the example of 2-cells after the first division in the 3D culture, during 14.5 hours.

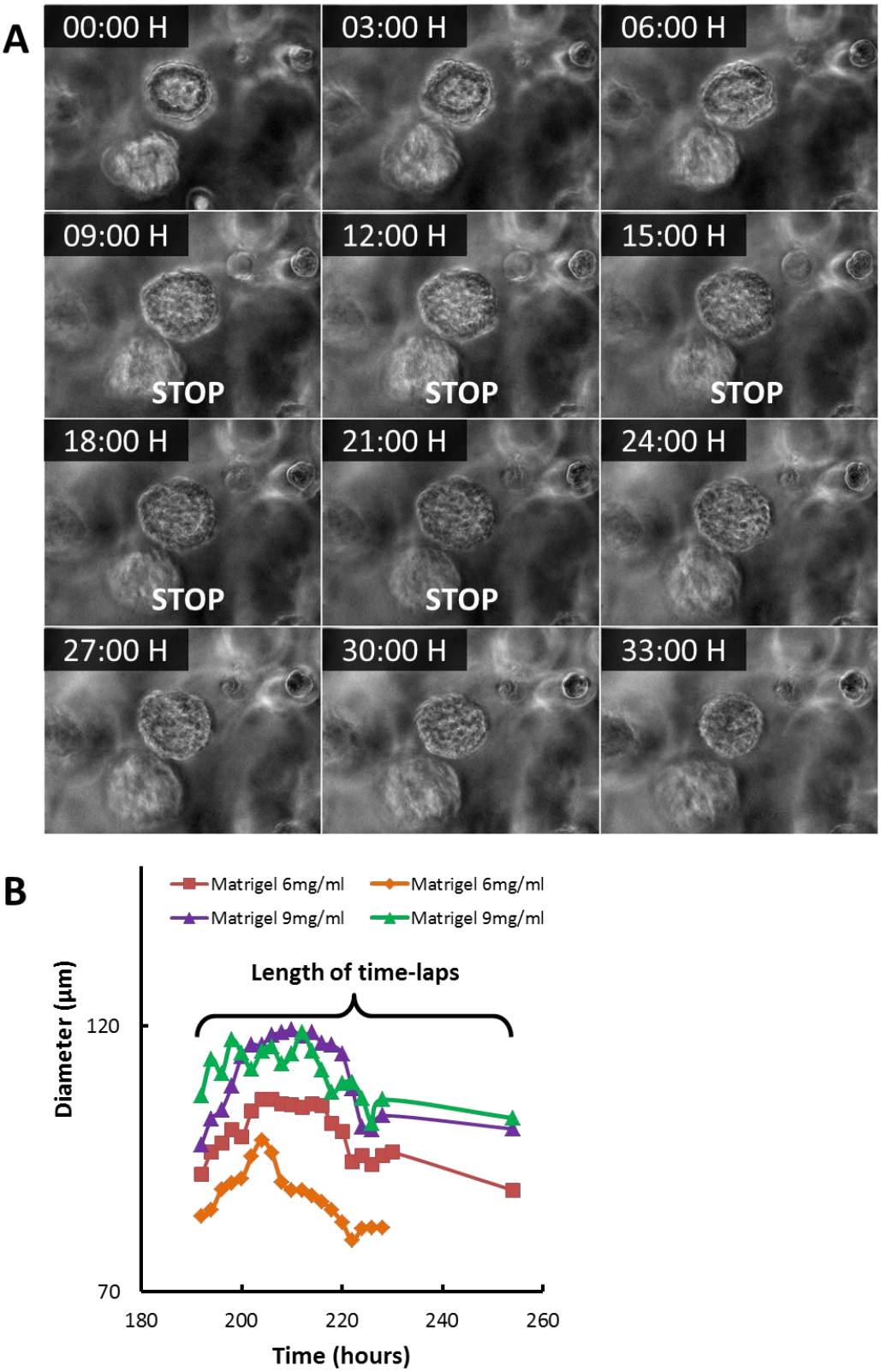

Figure 4-8 Rotational movement at the late stage of the acinus formation. A) Sequence of images of time-lapse acquisition of an acinus with a visible lumen. Images marked with STOP show the time at which acini stopped rotation and rest intact. Time scale presents the length of the time-lapse acquisition. **B)** Analysis of growth during the period of "STOP rotation" indicating that proliferation has been arrested for in average 20 hours. Time-scale represents the total time of culture not the length of the time-lapse.

4.2.4 RWPE1 form polarized acini

The protocol for immunofluorescence has been established for 3D culture and representative markers of apical, lateral, and basal membrane were chosen. The results of this part of immunostaining and microscopic analysis optimization are described in Materials and Methods. The basal membrane, which is in the direct contact with the extracellular matrix, is visualized by integrin staining. These surface protein play crucial role in the proper acini formation and homeostasis (Park *et al.*, 2006). Lateral surface has been stained with E-cadherin, a protein which is highly present in adherent junctions (see Chapter 2.1). Apical membrane has been indirectly indicated by the position of the Golgi-apparatus which in the properly polarized acini is position towards lumen. Formation of lumen has been visualized by the use of caspase-3 marker that stains apoptotic cells. Figure 4-9 presents the representative markers that delineate the three surfaces.

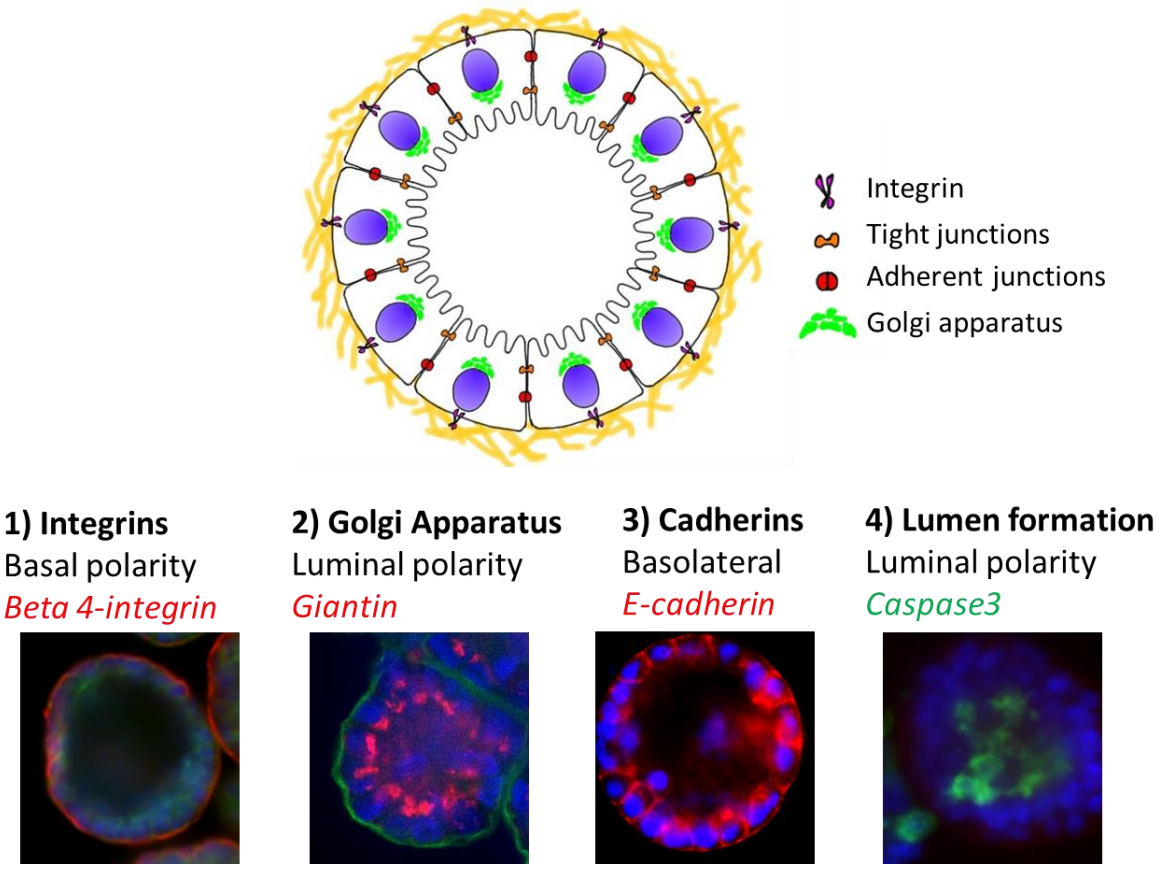

Figure 4-9 Visualization of polarity in acini of RWPE1 prostatic epithelial cells. Average diameter of RWPE1 acini is ~100-120 µm.

Acinus is defined by the presence of lumen but also by established apico-basal polarity described in chapter 1. Acini of RWPE1 cells are formed within 7-9 days through clonal division and lumen is formed by apoptosis of inner cells around day 5 (Figure 4-10A). However, with the high resolution microscopy it has been possible to observe the formation of lumen in the acini

as early as after 4 days (Figure 4-10B) by the mechanism that did not originate from apoptosis. Conversely, it is visible that polarized peripheral cells move away to open up small lumen, which has been proposed as another possible mechanism for lumen formation (Tanner *et al.*, 2012). Therefore, two mechanisms were observed for lumen formation by RWPE1 cell model.

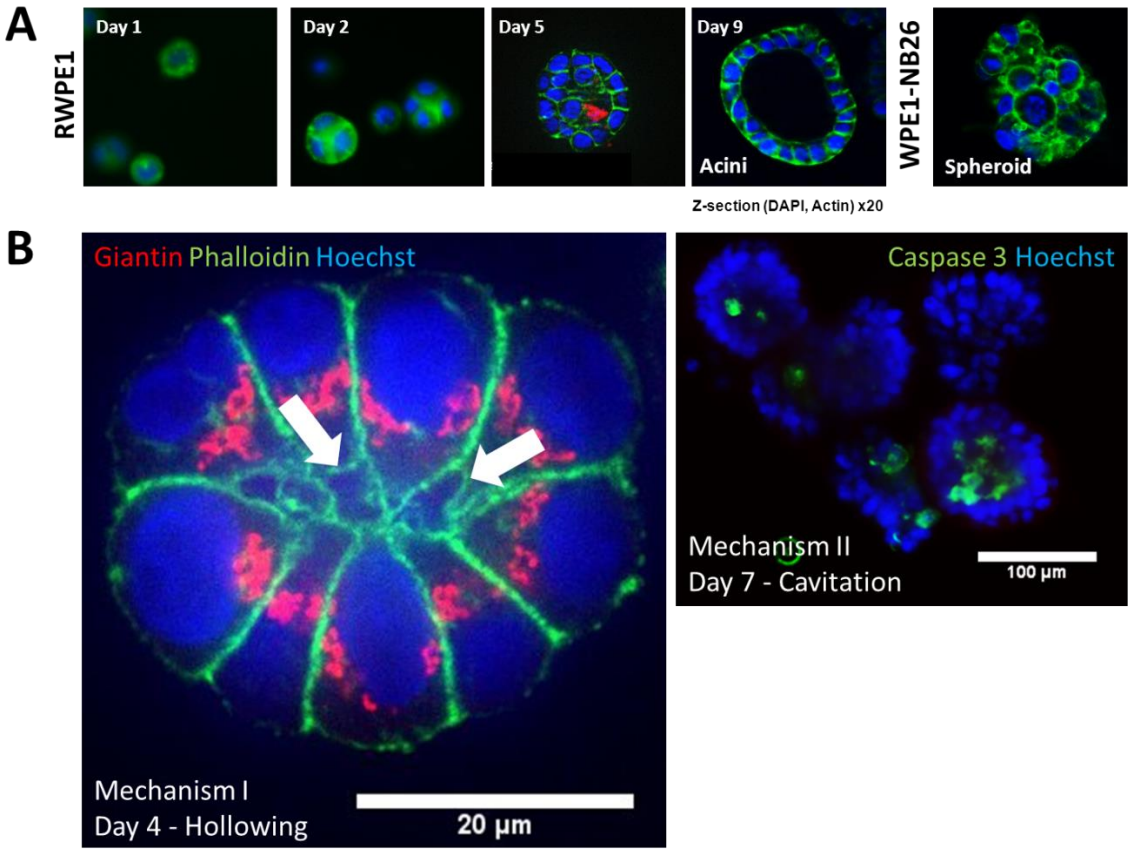

Figure 4-10 Formation of an acinus as visualized by fluorescent microscopy. A) Phalloidin that delineated the cellular membrane is a marker for F-actin and nuclei in blue were stained with Hoechst. At day 5 the apoptotic inner cells were stained with caspase -3 in red. To illustrate the difference in cellular organization also spheroid, aberrant solid cellular mass is presented. **B)** On the left, zoom of the RWPE1 structure grown for 4 days in *top-coat* conditions. Arrows indicate lumen opening by hollowing mechanism. On the right, group of RWPE1 acini on day 7 that form lumen by cavitation (apoptosis). Golgi apparatus has been stained to indicate the apical membrane polarity (anti-giantin in red). Scale bar 20 µm and 100 µm respectively.

Polarity is established in the later stage of acini growth

The process of establishment of the polarity of RWPE1 cells has not been described, it has been only presented that these cells form polarized acini with lumen. It is expected by comparison to other 3D epithelial models that polarity is established in the moment of the first division and maintained in later stages of development. In order to observe the formation of an apical surface 4 plates of 3D culture were launched simultaneously to be fixed and stained after 4 days, 6 days, 8 days, and 10 days. These time points were chosen as day 4 should bring structures before they start to form lumen, day 6 is the time of the lumen formation, and day 8

and day 10 should be associated with polarized acini with distinct lumen that maintain their structure.

Interestingly, cells presented in majority cases a proper apical polarity and the beginning of lumen formation already at day 4 (Figure 4-11). At day 6 the lumen is established and polarity maintained. In some cases, the Golgi-apparatus ribbon is broken and stays on both sides of the nucleus as indicated by the arrow. This unexpected positioning of the Golgi apparatus is rather rare at this stage of the culture. However, after day 8 even though the lumen is present, there is a loss of the apical polarity presented by dispersed Golgi-apparatus or by its inversed position.

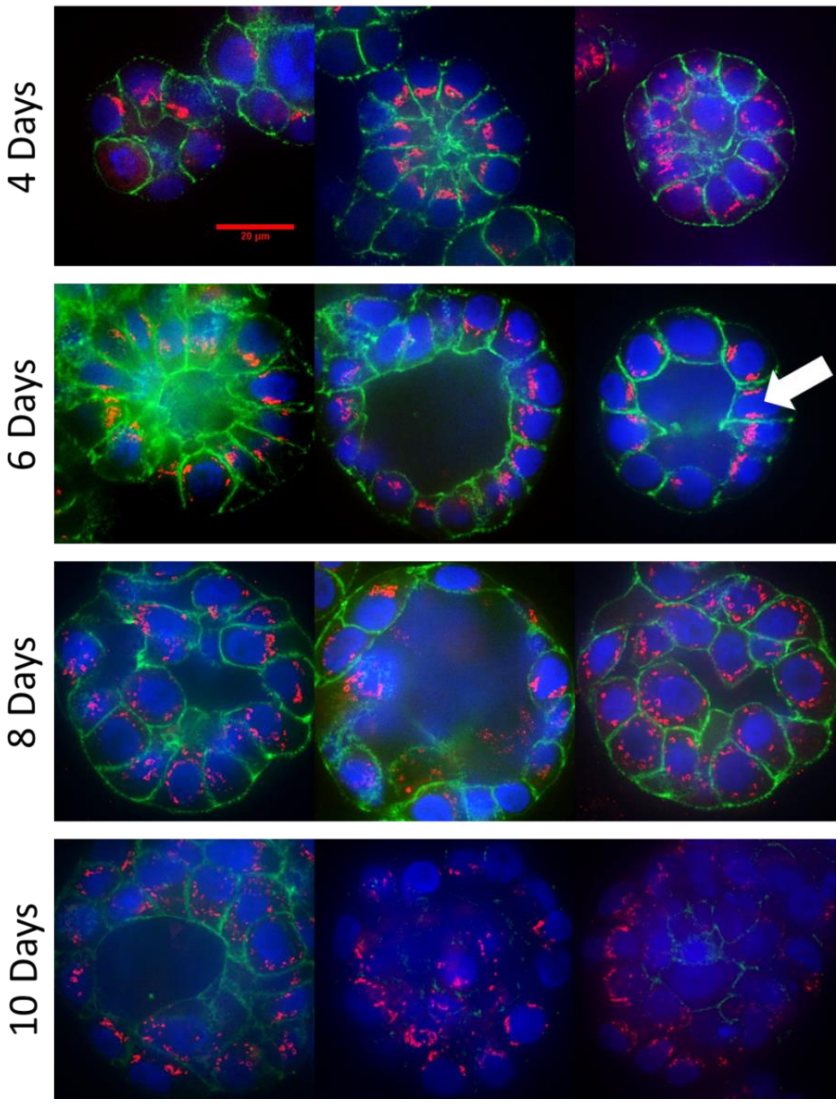

Figure 4-11 RWPE1 acini growth and polarity in development visualized by position of Golgi-apparatus (red, anti-giantin) and F-actin (green, Phalloidin) at day 4, 6, 8 and 10. Nuclei are stained with blue (Hoechst). Scale bar for all images 20 µm.

To further observe the development of RWPE1 acinus it has been verified if the polarity is maintained at the very early stage. Because it has been shown that the polarity can be more

promoted by top-coat protocol due to the anisotropic conditions of the environment which gives a strong cue to orient the polarity (Zegers *et al.*, 2003), both protocol were compared.

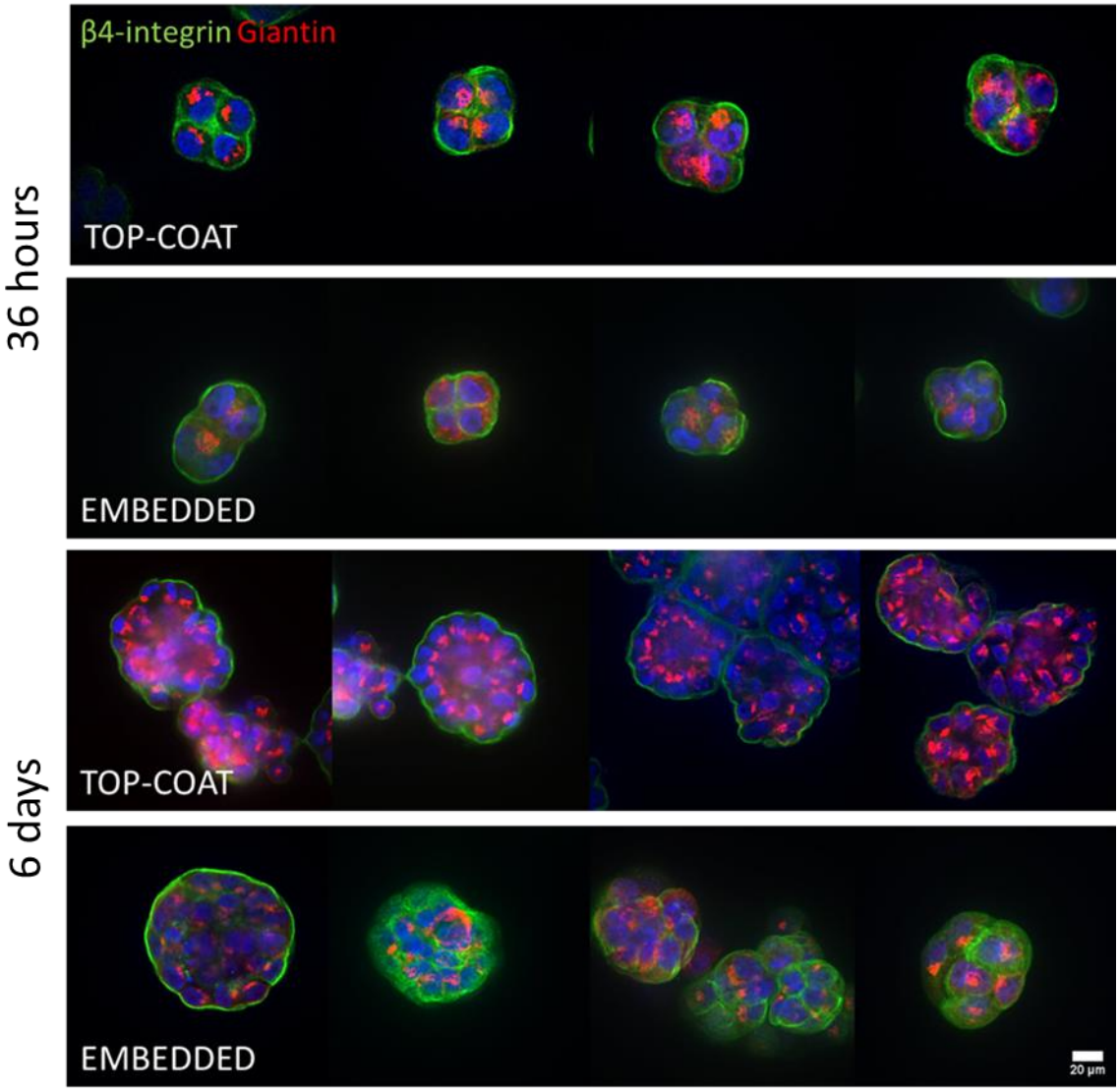

Figure 4-12 Observation of polarity of RWPE1 cells cultured according to top-coat and embedded protocol after 36 hours and 6 days of 3D cell culture. Scale bar for all images 20µm

At the early stage of growth, neither in top-coat nor in embedded conditions, structures were not polarized as observed by the position of β4-integrin and Golgi-apparatus. In both cases, β4-integrin was visible in lateral surfaces while Golgi-apparatus was dispersed with a random position within the cell (Figure 4-12 – "36 hours" panel). However, baso-apical polarity has been established after 6 days as expected, but surprisingly only in top-coat protocol (Figure 4-12 – "6 days" panel). Because micropatterning techniques allow controlled and repeatable growth of the cells (Rodriguez-Fraticelli *et al.*, 2012), presence or absence of polarity has been quantified by use of round micropatterns coated with matrigel (more details in Materials and Methods).

As expected and reported in literature (Wang *et al.*, 2013), MCF10-A cells formed majority of polarized structures (Figure 4-13). 76% of observed structures presented a proper organization of Golgi-apparatus. In the same conditions, RWPE1 cells proliferated more rapidly and only 14% of structures were polarized (Figure 4-13). As verified, RWPE1 cells establish polarity around day 4, however, after 8 days numerous structures are not polarized.

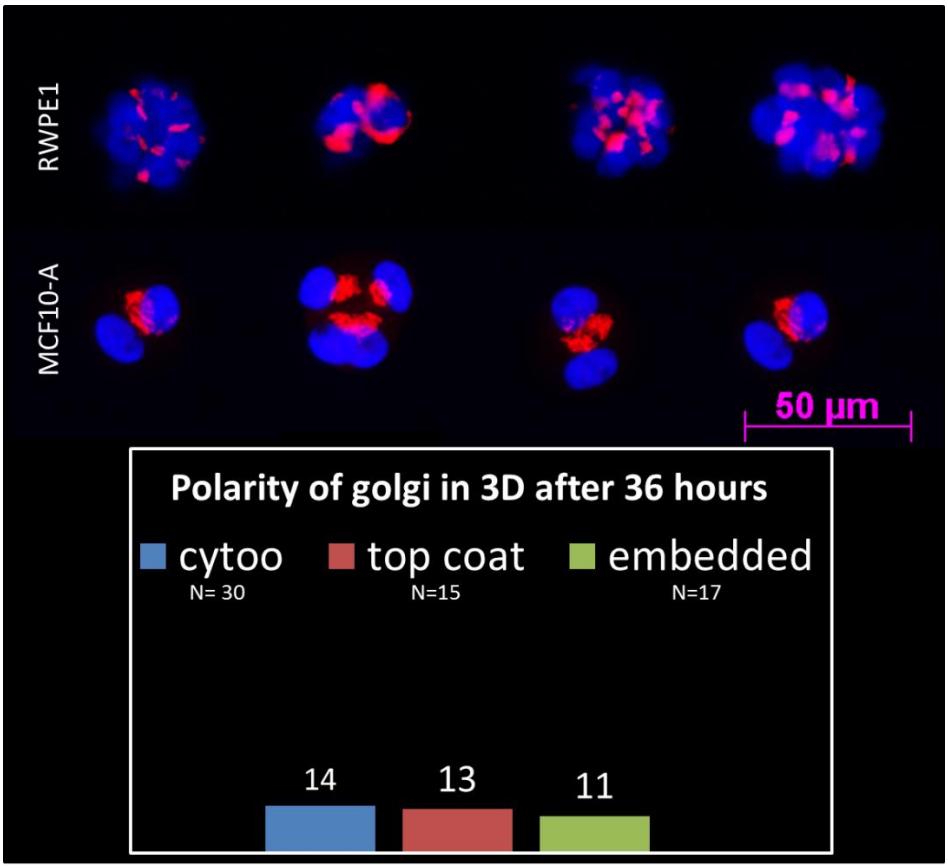

Figure 4-13 Organization of RWPE1 and MCF10-A cells on round micropatterns coated with Matrigel. Cells were stained with anti-Giantin for Golgi-apparatus. A bar chart indicates percent of polarized structures of RWPE1 cells within the culture after 36 hours on patterns (Cytoo) compared to top-coat and embedded protocol. Scale bar 50 µm.

We have further asked the question whether the polarity at early stages depends on the ECM composition. In order to verify which proteins play an important role in development of RWPE1 cell micropatterns were used. Cells were seeded on disc-like micropatterns coated with Matrigel, Collagen-1, Laminin-1, and Fibronectin respectively (Figure 4-14A). Only structures containing 2-cells that originated from a cell division were measured. The control coated with Matrigel induced polarity in 15% of observed structures (Figure 4-14B), which is consistent with what has been observed before (Figure 4-13). Laminin-1 induced polarity in 35% of the structures population while collagen-1 25% and fibronectin 18%. Interestingly, percent of polarized structures does not correspond proportionally to the area of the pattern that the cells have occupied (Figure 4-14C). A high percent of polarized structures on laminin-1 is associated with a relatively high cell adhesion area, but it is not a rule (Figure 4-14C). Fibronectin-coated

patterns promoted equivalent cell adhesion, however, the population of polarized cells was lower (Figure 4-14B).

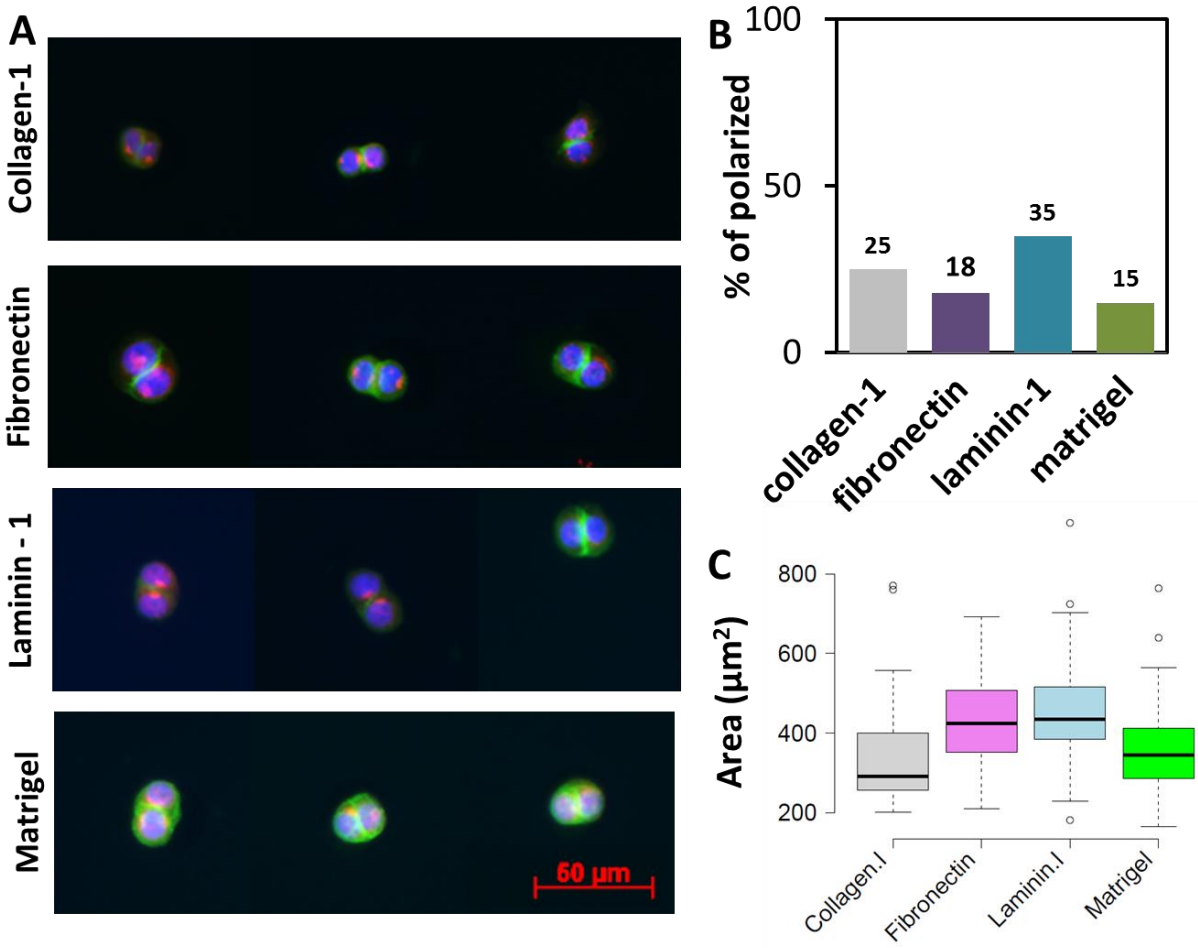

Figure 4-14 Effect of the ECM signaling on cell polarity at early stages of development. A) Immunofluorescent images of RWPE1 cells on patterns coated with different ECM proteins. Cells were stained with anti-Giantin (red), Phalloidin (green) and Hoechst (blue) in order to detect presence of the apical polarity. Scale bar 50µm. **B)** A bar chart indicates the percent of the structures polarized as a function of the protein coating. **C)** A boxplot present the area of attachment of cells in dependence of the protein type.

4.3 Discussion

In vitro prostate models include numerous established cells lines, however, only few of them recapitulate **glandular tissue organization** when cultivated in 3D culture on laminin-rich basement membrane (Matrigel). These models compared to breast epithelial cell lines (i.e., MCF10-A) are not widely studied. In here, RWPE1 cell were investigated as a potential model to study development of prostate and carcinogenesis. Reports on culture of RWPE1 cells present contradictory conditions for acini growth. Two studies in particular were considered; the first that introduced the establishment of RWPE1 cell line (Bello *et al.*, 1997) and second that verified in details the requirements for their culture (Tyson *et al.*, 2007). Introduced cell line was cultivated within KSFM support with EGF and BPE, but without diluted Matrigel in culture medium and fatal bovine serum. Furthermore, influence of EGF concentration on acini formation has been quantified and low concentrations (1,5 ng/mL) were present in the culture. Controversially, Tyson et al quantified in details each particular component including presence or absence of BPE, EGF and FBS, and presented results not complaint with the initial report of Bello *et al.* . In our case, the highest efficiency of acini formation has been observed with high levels of EGF (100 ng/mL), 2% v/v FBS and absence of BPE. The problem of heterogeneity of structures (acini, spheroids, branching and dysmorphic) has been eliminated by addition of 2% v/v of Matrigel (~0,2 mg/ml) into culture medium. This strategy has been widely described for MCF10-A model (Lee *et al.*, 2007) and after optimization the following composition of culture medium has been acquired for further experiments presented in this chapter; KSFM, 50ng/mL EGF, 2% v/v FBS and 10% v/v Matrigel (~0,9 mg/ml).

Development of an acinus in vitro includes several stages and is a **dynamic process**. Group of Pearson et al was the first to show that cells within acini are highly active and motile (Pearson and Hunter, 2007). Recently two reports on the **coherent rotation** of MCF10-A cells within acini indicated that angular motion is crucial for acinus formation (Tanner *et al.*, 2012; Wang *et al.*, 2013). It has been discovered that the rotational movement is associated with formation of a basement membrane. Acini rotate until around day 4, when the deposited by cells laminin layer becomes compact (Wang *et al.*, 2013). Dissolution of hydrogel around mature acini and their re-culture in the new Matrigel environment recovers the mechanism of rotation. This indicates the importance of laminin-integrin signaling in formation and maintenance of acini. Indeed, it is possible to change the malignant phenotype and obtain acini in 3D culture when blocking β1-integrin that is known to be overexpressed in tumors (Park *et al.*, 2006). As we showed, RWPE1 cells end the rotation in the late stage of the culture when the lumen is already formed. However, these acini are stable only for ~20 hours, and subsequently continue to move and contract in size. This phenomena has not been previously described, however, it can be associated with the deficiency of p53 in RWPE1 cells (Coppe *et al.*,

2008). It has been shown that P53 deficient mammary epithelial cells either undergo apoptosis or lack the growth arrest in dependence on the passage number (Seewaldt *et al.*, 2001).

Polarity and presence of lumen are intrinsic properties of polarized glandular tissue. How **lumen formation and polarity establishment** are connected remains undiscovered. As mentioned in Chapter 2, two mechanisms for acinus formation were proposed (Bryant and Mostov, 2008). One considers aggregation as an initial process (Bryant and Mostov, 2008) followed by establishment of polarity (Debnath and Brugge, 2005) and subsequent lumen formation by apoptosis of luminal cells. This process has been observed in 3D mammary cell cultures (MCF10-A) and in *in vivo* mouse mammary buds formation (Debnath *et al.*, 2002). It is thus indicated that initially important is polarity and lumen is formed consecutively. However, another model called hollowing, considers rapidly polarizing cells in which intracellular vesicles are delivered to the apical cell surface, creating a luminal space. This mechanism is present in 3D cell culture of kidney cells (Martin-Belmonte *et al.*, 2007) and in vascular development (Davis and Camarillo, 1996; Kamei *et al.*, 2006). It is suggested that the model for lumen formation is cell type dependent, however, we observed that RWPE1 cells clearly exhibit both types of mechanisms for lumen initiation in matrigel 3D culture in parallel (Figure 10). This result is consistent with another report that showed MDCK cells can follow both mechanisms depending on the cell seeding concentration and the ECM applied (Martin-Belmonte *et al.*, 2008). With increased cell concentration, cellular aggregation on collagen matrices is favored while when grown on Matrigel hollowing mechanisms is taking major role. Interestingly, authors show also that when knocked down Cdc42 (used by MDCK cells to establish apical surface) a mechanism of apoptosis replaces intracellular vesicles mechanism.

Contrary to what have been shown for MCF10-A cell (Wang *et al.*, 2013), RWPE1 cells are not polarized at very early stages of acini formation. **Lack of polarity during first 48 hours** has been tested according to embedded protocol, *top-coat* protocol and also on patterns, which normalize the culture and provide high signal reproducibility between cells (Thery, 2010). The number of polarized structures at this stage is consistent among tested protocols and falls around 13%. Moreover, as expected on the basis of the literature, laminin-1 controls lumen formation (Bello-Deocampo *et al.*, 2001). Here, by using laminin-1 patterns we showed that it significantly increased number of structures having lumen form 14% to 35% when compared with matrigel-coated control. Our results are consistent with a work of Rodriguez-Fraticelli *et al.* who have shown on MDCK model that laminin-1 induces proper polarity and lumen formation (Rodriguez-Fraticelli *et al.*, 2012). In contrast, MDCK cells have had low adhesion area on laminin-1 (~200μm^2 on 700μm discs) patterns in relation to collagen-1 and when compared to our results (~450μm). The reason behind can be cell-line-specific. Moreover, knowing the population of cells that are polarized at the early stages of morphogenesis might allow estimating heterogeneity of mechanism used to form acini by fact that hollowing occurs early and in between polarized cells.

Despite the lack of polarity at early stages, starting with day 4 majority of structures in top-coat conditions presented a proper polarity as indicated with β4-integrin for basal membrane and Golgi-apparatus (anti-giantin) for apical surface. However, well-established lumens appear at day 6 and are maintained throughout day 8 and day 10. It has been also observed that structures formed lumen but were still lacking appropriate apical polarity among all of the cells surrounding lumen. Surprisingly, the polarity established during earlier stages of cell culture is significantly disrupted around day 10. Because RWPE1 cells are not widely studied, observed effects (not reported for other epithelial cells) again might be specific to cell-line. If so, this model can serve to answer intriguing question whether polarity is necessary to maintain lumen and what is the long-term effect of its perturbation. To date tumorigenesis is mainly described as uncontrolled proliferation of cells followed by filling up of the lumen (Debnath and Brugge, 2005), however, mechanisms behind are still poorly understood.

Additionally, embedded protocol is ineffective in formation of acini at any stage of the culture when considered presence of lumen and polarity. Only 16% of structures at day 6 were polarized while the rest had high expression of β4-integrin marker in lateral surfaces and dispersed Golgi-apparatus among the cells cytoplasm. In general it is accepted that embedded culture is technically more correct because cells do not have any external anisotropic cue that could orient the polarity of cells at the beginning (Zegers *et al.*, 2003). A possible reason of decreased efficiency of lumen formation is the matrigel rigidity which can directly influence the phenotype (Paszek *et al.*, 2005).

4.4 Conclusions

Optimization of growth and culture conditions of a new cell model in the BIOMICS laboratory was the first important step of this thesis.

We have shown that RWPE1 cells can serve as a model to study acinar morphogenesis of prostate. In *top-coat* conditions acini are successfully obtained and proper polarity has been detected. The processes of establishment and maintenance of polarity in RWPE1 model are more complex compared to MDCK and MCF10-A models. Structures at early stages are not polarized and only top conditions promote growth of differentiated acini. We have shown also, that process of lumen formation within the same cell culture can proceed by cavitation and by hollowing. Formed acini in majority cases do not undergo growth arrest which in particular experiments can induce technical problems. A dynamic development reflected by the coherent rotational movement has been observed similarly as for other epithelial cells models. Despite this cells serve today as a model, more experiments are necessary to perform broader studies on prostate acini morphogenesis to understand the specificity of prostate development and to determine physical, genetic, and chemical factors that induce carcinogenesis.

The established optimized conditions for RWPE1 3D cell culture now provide systematically ~62% of acini population within the culture. However, limitations of this standard well-format culture (described in Chapter 2.4) impede high-throughput and high-content studies. Therefore, to overcome the technological gap new methods have been developed to standardize the 3D culture in order to provide a population of homogenous structures and amenable high-throughput analysis.

With the optimized protocol for cell culture, immunofluorescence and microscopic acquisitions, for future experiments RWPE1 cells served as a model of polarized acini. By the use of RWPE1 cells three main technologies for 3D epithelial cells culture were developed:

- Droplet microfluidic system for cell encapsulation which aims to bring high throughput flow-based analysis of 3D structures and control over environment (Chapter 5)
- Circular microchannels for tubule-like epithelial culture (Chapter 6)
- Lens-free imaging technique to distinguish acini from spheroids without necessity for labeling (Chapter 7)

5. Standardization of 3D cell culture using microfluidics and flow-based analysis

This chapter introduces microfluidics technologies with a special focus on droplet microfluidics. With the aim to apply microsystems for 3D epithelial cell culture, a droplet microfluidic platform has been developed to encapsulate cells in beads composed of Matrigel. Chapter 5 describes development, optimization of the system, and its applications.

Key findings

- PFPE-PEG surfactant in HFE7500 oil stabilizes Matrigel microfluidic droplet formation
- Encapsulated epithelial cells form polarized acini in Matrigel beads
- Encapsulation provides a possibility for high throughput flow-based analysis
- Encapsulation allows isolating single cells – acini formation occurs only by cavitation mechanism
- 3D culture in beads provide more homogenous in size population of acini
- Prostate epithelial cells rely on autocrine signaling to develop into acini
- Encapsulation promises high control over environment: size, rigidity, constraint

5.1 Introduction to microfluidics

For centuries chemist's tool-kit consisted of macroscopic round-bottomed flasks, test tubes and distillation columns all made from glass. Today, development in organic chemistry is visible in terms of analysis, but for fundamental laboratory methods chemists continue to use the same glass-ware as decades ago. Similarly, in cell biology, conventional 2D cell culture systems, mainly micro-well plates, flasks and Petri-dishes provided a satisfactory source of information to understand the basics of cell biology, and today they continue to be used extensively on a daily basis. Despite the use of robotic liquid dispensing stations, the transition from 384-well format into 1536-well format is still challenging due to the edge effects and uncontrolled evaporation. Standard 2D culture has met its limits in decreasing the scale of the experiments and it is more and more generally accepted that cell biology needs to acquire third dimension, in order to recreate more accurately *in vivo* environment. With the increasing interest to develop new *in vitro* models with more physiological chemical and mechanical properties, droplet microfluidics seems to be a promising technology as detailed below.

In general, droplet microfluidics is a technology that relies on forming and manipulating droplets of controlled volume (usually from μL to pL) that are carried by the immiscible phase (Huebner *et al.*, 2008; Song *et al.*, 2006). Droplet microfluidics ensures formation of monodisperse emulsions♣ (water-in-oil or oil-in-water) in a highly controlled manner with a high throughput (up to 100kHz,(Baret *et al.*, 2009; Chiu *et al.*, 2009)).

Droplet microfluidics has found its application in biology due to the following properties:

- high-throughput formation of thousands of identical aqueous droplets
- use of small volumes of reagents
- high-control over flow conditions provides control over size of formed droplets
- a single droplet acts as a micro-bioreactor
- possibility to acquire built-in analysis

A primary goal for microfluidics is to enhance the capabilities of investigators in biology and medical research. One of the biggest strengths is the scale of microsystems that is well matched to the physical dimensions of most of microorganisms and cells, providing tools able to manipulate biological objects at their appropriate environments with a control that cannot be easily achieved by standard culture techniques. Furthermore, because such systems support cell culture, the opportunity to integrate analytical devices to probe the biochemical processes at microscale is advantageous.

♣ emulsions – mixtures of two or more immiscible liquids

5.1.1 The scale makes the difference

The field of microfluidics is characterized by manipulating liquids at microscale at which fluid phenomena that dominate liquids are measurably different from those that dominate in macroscale.

Reynold's number

One of the important characteristics that give high control over flow and diffusion is a laminar flow. A Reynold's number (*Re*) is a dimensionless quantity that defines the ratio of inertial to viscous forces in a fluid; it is proportional to the characteristic fluid velocity (v; m s^{-1}) and length scale of the system (*w*; m) and inversely proportional to the fluid viscosity (η; kg m^{-1} s^{-1}).

$$\text{(Eq. 1)} \qquad Re = \frac{w\,v}{\eta}$$

Laminar flow is characterized by low *Re* (<2000, in microfluidics typically < 1) and is in contradiction to our daily life intuition on fluids where the flow is turbulent (*Re* > 2000). In microfluidic channels, low values of *Re* affirm that viscous forces dominate over inertial forces, and as a result flows are linear. Already a decade ago, Felice C. Frankel has taken the most famous image (Figure 5-1A) to introduce one-phase microfluidics and the laminar flow. The image illustrates infused colored water dyes into microchannels that downstream flow along-side. As the mixing occurs only by diffusion the colors of dyes are maintained indicating flow linearity.

In laminar flow diffusive mixing is slow and depends on the size of molecules, the viscosity of liquids and the characteristic distance. In one-phase microfluidics the ability to sustain parallel streams of different solutions is advantageous for example for formation of concentration gradients within microchannels (Gunawan *et al.*, 2006; Tian *et al.*, 2012) (Figure 5-1B). However, when considered fast reactions laminar flow has its drawbacks. In such case when reagents are initially in separate streams reaction does not proceed uniformly throughout the width of the channel.

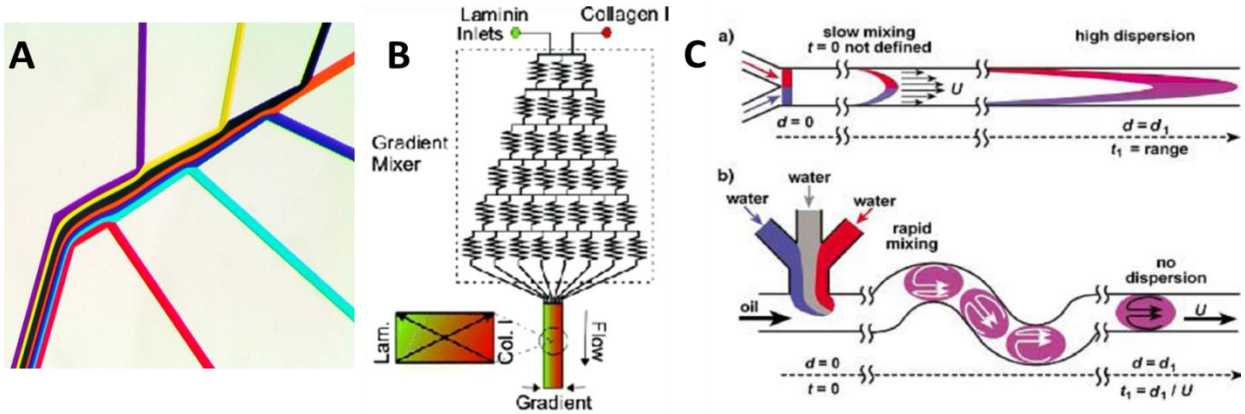

Figure 5-1 Laminar flow in one-phase microfluidics. A) A photo micrograph of colorous water dyes injected into a microfluidic system. Downstream color water dyes flow along-side indicating presence of laminar flow. Source: Felice Frankel **B)** Formation of gradient of Collagen I and Laminin by use of geometrical architecture of channels to control diffusion. Authors studied the effect of ECM proteins on cell migration. Source: (Gunawan *et al.*, 2006). **C)** Schematic comparison of continuous-flow (slow mixing and high dispersion) and drop-based microfluidics (rapid mixing and no dispersion). Source: (Song and Ismagilov, 2003).

Furthermore, the flow through a channel has a parabolic profile (for pressure-driven flows) (Figure 5-1C) which results in significant dispersion of reagents along the channel. The parabolic flow (called also Taylor-Aris dispersion) occurs due to the shear forces applied by channel walls on the fluid and thus the fluid at the center of the channel moves faster than the fluid by the edge. Compartmentalization of the fluid into a form of discrete droplets eliminates numerous problems of one-phase microfluidics (Figure 5-1C) (Song and Ismagilov, 2003) and presents several advantages which will be described in further parts of this introduction.

Capillary number and droplet formation

Droplet formation in a basic microfluidic system is based on combining two immiscible fluids (dispersed♣ and continuous phase♦). By the geometry (described in details further parts of the introduction) of the channels a shear force is generated, surface tension tends to reduce the interfacial area while viscous stresses extend the interface. As a result destabilized interface breaks into droplets. The process of droplet formation is therefore dependent on the ratio of viscous to interfacial stresses described by capillary number (*Ca*). *Ca* is proportional to viscosity (η; kg m^{-1} s^{-1}) and to characteristic fluid velocity (v; m s^{-1}) and inversely proportional to surface tension (γ; kg s^{-2}) between immiscible liquid phases.

$$Ca = \frac{\eta v}{\gamma} \qquad \text{(Eq. 2)}$$

In two-phase microfluidics, in between two immiscible fluids, a surface tension affects the dynamics of the free surface. If there would not be an interfacial tension between two

♣ Dispersed phase –usually aqueous phase which breaks into droplets
♦ Continuous phase – usually an oil phase which serves as a carrier fluid

phases, the streams would flow alongside. It has been experimentally shown that the process of droplets formation depends on Capillary number and the relative viscosity of continuous and dispersed phase (Tice *et al.*, 2004). At high *Ca* values the diameter (*R*) of droplets can be predicted by Equation 3:

$$\text{(Eq. 3)} \qquad R \sim \frac{\gamma}{\eta v} w = \frac{w}{Ca}$$

,where *w*(m) is a cross-sectional dimension of the channel. At values Ca > 1 formed droplets have diameter smaller than the diameter of the channel in which the process of droplet formation occurs.

5.1.2 Before forming droplets

The success or defeat of a droplet microfluidic experiments depends on numerous parameters. Droplet formation is highly sensitive to chemical properties of channels surface or physical properties of the liquid phases. Thus it is important to appropriately choose the material used for the fabrication and the fluids used for droplet formation. A successful, clean transport of reagents (flow of the aqueous phase) occurs when the continuous phase (carrier fluid) wets the walls of the channels preferentially over dispersed phase. Moreover, geometry of the channels determines the output of the system. The size of the droplet upon equal flow rate conditions can vary upon alterations in surface hydrophobicity or fluids viscosity, but also upon presence of the surfactant, which changes the surface tension between two phases.

Surfactants in droplet microfluidics play crucial role. A high surface to volume ratio increases importance of the interfacial effects. Therefore, emulsions need to be stabilized with surfactants which by reducing surface tension between phases prevent the natural process of coalescence. As it is described in Chapter 9.1.1 (supplementary results), choice of the oil and a compatible surfactant that stabilizes droplets of aqueous-phase can be challenging. Additionally, appropriate hydrophobic surface for water-in-oil emulsion has to be chosen to control wetting of the channel walls by continuous phase and prevent wetting of an aqueous phase. Methods of silanization or siliconization are commonly used to improve systems performance (Martin *et al.*, 2003).

Control over flow in simple T-junction and flow-focusing devices

The simplest way to induce flow in the microchip is to use gravity forces. Liquids in containers are positioned above the microfluidic chip at the desired distance; the higher the containers are, the higher flow will be induced. Another advantage of introducing flow by gravity is its steadiness. The problem appears when the liquid has a significant viscosity or when high flow rates are desired. In this case, to induce flow through the microfluidic channel one needs to install the container at the height that is not any more accessible from the

practical point of view. For this reasons, researchers employed syringe pumps, which are recently widely used due to their simplicity in operation and accessibility (no need for computer-control, external pressure source etc.). Often encountered limitation of syringe pumps is relied to the high-sensitivity of the droplet-formation process to the flow steadiness. It has been shown, that syringe pumps can induce oscillations in the flow-rate which influence directly the output of the system (Korczyk *et al.*, 2011). Authors compared the performance of syringe pumps (Harvard®) with a home-made system based on the pressurized containers and steel capillaries, which is characterized by stable flow as measured by the size dispersity of the formed droplets (Figure 5-2A). Today, some manufacturers achieved to eliminate flow oscillations, for example Nemesys syringe pumps.

Indeed, numerous commercial solutions were introduced that are based on adjusting a gas pressure in order to induce the flow (Figure 5-2C). This includes, for example, Fluigent systems (France), Elveflow Elvesys plug&play systems (France) (Figure 5-2B), or Syrris systems (Worldwide).

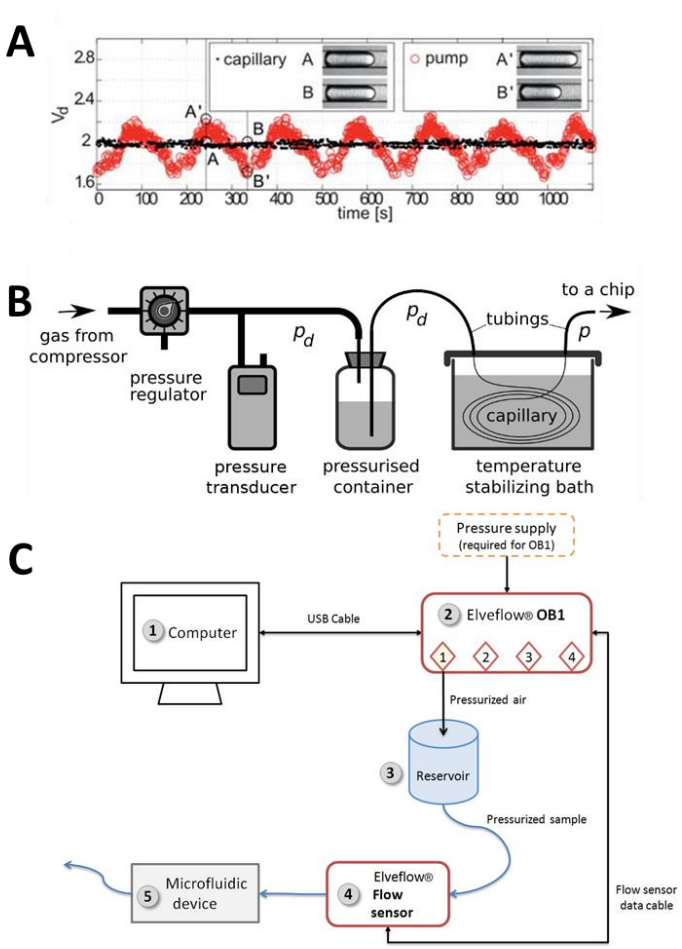

Figure 5-2 Control over flow rate in flow-focusing and T-junction microchips. A) Comparison of flow steadiness of syringe pumps and home-made pressurized system **(B).** Volume of consecutive droplets has been measured for both methods. **C)** A scheme of the commercially

available plug&play set-up to control flow rates in microfluidic devices. Source: A) and B) reprinted (Korczyk *et al.*, 2011) and C) www.elveflow.com

Microfabrication

The origins of microfluidic techniques start with the dynamic development of methods to fabricate microelectronic circuits (Whitesides, 2006). Those methods inspired researchers from other areas of science to create microchips with channels in range of 10 µm – 100 µm.

An important parameter that can define the success of the microfluidic experiment is the material used for the fabrication process. It is necessary to consider, for instance, resistance to solvents, optical transmissivity, or hydrophobicity. Each of these parameters can disturb appropriate function of the microchip. For high organic solvent resistance glass microchips can be considered but they are associated with the high-cost of fabrication processes. Similarly, 3D printing techniques did not find wide application. Today, most of the microfabricated systems are made with silicon, silica or glass (Figure 5-3), however, in the laboratory level two other groups are becoming widely used – thermoplastic polymers and PDMS. Application of these materials ensures more facile microfabrication processes that allow prototypes preparation. Furthermore, microfabrication in these two types of materials is cheaper than in silicon, silica or glass.

Microfarbication with polydimethylosiloxane (PDMS) (Xia and Whitesides, 1998) is based on soft photolithography process while in case of a rich group of thermoplastic polymers microfabrication occurs upon embossing (Martynova *et al.*, 1997), injection molding (McCormick *et al.*, 1997), or thermoforming (Giselbrecht *et al.*, 2006). Figure 5-3 presents approximate number of publications referencing different materials used for microchips fabrication in years 2000-2008 (Tsao and DeVoe, 2009).

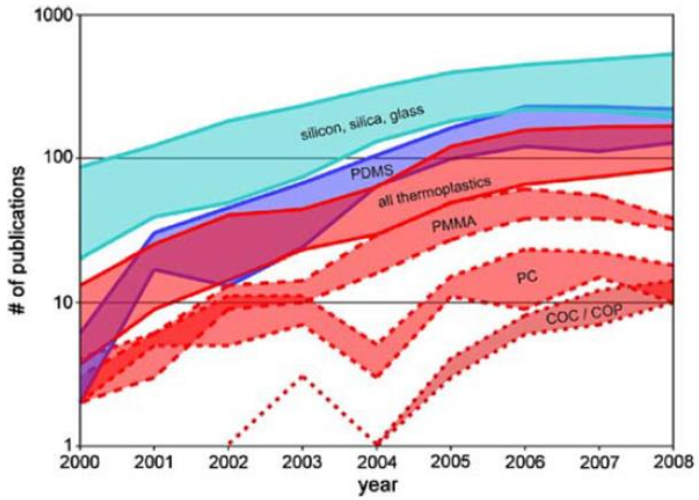

Figure 5-3 Applicability and popularity of various materials used for microfabrication in years 2000-2008. Source: (Tsao and DeVoe, 2009)

Since 2000, a group of silica and silicon (this includes glass and silica capillaries) are the dominantly used materials for microfluidics. Another widely used is family of thermoplastic polymers which includes polycarbonates (PC), polymethylmethacrylates (PMMA) and cyclic olefin polymers (COP) or copolymers (COC). The advantage to use thermoplastic polymers relies on: *i)* low cost, *ii)* relatively simple channel fabrication, *iii)* acceptable optical transmissivity in VIS spectrum, and *iv)* good solvent and chemical compatibility. However, precautions need to be taken in experiments that require use of aggressive organic solvents. The properties of thermoplastic polymers vary and their application is assay-dependent. Furthermore, sealing of the open microchannels is necessary to produce the final microfluidic chip and this step is critical, not universal and considered as a drawback.

Aforementioned PDMS is the second that is highly employed and found its application after introduction of soft photolithography methods (Xia and Whitesides, 1998). Since PDMS microchips were used for experiments described in this thesis the introduction chapter will be limited to soft lithography fabrication techniques.

Soft lithography with Poli(dimethylsiloxane)

PDMS fulfills majority of the requirements for the most suited material for microfluidic chips fabrication. Its properties are:

- Inexpensive and allows rapid prototyping
- Flexible with controlled rigidity
- Optically transparent (down to 230 nm)
- Impermeable to water
- Non-toxic to cells
- Permeable to gasses

There are several disadvantages of PDMS as a material for microfabrication, and these include for example swelling when exposed to solvents (parameters of channels might change) or difficulties to achieve stable inlet-tubing connection (for high flow-rate experiments). These parameters, however, did not have significant influence on the experiments performed in this thesis and therefore, PDMS was a material of choice.

Soft lithography, a fabrication process, begins with the preparation of a design of the channels which will be further printed on the transparency. A rapid prototyping is cost-effective compared to standard chrome masks, however, the resolution is significantly lower (>20μm in rapid prototyping and ~500 nm for a chrome mask). The experimental procedure is based on the uniform deposition of a photoresist (for example SU-8) on a silicon wafer (Figure 5-4A). Subsequently, a photomask is acquired to produce a *master* by contact-photolithography (Figure 5-4B).

The next step in the process is replica molding. PDMS is supplied in two components, a base (elastomer) and a curing agent. Polymerization is based on the reaction of silicon groups present in the curing agent with vinyl groups from the base. A mixture of base and curring agent (10:1) is poured over the master and allowed to polymerize (60 minutes in 60˚C) (Figure 5-4C). Polymerized elastomer, *replica*, has the embossed microstructures (or microchannels). Although, traditional soft lithography is based on the use of photoresist, masters can be fabricated by many other techniques (for example direct milling, embossing). The final step in microfluidic device preparation is bonding of the replica with a flat slab of the PDMS or glass. Sealing can be reversible, due to the weak Van der Waals interactions, or irreversible upon exposure of both surfaces to oxygen or air plasma (Chaudhury and Whitesides, 1991). It is possible to seal PDMS irreversibly with PDMS, glass, Si, SiO_2, quartz, polystyrene and polyethylene (Duffy *et al.*, 1998).

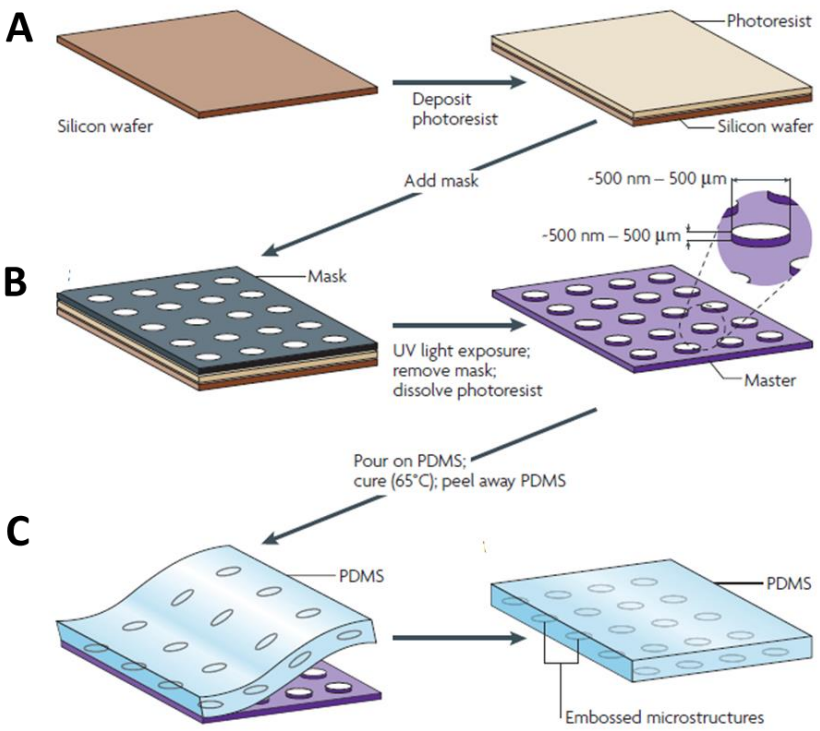

Figure 5-4 Stages of soft photolithography process. Source: (Weibel *et al.*, 2007)

5.1.3 Formation of droplets in a microscale

Droplet microfluidic is an expanding subgroup of microfluidics and simply aim to form water-in-oil or oil-in-water emulsions by using microfabricated chips. Droplet microfluidics ensures high-throughput formation of droplets of controlled *i)* size, *ii)* shape, and *iii)* monodispersity. Moreover, each single droplet can react as a single chemical or biological reactor and multiple reactions can be performed in parallel. With the high-throughput and

increasing availability of microfluidic systems, droplets become to be considered as an important tool in drug delivery and biosensing. To effectively serve as miniaturized test-tubes, a high control over size and morphology has to be ensured, as these parameters strongly affect biological and chemical properties of the sample. For example, the diffusion of nutrients or reagents will strongly depend on the droplet size, which defines the distance over which diffusion takes place. Traditional methods to form emulsions, for example, direct agitation of immiscible fluids results in significant polidispersity. By contrast, droplet microfluidics generates droplets with size variations smaller than 1% (Nisisako *et al.*, 2006).

Among many, there are four main techniques used to form droplets which include:

- T-junction
- Flow-focusing
- Dielectrophoresis (DEP)-driven droplet formation
- Electrowetting on dielectric (EWOD)

T-junction and Flow-focusing methods will be discussed here as both techniques fall in the group of planar microchips where principle of droplet formation is based on the use of continuous flow of oil and aqueous phase. Due to the simplicity in fabrication and operations, flow-focusing systems were used for experiments presented in this chapter.

T-junction

Formation of droplet in T-junction is governed by the geometry of the channels, where the inlet channel with the dispersed phase is positioned perpendicularly to a channel that contains the continuous phase (Figure 5-5A). It has been first presented by Thorsen *et al.* and gave a birth to droplet microfluidics (Thorsen *et al.*, 2001). The mechanism of droplet formation is based on the shear forces generated by the continuous phase that induces a pressure gradient on the tip that entered the continuous channel (Figure 5-5B). As a consequence, the dispersed phase is elongated in the main channel until the forming neck narrows and breaks into a droplet (Figure 5-5C)(Garstecki *et al.*, 2006). The size of the droplet is mainly controlled by the fluid flow rates, but depends also on the width of the channel, and on the relative viscosity between both phases (Tice *et al.*, 2004). T-junction systems are not limited only to a single inlet of dispersed phase, and by combination of numerous inlets (Figure 5-5D) more complicated experiments can be performed inside each single droplet, including protein crystallization (Zheng and Ismagilov, 2005) or chemical reactions (Cygan *et al.*, 2005).

Flow-Focusing

Based on a similar idea as the aforementioned T-junction systems, in flow-focusing dispersed and continuous phases are forced through a narrow part of the outlet channel (Anna *et al.*, 2003)(Figure 5-6A). Recently, simpler configurations without the nozzle are also applied

(Figure 5-6B). Due to the design in which the continuous-phase channels focus their flow at the intersection with the dispersed phase, the flow-focusing systems utilize a symmetric shearing which brings higher control over droplets formation. During droplet formation, the dispersed phase enters the intersection regions and temporarily limits the flow of continuous phase into the outlet. This results in the increased pressure that narrows the dispersed phase stream and results in the controlled breaking into droplets (Nie *et al.*, 2008). It has been observed that the size of the droplets can be altered by the design of the device (Tan *et al.*, 2006) the properties of liquids, and the flow rates of two immiscible phases (Cramer *et al.*, 2004; Garstecki *et al.*, 2004). Therefore, each system requires optimization in order to produce droplets of desired properties.

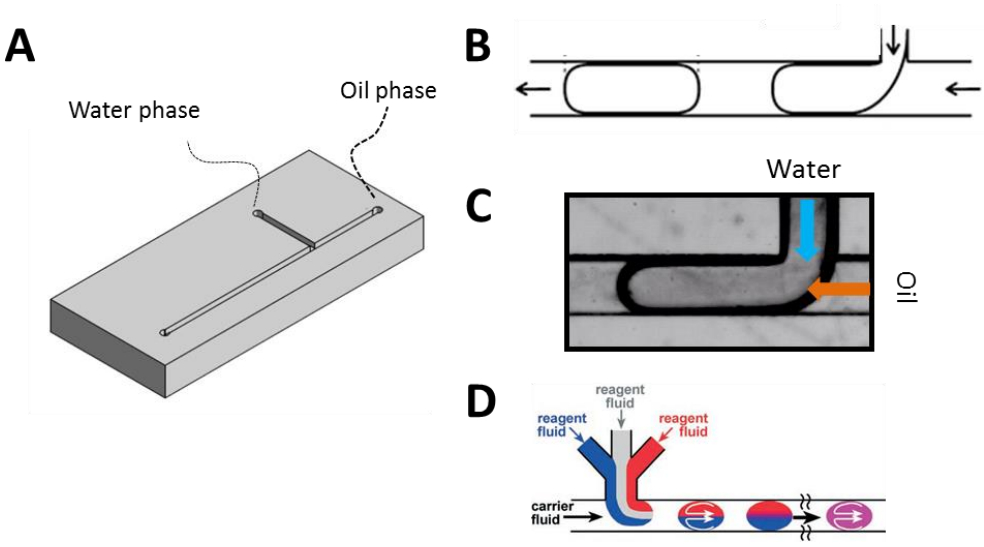

Figure 5-5 Microfluidic T-junction system for droplet formation. A) 3D visualization of a simple T-junction microfluidic chip. Droplet formation process represented schematically (**B**) and by phase contrast image (**C**). (**D**) Modified T-junction system for droplet formation composed of multiple fluids (reagent in fluid blue and reagent in fluid red). Source: Illustration B has been reprinted from (Garstecki *et al.*, 2006), image D reprinted from (Song *et al.*, 2006)

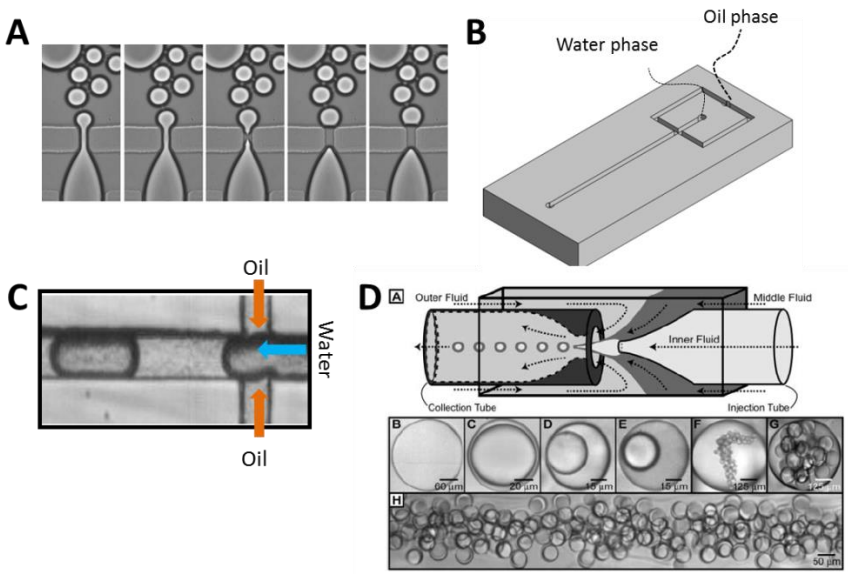

Figure 5-6 Microfluidic flow-focusing system for droplet formation. A) Original first flow-focusing device containing an orifice. **B)** 3D visualization of a simplified flow-focusing microfluidic chip. **C)** Phase contrast microphotograph illustrates the process of droplet formation. **D)** Capillary-based systems for droplet formation or multi emulsion formation. Source: A) reprinted from (Anna *et al.*, 2003); D) reprinted from (Utada *et al.*, 2005)

Many variations of the simplest flow-focusing geometry were introduced. Depending on the fabrication method, flow-focusing devices can have a planar geometry (on a polymeric chip) or have a capillary-based design, where the capillary of dispersed phase is inserted in the capillary of continuous phase, which forms an outer shell around the dispersed phase (Utada *et al.*, 2005). Such configuration enables more complex configuration composed of multiple capillaries that allow producing highly-controlled multi emulsions (Figure 5-6C). Since droplet size depends on various parameters, including the channels size which plays an important role in the final output, Lee *et al.*, proposed a microchip with altered channel dimensions by applying pneumatically controlled walls (Hsiung *et al.*, 2007).

Flow-focusing methods are mainly used to produce highly controlled water-in-oil emulsions, but reports present also generation of micro-bubbles (Garstecki *et al.*, 2004), double emulsions (Utada *et al.*, 2005), oil-in-water emulsions (Maan et al., 2013) or aqueous droplets coated with a polymer (Takeuchi *et al.*, 2005).

5.1.4 Cell encapsulation

The technology of cell microencapsulation aims to immobilize cells in an isolated microenvironment that maintains cells intact and supports cellular functions. Moreover, culture of cells in 3D microenvironments offers the ability to control shear forces, the manipulability and reconfigurability of hydrogel beads or capsules, and more importantly sufficient transport of nutrients and waste exchange (McGuigan and Sefton, 2007; Orive *et al.*, 2004). The high potential that lies in cell encapsulation has been observed as early as in 1933,

when Bisceglie enclosed tumor cells in a polymer membrane and transplanted them into a pig's abdominal cavity. Interestingly cells survived long enough to conclude, what we know today, that encapsulation prevents immune rejection of implanted cells (Chang, 1964). Except reports on cell encapsulation in aqueous droplets separated by oil (Brouzes *et al.*, 2009), the most commonly employed materials are hydrogels due to their high biocompatibility (Williams, 2009).

Hydrogels and cell encapsulation

Hydrogels are water-swellable polymers that enable nutrients and waste exchange, display tissue-like mechanical properties, and are highly biocompatible. Their role is to mimic the extracellular matrix, a natural environment of cells within tissues. These properties make hydrogels highly attractive as biomaterials for cell growth, cell encapsulation (Zimmermann *et al.*, 2007) or tissue engineering (Balakrishnan and Banerjee, 2011).

Hydrogels in general, can be divided into two groups: synthetic hydrogels that are obtained in the laboratory and natural hydrogels. The latter group further divides into protein based (collagen, gelatin, fibrin) and polysaccharides (alginate, pectin, hyaluronic acid, chitosan and agarose). Synthetic hydrogels include i.e., poly(ethylene glycol) (PEG) or poly(vinyl alcohol) (PVA). Table 5-1 shows the broad use of hydrogels as biomaterials for drug delivery, encapsulation, and for scaffold formation.

Considered the particular properties of natural and synthetic hydrogels only few fulfill the requirements for droplet microfluidic cell encapsulation. Materials that require UV radiation (PEG), high-temperature thermal treatment (Elastin-like polypeptides), toxic crosslinking agents (PEG with azide and alkyne groups) might have limited application due to their possible toxicity. On the other hand, materials that require multistage polymerization risk complicating significantly the design and operation of microfluidic device.

Requirements for cell encapsulation

There are three key components to be considered in cell microencapsulation:

1) Cells and their specific requirements of culture
2) Type of hydrogel
3) Microencapsulation technology

Since different cell lines have their own unique properties, the first point defines the most important requirements for the experiment and directly influences on the choice of the hydrogel material and encapsulation technology so that the highest biocompatibility is achieved. Moreover, choice of the hydrogel-type dictated by cell requirements should not affect the process of microencapsulation. As has been discussed above, physical parameters of the dispersed phase need to be considered to not to impact the process of droplet formation. The

method used for cell encapsulation has to be reproducible and of a high throughput to produce sufficient number of cell-laden microgels. Highly monodispersed microgels are required to enable control over average cell number per droplet (or a microgel) and to study the role of the microenvironment on the cell fate.

Conventional methods effected in a high polidispersity of microgels (in the range of 10 to 50%), large microgels diameters (up to 1 mm), and need of high amounts of reagents. These methods include hydrodynamic dripping (Levee *et al.*, 1994), extrusion methods (Rabanel *et al.*, 2009; Schwinger *et al.*, 2002), bulk emulsification (Batorsky *et al.*, 2005), and electrostatic dripping (Poncelet and Neufeld, 1989).

Droplet microfluidics techniques provide, at the same time, superior control over polymerization process of various hydrogels and over the size of the produced droplets. Therefore, these systems are broadly used for cell encapsulation purposes (Velasco *et al.*, 2012) (Table 5-1) and have been used during this thesis to encapsulate epithelial cells in Matrigel beads.

Table 5-1 Summary of selected hydrogel applications in tissue engineering. Source: (Slaughter *et al.*, 2009)

Intended tissue	Cell type(s) studied	Hydrogel type(s)	Hydrogel function(s)
Bone	Osteoblasts	PEG–PLA [a]	Drug delivery, Encapsulation
Bone	Osteoblasts	Peptide amphiphile–Ti composite	Encapsulation, Implant
Bone	Fibroblasts	PEG	Scaffold
Cardiovascular	Bone marrow cells	Fibrin	Cell delivery, Scaffold
Cardiovascular	Embryonic carcinoma	PEG	Encapsulation
Cardiovascular	Cardiomyocyte, Endothelial, ESCs	SAP	Encapsulation, Scaffold
Cardiovascular	Hepatocytes	HA, Alginate, Carboxymethylcellulose	Scaffold
Cartilage	Chondrocytes	Fibrin	Cell delivery, Scaffold
Cartilage	Chondrocytes	PEO Semi-IPN	Drug delivery, Encapsulation
Cartilage	Chondrocytes	PEG	Drug delivery, Encapsulation
Cartilage	ESCs	PEG	Drug delivery, Encapsulation
Cartilage	Chondrocytes	PVA	Encapsulation
Cartilage	Chondrocytes	PEG	Encapsulation
Cartilage	Chondrocytes	PEG	Encapsulation
Cartilage	Chondrocytes	PEG	Encapsulation
Cartilage	Chondrocytes	PEG–PLA–PVA [a]	Encapsulation
Cartilage	Chondrocytes	Alginate	Encapsulation
Cartilage	Chondrocytes	Collagen	Encapsulation
Cartilage	Chondrocytes	Collagen, HA	Encapsulation
Cartilage	Chondrocytes	PEG–PLA [a]	Encapsulation, Scaffold
Cartilage	MSCs	PEG	Encapsulation, Scaffold
Cartilage	Chondrocytes, MSCs	PEG	Encapsulation, Scaffold
Cartilage	Chondrocytes	PLLA [b], Agar, Gelatin	Encapsulation, Scaffold
Cartilage	Chondrocytes	HA, Collagen	Encapsulation, Scaffold
Cartilage	Chondrocytes	Fibrin	Encapsulation, Scaffold
Cartilage	Chondrocytes	SAP	Encapsulation, Scaffold
Cartilage/Bone	–	Alginate, HA	Bioreactor, Scaffold
Connective Tissue	Fibroblasts	HA	Encapsulation, Scaffold
ECM	Fibroblasts	HA, Chondroitin Sulfate, Gelatin	Encapsulation, Scaffold
Eye	–	HA	Barrier, Scaffold
Eye	–	PHEMA	Scaffold
Facial	Chondrocytes	Alginate	Encapsulation, Implant
Facial	–	HA	Space-Filler
Intraperitoneal	–	HA	Barrier
Intraperitoneal	–	PEG, PEG/PLA [a]	Barrier, Drug delivery
Intraperitoneal	–	PEG	Drug delivery
Neural	–	Collagen	Drug delivery
Neural	Neuroprogenitors	SAP	Entrapment, Scaffold
Neural	–	PHEMA–MMA	Scaffold
Pancreatic	Islet of Langerhans	PEG	Encapsulation
Pancreatic	Islet of Langerhans	PEG–PLA [a]	Encapsulation
Skeletal Muscle	Myoblasts	PHEMA	Scaffold
Skin	–	Collagen	Drug delivery
Skin	–	Fibrin	Glue
Skin	Fibroblasts	HA	Scaffold
Spinal cord	–	PHEMA	Drug delivery, Scaffold
Spinal cord	Astroglial cells	Collagen	Encapsulation
Vascular	–	PEG	Barrier
Vascular	–	PEGDA	Drug delivery
Vascular	–	Alginate	Drug delivery
Vascular	–	Gelatin	Drug delivery
Vascular	–	HA	Drug delivery
Vascular	–	PEG	Drug delivery, Scaffold
Vascular	hESCs	HA	Encapsulation
Vascular	MSCs, Primary smooth muscle	PEG	Encapsulation
Vascular	Endothelial cells	P(PF-*co*-EG)	Encapsulation
Vascular	hESCs	Dextran	Encapsulation, Drug delivery
Vascular	Smooth muscle cells	PEG	Scaffold
Vascular	Endothelial cells	PEG	Scaffold
Vocal Cord	–	HA–Gelatin	Scaffold
Vocal Cord	–	Collagen, Alginate	Scaffold

[a] PLA = poly(lactic acid). [b] PLLA = poly(L-lactic acid).

5.2 Controlled 3D culture in Matrigel-droplet microfluidics shows that acinar development relies on autocrine signaling

Presented in this chapter work has been a basis to a recently submitted publication in Nature Communications journal under the title: "Controlled 3D culture in Matrigel-droplet microfluidics shows that acinar development relies on autocrine signaling".

Contributing authors: M. E. Dolega, F. Abeille, N. Picollet-D'hahan, X. Gidrol

M.E.D, X.G and NPD designed research; M.E.D. performed research; F.A. master prefabrication; M.E.D, X.G and NPD analyzed the data; M.E.D, X.G and NPD wrote the paper.

5.2.1 Abstract

3D culture systems are a valuable tool for modeling morphogenesis and carcinogenesis of epithelial tissue in a structurally appropriate context. We present a novel approach for 3D cell culture based on a flow-focusing microfluidic system that encapsulates epithelial cells in Matrigel beads. As a model we use prostatic and breast cells and assay for development of acini, polarized cellular spheres enclosing lumen. Each individual bead on average acts as a single 3D cell culture compartment generating one acinus per bead. Compared to standard protocols microfluidics provides increased control over the environment leading to a more uniform acini population. The increased facility of bead manipulation allowed us to isolate single cells which carry sufficient autocrine signals to fully develop into acini in an environment composed only of Matrigel. Furthermore, combination of our microfluidic approach with large particle FACS opens new avenues in high throughput screening on single acini.

5.2.2 Introduction

Although relatively well understood in mouse and to some extent in rat, the molecular mechanisms and gene networks that control acinar development are far less characterized in humans because of the lack of appropriate models (Pearson *et al.*, 2009). The recent development of three-dimensional (3D) cultures of epithelial cells from different organs (prostate, breast, kidney, etc.) in Matrigel offers real potential as a model for human acinar development (Mailleux *et al.*, 2008; O'Brien *et al.*, 2002; Pearson *et al.*, 2009; Zegers *et al.*, 2003). Indeed, cells within a tissue interact with neighboring cells and with the extracellular matrix (ECM) through chemical and physical cues. Cell-cell and cell-ECM interactions

establish a 3D communication network that maintains the specificity and homeostasis of the tissue. Three-dimensional cultures that re-establish such physiological interactions can model real tissues better than conventional 2D cultures. In such a 3D context and with appropriate factors in the culture medium, epithelial cells are able to develop acinar structures. Research has established that first, either a precursor cell proliferates or cells aggregate to form small 3D clusters of randomly oriented cells consisting of two cell populations: outer cells having contact with the ECM and inner cells surrounded only by other cells. Second, cells in the outer layer develop an apico-basal polarity and no longer respond to proliferative signals. Third, differentiation of the outer cells is followed by apoptotic death of inner cells that results in the formation of the hollow lumen, and the acinar structure remains hollow thereafter (Bryant and Mostov, 2008; Mailleux *et al.*, 2008). Although these different stages in acinar development are well documented, the molecular factors that guide the actions of a single cell during that process are still poorly understood.

The main reason for the relatively slow progress comes from difficulties in manipulating, treating and controlling the structures and the environment around them in 3D. However, standard 3D culture formats performed in microwell plates present some limitations that hamper their applicability to high throughput screening (HTS) for pharmaceutical studies and also limit the ability to address basic questions regarding acinar development and carcinogenesis. Indeed, in such formats, control over the environmental physical parameters including size, stiffness, and porosity remains limited (Hebner *et al.*, 2008). Moreover, the presence of Matrigel creates a physical barrier that prevents or decreases the efficiency of several standard techniques used in 2D culture (i.e., direct transfection with siRNA and cell lysis for RNA or DNA extraction). Additionally, phenotypic analysis based on immunofluorescence and subsequent confocal microscopic observation, which can reveal the presence of the lumen and the position of polarity markers, (Lee *et al.*, 2007) is time-consuming. Hence, this well-plate format is not suitable for screening applications that require reproducibility, rapid and robust handling and large-scale analysis. The complexity of analysis is in itself an obstacle, and consequently, there are only a few reports on 3D screens of epithelial cells (Hubbell, 2004; Khademhosseini *et al.*, 2006; Lee *et al.*, 2008). Finally, because multiple cells are grown in 3D embedded in Matrigel, the resulting mixture of individual and clustered cells makes it very difficult to answer basic biological questions such as whether a single cell can promote the formation of a fully differentiated acinus. These model systems cannot determine whether aggregation or proliferation presides in the first stage of cluster formation of unpolarized cells or whether the neighboring cells influence terminal differentiation and acinar formation.

Therefore, there is critical need for new technologies that would allow for the following: i) higher control over the size and composition of the environment surrounding the cells; ii) isotropic conditions throughout the culture; iii) flow-based high throughput assays; and iv)

control over cell concentration, facilitating the isolation of single structures with which to study, for instance, paracrine/autocrine effects on the development of 3D structures. Microfluidics is a promising approach to 3D epithelial cell culture that addresses all four points.

Recent developments in droplet microfluidics for 3D culture include in-droplet formation of spheroids (Alessandri *et al.*, 2013; Kim *et al.*, 2011) and the isolation of encapsulated cells from the immune system in the case of cell-implants (Jun *et al.*, 2013). Depending on the cell type and the application, the hydrogel type varied from biologically inert, including alginate or agarose, to collagen for cell proliferation and further tissue engineering (Matsunaga *et al.*, 2011). Interestingly, depending on the hydrogel used, microfluidic systems have differed dramatically generating a significant lack of universality. As collagen or Matrigel promotes growth and differentiation of various cell types (Kleinman *et al.*, 1981) and governs the development of acini or cysts in traditional 3D culture, it is surprising that there have been no report on the formation of droplets composed of Matrigel to date.

In this study, we developed a droplet microfluidic system for cell encapsulation in Matrigel microbeads. The microfluidic operational parameters were optimized to eliminate droplet coalescence issues and to provide high cell viability. In such appropriate conditions, each individual microbead acts as a single-cell culture compartment generating on average one acinus per bead. Matrigel microbeads served as microcarriers for flow-based high-throughput analysis and thus opened new possibilities for performing high throughput screens on 3D culture structures in biological and pharmaceutical research. Furthermore, we show that 3D cell culture in Matrigel beads provides a unique system where acinar development can be traced from the very first division to the final developmental step, under temporally and spatially controlled conditions. Finally, we were able to trap a single prostate cell and drop it into each well of a 384-well microtiter plate. This original approach allowed us to demonstrate that one single prostate cell, without any interaction with neighboring cells, was able to proliferate and differentiate into an acinus within 6 days. This indicates that acinar development proceeds through clonal growth from single cell and relies on autocrine signals to differentiate.

In future applications, we anticipate that the wide dynamic range and high sensitivity of this microfluidic system will provide maximally flexible conditions under which to probe further biological questions that have been previously inaccessible due to the limitations imposed by 3D culture conditions.

5.2.3 Result 1 - A microfluidic device to generate Matrigel-containing monodisperse beads amenable to high content screening

We used the most basic design of flow-focusing (FF) junction (Anna *et al.*, 2003) for the formation of droplets. Because Matrigel is a complex material composed of over 1800 proteins (Kleinman and Martin, 2005), the choice of the oil and the surfactant was crucial. Supplementary results on the optimization of the experimental setup are presented Chapter 9.1.1. We tested various surfactant combinations at different concentrations (Chapter 9.1.1 Table 9-1) and obtained weak stability of the droplets collected at the outlet. To further minimize the coalescence of droplets just before leaving the channel, we designed a planar outlet tubing connection. The commonly used surfactants that we tested did not provide sufficient droplet stability. Because Matrigel is composed of ~30% of collagen, we assumed that the methods established for collagen droplet formation (Matsunaga *et al.*, 2011) would be suitable for Matrigel. Conversely, lecithin and other types of surfactant/oil systems used for cell encapsulation caused cell death of epithelial cells (Figure 5-7). Indeed, we observed that epithelial cells can be highly fragile depending on the presence and the type of the surfactant. We found that the PFPE-PEG surfactant (Brouzes *et al.*, 2009; Holtze *et al.*, 2008) was suitable in our microsystem and was biologically inert. Interestingly, the droplets do not undergo coalescence only in HFE7500 oil contrary to previous reports for aqueous droplets in FC40.

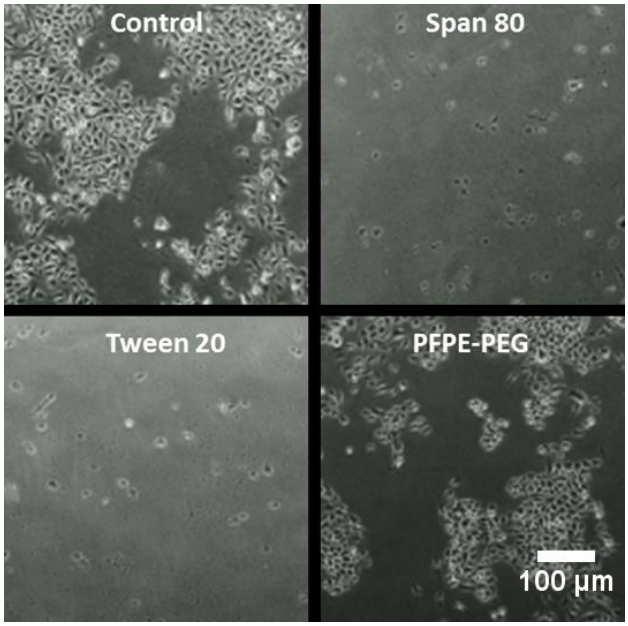

Figure 5-7 Biocompatibility test of chosen surfactants and their effect on cell viability as tested in standard 2D culture.

We modified the basic design of the FF junction system in the experimental device by adding a wide serpentine channel (Figure 5-8A) that served as a reservoir for the Matrigel mixed with cells. In this way, direct injection of 100 μL of the Matrigel phase was possible by simple pipetting. Size of the droplets which depends on the rate of flow of particular phases (Qoil = Q_1 and QMatrigel = Q_2) was controlled by syringe pumps. The significant difference in the viscosity of perfluorinated oil and Matrigel limited the minimal size of the droplets (Figure 5-8C). Therefore, to span a spectrum of the bead size from 100 μm to 500 μm, we used three different devices with 100 μm, 250 μm and 400 μm channels each having a square cross section. The flow rate for the majority of the experiments in a 250 μm device was Q_2 = 400 μL/h for Matrigel and Q_1 = 1600 μL/h for oil. Due to the properties of Matrigel (liquid at 4˚C and polymerized at 37˚C), all manipulations were carried out at 4˚C. We found that 15 minutes of encapsulation time produces thousands of beads and maintains high viability of cells for 24 hours that would otherwise suffer due to the prolonged residence in the cold. Formed hydrogel droplets are collected in oil in a tube and allowed to polymerize for 20 minutes at 37°C. Cell-containing polymerized beads were transferred into culture media and maintained in a multiwell plate. We tested bead stability and observed slow dissolution (Figure 5-8D) and aggregation. Dissolution of beads had direct influence on the cell phenotype as 65% of structures in unstable beads presented inversed polarity (Figure 5-9A). The addition of 1% v/v of Matrigel into the culture medium prevented both phenomena and restored bead stability with only 5% change in size during the first 7 days and 18.5% after 20 days. In the control without Matrigel, bead dissolution reached 30% after 7 days and 44% after 20 days. This level of bead stability is satisfactory considering that the typical time scale of experiments in epithelial 3D culture falls between 7-21 days (Debnath *et al.*, 2003). A 10% increase in the concentration of Matrigel in the culture medium prevented proliferation of cells in beads (Figure 5-9C), possibly due to limited diffusion and exchange of nutrients. We also observed that decreased bead stability induces encapsulated cells to leave the Matrigel and initiate a 2D culture at the bottom of the well instead (Figure 5-8E). Another controllable parameter was the initial number of cells per bead, which can be set by altering the cell density in Matrigel. As it follows a Poisson distribution for any particular bead size, the initial concentration of cells can be calculated such that the average droplet will contain a single cell per bead (Chapter 9.2.2 Methods in microfluidics). Thus, we have developed a microfluidic system that enables the formation of Matrigel droplet containing well-controlled 3D epithelial structures.

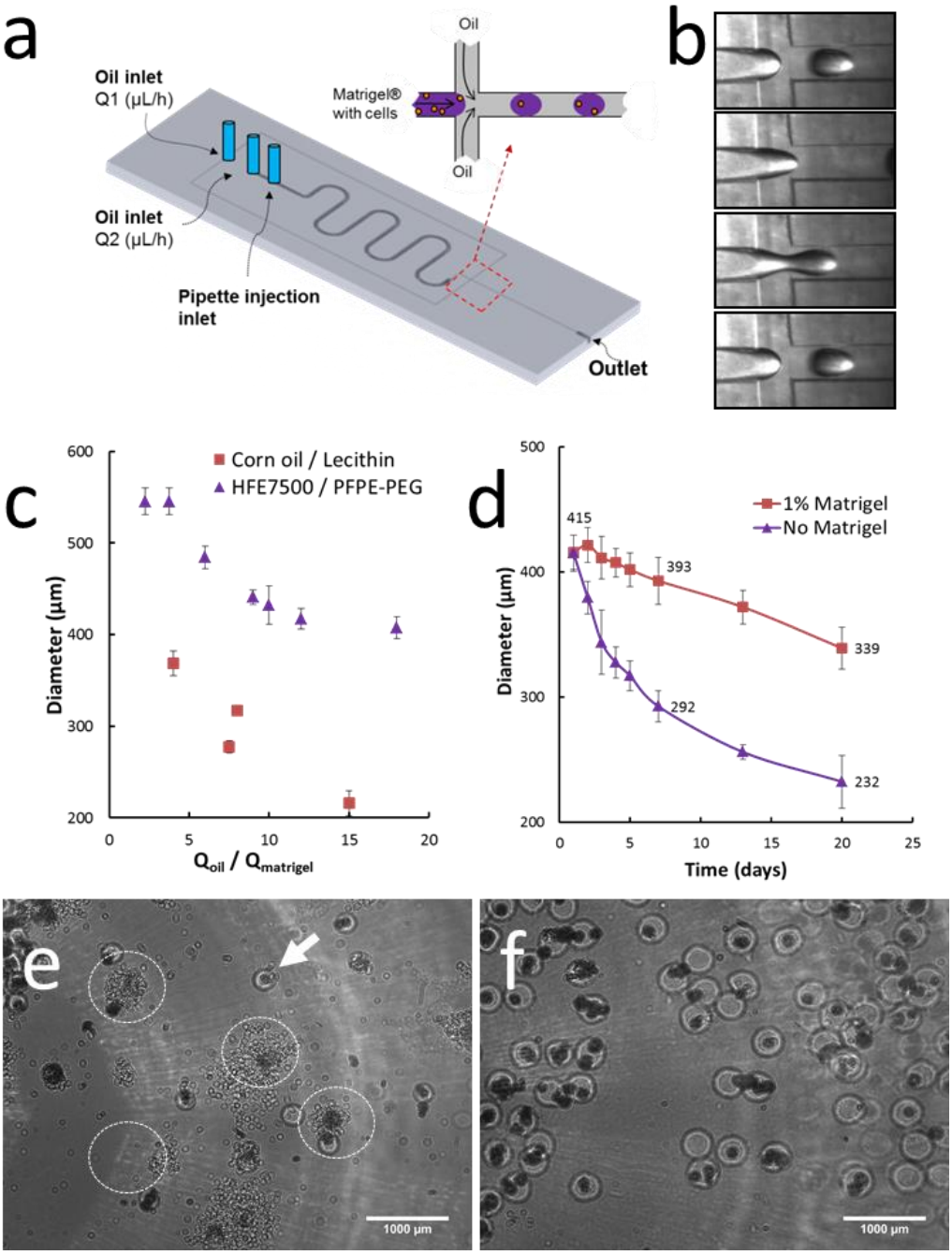

Figure 5-8 Formation and stability of Matrigel droplets. A) Schematic representation of an experimental setup. The long serpentine channel was used as a reservoir for the injected Matrigel with cells. B) Formation of a Matrigel droplet in the 400 µm channel of a flow-focusing system. **C)** Dependence of the size of the droplet on the ratio of rate of flows for perfluorinated oil and for corn-oil. **D)** Graph shows the dissolution, which is reflected in changes in size of beads kept in different culture media - pure or containing 1% diluted Matrigel. **E)** As a consequence of dissolution (size change indicated by arrow), cells escape the beads and form 2D culture monolayers (marked with circles), but maintaining cells in culture media containing 1% Matrigel prevents this effect **(F).**

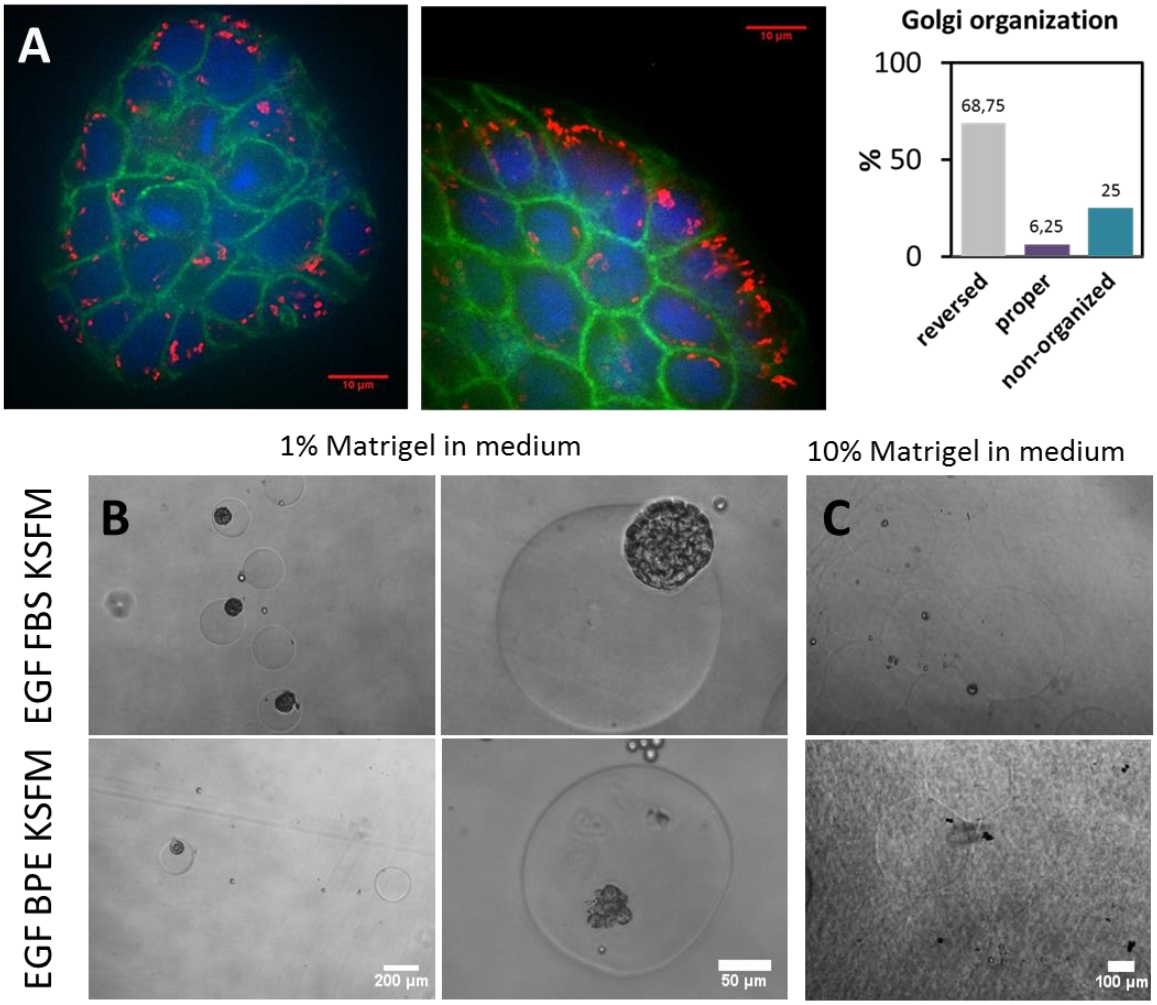

Figure 5-9 Importance of culture medium composition on beads stability and cell growth. A) Beads instability promotes inversed polarity in RWPE1 structures. **Left:** Fluorescent images of encapsulated structures stained for Golgi apparatus (anti-Giantin; red), Actin (Phalloidine; green), and nuclei (Hoechst; blue). **Right:** The bar chart presents the population of structures with reversed, proper and non-organized polarity. (n = 42) **B)** 1% matrigel stabilizes beads, prevents aggregation and promotes growth, while **(C)** 10% limits the diffusion of nutrients and as a consequence cells do not proliferate. Visible differences were observed when cultured with KSFM used for 2D culture (EGF BPE KSFM) and for 3D culture (EGF FBS KSFM). Compositions of culture medium for both types of culture are described in details in Materials and Methods (Chapter 9). Scale bar A) 10 µm and B), C) as indicated.

In addition, we also designed our system to take into account several requirements of high-throughput and high-content analyses. While such analyses are relatively simple in 2D culture either through automated microscopic acquisition or the use of a fluorescently activated cell sorter (FACS), appropriate analytic methods are lacking for 3D culture. It has been shown that encapsulation of microorganisms (Eun *et al.*, 2011) and cells (Brouzes *et al.*, 2009) into beads that serve as microcarriers allows for flow-based analysis methods. In these experiments, we used the MCF10A-GFP breast epithelial cell line, which forms acini within 14-20 days in 3D culture (Debnath *et al.*, 2003). We chose this cell line for two reasons: first, to demonstrate the feasibility of this system with other cellular models, and second, because of the availability of this stable GFP-expressing cell line in the laboratory. We transfected cells for 48 hours in standard 2D culture using a siRNA targeting GFP (siGFP) and AllStar (siAllstar) as a control. Subsequently, the transfected cells were trypsinized and encapsulated in Matrigel beads 250 µm in diameter. For each condition, we prepared approximately 1000 beads. During the 5-day incubation in beads, the cells proliferated and formed 3D structures (Figure 4-10A). We verified by fluorescent microscopic observations that the level of green fluorescence of the cells in control (Figure 5-10B) was higher compared to the siGFP sample (Figure 5-10B), as expected. We used large-particle FACS (LP FACS) to analyze the level of fluorescence of transfected cells in beads in a high-throughput format. As a result, we obtained data points characterized by the Time of Flight (TOF), which indicates the axial size of the sample, as well as the signal of Optical Density of the object (EXT) (Figure 5-10D). We defined the regions for noise, empty beads, and beads with cells by observing the changes in the EXT, TOF and the fluorescence (FLU) intensity parameters (Figure 5-10E-G). EXT and TOF provide information about the physical properties of the beads themselves, while FLU supplies data concerning the presence or absence of the fluorescent cells. We observed a weak signal of fluorescence in empty beads that originates from the Matrigel, which normally expresses low autofluorescence. We quantified the fluorescence of transfected cells and observed a 36% decrease in fluorescence for cells treated with siGFP cells compared to the controls (Figure 5-10C). The analysis was performed on ~700 beads within 5 minutes per condition. We believe the approach described here could be used for any high content analysis of 3D structures, either spheroids or acini, challenged with drugs, siRNA, miRNA, expression vectors, etc.

Chapter 9.1.2 presents preliminary results on direct 3D siRNA transfection on structures encapsulated in Matrigel beads.

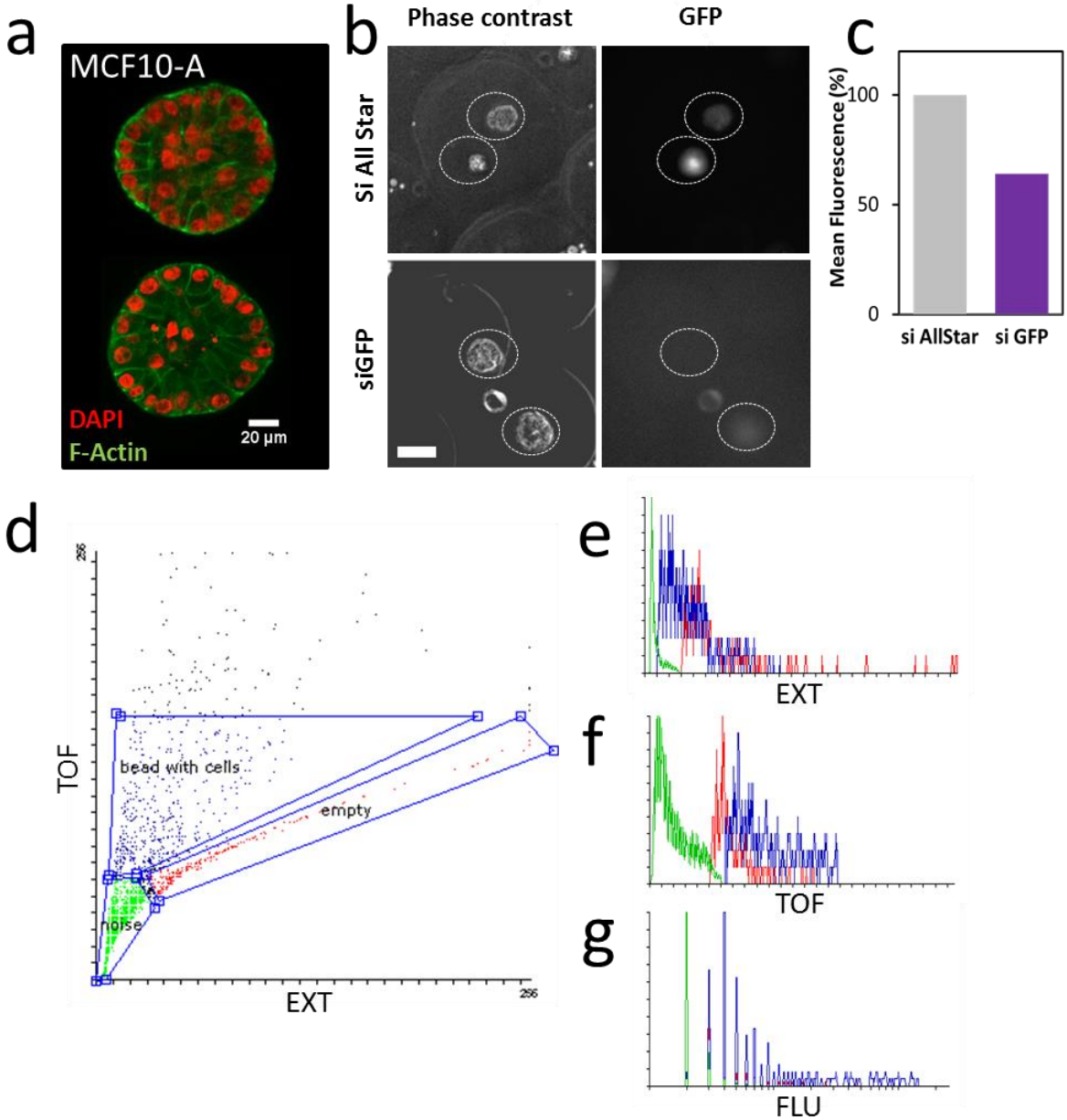

Figure 5-10 Large particle FACS (LP-FACS) analysis of 3D structures grown in beads. A) Encapsulated MCF10-A grow into acini as shown by Phallodin (green) and Hoeschst (red) staining. Scale bar 20 µm **B)** Phase contrast and fluorescent images of MCF10A-GFP cells treated with a control siRNA (siAllstar) and with siGFP. Fluorescent images represent equal times of the exposure therefore indicate the effect of decreased fluorescence in cells treated with siGFP. Scale bar 100 µm **C)** Quantification of transfection efficiency as measured by LP-FACS. **D)** The output signal indicates the dependence of the axial size (TOF) and optical density (EXT) of every object analyzed. By analyzing points based on EXT **(E)** and TOF **(F)** combined with a fluorescent signal **(G)** we distinguished beads containing cellular structures from empty ones

5.2.4 Result 2 - A single prostate cell proliferates and differentiates into an acinus

Typically, we encapsulate a single cell per bead and observe its growth and capacity to form a lumen. To prove the suitability of the system for epithelial cell culture we have used an immortalized prostate cell line RWPE1 that forms acini within 6-8 days when supported with Matrigel (Bello-Deocampo *et al.*, 2001; Webber *et al.*, 1997). Matrigel beads with encapsulated cells were pooled together and cultivated in multi-well plates and observed by means of phase contrast microscopy (Figure 5-11B). Because of the average size of the acini, which vary from approximately 90-120 µm in diameter depending on maturity, we used the 250-µm device to produce beads of 250 µm in diameter. At this bead size, the nutrients freely reach cells and there is no risk that the structure will become bigger than its surrounding environment, which would result in cellular reorganization into a monolayer. Cell viability was not influenced by the performance of the system (Figure 5-11C). Increased flow rate for high-throughput production of droplets, which induces circulation of a droplet internal liquid (Jakiela *et al.*, 2012), did not affect cell viability. We further investigated the rate of growth by measuring the diameter at different time points assuming a spherical geometry at all stages (Figure 5-11A). In comparison with standard 3D culture, acini in beads presented a higher rate of growth at day 5, which might be a result of the presence of nutrients in excess (Figure 5-11A). On day 7, the average size of an acinus in standard culture was 100 µm (analyzed structures, n = 35) *versus* 120 µm (analyzed structures, n = 27) when grown in beads. Furthermore, the homogeneity of the size of structures grown in beads was statistically higher compared to structures grown under embedded conditions (Figure 5-11A and inset Figure 5-11A). We further evaluated the efficiency of lumen formation by delineating cell membranes by phalloidin staining and subsequent confocal observation. We included structures that initiated or completed lumen formation in the category of lumen formation, as presented in Figure 5-11D. Spheroids were characterized and counted as structures with tightly packed cells in the lumen. We found that, after 6 days in culture, 80% of the 3D structures exhibited lumen formation while only 20% were classified as spheroids (Figure 5-11D). The average size of the lumen-forming structures was slightly bigger (72 µm) compared to spheroids (67 µm). Interestingly, contrary to the top-coat conditions which induce ~70-80 % of acini only 16% of RWPE1 3D structures showed detectable lumen formation when cultivated in the 3D embedded culture (please refer to Chapter 4).

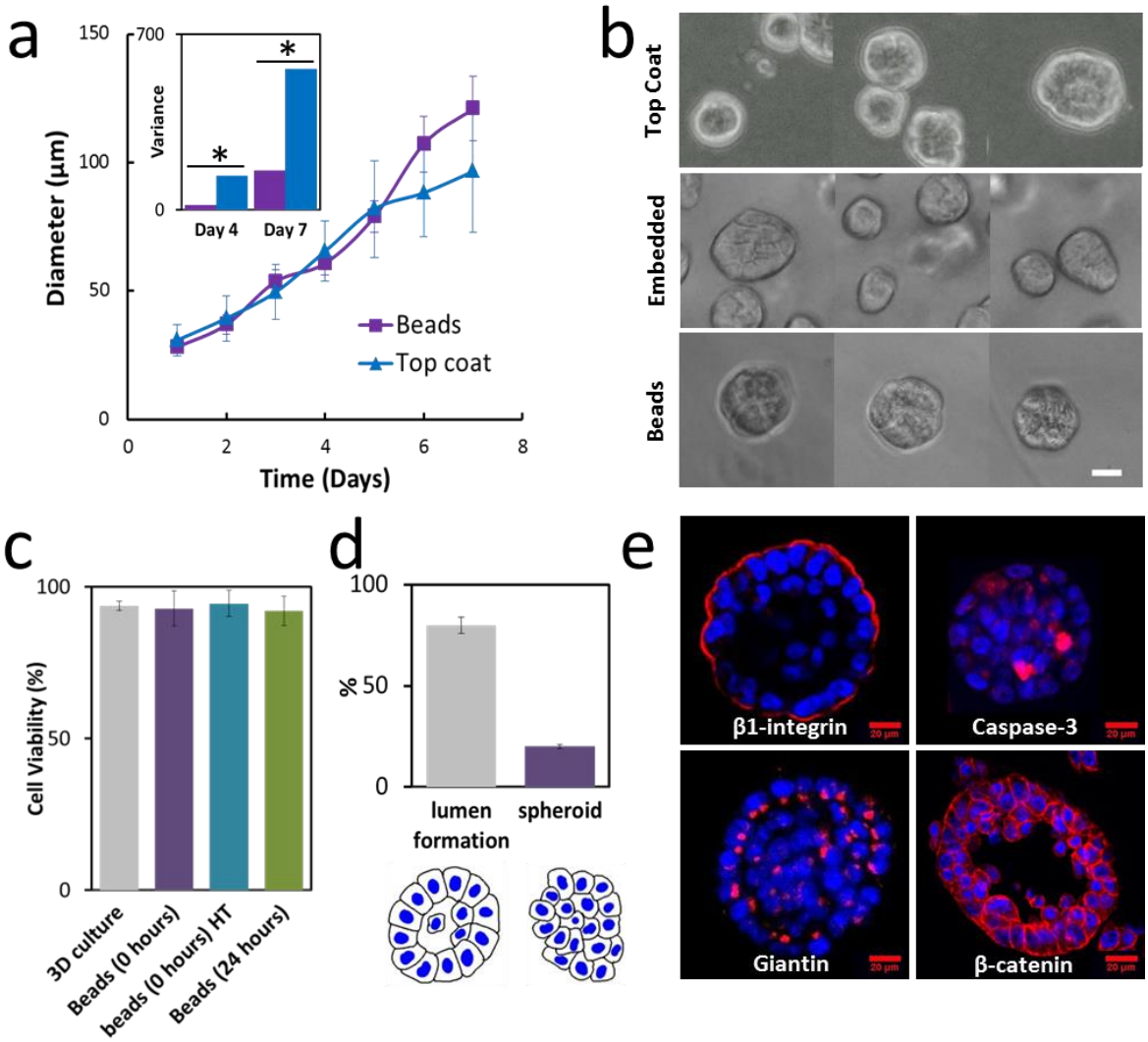

Figure 5-11 Epithelial cell culture in beads. A) Graph shows the rate of growth (according to the diameter) of 3D structures culture in beads (violet) and in *top-coat*s (blue) over 7 days. Inset represents the difference in variance of diameter between these two protocols and * indicates the statistically significant difference in variance as tested with F test (at significance level 0.05). **B)** Phase contrast images of structures grown in beads as isolated cells and under embedded and *top-coat* conditions. Scale bar 20 µm. **C)** Encapsulation of cells in a microfluidic system does not influence the viability as compared to standard 3D culture. **D)** Efficiency of lumen formation within the 3D structures grown in beads for 6 days. **E)** Acini grown in beads have proper polarity as shown with b1-intergrin, giantin and β-catenin. Lumen formation occurs via apoptosis as shown by active-caspase 3 staining. Nuclei were stained with Hoechst (blue). Scale bar 20 µm.

Encapsulation of a single cell per bead provides homogenous conditions in the whole culture and also provides a physical barrier to prevent the migration and the aggregation of cells. With standard 3D conditions, when cells are cultured together it is impossible to investigate whether acini formation proceeds by clonal growth from a single cell (hollowing) or via a process of aggregation and subsequent differentiation (cavitation). Culture performed in beads provides the first system in which acini development can be traced from the very first cell division and the underlying mechanism can be temporally and spatially defined. The process of lumen formation is dependent on the establishment of the apico-basal polarity of cells (Bryant and Mostov, 2008). In beads, lumen formation relies on the mechanism of apoptosis of cells in the center of the structures, which we showed by active-caspase-3 immunostaining (Figure 5-11E). The apico-basal polarity is established along the lumen formation, which we confirmed with a basal ß1-integrin marker, a baso-lateral ß-catenin marker and giantin, which recognizes the Golgi apparatus of apical membranes (Figure 5-11E). We also performed cryo-sectioning to show the feasibility of this technology and to address the issue of lumen formation (Figure 5-11E –ß-catenin staining). We have been able to show unambiguously that one single prostate cell can form a fully polarized acinus. However, we do not know how neighboring cells may influence this process.

5.2.5 Result 3 - Single prostate cells rely on autocrine signals to initiate acinus formation

In the majority of *in vitro* cell culture techniques, cells proliferate in an environment rich with signals originating from neighboring cells. According to the generally accepted concept of glandular tissue development based on *in vitro* 3D culture, the acinus is formed by cellular proliferation or aggregation and subsequent apoptosis of cells that do not have contact with the extracellular matrix (ECM) (Debnath *et al.*, 2003). To date, classical 3D culture techniques have not allowed the analysis of pathways crucial in development from single cells that are isolated from paracrine signals. We used our microfluidic encapsulation technique to maintain a single cell with a controlled size and microenvironment in complete isolation from other cells. To this end, we dispensed microbeads in microtiter plates in a manner such that a single well contained a single microbead encapsulating a single cell (Figure 5-12A and 5-12B). Typically, we chose 384-well plates due to their low well surface, which allowed microscopic observation of the entire area at once. With this experimental design, a single cell can clonally expand and form an acinus solely relying on its own genetic program and autocrine signals. We expected that the cell seeding concentration might be a limitation as it has been observed that when insufficient, it might significantly lower or prevent the proliferation of cells in *in vitro* culture (Prokop *et al.*, 2004). In standard 3D culture, we observed that a high seeding density accelerated the rate of growth and acini development (please refer to chapter 4). On average, approximately 15% of wells contained isolated single-encapsulated cells, and interestingly, in

the majority of cases, they divided and formed organized structures as detected by phase contrast and fluorescent microscopy (Figure 5-12C and 5-12D).

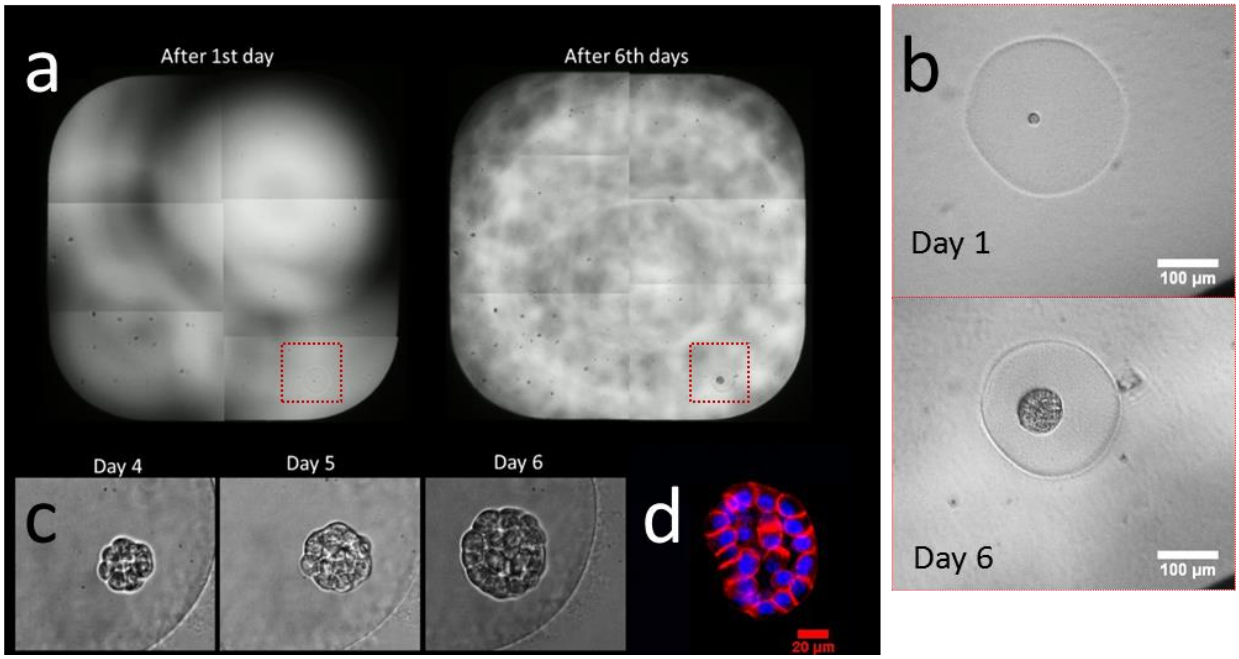

Figure 5-12 Isolated single cells rely on autocrine signals to develop into an acini. A) Beads with a single cell were isolated by dispensing into a single well of a 384 well plate and kept in culture for 6 days. The images present an overall view over the surface of a single well. **B)** and **C)** Phase contrast images presenting the growth of the acinus over time starting from a single cell. Scale bar 100 µm **D)** Fluorescent staining for actin (red) and DNA (blue) reveals the early formation of a lumen.

5.2.6 Result 4 - RNA extraction for transcriptome analysis

We tested whether our microfluidic encapsulation technology allows sufficient, high-quality RNA extraction. Trizol is a commonly used reagent for RNA extraction based on the phase separation but in the case of low cell number (some hundreds of cells) this approach proved inefficient. Instead, we evaluated popular kits specifically adapted for low cell density samples based on lysis by the buffer and further extraction through membrane columns. Those kits in standard 3D culture are not able to sufficiently digest the matrigel. As observed, lysis buffer (from Qiagen RNeasy Mini kit) was dissolved matrigel beads during first few seconds of the reaction and proved to be suitable for RNA extraction from encapsulated cells. A range of cell number (10^2, 10^3, 10^4, and 10^5 cells) has been tested in order to determine the minimal required amount of cells for RNA extraction and detection.

Table 5-2 Determination of minimal cell number for RNA extraction and further UV/VIS detection♣

Sample ID	ng/uL	A260	260/230	260/280	Const.
10 2	1,80	0,045	0,57	1,24	40
10 3	2,61	0,065	0,51	1,29	40
10 4	3,61	0,090	0,15	-6,14	40
10 5	48,75	1,219	1,48	2,01	40

RNA yields from cell number lower than 10^5 were insufficient for detection by spectrophotometric methods (Table 5-2) and thus for further analysis we used an electrophoresis-based bioanalyzer (using Picokit specially designed for RNA concentrations as small as 50 pg / µL). We were able to detect RNA from 10^3 cells but not from 10^2 cells (Figure 5-13A).

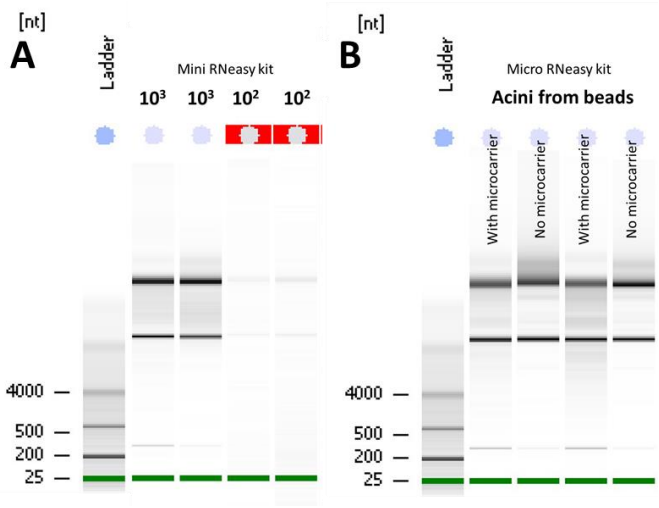

Figure 5-13 RNA extraction with A) RNeasy mini kit from 10^2 and 10^3 cells, and B) RNeasy microkit from acini grown in beads.

Since the RNeasy Mini kit is prepared to extract RNA from samples of 10^5, we decided to apply a corresponding RNeasy Micro kit that serves to extract RNA from as little as 10^2 cells. With the new kit we have successfully extracted RNA from Acini grown in Matrigel beads (around 100 acini ~5000 cells) (Figure 5-13B).

With the established protocol we extracted and analyzed RNA from isolated in 384 well plate cells at three different times points. The day 1 indicated in here a time before the first cell division occurs but after the encapsulated cell accommodates into the new environment. Because of the limited number of cells on day 1 we encapsulated a single cell per bead and exceptionally pooled them together for 5 hours. For day 3 and day 6 we isolated cells and after

♣ 260 nm determines the nucleic acid concentration; 280 nm determines the protein concentration; 230 nm determines presence of other contaminants; A260/A230 and A260/280 ratios are used to assess RNA purity

certain point of time we aspirated them from the wells and pooled together for the RNA extraction (79 structures at day 3 and 55 structures at day 6). As measured with Bioanalyzer, we obtained a good quality RNA (Figure 5-14) that is reflected by two intensive bands for 18S and 28S ribosomal RNA and the RNA integrity number (RIN) has fallen above 9. The concentration of the RNA was on the level of ~40 pg/µL which gives ~0,2-0,5ng of total RNA. This range of the total amount of RNA is low but recent advances allow amplifying RNA from as little as 1ng in total (Dafforn *et al.*, 2004; Scherer *et al.*, 2003) (also with commercially available kits i.e., Invitrogen Arcturus kit for RNA amplification) or from a single cell (Picelli *et al.*, 2014). Extracted RNAs were sent to the outsourcing platform for transcriptome analysis.

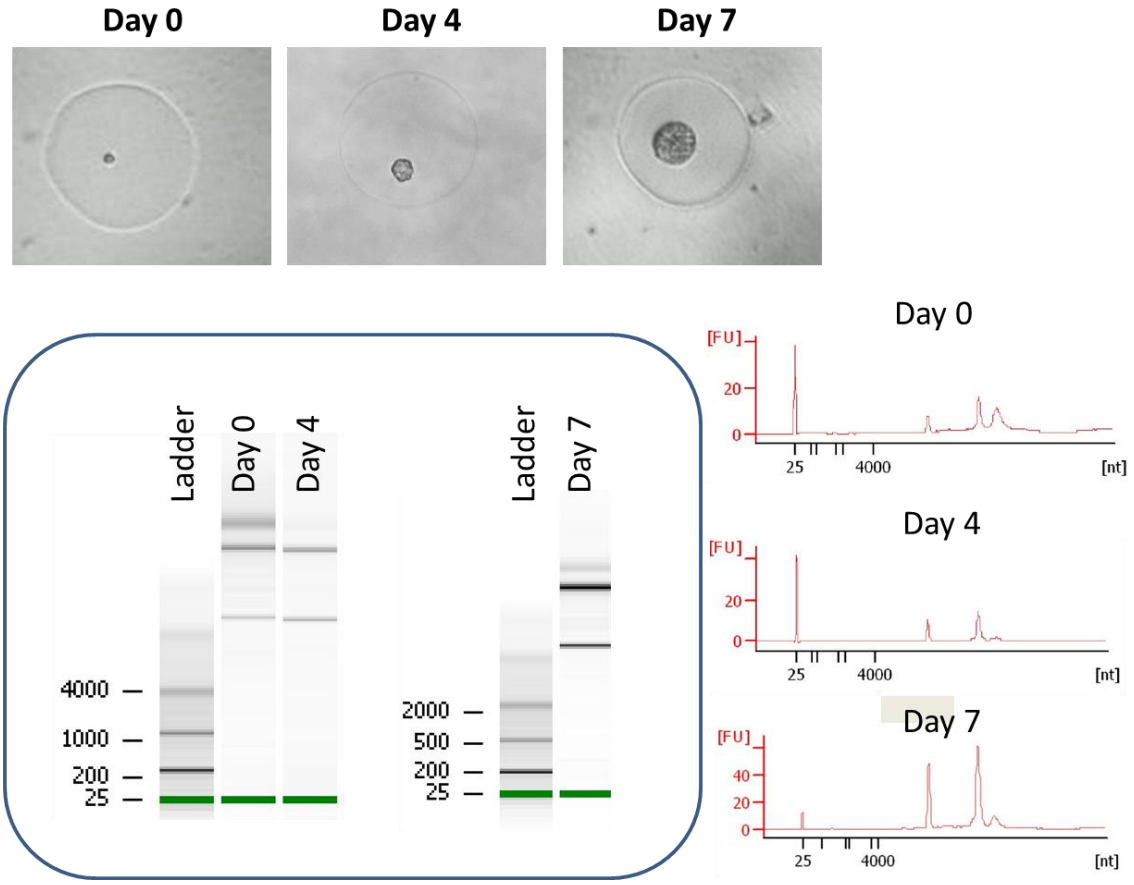

Figure 5-14 RNA extraction from isolated acini in 384-well plates. RNA has been isolated at day 0, day 4 and day 7 by using a RNEasy Micro Extraction kit (Qiagen). Extracted RNAs were analyzed with Bioanalyzer.

5.2.7 Discussion

The use of the extracellular matrix naturally extracted from a tumor, namely Matrigel, opened new avenues in *in vitro* cell culture. Its composition is highly complex (Hughes *et al.*, 2010) and not fully characterized, but it is irreplaceable for 3D cell culture assays such as acinar formation, tubulogenesis, angiogenesis, etc. However, to date the microenvironment of these 3D cultures is still poorly controlled, making studies on mechanical or chemical cues and intercellular signaling limited. Furthermore, to promote isotropic conditions in 3D culture, cells are often immobilized in the gel and analysis is mainly based on microscopic acquisitions. To access the information on polarity, it would always be necessary to use immunochemistry and microscopic analysis because the presence of the signal as well as its position within the cell is important. Thus, there is a need for a technology that would permit simpler observations of phenotypic changes such as increased proliferation, apoptosis or the presence of mesenchymal markers. To fill this technological gap, we present here a microfluidic approach to generate Matrigel droplets for cell encapsulation and subsequent cell culture in a 3D microenvironment. The system allows for massive production of single biological reactors, which on average generate a well-controlled single 3D epithelial structure.

Considering 3D culture in general, one can find a variety of different approaches (for review (Kobel and Lutolf, 2011)) including droplet microfluidic to generate collagen microbeads for 3T3 NIH and HepG2 cells-based macroscopic 3D tissue architecture (Matsunaga *et al.*, 2011). However, there are far fewer reports on epithelial 3D cell culture. Chen *et al.* proposed a 3D microfluidic method that encompasses continuous medium perfusion through microchannels located along an MCF10-A cell culture chamber (Chen *et al.*, 2011). Another report focused on the organization of the ECM and presented a system to study the importance of the orientation of collagen fibers on epithelial cell branching in 3D (Brownfield *et al.*, 2013). A broadly used micropatterning techniques brought superior control over the composition, size and thus confinement and organization of cells in 2D culture (Thery, 2010). However, the application of patterns is limited in 3D cell culture due to anisotropic mechanical properties sensed by cultivated cells. The substrate is rigid at the bottom while there is only culture medium at the top of the culture. Under these conditions, orientation of apico-basal polarity is forced rather than established by cells. Furthermore, there is a significant difference in the phenotype of cells that were cultivated on a 3D ECM compared to those cultured on a matrix of exactly the same composition that has been flattened to provide a 2D surface (Cukierman *et al.*, 2001).

Inspired by the micropatterning-based microenvironmental control for 2D cultures, we developed a droplet microfluidics approach to generate, for the first time, Matrigel droplets that would optimize the microenvironmental control of 3D epithelial cell culture. This technology, also relying on a simple microfluidic principle, requires extensive optimization of

the operational parameters of the system and of the stability of formed beads. Combining recent advances in microfluidics concerning channels treatment (Mazutis *et al.*, 2009), surfactant (Holtze *et al.*, 2008), oil and a process of cell encapsulation (Joensson and Svahn, 2012), we succeeded in creating a long-term (up to 2 weeks) 3D cell culture in Matrigel beads. These 3D epithelial structures formed a lumen and presented a proper basal and apical polarity (Debnath *et al.*, 2003), which we confirmed by immunostaining techniques. The proportion of structures with a lumen was comparable to those obtained using traditional 3D culture of RWPE1 prostate cells. The existing literature on the mechanisms of lumen formation *in vitro* indicates first clonal division and further apoptosis (anoikis) (Mailleux *et al.*, 2008). However, it has been shown that, for instance, MDCK cells grown in solution when aggregated are also capable of forming a lumen but with an oppositely oriented polarity(Wang *et al.*, 1990). By using a microfluidic approach and single cell containing-Matrigel droplets, we eliminated a possible mechanism of aggregation while maintaining paracrine/autocrine signaling. Thus, the whole population of acini has its origins from the same mechanism of development and has been exposed to exactly the same microenvironment (regarding size, composition and homogeneity). The rate of growth of acinar structures from a single cell was comparable to the rate seen in a more traditional 3D culture. Furthermore, the population of formed acini was more homogenous in size compared to when top-coat and embedded protocols were used. Superior control over homogeneity of grown structures is of great importance as it has been reported that tumor-like spheroids' response to treatment was size-dependent (Celli *et al.*, 2014).

To date, a limited number of reports presented high-throughput screen studies on epithelial cell cultivated in 3D due to the difficulties in detection automation and heterogeneity of the structures grown freely on Matrigel. The microfluidic approach of cell encapsulation we are proposing not only supplies cells with an ECM environment that promotes growth and differentiation but also keeps each single bead as a floating object that can be easily aspirated, dispensed or carried by flow. Thus, the use of flow-based FACS-like monitoring of beads is possible for high-throughput analysis of the relative size of the object, light dispersion and fluorescent signal. The limitation and accessibility is determined by the size of the object, which is non-compatible with standard FACS machines. However, it is possible to choose an LP-FACS or to construct a dedicated microfluidic platform according to previously described protocols (Mazutis *et al.*, 2013).

After demonstrating the ability to isolate a single cell per bead in a single well, we showed that the acinus relies on autocrine signals to initiate its full development. The distinction between autocrine and paracrine signals is of great importance to further understand the development of a given tissue. For example, it has been shown that branching morphogenesis relies on complex signaling between epithelial and mesenchymal cells through both paracrine and autocrine factors, while autocrine signaling of Hedgehog has been identified

as important in developing tissues from Drosophila to mammals (i.e. in neural stem cells (Cai *et al.*, 2008), large B-lymphoma (Singh *et al.*, 2010) and cerebellar dysplasia in the developing brain (Wang *et al.*, 2004)). The discovery of an autocrine signaling pathway often came along with the introduction of a new technological improvement. Here, we propose an approach that allows for the isolation of a single cell into a homogenous 3D environment simply by dispensing beads into separate wells. Multiple structures are grown separately but in parallel, originating from the same passage. This parallelization would allow the generation of sufficient encapsulated cells for large scale genomics analysis to reveal molecular mechanisms and gene networks that play a crucial role in acinar development and possibly in acinar carcinogenesis. The throughput of cell/bead complex isolation could be further improved by using robotic liquid dispensing stations. In a broader perspective, this system can serve universally either for single cell encapsulation/isolation to study autocrine signals or to control paracrine signals originating from co-culture microreactors.

An encapsulation approach has been applied to study single cells or spheroids, but to date it was not used on epithelial cells due to the necessity of using Matrigel as a material for the formation of beads. The technology we propose can be applied to various cell types that would require Matrigel to proliferate and differentiate. Furthermore, this is the first technique that allows for the analysis and subsequent sorting of 3D living cells. The high-throughput nature of the encapsulation approach relies on the i) simultaneous formation of hundreds of thousands of homogenous bioreactors, ii) possibility of using automated liquid-dispensing robots to manipulate beads, and iii) use of the flow-based analytical methods. Thus, this system opens new avenues of research in both epithelial development and carcinogenesis.

Although tumor development is undoubtedly governed by genetic alterations and biochemical cues, the mechanical cues are finding their moment of general interest (Butcher *et al.*, 2009). However, in 3D culture, studying internal and external forces by altering the environment has been challenging. The spherical environment provided by beads can be considered isotropic for mechanical properties, composition and the diffusion of nutrients. Under such conditions, the apico-basal polarity and organization is governed and established by cells. Because the process of droplet formation is highly repeatable under laminar flow conditions, it is possible to produce thousands of identical bioreactors. As the Matrigel lacks control over rigidity and is considered to be a compliant matrix, only polyacrylamide-Matrigel coated substrates have thus far been used to study the effect of stiffness on the function, organization and differentiation of cells (Paszek *et al.*, 2005). Use of the beads and a corresponding approach to control rigidity of the environment by altering the mechanical properties of a second gel that immobilizes the beads (preliminary results are presented in Chapter 9.1.3), we anticipate that our microfluidic system can do the same for 3D culture as micropatterning techniques do for 2D culture.

6. Mimicking ductal environment of exocrine glands using circular-shaped microchannels

Presented in this chapter work has been motivated by the ANR Brocoli (2011-2014) project which aims to identify new biomarkers in prostate cancer by analysis of epithelial secretion liquids. The core of Brocoli project was to characterize a novel 3D culture system using polyelectrolyte (PE) scaffolds to construct *in vitro* 3-dimensional (3D) culture models of prostate tissue and to discover ways to control the microenvironment of cell growth so as to understand (i) the exocrine gland morphogenesis into cell differentiation, and (ii) acini formation and to understand the breakdown of tissue architecture and disorganisation of acini during disease and cancer. The approach aimed to create 3D branched luminal structures by seeding epithelial cells on polyelectrolyte films of a form of tubules. Polyelectrolyte films were chosen because they are an ideal material for scaffold preparation due to *i)* the simplicity of layer-by-layer♣ method of assembly, *ii)* possibility to modulate surface properties, *iii)* low cost and *iv)* no cyto-toxicity. We have shown that cell phenotype (morphology, adhesion, apoptosis etc.) can be modulated by the charge of the terminating polyelectrolyte layer. Publication describing this work is presented in *Chapter 7 – Other Publications*.

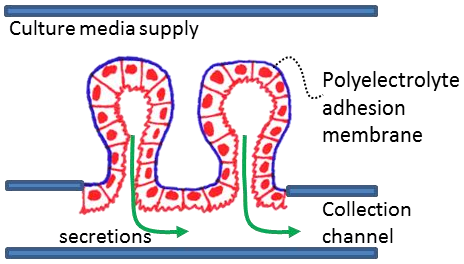

Figure 6-1 Schematic representation of a microfluidic system for collection and further analysis of epithelial secretion liquids.

The initial approach for the lab-on-chip device to analyze secretions liquid was based on preparation of a tubular mold whose shape resembles a set of tubules terminated with a cyst (Figure 6-1). Parallelization is needed due to low-concentration of secreted molecules. Subsequently polyelectrolytes (PAH and PSS) will be assembled according to layer-by-layer

♣ Polyelectrolytes are able to form complexes with oppositely charged species that are stabilized by electrostatic interactions. Layer-by-layer assembly relies on alternate coating of surface with positively and negatively charged polyelectrolytes (i.e., Polyallylamine hydrochloride and poly(sodium 4-styrene sulfonate)).

technique in order to prepare substrate for cell growth. Cells infused into these polyelectrolyte-formed niches (dimensions: height of the tubule 100 μm and width 80 μm) attach and proliferate to form confluent epithelial layers. Such constructs would be kept inside a microfluidic chip containing two compartments; first for the collection of secretions and second for culture media supply and epithelial layer stimulation.

However, little is known how epithelial cells proliferate in such constraint environments and what are the differences between standard and micro-scale cell culture in case of i.e., diffusion of nutrients and oxygen. Therefore, a simple prototype has been developed. It served to i) confirm polyelectrolytes films assembly, ii) show feasibility of cell infusion and subsequent adhesion and growth on polyelectrolyte films, iii) verify the limits that result from the micro-scale of the device. One of the important advances is the simplicity of circular channels fabrication which is rapid and does not require use of any specialized equipment. Results are presented below in the form of a publication.

List of authors: Monika E. Dolega, Jayesh Wagh, Sophie Gerbaud, Frederique Kermarrec, Jean-Pierre Alcaraz, Donal K. Martin, Xavier Gidrol, Nathalie Picollet-D'hahan

The publication would not take place without following authors' contributions:

Design of research:	M.D., X.G., D.M., N.P.D.
2D cell culture:	M.D., S.G., F.K.,
3D culture, immunostainng:	M.D., J.W.
Fabrication of systems:	M.D., J.W.
Polyelectrolyte coatings:	M.D., J.W., J-P.A.
Microscopic acquisitions:	M.D., J.W.
Analysis of results:	M.D., X.G., D.M., N.P.D.
Manuscript preparation:	M.D., X.G., D.M., N.P.D.

OPEN ACCESS Freely available online

PLOS | ONE

Facile Bench-Top Fabrication of Enclosed Circular Microchannels Provides 3D Confined Structure for Growth of Prostate Epithelial Cells

Monika E. Dolega[1,2,3], Jayesh Wagh[1,2,3], Sophie Gerbaud[1,2,3], Frederique Kermarrec[1,2,3], Jean-Pierre Alcaraz[4], Donald K. Martin[4], Xavier Gidrol[1,2,3], Nathalie Picollet-D'hahan[1,2,3]*

1 Univ. Grenoble Alpes, iRTSV-BGE, Grenoble, France, **2** CEA, iRTSV-BGE, Grenoble, France, **3** INSERM, BGE, Grenoble, France, **4** UJF-Grenoble 1, CNRS, TIMC-IMAG UMR 5525 (SyNaBi), Grenoble, France

Abstract

We present a simple bench-top method to fabricate enclosed circular channels for biological experiments. Fabricating the channels takes less than 2 hours by using glass capillaries of various diameters (from 100 μm up to 400 μm) as a mould in PDMS. The inner surface of microchannels prepared in this way was coated with a thin membrane of either Matrigel or a layer-by-layer polyelectrolyte to control cellular adhesion. The microchannels were then used as scaffolds for 3D-confined epithelial cell culture. To show that our device can be used with several epithelial cell types from exocrine glandular tissues, we performed our biological studies on adherent epithelial prostate cells (non-malignant RWPE-1 and invasive PC3) and also on breast (non-malignant MCF10A) cells We observed that in static conditions cells adhere and proliferate to form a confluent layer in channels of 150 μm in diameter and larger, whereas cellular viability decreases with decreasing diameter of the channel. Matrigel and PSS (poly (sodium 4-styrenesulphonate)) promote cell adhesion, whereas the cell proliferation rate was reduced on the PAH (poly (allylamine hydrochloride))-terminated surface. Moreover infusing channels with a continuous flow did not induce any cellular detachment. Our system is designed to simply grow cells in a microchannel structure and could be easily fabricated in any biological laboratory. It offers opportunities to grow epithelial cells that support the formation of a light. This system could be eventually used, for example, to collect cellular secretions, or study cell responses to graduated hypoxia conditions, to chemicals (drugs, siRNA, …) and/or physiological shear stress.

Citation: Dolega ME, Wagh J, Gerbaud S, Kermarrec F, Alcaraz J-P, et al. (2014) Facile Bench-Top Fabrication of Enclosed Circular Microchannels Provides 3D Confined Structure for Growth of Prostate Epithelial Cells. PLoS ONE 9(6): e99416. doi:10.1371/journal.pone.0099416

Editor: Ted S. Acott, Casey Eye Institute, United States of America

Received December 19, 2013; **Accepted** May 14, 2014; **Published** June 19, 2014

Funding: This research was funded by a grant from the French Agence Nationale pour la Recherche (ANR-11- BSV5-009) and supported by the CEA IRTELIS international PhD program. The funders had no role in study design, data collection and analysis, decision to publish, or preparation of the manuscript.

Competing Interests: The authors have declared that no competing interests exist.

* Email: nathalie.picollet-dhahan@cea.fr

Introduction

Model systems that recreate the architectural features observed in tissues and in tumours are of prime interest to study morphogenesis and carcinogenesis. Indeed in order to better mimic the reality of tissues compared to standard 2D culture, a growing number of 3D cell culture devices are being introduced to provide controlled mechanical, chemical and biological cues [1]. Numerous approaches have emerged that are aimed to control the spatial and temporal properties of the cell microenvironment (e.g. stiffness, 3D structure, micropatterning, shear stress). Endothelial cells cultured within a chamber capable of applying physiological shear stresses are induced to differentiate due to stimulation of specific integrin/endothelial cell-mediated signalling cascades [2]. Also, epithelial cells cultured on soft extracellular matrix gels organize themselves into polarized structures that strongly resemble functional tissue in vivo [3,4]. For in vitro studies of vascular tissue, lab-on-chip (LOC) systems [5] that incorporate a unique 3D and dynamic microenvironment with high spatiotemporal precision provide a physiologically relevant way to reproduce vascular tissues.

However, despite the high prevalence of life-threatening diseases and cancers that affect exocrine glands, there are fewer reports of LOC systems to investigate exocrine ductal/acinar systems. We report here a microfluidics-based system that is simple to fabricate and provides 3D scaffolds that mimic epithelial-lined ductal systems of glandular tissues.

Microfluidics in general provides advantages such as *(i)* manipulation of liquids and objects at the microscale, *(ii)* high precision in controlling flow in low Reynolds number regimes ($<<1$), and *(iii)* facilitation of high-throughput experimentation by on chip parallelization and greatly reduced volume of expensive reagents and number of cells. Moreover, microfluidic systems have already allowed multiple biological studies including protein crystallization [6], collection of cellular secretions [7], blood circulation [8], angiogenesis [9] and cellular co-cultures [10].

Fabrication of microfluidic devices usually is based on micromachining of polymers such as poly(methyl methacrylate) [11], polycarbonate [12] or soft lithography with the use of polydimethylsiloxane (PDMS) [13]. The first technique requires the use of a milling machine and additional chemical treatments to bond different surfaces, while the latter relies on the use of highly equipped and specialized clean room facilities. To date, the most

common profile of fabricated microchannels is rectangular. However, that profile does not reflect biological reality and more particularly the rheology of circular ducts (e.g. venules, arterioles, capillaries) nor tubular epithelial structures that are found in vivo. The rectangular microfabricated profile limits bio-applications and needs to be improved.

There are previous reports of the fabrication of microchannels in materials suitable for cell culture. Among them, Tien's group used a similar method to fabricate circle channels in collagen hydrogels and investigates biology issues [14–16]. Wilson et al also described a method to obtain circular channels by combining mechanical micromilling with soft lithography [17]. Another approach relied on gas infusion into rectangular channels filled with a pre-polymerized agent [18,19]. Despite the successful fabrication with the above techniques, they remain complex and time-consuming. A different approach to form circular channels was based on the moulding of nylon threads [20] or metal microwires [21] embedded inside a block of cross-linked PDMS and then removal. The technique did not require any bonding and created multichannel devices with circular channel diameters around 20 µm for microwires and larger than 50 µm for nylon threads. However, it was necessary to swell the PDMS with ethanol, triethylamine or chloroform for several hours before removal of threads or wires from the mould. That process therefore excludes the potential use of such systems for biological experiments due to the detrimental effect of organic swelling-solvents on living cells. A similar approach was also presented by Perry et al [22] for optically based flow cytometry studies of red blood cells. However, all these microfluidics systems are based on complex manufacturing processes that only a laboratory experienced in the field can reproduce. Furthermore, the previous systems lack biological validation with adhering cells and further characterization using specific markers of the organization or the morphology of the cells lining the walls of the tubes.

To overcome these limitations, we present a ready-to-use, simple and rapid method to fabricate single straight circular channels of various diameters for studies of adherent cells and for manipulation of the cellular microenvironment. Our technique takes about 2 hours and is based on the use of glass capillaries combined with corresponding needles that together serve as a mould for PDMS or hydrogel-based devices. We show here the biocompatibility of our system with various epithelial cells lines that grow stably inside the microchannels. Epithelial cells were chosen for three reasons. First, in 3D culture, they reproduce essential structural features of glandular epithelium in vivo, with the presence of a centrally-localized, hollow lumen and the polarization of cells surrounding that lumen. Second, we previously observed that some polyelectrolytes (PE)-terminating films preferentially modulate the 2D growth characteristics of prostatic cancerous cells [23]. Third, our previous data showed that prostatic cancerous cells are able to organize in 3D-confined tubular scaffolds [23]. In this study, we go further in showing the influence of the 3D microenvironment in tubes on epithelial cell morphology and proliferation by coating the microtubes either with a layer-by-layer assembled PE film or with Matrigel The PE film provides a tunable surface environment for external manipulation of cells and the Matrigel is typically used to mimic the complex extracellular environment found in many tissues. Our microchannel system allowed formation and access to an artificial lumen that allowed us to study cell morphogenesis and the events occurring during cells populating the lumen, such as in carcinogenesis. The microchannel ductal system allowed us to perform immunostaining and fluorescence microscopic observations of cells fixed inside the microchannel directly and without any special adjustment of the lumen.

Materials and Methods

1. Fabrication of Microchannels

A step-by-step protocol to fabricate enclosed circular channels is presented in Figure 1 and is fully detailed in Figure S1 and Table S1 in File S1. The enclosed 3D cellular scaffolds were fabricated using glass capillaries as the mould to form circular microchannels (Figure 1). This bench-top fabrication procedure enables the preparation of multiple channels in parallel. For each experiment around 10 tubes were manufactured at one time within only two hours. Glass capillaries were mounted with needles which were immobilized by a drop of nail polish (Figure S1 in File S1). The capillary/needle assembly was positioned on two stacks to enable microscopy observations by controlling the distance between the channel and the surface of the PDMS. Degassed PDMS was poured into a petri dish to submerge the entire capillary architecture and then left to polymerize. After the PDMS had solidified it was removed from the petri dish and cut at the middle point of the needle to allow access to the assembly. Needles and subsequently, glass capillaries were gently removed with pliers (Figure S1 in File S1). This appropriate choice of capillaries (diameters and walls thicknesses) eliminates the need use ethanol or chloroform for smoothing PDMS prior to removing the capillaries. With these proper dimensions capillaries have also a very low tendency to break (less than 10% of capillaries, on n = 10 used in this work). New needles were inserted to allow injection of chemicals, nutrients and cells.

2. Coating of Microchannels

For biological assays, the inside of the PDMS microchannels was coated with a thin film of either polyelectrolytes or Matrigel (BD Biosciences, San Jose, CA, Ref 356231), which is widely used for 3D culture of epithelial cells due to its ability to promote specific cellular organization [3] and in case of endothelial cells for sprouting experiments. The thin film of polyectrolytes was achieved using Layer-by-Layer (LbL) assembly of the polyelectrolytes PSS (poly (sodium 4-styrenesulphonate; Sigma 243051)) and PAH (poly (allylamine hydrochloride; Sigma 283223)). They present different surface charges (polyanions for PSS and polycations for PAH) depending on the choice of the terminating layer. Also, the number of coatings modulates the mechanical and chemical properties. The process of deposition previously described [24] was adapted to this format of the microchannels (see Figure S2 in File S1). Since the polyelectrolytes bind Rhodamine B (Sigma, Ref R6626), the uniform coating of polyelectrolyte inside PDMS microchannels was confirmed by including Rhodamine (10 µg/ml) with the polyelectroytes. The microchannels were coated with the Rhodamine B/polyelectrolyte solution for 5 min at a flow rate of 1 $ml.h^{-1}$ using a syringe pump.

The thin film of Matrigel was achieved by adapting a protocol for coating that is commonly used for 2D culture on glass and plastic substrates. We infused a diluted Matrigel (1:40 in culture medium) into the microchannels for 30 minutes at RT and then washed the Matrigel solution out by culture medium.

3. Cell Lines and 2D Cell Culture

Adherent epithelial prostate cells (non-malignant RWPE-1 and invasive PC3) and breast (non-malignant MCF10A) were used. These cells form tree-like tubule structures with a hollow lumen when cultured in 3D [4], which mimic the *in vivo* glandular epithelial tissue architecture [25]. RWPE-1 (ATCC Ref. CRL-

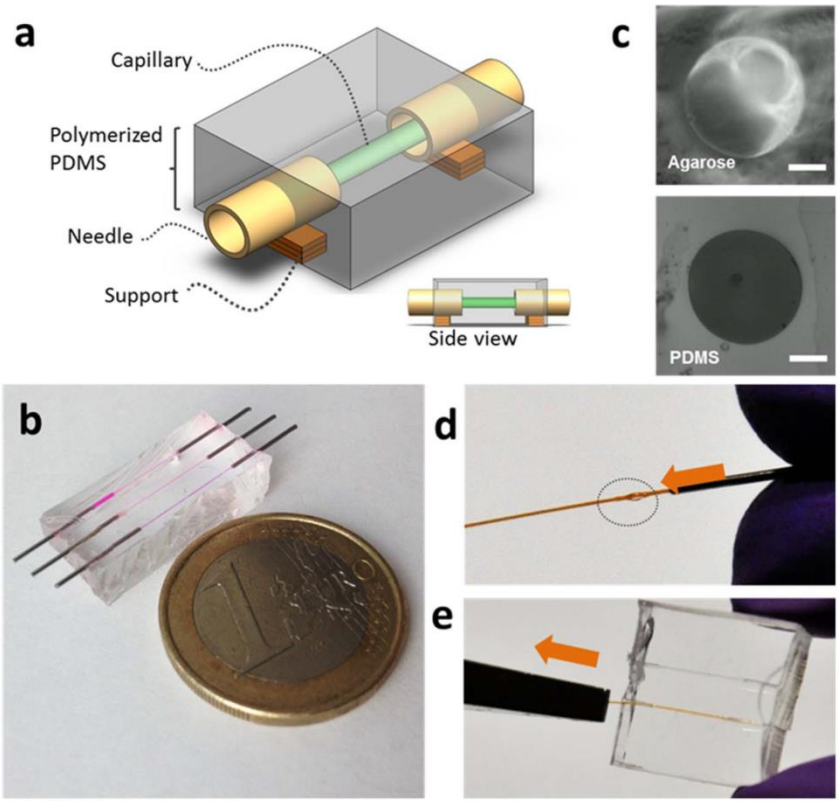

Figure 1. Microchannels fabrication process. Scheme of the device (**a**); Microphotograph of the device. One Euro coin added as a scale (**b**); Phase contrast pictures of cross section of channels fabricated in PDMS and agarose (**c**); Steps of fabrication (**d**) and (**e**). More detailed information provided in Figure S1. Scale bar 50 µm.
doi:10.1371/journal.pone.0099416.g001

11609) and MCF10A (ATCC Ref. CRL-10317, gift from Odile Filhol, Inserm U1036, CEA Grenoble, France, [26]) cells respectively mimic normal prostate and breast epithelial cell behaviour as characterized by a well-established polarized morphology [4], whereas PC3 cells (ATCC Ref. CRL-1435) represent tumorigenic cells at a highly invasive stage of neoplastic transformation with the loss of acinar morphogenesis. PC3 cells (prostate carcinoma) were routinely cultured in RPMI Glutamax culture medium (Invitrogen, Ref. 61870-010) supplemented with 10% fetal calf serum (PAA, Ref. A15-101) and 1% penicillin/streptomycin (Invitrogen, Ref. 15140-122). RWPE-1 cells (non-neoplastic human prostate epithelial cells) were maintained in KSFM (Life Technologies, Carlsbad, CA, Ref. 17005-075) supplemented with 5 $ng.mL^{-1}$ epidermal growth factor (EGF) and 50 $\mu g.mL^{-1}$ bovine pituitary extract. For passaging, cells were washed with Dulbecco's Ca^{2+}/Mg-free PBS (D-PBS, Life Technologies, Ref. 14190) and incubated with 1 mL trypsin-EDTA (Lonza, Basel, CH, Ref. CC-5012, 0.25 $mg.mL^{-1}$) for approximately 7 minutes, as previously described. MCF10A cells were maintained and cultured according to the protocol of Debnath et al [27]. All cells were routinely cultured in a humidified atmosphere at 37°C and 5% CO_2. For all experiments cells were supplied every day with fresh culture medium.

4. 3D Cell Culture

Acinar morphogenesis assay was performed according to the previously published top-coat protocol [3]. Matrigel was thawed overnight and poured into either 4-well (160 µL of Matrigel, 500 µL of culture medium) or 8-well Labtek (90 µL of Matrigel, 250 µL of culture medium) plates on ice. Then, the plates were incubated for 30 minutes at 37°C in order to polymerise the Matrigel. After polymerizing the Matrigel cells were seeded in half the final volume (e.g. 5000 cells in each well of the 8-well Labtek plate) and allowed to adhere for approximately 45 minutes. The top coat layer of 8% Matrigel in culture medium was slowly poured over the attached cells. The culture medium was changed every other day.

5. Immunostaining in 2D and in 3D Culture

For 3D culture cells were fixed with 4% (v/v) paraformaldehyde (PFA) in PBS for 20 minutes and then washed once with PBS. 2D cultures were maintained until the cells attained 70% confluency and then were fixed with 4% (v/v) PFA in PBS for 20 minutes and then washed once with PBS. To prevent the nonspecific adsorption of antibodies, the cells were incubated with 0.1% BSA and 10% goat serum for 1 hour. The primary antibodies (anti-Giantin, Abcam ab24586, 1/500; anti-caspase 3 active, Millipore AB3623, 1/300; anti-beta4-integrin, Millipore MAB1964, 1/250; anti-centrosome, kind gift from M. Thery, CEA Grenoble, F) were dissolved in PBS^{+}, Tween20 0.05%, and 5% goat serum. The cells were incubated for 1 hour with the appropriate antibody and then washed 4x with for a total of 45 minutes. The cells were then incubated with secondary antibody (Jackson, dilution 1/500 in PBS^{+}, Tween20 0.05%, and 5% goat serum). Cells were subsequently washed 4 times for

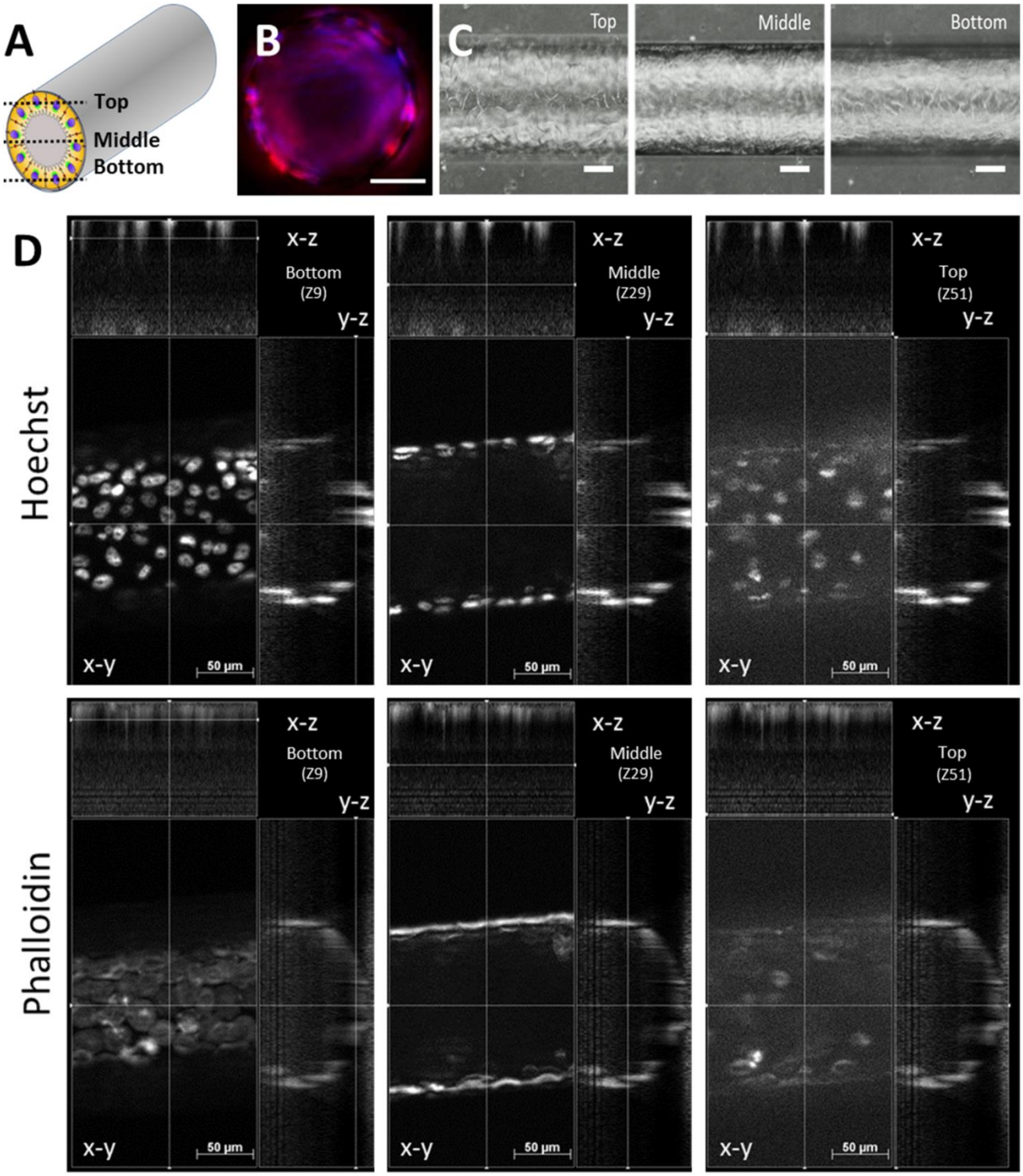

Figure 2. Epithelial cellular organization and proliferation inside fabricated microchannels. A. Schematic representation of an epithelial cell monolayer covering the inner wall of the circular channels fabricated in polydimethylo-siloxane (PDMS). **B.** Cross-section of a microchannel formed in PDMS and coated with Matrigel. Cells infused into channels adhere to 3D-confined scaffolds and form a confluent layer (Actin in red, nuclei in blue). Bar 50 µm. **C.** Organization of MCF10A cells forming a confluent monolayer after 5 days of growth inside a Matrigel-coated tube (diameter 150 µm). Phase contrast images. Note that the focus of each image is at different plane (top, middle and bottom of the tube as indicated in A.). Scale bar = 100 µm. **D.** Apotome Z-stack of PC3 cells on PSS substrate stained with Hoechst (top panel) and Phalloidin (lower panel). Separate-channel images are shown and three positions of the tubes (as indicated in A) are viewed.
doi:10.1371/journal.pone.0099416.g002

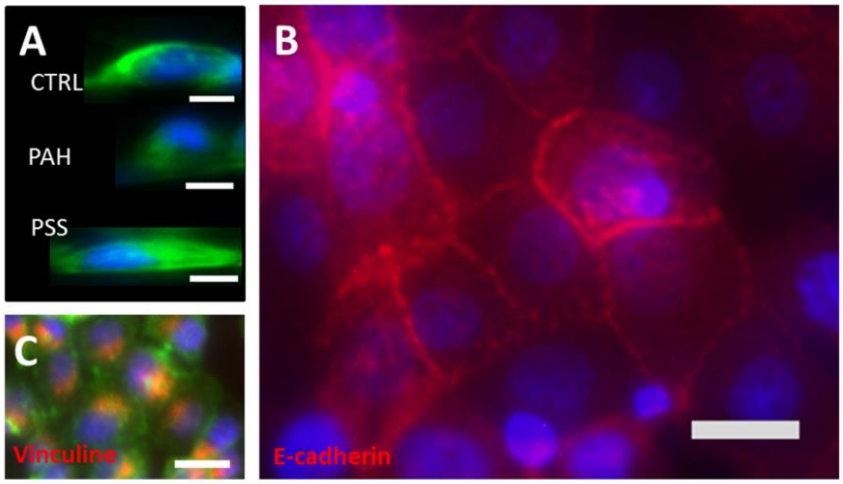

Figure 3. Epithelial cellular morphology and adhesion inside fabricated microchannels. A. Focus at midline of a circular channel provides direct view of RWPE1 cell and nuclei shape that vary according to PE coating. Bar 10 µm. **B.** Membrane junction structures of RWPE1 cells adhering in tubes. Expression of E-Cadherin (red) reveal intercellular junctions formed in the confluent monolayer of cells lining the inner wall of the tubes (240 µm diameter). Nuclei in blue (DAPI). Scale bare 25 µm. **C.** Adhesion of PC3 cells in Matrigel coated channels of 150 µm in diameter. Focal adhesion points (Vinculin) in red, nuclei in blue (DAPI) and actin in green (Phalloidin). Scale bare 25 µm.
doi:10.1371/journal.pone.0099416.g003

15 minutes with PBS. Nuclei and actin were stained as described hereafter.

6. Static and Flow-based Infusion of Cells into Microchannels

Chemical dissociation of the cells was carried out by incubation for 5 min at 37°C in Trypsin-EDTA (Life Technologies, Ref. 25300-054) in calcium/magnesium-free PBS. Cells were then infused into microchannels using syringe/tubing connected to the device at high concentration of 3×10^6 cells.mL^{-1} in order to infuse a sufficient number of cells into the microchannel. A syringe pump with an adjustable flow rate was the best choice to provide a gentle and controlled infusion. For static experiments, the chip with cells was positioned within a petri-dish and immersed in culture medium to prevent any evaporation from the channels. It is unnecessary to apply a constant flow of culture medium through the microchannel. For flow experiments, cells were infused into microchannels and kept in static conditions for 24 hours to promote satisfactory cellular adhesion. Stable and continuous flow was introduced by use of Fluigent pressure pumps (Fluigent, France). Pressurized containers with culture medium were set up within the CO_2 and temperature controlled chamber. The flow rate was adjusted around 5–10 µL.h^{-1} (~10 mbar) and adhesion and proliferation of cells were observed in time. All samples were kept in a humidified incubator at 37°C and 5% CO_2.

7. Immunostaining and Viability Test in Microchannels

Phalloidin was used to identify cortical actin filaments, which follow the contours of the plasma membrane and hence provide a reasonable means to delineate the extent of the cell and its membrane. E-cadherin was used to detect cell-cell junctions. Immunostaining in microchannels was carried out by infusion with a syringe pump at room temperature throughout. RWPE-1 cells were plated in microchannels at a density of 6×10^6 cells.mL^{-1} of culture. After the cells had formed a confluent layer (between 5–7 days), they were fixed for 20 minutes with 4% (v/v) PFA in a solution composed of 10% sucrose in cytoskeleton buffer (solution A). Then cells were washed with solution A and permeabilized for 3 minutes with 0.1% Triton TX-100 in solution A. The PFA auto-fluorescence was quenched by TBS 1X for 10 minutes, followed by washing with PBS for 30 minutes. Non-specific sites were blocked by exposure to 10% goat serum and 3% BSA in PBS and cells were incubated with the primary antibody for 1 hour. The primary antibody was E-Cadherin (Abcam, Ref. ab1416) diluted to 1/50 in 0.1% Tween-20 and 1% BSA in PBS. Cultures were then washed for 30 minutes with PBS and incubated with anti-mouse Cy3 conjugated secondary antibody (Jackson, Ref. 115-162-062) diluted to 1/1000 and Phalloidin FITC (Sigma, Ref. P5282) diluted to 1:1000 in 0.1% Tween-20 and 1% BSA in PBS for 20 minutes. After washing for 30 minutes with PBS, nuclei were counterstained with Hoechst (Life Technologies, Ref. H-1399), diluted to 1:7000, for 5 minutes. A last wash was performed for 10 minutes and Dako fluorescent mounting medium was infused manually.

Focal adhesion points were detected by labelling using Vinculin. For Vinculin immunostaining cells were pre-permeabilized for 40 seconds with Triton X-100 and fixed with 4% (v/v) PFA in PBS for 20 minutes and washed once with PBS. To prevent any nonspecific antibody adsorption cells were incubated with 0.1 BSA and 10% goat serum for 1 hour. Primary antibody against Vinculin (Sigma, Ref. V9131) at 1:700 dilution (dissolved in PBS$^+$, Tween 20 0.05%, and 5% goat serum) was incubated for 1 hour and followed by 4 PBS washes in total for 45 minutes. Cultures were then incubated with anti-mouse Cy5 (Jackson, dilution 1/500 in PBS$^+$, Tween 20 0.05%, and 5% goat serum). Microchannels were subsequently washed 4 times for 15 minutes with PBS. Nuclei and actin were stained as described above. A Live/Dead Viability test was performed by use of Calcein AM (Molecular probes, C3099) and Propidium Iodide (Molecular Probes, V13245) according to the manufacturer's protocols provided with the products.

8. Fluorescence Microscopy

The microchannels with cells inside were observed using the AxioImager Z1 Zeiss microscope with a 20x objective equipped with the straight Apotome module for z-stack acquisitions (one image in z-axis every 3 µm for a 150 µm-diameter tube). Images

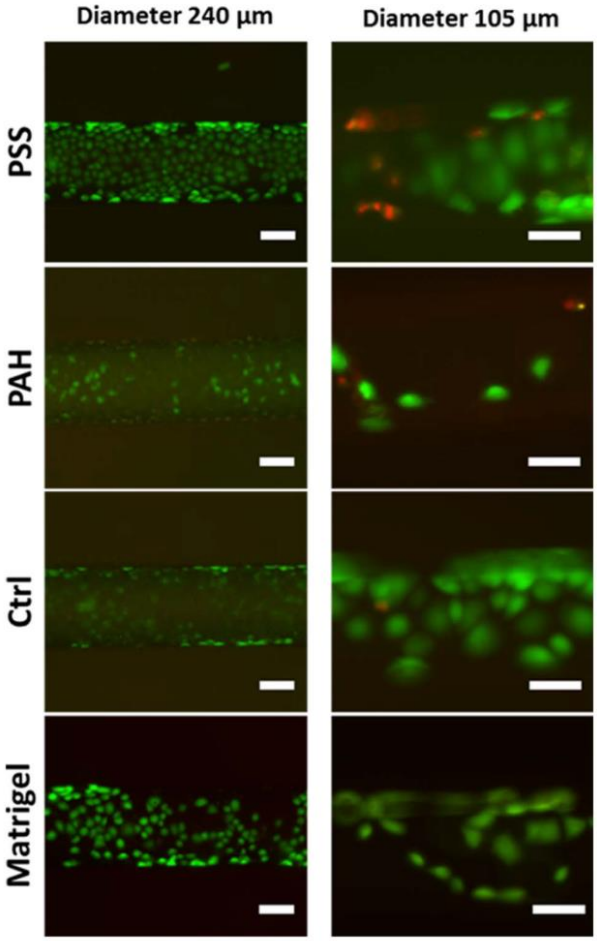

Figure 4. PC3 cell viability in microchannels. Calcein AM/propidium iodide test on PC3 cells in tubes of 105 µm (right) and 240 µm (left) coated with polyelectrolytes (PAH or PSS) and Matrigel. Note the limited adhesion and proliferation of cells in channels coated with PAH and non-coated (CTRL). In 105 µm channels we observe increased cellular death and the same effect of the type of coating. Scale bar 50 µm.
doi:10.1371/journal.pone.0099416.g004

were recorded using an AxioCam MRm monochrome digital camera mounted to the microscope.

Results and Discussion

Our motivation for this work was to develop polyelectrolyte 3D scaffolds in order to create new cell-culture devices that more closely mimic the natural physiological ductal environment found in exocrine glands. The present work described in this manuscript provides a detailed protocol for bench-top rapid fabrication of circular channels for 3D cell culture (Figure 1 & Figure S1 in File S1). The novelty of our system is based on its simplicity (Figure 1a). The fabrication process provides a high rate of success (nearly 90%) by the use of glass capillaries with thick walls (Table S1 in File S1), which are recommended to overcome potential for capillary breakage. Our process is cheap since it required low-cost materials, products and consumables (glass capillaries, needles, polymers). Therefore it is suited to parallelization. For convenience, about 10 tubes were manufactured at one time in this work to study different conditions but in fact, there is no limitation except the size of the support we are using. Therefore costs for performing these experiments in a larger scale setup are not more critical than for single experiments. This advantage opens the avenue towards further analysis (dose-response assays for instance) supported by an extensive statistical analysis according to specific needs. Compared to other existing methods, our fabrication of circular microchannels does not require the use of any complicated or specially adjusted moulds. The thick-called glass capillary is versatile since it can be used with different soft polymeric materials to form the microchannels, including agarose for example. Our method is limited to forming single microchannels, but which remains an advantage since it is much simpler compared to other existing methods and it provides more rapid fabrication. Although our method in its present description provides a very simple means to prepare microchannels to support ductal-like epithelial structures, it does provide a basis for future construction of more complex networked 3D microchannel scaffolds. Such future complex systems would include the capability for co-cultures of epithelial cells with stromal cells (fibroblasts, smooth muscle, endothelial cells) in order to reproduce functional tissues. Such a complex system could follow the same protocol of fabrication as the one presented here but would utilize another type of material, such as from within the hydrogels group. Although PDMS is easy to use, is biocompatible, has elastomeric properties, is flexible and perfectly transparent, it is only permeable to gases and does not allow for the diffusion of liquids. Applying our method to hydrogels, for example, would allow the possibility to *(i)* embed fibroblasts (or other type of cell) in the hydrogel and infuse epithelial cells into the microchannels so that the direct contact between two types of cells would be limited or *(ii)* infuse fibroblasts into the microchannels and culture them until confluence followed by the infusion of the second type of cells. One another possibility would be also to use sacrificial core and polyelectrolytes coating as previously demonstrated [34].

As a proof of concept for applying our method to such other biomaterials and to demonstrate the versatility of our technique for other types of temperature-dependent gels, we fabricated microchannels in agarose. Microchannels of 150 µm in diameter were fabricated in an agarose gel (3% w/v) following the same protocol as for PDMS (Figure 1b–c). Agarose is biologically inert and it can also be modified to promote cellular adhesion [28]. Cell culture, immunostaining and fluorescent microscopic observations can be performed directly without any extra manipulation. Moreover, the rounded-shape of our fabricated microchannels and the compatibility of our device with biopolymer coatings (e.g. Matrigel, LbL-assembled polyelectrolytes) allow extending bio-applications to 3D cell culture to flow-based assays which more closely mimic the physiological context of exocrine gland function.

Since cells do not adhere well to untreated PDMS, several treatments can be applied including plasma treatment and further amine functionalization [29], protein absorption or boiling water [30] to promote cellular adhesion. We chose to modify the microchannels by the simple method of layer-by-layer assembly of alternating polyanionic (PSS) and polycationic (PAH) materials [31]. This assembly produces a different surface charge that depends on the choice of the terminated PE layer, a modulation of the mechanical properties of the surface that depends of the number of layers assembled, and is also known to produce a surface that is compatible with cell adhesion [24]. Moreover we previously demonstrated quantitatively that PSS and PAH coatings alter the growth, attachment and spreading of prostate epithelial cells [23].

In this study we used three different types of human epithelial cells types to validate that the microchannels constitute a proper

3D microenvironment. In 3D culture, normal cells form indeed tubules, organized as a tree-like structure mimicking the in vivo glandular epithelial tissue architecture. Tubules connect terminal ductal lobular units, namely acini that are the smallest functional units of the prostate and the breast. Acini and tubules are formed by lumen-enclosing monolayers of cohesive cells and are respectively spherical and cylindrical. These cells models are routinely used in our lab to investigate 3D constructs in bulk Matrigel cultures (Figure S2 in File S1) and do properly differentiate into normal, hollow and well differentiated acini (for RWPE1 and MCF10A) [3]. As expected, PC3 cells in our hands form non-differentiated tumor-like spheroids (data not shown). Moreover these models are known to exhibit an exocrine activity, such as RWPE1 for example previously shown to secrete PSA (Prostate Specific Antigen) [35–36]. However, similar to other labs working with such bulk Matrigel 3D cultures, it is not possible to access in real-time the secretions from acini/ductal structures that form spontaneously in the bulk Matrigel.

Our results in this report demonstrate *i)* conditions required for cells to attach and grow as a confluent and viable monolayer on the walls of the microchannel (Figure 2A–B) just as standard 2D cell culture on dishes (Figure S2 in File S1) and *ii)* the formation of a light in the centre of the microchannels, for example as a basis for creating acini/ductal structures for the collection of secretions in real-time. Our phase contrast results show that all cell lines adhered and proliferated inside fabricated microchannels of 150 µm of diameter and formed a confluent monolayer covering the inner wall of the microchannel in static conditions after approximately 5 days (Figure 2C), as also demonstrated with simultaneous staining for Phalloidin and nuclei observed with confocal imaging (Figure 2D). The Apotome z-stack in Figure 2D provides a large-area 2D projection of the entire microtube. Focal adhesion sites were identified by Vinculin immunostaining and are shown here for PC3 as a representative result consistent with what we observed on all our models (Figure 3). Vinculin is a cytoskeletal protein associated with cell-cell and cell-matrix junctions, where it is thought to function as one of several interacting proteins involved in anchoring F-actin to the plasma membrane. We show that a microchannel coated with either a single PSS layer or a layer of Matrigel promotes cellular adhesion and proliferation of epithelial cells when observed with phase contrast and fluorescent microscopy (Figure 2). The PE deposition inside microchannels was confirmed by addition of Rhodamine B into polyelectrolyte solution and observation under microscope (Figure S3 in File S1). By contrast to PSS and Matrigel, a single layer of PAH slowed down cell proliferation and spreading, similar to a previous report [23]. It is commonly assumed that positively charged surfaces promote cell adhesion and proliferation [32]. However, PAH-terminal films support cell culture selectively depending on the cell line; for example, positively for neuronal cells while negatively for skeletal muscle cells [33]. The observed limited adhesion of epithelial cells in PAH-coated microchannels was also illustrated by the height of the cell and the position of nucleus (Figure 3A) as compared to PSS (spread cellular profile) and uncoated PDMS surface (rounded shaped cells). The ultimate commitment of a cell to adhere, differentiate, proliferate or migrate is a well-coordinated response to its molecular interaction with the components of the extracellular matrix (ECM) and surrounding cells. To further characterize cellular structures formed in the microchannels, expression of E-Cadherin was observed by the epithelial cells (Figure 3B). The expression of E-cadherin, a marker of lateral membrane domains, shows that our ex vivo microchannel provides an environment for the proper architecture and differentiated function of epithelial tissue. E-cadherin is also often used to quantify epithelial to mesenchymal transition and hence was chosen here to validate that our cells do not undergo phenotypic alteration. The luminal expression of Golgi in 3D (Figure S2 in File S1) also demonstrated that acinar differentiation was in line with cell polarization. This polarity was observed both in 2D and in 3D with the luminal expression of Giantin and of the centrosome (Figure S2 in File S1). This polarized organization of cells that we could observe in 2D does not mean that cells in 2D will undergo the same functional phenotype that they do in 3D. It is indeed well-known that the function of secretory cells such as breast epithelial cells [37] changes dramatically from the classical 2D culture plates to even Matrigel cultures. Also, the responses of tumor tissues to anti-cancer drugs are radically different between 2D and 3D cultures [38].

To assess the biocompatibility of the fabricated scaffolds we performed viability assays on PC3 cells cultured in microchannels of various diameters (Figure 4). For those assays we chose the smallest diameter of the channel to be 105 µm, since this is a dimension that is similar to the acinar and tubular structures existing in vivo. For comparison, we utilised a microchannel of 240 µm in diameter as our reference of stable proliferation of cells inside microchannels. We based our viability tests on two parameters; the intercellular esterase activity as indicated by calcein AM and plasma membrane integrity as verified by propidium iodide. By observation of the live/dead cell ratio we could find the best conditions for the cell culture inside the microchannels. We tested several coatings (PAH, PSS, no coating and Matrigel coating) and we found the best to be the PSS and Matrigel coatings (Figure 4). As previously observed and quantified, we confirm that PAH limits cellular adhesion and proliferation in comparison to the PSS and Matrigel coatings which provided cellular organization within the tubes [23]. Moreover we verified the importance of the diameter of the channels on two representative dimensions (240 µm and 150 µm). In static conditions we noticed that the cellular proliferation and viability are limited in 105 µm microchannels, as compared to the microchannels of 240 µm diameter where the growth of cells varied only according to the type of coating (Figure 4). We explain these results by the limited diffusion of nutrients in the smaller channels. In 105 µm channels the effect of surface coating also plays important role; however, we observed that cells proliferated mostly at the terminal ends of the channels which suggests limited diffusion of fresh nutrients into the channel. The observed lack of growth might also relate to the lack of oxygen. Interestingly our system could be useful to create defined and gradual hypoxia conditions without any need for special hypoxic incubator. This limitation can be overcome when perfusing channels with a continuous flow of nutrients without affecting cell viability and adhesion. Indeed we did not observe any cellular detachment due to the presence of the flow (see Movie S1 in File S1). As expected and observed using time-lapse microscopy, detachment during mitosis obviously occurs inside channels but the daughter cells following division consequently re-attach to the substrate. The precise and careful adjustment of the flow rate and pressure values during cell infusion and culture has prevented cells removal during division. Therefore, cells during mitotic detachment are capable to maintain in the channel and adhere. All observations taken together, the size of channels does not hamper the proper cellular division, adhesion and organization inside cylindrical tubules. Further experiments are under progress in our group to finely investigate the effect of flow on cellular function (secretions). In the current study we succeeded in validating the feasibility, usefulness and biocompatibility of our microchannels and their adequacy with our epithelial models. Detecting secretions and demonstrating

a functional assay on exocrine cells represent our ultimate goal. In this context microsystems offer a distinct advantage with the high volume to surface ratio of capillaries. While small scale is responsible for limited cell growth in static conditions due to the quick starvation (as shown for small channels of 100 µm diameter), any tiny secretions are more concentrated in a small volume which simplifies the detection. To that end, the proposed system in the future would be easily combined with mass spectrometry techniques for secretomics-based analysis.

Conclusions

Our technique provides a simple, low cost and versatile means to fabricate circular-shaped microchannels that are well-adapted for bio-applications. Epithelial cell behaviour can be modulated in microchannels by altering the surface charge of the microenvironment (PE) or by mechanical constraint (i.e. by adjusting the diameter of the microchannel). Our method produces a device that is easily combined with microfluidic flow systems for extensive studies of cell culture in dynamic environments and of further 3D tubulogenesis models. We believe that these circular microchannels can successfully serve for diverse epithelial cell types from exocrine tissues but also for endothelial and blood flow experiments, cellular secretion collection and co-culture systems, monitoring cellular processes in 3D and studying the dynamic flow effects on cell function. Moreover, it is a simple and rapid fabrication process that could be easily integrated in any biological laboratories.

Supporting Information

File S1 Contains Figure S1, A serie of photographs detailing the fabrication process. Figure S2, Epithelial cellular organization in 2D and 3D. Figure S3, Rhodamine staining of polyelectrolyte-coated PDMS channels. Table S1, Guide for choice of capillaries and needles for the microfabrication process.
(DOCX)

Movie S1 Presents the monolayer formation of MCF10A cells within first 15 hours culture with adjusted flow of culture media.
(DOCX)

Acknowledgments

We thank Odile Filhol INSERM U1036, CEA, Grenoble, France who kindly provided MCF10A cells.

Author Contributions

Conceived and designed the experiments: MED JPA DKM XG NPD. Performed the experiments: MED JW SG FK. Analyzed the data: MED XG DKM NPD. Contributed reagents/materials/analysis tools: MED JW SG FK JPA XG NPD. Wrote the paper: MED DKM XG NPD.

References

1. Lutolf MP, Hubbell JA (2005) Synthetic biomaterials as instructive extracellular microenvironments for morphogenesis in tissue engineering. Nature Biotechnology 23: 47–55.
2. Riha GM, Lin PH, Lumsden AB, Yao QZ, Chen CY (2005) Roles of hemodynamic forces in vascular cell differentiation. Annals of Biomedical Engineering 33: 772–779.
3. Dolega ME, Allier C, Vinjimore KS, Gerbaud S, Kermarrec F, et al. (2013) Label-free analysis of prostate acini-like 3D structures by lensfree imaging. Biosens Bioelectron 49c: 176–183.
4. Debnath J, Brugge JS (2005) Modelling glandular epithelial cancers in three-dimensional cultures. Nature Reviews Cancer 5: 675–688.
5. Whitesides GM (2006) The origins and the future of microfluidics. Nature 442: 368–373.
6. Dolega ME, Jakiela S, Razew M, Rakszewska A, Cybulski O, et al. (2012) Iterative operations on microdroplets and continuous monitoring of processes within them; determination of solubility diagrams of proteins. Lab on a Chip 12: 4022–4025.
7. Huang N-T, Chen W, Oh B-R, Cornell T, Shanley TP, et al. (2012) An integrated microfluidic platform for in situ cellular cytokine secretion immunophenotyping. Lab on a Chip 12: 4093–4101.
8. Shevkoplyas SS, Gifford SC, Yoshida T, Bitensky MW (2003) Prototype of an in vitro model of the microcirculation. Microvascular Research 65: 132–136.
9. Song JW, Munn LL (2011) Fluid forces control endothelial sprouting. Proc Natl Acad Sci USA 108: 15342–15347.
10. Rao N, Evans S, Stewart D, Spencer KH, Sheikh F, et al. (2013) Fibroblasts influence muscle progenitor differentiation and alignment in contact independent and dependent manners in organized co-culture devices. Biomedical Microdevices 15: 161–169.
11. Brown L, Koerner T, Horton JH, Oleschuk RD (2006) Fabrication and characterization of poly (methylmethacrylate) microfluidic devices bonded using surface modifications and solvents. Lab on a Chip 6: 66–73.
12. Martin PM, Matson DW, Bennett WD, Hammerstrom DJ (1998) Fabrication of plastic microfluidic components. Proceedings microelectronic Engineering, Santa Clara, Ca, 41/42: 493–496.
13. McDonald JC, Whitesides GM (2002) Poly(dimethylsiloxane) as a material for fabricating microfluidic devices. Accounts of Chemical Research 35: 491–499.
14. Golden AP and Tien J (2007) Fabrication of microfluidic hydrogels using molded gelatin as a sacrificial element. Lab on Chip 7 (6): 720–5.
15. Price GM and Tien J (2011) Methods for forming human microvascular tubes in vitro and measuring their macromolecular permeability. Methods Mol Biol 671: 281–93.
16. Wrong KH, Chan JM, Kamm RD, Tien J (2012) Microfluidic models of vascular functions. Annu Rev Biomed Eng 14: 205–30.
17. Wilson ME, Kota N, Kim Y, Wang Y, Stolz DB, et al. (2011) Fabrication of circular microfluidic channels by combining mechanical micromilling and soft lithography. Lab on a Chip 11: 1550–1555.
18. Fiddes LK, Raz N, Srigunapalan S, Tumarkan E, Simmons CA, et al. (2010) A circular cross-section PDMS microfluidics system for replication of cardiovascular flow conditions. Biomaterials 31: 3459–3464.
19. Abdelgawad M, Wu C, Chien WY, Geddie WR, Jewett MAS, et al. (2011) A fast and simple method to fabricate circular microchannels in polydimethylsiloxane (PDMS). Lab on a Chip 11: 545–551.
20. Verma MKS, Majumder A, Ghatak A (2006) Embedded template-assisted fabrication of complex microchannels in PDMS and design of a microfluidic adhesive. Langmuir 22: 10291–10295.
21. Jia Y, Jiang J, Ma X, Li Y, Huang H, et al. (2008) PDMS microchannel fabrication technique based on microwire-molding. Chinese Science Bulletin 53: 3928–3936.
22. Perry H, Greiner C, Georgakoudi I, Cronin-Golomb M, Omenetto FG (2007) Simple fabrication technique for rapid prototyping of seamless cylindrical microchannels in polymer substrates. Review of Scientific Instruments 78 (4): 044302.
23. Picollet-D'hahan N, Gerbaud S, Kermarrec F, Alcaraz JP, Obeid P, et al. (2013) The modulation of attachment, growth and morphology of cancerous prostate cells by polyelectrolyte nanofilms. Biomaterials 34 (38): 10099–108.
24. Ting JHY, Haas MR, Valenzuela SM, Martin DK (2010) Terminating polyelectrolyte in multilayer films influences growth and morphology of adhering cells. IET Nanobiotechnology 4: 77–90.
25. Mailleux AA, Overholtzer M, Brugge JS (2008) Lumen formation during mammary epithelial morphogenesis: insights from in vitro and in vivo models. Cell Cycle 7: 57–62.
26. Deshiere A, Duchemin-Pelletier, Spreux E, Ciais D, Combes F, et al. (2013) Unbalanced expression of CK2 kinase subunits is sufficient to drive epithelial-to-mesenchymal transition by Snail1 induction. Oncogene 32: 1373–1383.
27. Hebner C, Weaver VM, Debnath J (2008) Modeling morphogenesis and oncogenesis in three-dimensional breast epithelial cultures. Annual Review of Pathology-Mechanisms of Disease 3: 313–339.
28. Su Y, Chu B, Gao Y, Wu C, Zhang L, et al. (2013) Modification of agarose with carboxylation and grafting dopamine for promotion of its cell-adhesiveness. Carbohydrate Polymers 92: 2245–2251.
29. Glass NR, Tjeung R, Chan P, Yeo LY, Friend JR (2011) Organosilane deposition for microfluidic applications. Biomicrofluidics 5(3): 36501–365017.
30. Joong Yull P, Dongchan A, Yoon Young C, Chang Mo H, Takayama S, et al. (2012) Surface chemistry modification of PDMS elastomers with boiling water improves cellular adhesion. Sensors and Actuators B (Chemical) 173: 765–771.
31. Decher G, Hong JD, Schmitt J (1992) Buildup of ultrathin multilayer films by a self-assembly process: III. Consecutively alternating adsorption of anionic and cationic polyelectrolytes on charged surfaces. Thin Solid Films.
32. Bledi Y, Domb AJ, Linial M (2000) Culturing neuronal cells on surfaces coated by a novel polyethyleneimine-based polymer. Brain Research Protocols 5: 282–289.

33. Dhir V, Natarajan A, Stancescu M, Chunder A, Bhargava N, et al. (2009) Patterning of diverse mammalian cell types in serum free medium with photoablation. Biotechnology Progress 25: 594–603.
34. Ting JHY (2008) Diabetic retinopathy: Economic evaluations and cellular functions. PhD thesis, University of Technology Sydney, Australia.
35. Webber MM, Bello D, Kleinman HK, Hoffman MP (1997) Acinar differentiation by non-malignant immortalized human prostatic epithelial cells and its loss by malignant cells. Carcinogenesis 18: 1225–1231.
36. Nicotera TM, Schuster DP, Bourhim M, Chadha K, Corral DA, et al. (2009) Regulation of PSA Secretion and Survival Signaling by Calcium-Independent Phopholipase A(2)beta in Prostate Cancer Cells. Prostate 69: 1270–1280.
37. Vidi P-A, Bissell MJ, Lelievre SA (2013) Three-dimensional culture of human breast epithelial cells: the how and the why. Methods in molecular biology (Clifton, NJ) 945: 193–219.
38. Godugu C, Patel AR, Desai U, Andey T, Sams A, et al. (2013) AlgiMatrix (TM) Based 3D Cell Culture System as an In-Vitro Tumor Model for Anticancer Studies. Plos One 8: 13.

Supplementary Information S1

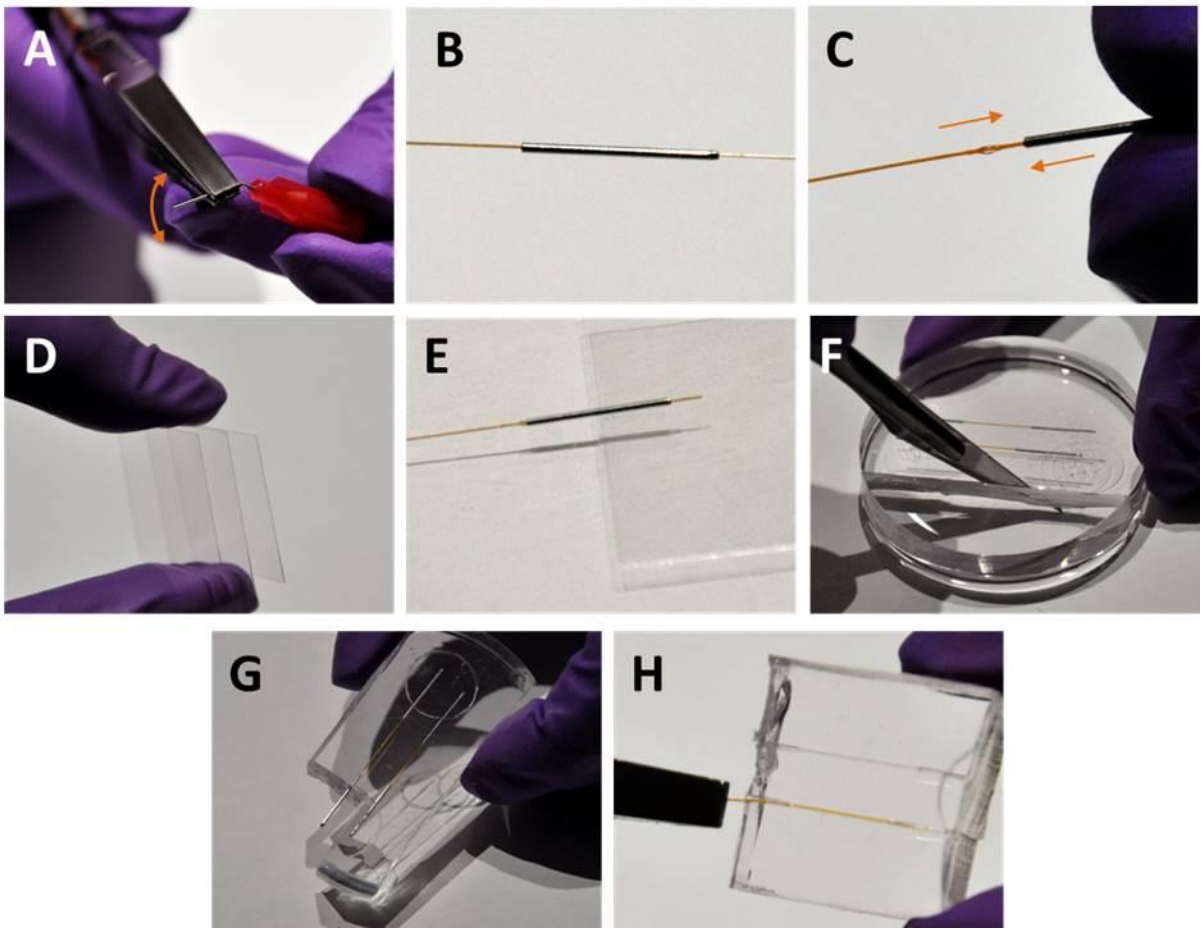

Figure S1 in File S1. A serie of photographs detailing the fabrication process. PDMS was prepared by extensive mixing of the elastomer with the curing agent in a 10:1 (wt/wt) ratio. During mixing air bubbles are introduced due to the viscosity of the solution and it is recommended to remove them by using a desiccator. Then the glass capillary is cut with scissors to a desired length, leaving an allowance of at least 1 cm to protrude from each side of the final construct. The needles are supplied with a plastic syringe connector that has to be cut carefully using a dremel tool or by hand with the use of pliers (**A**). Make sure that the metal part of needle has not been damaged or curved. Blow the needles with air to get rid of any inner contamination. The glass capillary is then aligned with the needle (**B**) so that the capillary protrudes from each end of the needle. To prevent any misalignment during further steps put a small drop of transparent nail polish on the surface of capillary at each end and slide the needle part so that the nail polish fills the space between the needle and the capillary (**C**). Triple glass cover slip towers are used to set up the distance between the channel and the surface of the petridish to ~550 µm (**D**). This step is crucial for further microscopic observations. In a 35 mm petridish (or other container of choice) support is inserted to keep the capillary/needle at controlled distance from the bottom (**E**). Degassed PDMS is then gently poured into a petri dish to completely cover the construct. The complete system is then placed in 65°C for 50 minutes to polymerize the PDMS. This process can be further accelerated with increased temperature. However, the plastic

petridish would then need to be replaced with high temperature resistant container. The polymerized PDMS is then removed with embedded capillary/needle construct and the support from the petridish and cut out using a scalpel thoroughly in the middle point of the needle perpendicularly to the channel at both ends (**F-G**). The cut part of the PDMS are gently removed from the needles and with the help of pliers the needles are pulled out first then the capillary from the PDMS (**H**). To prevent biological contamination, the device is sterilized by baking in an oven at 120°C for 30 minutes.

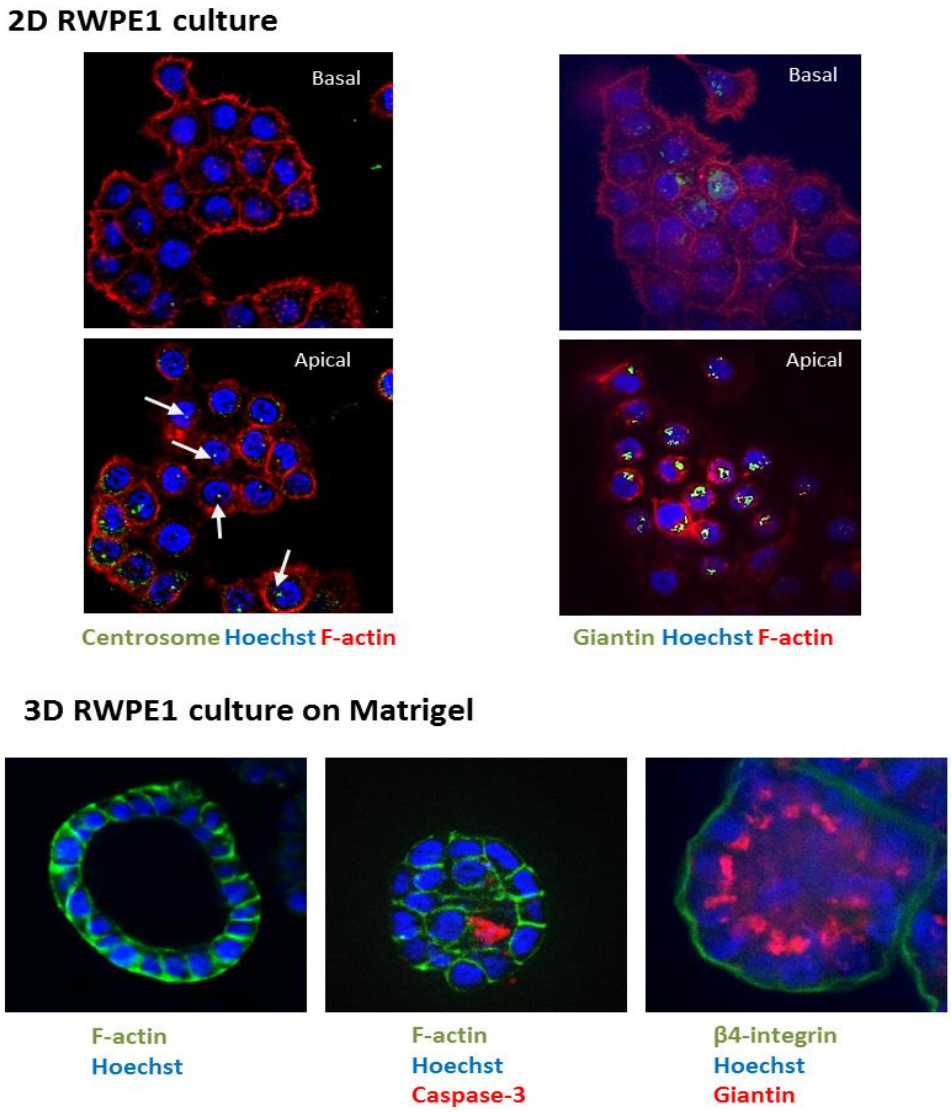

Figure S2 in File S1. Epithelial cellular organization in 2D and 3D.
Top panel: Immunostaining of nuclei (blue), F-actin (red) and centrosome (green, left panel) or Golgi (green, right panel) of RWPE1 cells after 72 hours culturing in 2D on plastic substrates. Cells were imaged by confocal at the interface cell membrane / surface (basal) and at the interface cell top / culture medium (luminal). The apical polarity is observed with centrosome staining (arrows) and Golgi staining. *Lower panel*: Immunostaining of nuclei (blue), F-actin (green) and caspase-3 (red, middle panel) and in the right panel, of Golgi (red) and B4-integrin (green) of RWPE1 cells culture in 3D Matrigel.

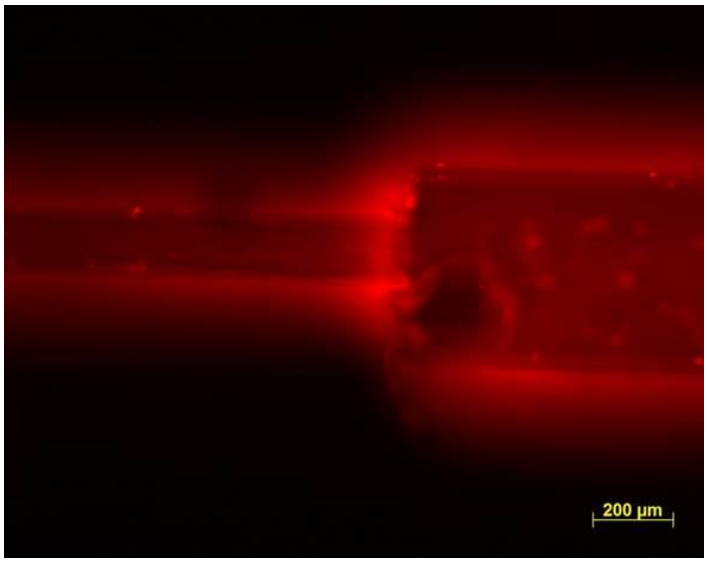

Figure S3 in File S1. Rhodamine staining of polyelectrolyte-coated PDMS channels. Channels were coated by constant infusion of the particular polyelectrolyte for 20 minutes followed by washing with PBS. To deposit a multilayer film, polyanions and polycations were infused alternatively, and between the changes of polyelectrolyte solution the tubes were washed thoroughly with MilliQ-grade water (18 MΩ cm).

Needle ref. (EFD Nordsen)	Needle ID	Needle OD	For channel	Capillary ref. (PolymicroTech.)
PN7018395	200 µm	420 µm	150 µm, 150 µm	TSP040105, TSP002150-10M
PN7018345	250 µm	520 µm	150 µm,240 µm	TSP002150-10M, TSP100245
PN7018272	410 µm	720 µm	363 µm	TSP005375-10M
PN7018233	510 µm	820 µm	435 µm	TSP320450

Table S1 in File S1. Guide for choice of capillaries and needles for the microfabrication process. Table S1 presents the dimensions of needles and capillaries that have been used for the experiments presented in this article. Depending on the desired channel size, a particular capillary and corresponding needle combination needs to be chosen. Therefore, Table S1 can serve as a guide for choosing a capillary/needle pair for the microfabrication process. We provide references for the materials we used. However, the fabrication process can also be performed with materials from other suppliers (e.g. Fibreguide industries or Beckman Coulter).

Movie S1 in File S1. Movie S1 presents the monolayer formation of MCF10A cells within first 15 hours culture with adjusted flow of culture media. Cells during mitotic detachment are capable to maintain in the channel and adhere.

7. Assessing the dynamic branching process of prostate cells using lens-free imaging

In chapter 5 droplet microfluidics systems for high-throughput and high-content analysis were presented. The principle relied on the encapsulation of epithelial cells into Matrigel beads, in order to provide a high-throughput analysis by using a flow-based FACS. Fluorescent analysis in FACS requires using immunofluorescence markers in order to describe phenotype of encapsulated cells. In this chapter, by applying lens-free systems a different approach for high-throughput has been proposed. Chapter 7.2 describes experimental lens-free application for 3D culture imagining and the label-free analysis, aiming to distinguish structures containing lumen from spheroids. Large field-of-view which significantly increases throughput of analysis, allowed also observing rare dynamic phenotypes during branching process in 3D culture (Chapter 7.3).

Key findings

- Lens-free 3D Imaging
  - Lens-free systems can serve to discriminate acini from spheroids by specific holographic patterns
  - large field-of-view (FOV) ensures rapid acquisitions to provide images of hundreds of structures at once;
  - FOV of the imaging set-up enables monitoring dynamic cellular 3D assemblies
- Environmental changes lead to branching-like phenotype of RWPE1 cells
  - Instability of Matrigel leads to the changes in compositions – Nidogen concentrates within the matrix
  - Time-lapse observations reveal distinctive dynamic phenotypes of collective cell migration
  - Observed branching-like process presents partial properties of the EMT process (invasion, increased motility and change in the cellular morphology, but β-catenin is maintained)
  - Altered environment leads to higher expression of β1-integrin, but not FAK or Rac1 (downstream effectors)
  - TGFβ1 inhibits branching-like process

7.1 Introduction to lens-free imagining

3D cell culture recapitulates properties of epithelial tissue *in vivo* by forming polarized spherical structures in Matrigel, acini (Chapter 1). However, development of new therapeutic agents by identification of genes responsible for a disease is hampered by problems in high-throughput analysis (Chapter 2). Analysis of 3D epithelial cell culture based on determination of acini (presence of lumen) vs. spheroids (solid mass) is time-consuming and requires confocal microscopy. Therefore, with the increasing development and high utility of lens-free (or as called also lens less) microscopy, we have applied such systems to observe 3D epithelial cells culture.

7.1.1 Operational principle

Lens-free imaging, as the name suggests, is a technique that does not require any lenses for observation of an object of micrometer (or even nanometer) scale size and has been introduced by several groups in 2007-2008 (Ji *et al.*, 2007; Naoghare *et al.*, 2007; Ozcan and Demirci, 2008). Lens-free microscopy employs charge-coupled device (CCD) or complementary metal-oxide semiconductor (CMOS) sensor to directly collect the light transmitted through observed samples (Bishara *et al.*, 2010; Coskun *et al.*, 2010; Seo *et al.*, 2010). To date, the performance of lensfree imaging has increased while keeping the design simple and effective. Rapid advances and commercialization in CMOS image sensor made attractive due to broad availability, low cost (~ 5-20 euros) and high pixel density sensor chips. In comparison to traditional techniques, standard optical microscopy allows to observe objects in field of view (FOV) of <1 mm^2 while lens-free imaging provides acquisition over a field of ~20 mm^2 (Figure 7-1) and allows to detect objects of size down to 100 nm (H1N1 virus) (Mudanyali *et al.*, 2013).

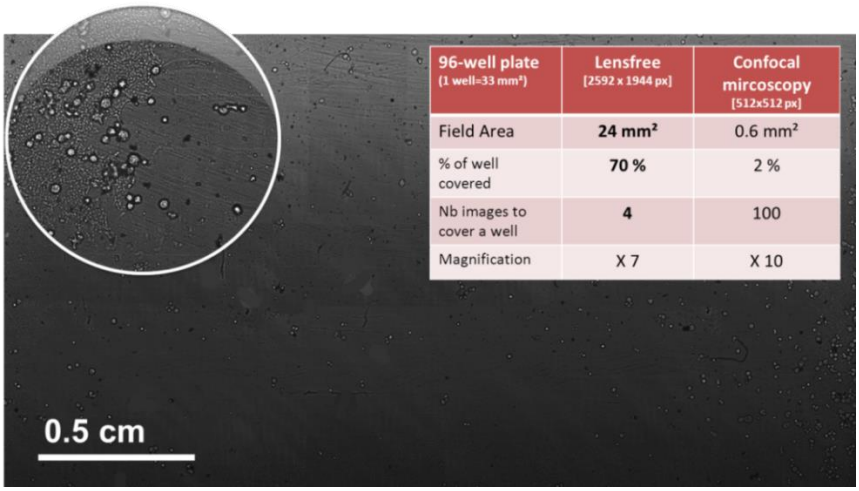

96-well plate (1 well=33 mm²)	Lensfree [2592 x 1944 px]	Confocal mircoscopy [512x512 px]
Field Area	**24 mm²**	0.6 mm²
% of well covered	**70 %**	2 %
Nb images to cover a well	**4**	100
Magnification	X 7	X 10

Figure 7-1 Raw lens-free image of an entire area of a well (1.8 cm^2) with a 3D epithelial cell culture on Matrigel. Inserted table compares performance of lens-free and confocal microscopy in imaging entire surface of a well of 96-well plate

7.1.2 Key components

Conventional lens-free holographic microscopy requires near perfect spatial coherence of the illumination which is obtained mainly by use of a laser that is focused and passed through a small aperture (~ 1-2 µm is in the order of a wavelength for spatial filtering). The system often utilizes a focusing lens to efficiently couple laser radiation with aperture (Garcia-Sucerquia *et al.*, 2006; Xu *et al.*, 2001). Recently simpler and cost-effective solutions based on using incoherent light were proposed. In lens-free new generation systems registered signal from the object does not spread across the entire sensor area. Therefore, the spatial coherence diameter required is small (Mudanyali *et al.*, 2010). The new approach is based on using a LED (light emitting diode) which is initially based on passing the light through a much larger aperture (~50-100 µm) (Figure 7-2).

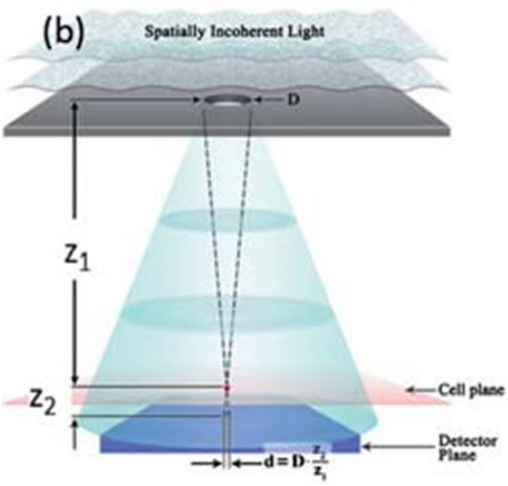

Figure 7-2 Schematic representation of the incoherent lens-free imaging system.
Typical parameters: z1 ≈ 2 - 5 cm; z2 < 1-2 mm; D ≈ 50-100 µm. Source: (Mudanyali *et al.*, 2010)

The second key component is the optoelectronic sensor array that serves to sample transmitted light pattern from each sample object. The FOV (field-of-view) of lens-free microscope is equal to the active area of the image sensor (either CMOS or CCD), and thanks to that a wide range of FOVs can be covered (typically in order of tens of mm^2). Compared to traditional lens-based microscopy, lens-free imaging significantly improves the imaging area. An important factor of sensors, that directly influences the output, is the pixel size. Smaller pixels improve the resolution of the images and fortunately the commercial trend for smartphone cameras goes into the right direction (recently ~1.4 µm pixel sizes).

7.1.3 Modes of acquisition

Bright-field lens-free microscopes present mainly two strategies of acquisition:

- Contact-mode shadow imaging microscopy (Lee *et al.*, 2011; Zheng *et al.*, 2011)
- Diffraction based lens-free microscopy (Cui *et al.*, 2008; Su *et al.*, 2010)

First group relies on minimizing diffraction by applying small distance between sample and a sensor (typically 1 μm). Practically this means that captured data corresponds to the shadows of the objects above the sensor. Because diffraction can be ignored final pictures are a two-dimensional representation. This technology is able to recognize various cell types in a heterogeneous cell solution based only on shape and contrast difference (Su *et al.*, 2009) (Figure 7-3A). Since this type of lens free imaging requires all objects to be in the same plane and close to the sensor, it excludes observation of bigger biological objects e.g., cell aggregates or tissue due to the complexity and size of an object.

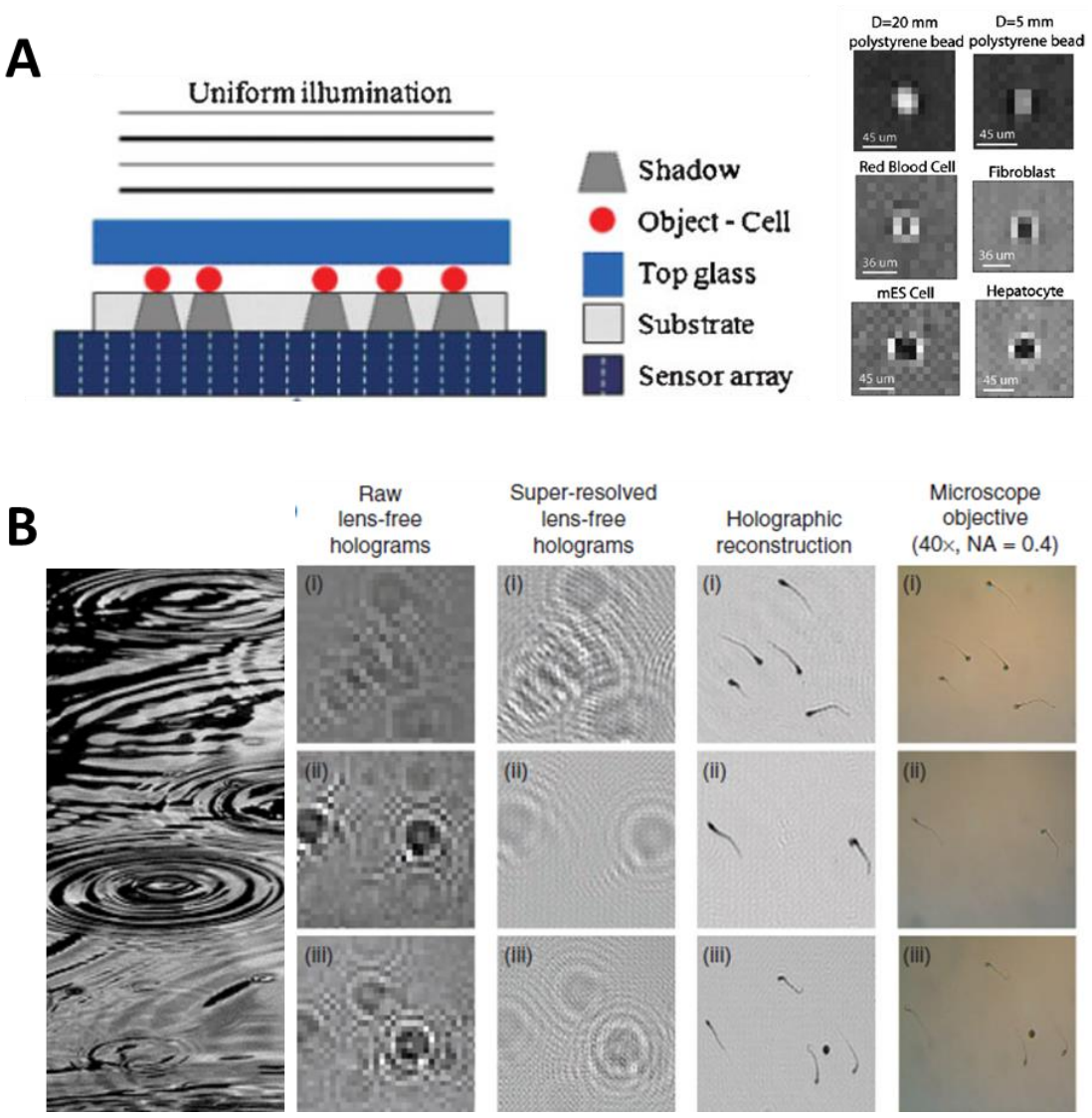

Figure 7-3 Lens-free imaging modes; A) Left: Scheme of a contact-mode shadow imaging microscopy. **Right:** shadows of different cells allow recognizing cell type by shape and contrast difference. **B)** Diffraction based lens-free microscopy. **Left:** An image of a water surface with water-rings that remind lens-free interference patterns. It is impossible to see the object that caused occurrence of the water rings, however, rings themselves provide the information about the object that felt into the water. **Right:** Holographic reconstruction of sperm cells. Source: A) (Su *et al.*, 2009) and B) (Mudanyali *et al.*, 2011)

Second type of lens less imaging microscopes relies on computational reconstruction in order to correct the effects of diffraction between the sample and the sensor (thickness of Matrigel layer in 3D culture is ~1 mm). This strategy allows obtaining 3D image of all objects in a sample that are at different distance from the image sensor at once. The scattered light from an observed object interferes with itself and the background light resulting in an interference pattern (i.e., a hologram). Interference patterns after digital reconstruction provide an image of analysed objects (Figure 7-3B).

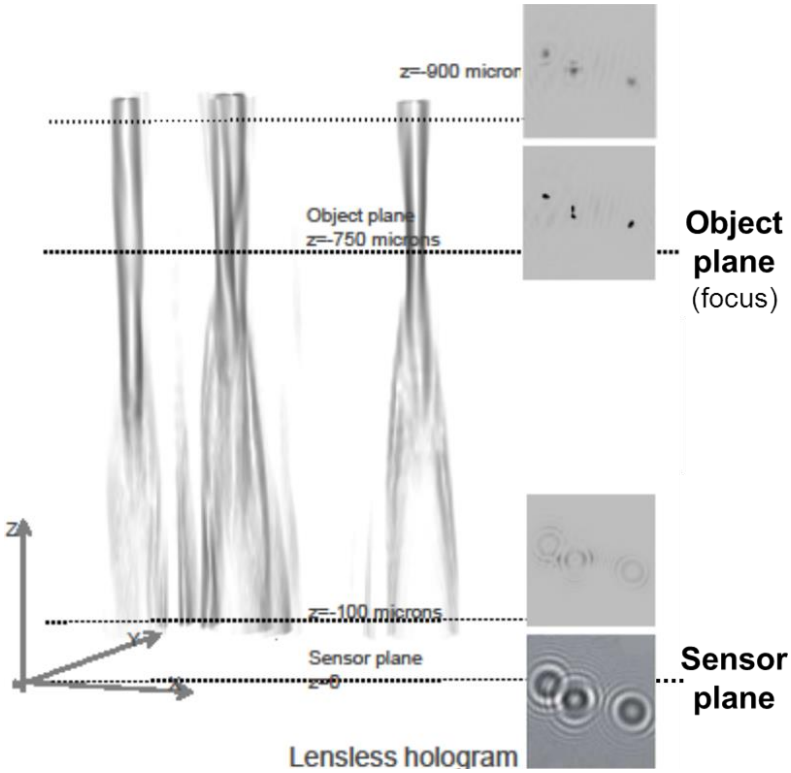

Figure 7-4 Light propagation and the resulting images according to the amplitude in lens-free holographic acquisitions. Source: C. Allier CEA-Leti

7.1.4 Techniques for image reconstruction

Fundamentally, two important reconstruction steps are required to visualize an object's image. The first, common for both acquisitions modes, and termed *pixel super resolution*[♣] (Park *et al.*, 2003) is used to overcome the resolution limit implicated by the pixel size. Therefore, in order to improve resolution in lens-free imaging pixel super resolution is acquired (Bishara *et al.*, 2010; Mudanyali *et al.*, 2011). Figure 7-3B presents super-resolved lens-free holograms as compared to raw images. The second reconstruction technique, which follows the super resolution process, takes into consideration the light diffraction which is the effect of the considerable distance (amplitude) between the object and the image sensor. Figure 7-4 presents

[♣] acquisition of ~10-20 images of the same scene, each image being acquired after a relative sub-pixel displacement between the image sensor and the scene or the illumination and the scene, then computer-based reconstruction of the scene by combining the images

the light path during the acquisition that to the amplitude images. Numerous approaches for amplitude and phase reconstruction have been introduced including iterative phase reconstruction (Fienup, 1982) and twin-image elimination algorithms (Denis *et al.*, 2008) that are widely used in digital holography. As a result of the second reconstruction step, amplitude and phase images of the object are generated

7.1.5 Advantages and drawbacks of lens-free holographic imaging

Lens-free holographic imaging offers high advancement in microscopy as compared to standard lens-based microscopes. The biggest improvement lies in the large field of view with at the same time high-resolution, which implicates numerous applications in biology. Because lens-free holographic systems have been introduced recently the majority of drawbacks are the result of to-date poor commercialization. Therefore, the user is forced to develop software to acquire and analyze images which limits the broad implementation of lens-free systems among researchers. Below a list of advantages and drawbacks is presented.

Advantages:

- Large FOV – 20 mm^2
- Large dynamic scale (acquisition on objects as small as viruses up to 3D multicellular large objects)
- Medium resolution ~ 1 - 2 µm
- Simplicity, small setup (fits easily into an incubator)
- Cheap (<200€)
- Applicable in time-lapsee acquisitions

Drawbacks:

- Not yet commercialized
- requires cooling system (sensor can heat up to 40'C when performing frequent time-point time-lapse observations)
- often requires reconstruction processes
- Limited to a single well observation (parallelized-sensor systems are recently under development, V.Haguet CEA/iRTSV/Biomics)

7.2 Label-free analysis of prostate acini by lens free imaging (Publication)

Published article is a result of collaboration between Biomics laboratory (CEA/DVS) and Leti (CEA/ DTBS). Dr. Cedric Allier has introduced lens free systems in CEA and used them previously, for instance, to observe bacteria and other objects of a single-cell scale. With the increasing need for high-throughput analysis in 3D cultures, collaboration has been established to perform, for the first time, observation of acini/spheroids in Matrigel by lens-free microscopy means.

The successful publication would not take place without following authors' contributions:

Planning of experiments:	M.D., C.A.,J-M.D, N.P.D., X.G.
2D cell culture:	M.D., S.G., F.K.,
3D culture, immunostainng:	M.D.
Microscopic acquisitions:	M.D., S.G.
Lensfree acquisitions:	C.A., M.D., S.V.
Holographic reconstructions:	C.A.
Metrics development:	C.A., P.M.
Analysis of results:	M.D., C.A., S.K., N.P.D., X.G.
Manuscript preparation:	M.D., C.A., S.K., N.P.D., X.G.

Biosensors and Bioelectronics 49 (2013) 176–183

Contents lists available at SciVerse ScienceDirect

Biosensors and Bioelectronics

journal homepage: www.elsevier.com/locate/bios

Label-free analysis of prostate acini-like 3D structures by lensfree imaging

Monika E. Dolega [a,b,c], Cédric Allier [d], Srikanth Vinjimore Kesavan [d], Sophie Gerbaud [a,b,c], Frédérique Kermarrec [a,b,c], Pierre Marcoux [d], Jean-Marc Dinten [d], Xavier Gidrol [a,b,c], Nathalie Picollet-D'Hahan [a,b,c,*]

[a] CEA, DSV iRTSV, Biologie à Grande Echelle, Biomics, 17 rue des Martyrs, F-38054 Grenoble, France
[b] INSERM, U1038, F-38054 Grenoble, France
[c] Université Joseph Fourier-Grenoble I, U1038, F-38041 Grenoble, France
[d] CEA, LETI, MINATEC, 17 rue des Martyrs, F-38054 Grenoble, France

ARTICLE INFO

Article history:
Received 14 March 2013
Received in revised form
29 April 2013
Accepted 2 May 2013
Available online 21 May 2013

Keywords:
Lensfree imaging
Prostate
Acini
3D culture
Morphogenesis
Cancer

ABSTRACT

We present a lensfree imaging method to analyze polarity in RWPE1 prostate epithelial cells that form polarized acini with lumen under standard tridimensional (3D) culture conditions. The first event in epithelial carcinogenesis is loss of polarity, followed by uncontrolled proliferation leading to metastasis. We demonstrate that it is possible to use optical signatures to discriminate 3D objects with distinct polarities in a large field of view. The three metrics we present here are designed as image processing tools to discriminate acini from spheroids without any 3D reconstruction. To demonstrate that our lensfree imaging platform may be used to study the 3D organization of epithelial cells, we analyzed and quantified the modulation of dynamic processes, e.g., the polarity of acini and the merging of polarized structures, upon transforming growth factor beta-1 (TGF beta-1) addition to the culture media. Hence, coupling lensfree microscopy with 3D cell culture provides an innovative tool to study epithelial tissue morphogenesis in a large field of view and to elucidate the regulation of growth, morphogenesis and differentiation in normal and cancerous human prostate cells. Moreover, such biosensor would be a powerful tool to follow cancer progression and to evaluate anti-cancer drugs.

1. Introduction

For many decades, cell biology experiments have been based on two dimensional (2D) cell cultures on rigid plastic substrates. Unfortunately, such culture conditions poorly reflect the reality of the cell microenvironment, which is composed of a fibrous network of proteins from the extracellular matrix (ECM) and neighboring cells in a tridimensional (3D) configuration. Cell culture in 3D offers a more realistic model of the in vivo microenvironment that favors polarized cell–cell and cell–ECM interactions (Pampaloni et al., 2007). Therefore, 3D cell culture is becoming routine in cell biology laboratories, and systems enabling the more complex reconstruction of tissues have been proposed (Mailleux et al., 2008; Pearson et al., 2009; Bryant and Mostov, 2008; O'Brien et al., 2002; Zegers et al., 2003). In this paper, we focus on the study of acini, which are the basic 3D structures constituting a secretory epithelium. The integrity of fully differentiated acini is determined by their apical and basal polarities, which are both characterized by specific cell–basement membrane contacts, intercellular junctions and luminal apoptotic cells (Debnath and Brugge, 2005). The maintenance of this polarity is critical for the structure and function of epithelial cells. The mechanisms controlling epithelial polarity and lumen formation are poorly understood (Pearson et al., 2009). Moreover, the disruption of apical polarity and the progressive transformation of acini into spheroids are key events in tumor progression. Therefore, the analysis of cell polarity is critical to assess epithelial development, integrity and homeostasis and to study the pathogenesis of epithelial tumors. To properly analyze polarity, in vitro 3D culture systems are necessary and are of increasing interest for cancer research because they recapitulate in vitro the alteration of the tissue architecture that precedes tumor development. Moreover, tissue architecture and the ECM influence the responses of tumor cells to signals from the microenvironment provided in a 3D context.

The imaging of 3D polarized structures in culture is not developing as fast as the 3D culture systems themselves. Immunofluorescence imaging of apical and basal polarity markers in fixed cells is the classical approach to study epithelial tissue phenotypes (Lee et al., 2007). It provides a way to follow the loss of apical

* Corresponding author at: CEA, DSV iRTSV, Biologie à Grande Echelle, Biomics, 17 rue des Martyrs, F-38054 Grenoble, France. Tel.: +33 4 38 78 67 78; fax: +33 4 38 78 59 17.
E-mail address: nathalie.picollet-dhahan@cea.fr (Nathalie).

0956-5663/$ - see front matter © 2013 Elsevier B.V. All rights reserved.
http://dx.doi.org/10.1016/j.bios.2013.05.001

polarity that is often described by the redistribution of tight junction proteins away from apical sites and by the filling of the lumen by disorganized cells, indicating that acini are transforming into spheroids (Hebner et al., 2008). However, the immunostaining approach presents some limitations (Yue et al., 2012), one being that it remains expensive because it is time-consuming and costly. In addition, data acquisition from living cells requires the use of transfection to induce the stable fluorescent expression of particular proteins, and the side effects on cellular function have to be considered (Baum et al., 2003). For clinical purposes, those traditional methods are not suited for the rapid and high-throughput counting/imaging of 3D cultures and the high-throughput evaluation of drugs that would cause high-throughput increase of the acinar forming ability of the cells while decreasing their invasiveness.

To overcome the above-mentioned limitations, a new imaging methodology to fully exploit the benefits of 3D cultures is needed. A direct imaging technique would (i) allow the observation of living cells, (ii) not require any staining, (iii) be time-efficient and (iv) enable high-throughput analysis and hence provide satisfactory statistical data.

As reviewed recently in Greenbaum et al. (2012), there is great potential for imaging without lenses, i.e., on-chip cell imaging and lensfree holographic microscopy. The resolution of these techniques is approximately 1 μm and can hardly compete with microscopy, but they offer several other advantages: the field of view (FOV) can cover up to several cm^2, the equipment is mostly compact in size; there is a wide range of readouts ranging from 1 nm to 1 mm; and they are easy to use. The e-Petri dish (Zheng et al., 2011), an on-chip cell imaging platform based on shadow imaging, challenges the superiority of video microscopy for applications such as cell migration assays. It allows continuous monitoring over a large field of view (24 mm^2), enabling the live imaging of thousands of cells simultaneously, but it remains limited to 2D cell culture. Moreover, the system requires a specific cell culture chamber and the customization and skillful integration of a sensor; 3D cell culture imaging with such a device has not yet been demonstrated. The second method, lensfree holographic microscopy, is very efficient for the detection of biological objects over very large FOVs (>20 mm^2) (Bishara et al., 2011; Mudanyali et al., 2011; Allier et al., 2010). Recently, it has been used to detect viruses (Mudanyali et al., 2013), to perform high-throughput 3D tracking of human sperm (Su et al., 2012) and to image microvessels from endothelial cells (Weidling et al., 2012). Little has been done to use lensfree holographic microscopy for monitoring cell culture (Moscelli et al., 2011), although it offers great promise for observing 3D cell cultures and even reconstructed tissues (Weidling et al., 2012; Isikman et al., 2011). Lensfree imaging could be used in difficult cellular assays for the quantification and analysis of complex cellular responses to address fundamental questions in developmental biology and to evaluate the effects of drugs in a physiological context.

Here, we use lensfree imaging to observe 3D structures from epithelial cells. We demonstrate that it is possible to use distinct optical signatures to quickly discriminate 3D objects of different polarities in a large field of view. Each object may exhibit either a well-ordered architecture (acinus) or a disrupted 3D structure with filled luminal space (spheroid). The three metrics we present here, i.e., gray level, Zernike features and the reconstructed holographic amplitude, are designed as image processing tools to discriminate acini from spheroids without 3D reconstruction. To illustrate the capabilities of our lensfree imaging platform, we showed how the 3D microenvironment influences 3D epithelial cell morphology and the merging of a population of cells. More specifically, we studied the effects of transforming growth factor beta-1 on acini size, lumen presence and acini merging, supported by strong statistical data.

This imaging system could be used extensively for studying cell–cell and cell–environment interactions by modulating the biochemical and mechanical stimuli within the ECM. We believe that this imaging system will be a powerful method for the large field analysis of multiple soluble effects, including fundamental and pharmacological research in carcinogenesis.

2. Materials and methods

2.1. Cell lines

RWPE1 and WPE1-NB26 cells were used in this study as models for normal and malignant epithelial acinar morphologies, showing two distinct and well-characterized phenotypes in 3D. The RWPE-1 cell line was obtained from ATCC (CRL-11609). This cell line was derived from non-neoplastic human prostate epithelial cells by immortalization with human papillomavirus (22). The WPE1-NB26 cells were derived from RWPE-1 cells by exposure to a direct-acting carcinogen, N-methyl-N-nitrosourea, and were purchased from ATCC (CRL-2852). The RWPE1 cells mimic normal prostate epithelial cell behavior as characterized by a well-established polarized morphology, whereas the WPE1-NB26 cells represent tumorigenic cells at a highly invasive stage of neoplastic transformation with the loss of acinar morphogenesis.

2.2. Cell culture (2D and 3D) and staining

RWPE1 and WPE1-NB26 cells were both maintained in KSFM (Life Technologies, Carlsbad, CA, ref. 17005-075) supplemented with 5 ng/mL epidermal growth factor (EGF) and 50 μg/mL bovine pituitary extract. The cells were maintained in culture until approximately 70% confluency. For passaging, cells were washed with Dulbecco's Ca^{2+}/Mg-free PBS (D-PBS, Life Technologies, ref. 14190) and incubated with 1 mL trypsin–EDTA (Lonza, Basel, CH, ref. CC-5012, 0.25 mg/mL) for approximately 7 min. The trypsin was neutralized with 2 ml trypsin neutralizing solution (Lonza, ref. CC-5002), and the cells were recovered by centrifugation and counted using a Scepter 2.0 Handheld Automated Cell Counter (Millipore, Billerica, MA, ref. PHCC 20060). For the acinar morphogenesis assay, the RWPE1 and WPE1-NB26 cells were cultured in 3D with KSFM (Life Technologies, ref. 17005-075) supplemented with 50 ng/mL EGF and 2% fetal bovine serum (FBS). The 3D culture was grown in Matrigel (BD Biosciences, San Jose, CA, ref. 356231) according to the top-coat protocol (8). The top-coat assay was preferred to the 3D 'embedded' assay because it requires less time and EHS (Engelbreth–Holm–Swarm Mouse Tumor) and because it facilitates imaging as the colonies are in a single plane (8). Briefly, Matrigel was thawed overnight and poured into 4-well (160 μL of Matrigel, 500 μL of culture media) or 8-well Labtek (90 μL of Matrigel, 250 μL of culture media) plates on ice. For polymerization, Matrigel was incubated for 30 min at 37 °C. Cells were seeded in half the final volume and allowed to adhere for approximately 45 min. The top coat layer containing 8% Matrigel was slowly poured over the attached cells. The culture media was changed every other day. All cells were routinely cultured in a humidified atmosphere with 5% CO_2 at 37 °C. To perform statistical analysis and to determine spheroid-to-acini ratios in the same field of view, a mix of WPE1-NB26 and RWPE1 cells was seeded onto 3D Labtek slide chamber and analyzed. To quantify the effect of TGF beta on acinar formation, we conducted an experiment in which TGF beta was added to RWPE1 3D cell cultures after 3, 5 and 10 days of culture.

After at least 8 days of 3D culture, the cells were fixed with 4% (v/v) paraformaldehyde in PBS for 20 min and washed once with PBS. Actin filaments were stained with TRITC phalloidin (Sigma-Aldrich,

St-Louis, MO, ref. P1951) at a 1:500 dilution for 20 min while nuclei were counterstained with Hoechst (Life Technologies, ref. H-1399) at a 1:7000 dilution. Glass cover slides were mounted on the glass slides with a Dako Fluorescent Mounting Medium kit (Dako, Glostrup, DK, ref. S3023) and stored at 4 °C before imaging.

2.3. Lensfree imaging and microscopy

Our lensfree imaging device is depicted in Fig. 1b. It is based on the technique introduced by Ozcan and Demirci (2008), Seo et al. (2009)). The setup consists of a LED emitting at 610 nm coupled to a 150 μm diameter pinhole and a CMOS image sensor. The characteristics of the three different sensors used during the experiments are detailed in supplementary information S-1. The LED is located 10 cm above the sensor and illuminates the slide chamber that contains the 3D epithelial cell culture. The chamber is put on the CMOS sensor such that the distance between the sensor plane and the cells is approximately 800 μm. An in-line holographic image is then formed on the sensor as a result of the interference between the partially coherent incident light and the light scattered by the cells and/or the acini. Fig. 1a shows the lensfree acquisition of a full chamber of an 8 well Lab-Tek® slide. To image a FOV as large as 9.4 by 7.3 mm^2, we composed a mosaic of 4 24 mm^2 lensfree acquisitions. The acini of interest could then be localized on the lensfree sensor monitoring the full chamber and finely re-analyzed using a fluorescence microscope for comparison. We used the AxioImager Z1 Zeiss microscope equipped with the straight Apotome module for z-stack acquisitions. The microscope was mounted with an AxioCam MRm monochrome digital camera. Optical sectioning of the fluorescent samples was performed to discriminate the 3D structures, i.e., acini with lumen versus spheroids.

3. Results

Our lensfree imaging device was used to image the fully differentiated multicellular assemblies that form acini. Fig. 1 shows the lensfree imaging device and images of a RWPE1 3D cell culture. One can visualize many 3D objects (> 1000) at a glance and look for rare events at the level of single 3D structures. Fig. 1d shows a zoomed-in region of Fig. 1a featuring the lensfree hologram of merged 3D structures, a single 3D object and single epithelial cells. The 3D cultures of epithelial cells are based on the support of cells with a naturally derived soft substrate that comprises a mixture of proteins and growth factors and that allows the homogenous interaction of the cells with their environment in three dimensions.

Successful 3D culture is mostly performed in the presence of Engelbreth–Holm–Swarm (EHS)-derived ECM that directs the induction of glandular epithelial polarity. Secretory epithelia are typically composed of acini (Fig. 2a), a bilayered cellular sphere, and tubules that are cylindrical monolayers forming a network between single acini. The polarity of the acini and the tubules result in the formation of an apical surface facing the lumen and a basolateral surface facing the extracellular matrix. The frequency of acinar formation is expected to be significantly different in RWPE1 and WPE1-NB26 cell lines (Bello-DeOcampo et al., 2001). Indeed, optical confocal sections of DAPI-stained cells after 8 days of growth in Matrigel show that the non-tumorigenic RWPE1 formed acini with well-polarized cells and a distinct lumen (Fig. 2b), whereas WPE1-NB26 cells did not differentiate efficiently and formed many more spheroids (Fig. 2e). The inability to undergo acinar differentiation correlated with their degree of malignancy (Bello-DeOcampo et al., 2001).

By comparing the RWPE1 and WPE1-NB26 3D epithelial cell cultures (Fig. 2) and hence acini (Fig. 2a) and spheroids (Fig. 2b), we observed significant differences between their lensfree holograms. The lensfree holograms of spheroids (Fig. 2f) showed a very bright spot in the middle whereas the holograms of acini with lumens were more uniformly black (Fig. 2c). The difference in gray-level intensity in the center of these two holograms is approximately 100 out of 255 with a background of 5 Gy-levels (Fig. 2i).

We found two other metrics able to discriminate acini with lumen from spheroids, i.e., the Zernike transform and the amplitude holographic reconstruction (see supplementary information S-2). Fig. S-1 shows the analyses based on the Zernike transform comparing the lensfree acquisition of the RWPE1 and WPE1-NB26 3D cell cultures (see supplementary information S-2).

A comparison of Fig. S-1a and f shows that in this experiment, the lensfree holograms of acini and spheroids were not very

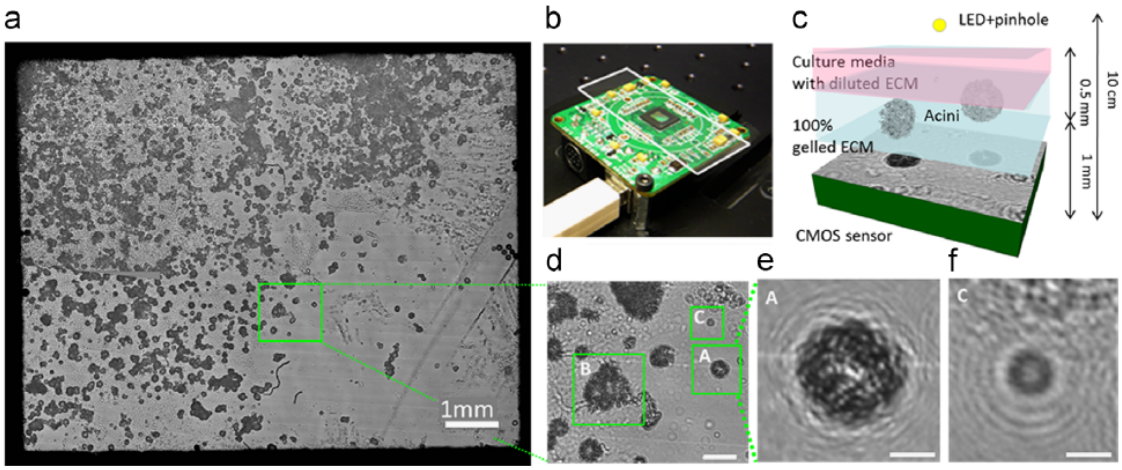

Fig. 1. Lensfree imaging of 3D cultures of epithelial cells. (a) Lensfree imaging of an 8-well Lab-Tek® slide chamber filled with a 3D culture of RWPE1 epithelial cells. Generally, each well contained thousands of acini. To image the entire chamber, we constructed a mosaic of four 24 mm^2 FOV lensfree acquisitions. The CMOS sensor is placed in contact with the chamber slide (b) and allowed to record the lensfree hologram resulting from the interference between the partially coherent incident light and the light scattered by the cells and/or the acini. Illumination is provided by a CMS LED emitting at 610 nm set 10 cm above the chamber. (c) Schematic of the lensfree imaging setup for 3D cultures of epithelial cells (not to scale). Epithelial cells are completely embedded within the extracellular matrix (ECM). (d) The expanded region of the white rectangle in (a) shows the lensfree holograms of (e) an acini (labeled A), merged acini (labeled B) and (f) single cells (labeled C). When the outline of the acini (Fig. 2) is drawn in the lensfree hologram (e), the single cell pattern (f) is much larger than the cell itself. The scale bars are 200 μm and 50 μm in (d) and in (e, f), respectively.

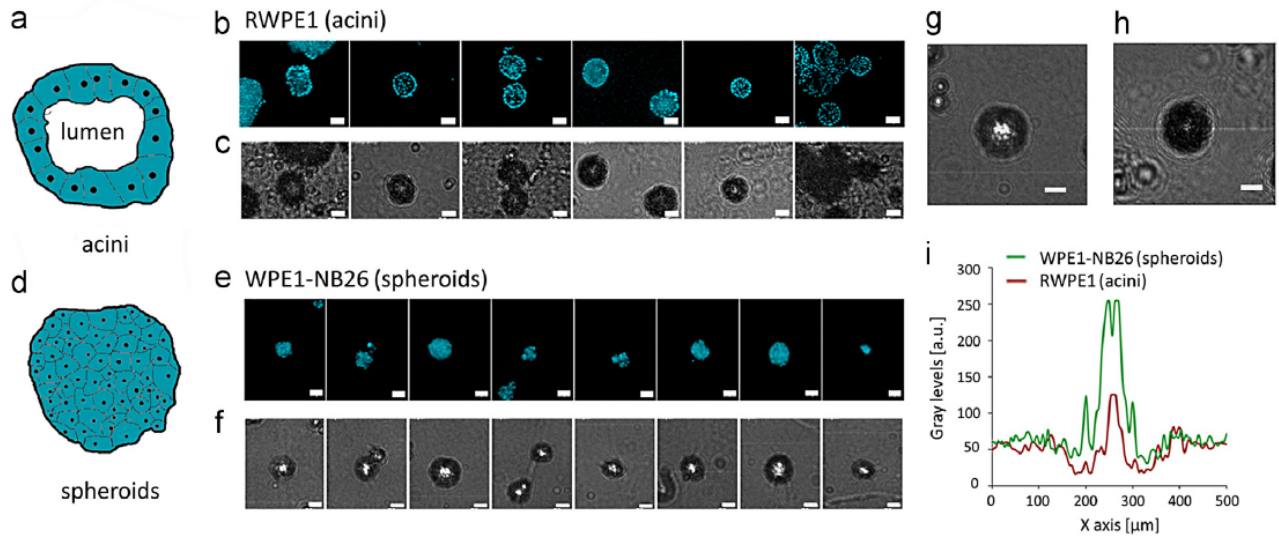

Fig. 2. Lensfree imaging and fluorescence microscopy of acini with lumen versus spheroids. Hoechst-stained 3D cell cultures after 8 days of growth in Matrigel of the (a–b) RWPE-1 and (d–e) WPE1-NB26 cells (20× magnification, scale bar 50 μm). These acquisitions show the strong difference in acinar formation, i.e., lumen or spheroids. The lensfree holograms of the acini with lumen and the spheroids, whose schematics are depicted in (a) and (d), respectively, present many differences (scale bar 50 μm). At the center of the pattern, the difference in gray-levels yields a value of 100 (onto a full scale of 255). This value is largely above the background noise of our lensfree imaging setup (5 Gy-levels standard deviation) and well above the mean gray levels of 50. Typical lensfree holograms of WPE1-NB26 cells (spheroids) (g) and RWPE-1 cells (acini) (h) scale-bar 50 μm. Intensity profiles measured on lensfree holograms showing the main axis of the WPE1-NB26 cells (spheroids, in green) and the RWPE-1 cells (acini, in red) (i). (For interpretation of the references to color in this figure legend, the reader is referred to the web version of this article.)

different in comparison with Fig. 2. Both the holograms of acini with lumen and spheroids showed a bright spot in the middle and there was less than a one-sigma difference ($N=50$) in the maximum intensity, which made it very difficult to discriminate the two structures. However, by averaging twenty lensfree holograms, we found a subtle halo in those of the acini with lumen (Fig. S-1b) that was not present in the averaged lensfree hologram of the spheroids (Fig. S-1c). To quantify this feature, we implemented a Zernike transform algorithm in ImageJ (Banada et al., 2007; Bae et al., 2012) (see Supplementary information S-2). By calculating the first twenty Zernike moment invariants over a large number of different lensfree holograms of acini (73 RWPE1 objects, 51 WPE1-NB26 objects), we found that three Zernike moments are discriminating, i.e., $|Z_{2,0}|$, $|Z_{4,0}|$ and $|Z_{6,0}|$ (Fig. S-1c, d, e, h, i). In particular, we determined that fixing a threshold to the $|Z_{4,0}|$ Zernike moment allows the measurement of a 1.7σ difference between the RWPE1 and WPE1-NB26 patterns (Fig. S-1j, k).

In some experiments, with a heterogeneous mixture of 3D structures (Fig. 3), the $|Z_{4,0}|$ Zernike moment varied by less than 1σ ($N=50$).

Performing a principal component analysis (PCA) using the first twenty Zernike moment invariants did not improve the discrimination. Where the differences between the acini and spheroids were too small to discriminate with lensfree imaging, we had to consider the 3D structures as 2D objects of which the transmission could be reconstructed by holographic amplitude reconstruction (Fienup, 1982; Soulez et al., 2007) (see Supplementary information). In principle, by applying a threshold to the reconstructed amplitude to detect the spheroids and local maxima to detect all the acini, we thought it is possible to discriminate the acini from the spheroids. To experimentally verify our hypothesis, we performed image reconstruction of the hologram obtained from the plate containing both spheroids and acini. The amplitude reconstruction of RWPE1 and WPE1-NB26 epithelial 3D cell cultures indicated that the percentage of spheroids was 8% ($N=109$) and 60% ($N=181$), respectively (Fig. 3c).

To further investigate the imaging capabilities of our system and to extend our observations, we performed a time course experiment to monitor the dynamic phenotypes induced upon the variation of culture conditions. As little is known about the influence of transforming growth factor on acini formation in a 3D culture of non-malignant prostate cells, we treated epithelial cells at very early stages of 3D culture and induced polarized acini formation with TGF beta-1. We built a dataset of 35 lensfree acquisitions over 9 days, from day 3 to day 12 after TGF beta-1 addition. In total, we acquired and analyzed approximately 10,000 lensfree holograms of single acini and multiacinar structures. Fig. 4 shows the effects of TGF beta-1 on acini size and on the process of multiacinar formation.

There was an inhibition of acinar growth that was dependent on the length of the TGF beta-1 treatment (Fig. 4a). In a control experiment, multiacinar structures predominate and the single acini reach the largest observed size, with a mean diameter of 125 μm and a maximum diameter up to 200 μm. The shorter the TGF beta-1 treatment, the smaller the single acini obtained (Fig. 4b). The mean acini diameter increased by a factor of approximately two in 9 days. Similarly, TGF beta-1 treatment of RWPE1 cells in 3D culture limited the formation of multiacinar structures that predominated in the control experiment. The ratio of the surface covered by multiacinar structures versus single acini was between 5 and 7 in the control experiments, whereas it did not exceed 3 in the presence of TGF beta-1.

Furthermore, we looked at the number of high intensity lensfree holograms (Fig. 5) because they correlated with the structures of spheroids (Fig. 2).

Performing a manual count (ImageJ, cell counter) on four 24 mm^2 lensfree acquisitions of RWPE1 3D cell culture on day 12 of the experiment, we found patterns with strong lensing effects at 34%, 22%, 32% and 13% ($N=1415$) on day 3, 5 and 10 of TGF beta-1 treatment, respectively. No high intensity lensfree holograms were observed with the control wells (Fig. 5g–j). These results are consistent with the measured local maxima distribution (75 Gy-levels noise tolerance, ImageJ). By applying a gray-level threshold at an arbitrary value of 175 (see threshold line in Fig. 5e, f), we found percentages of 26%, 21%, 33% and 16%, which are similar to the data obtained after the manual counting. There was thus a

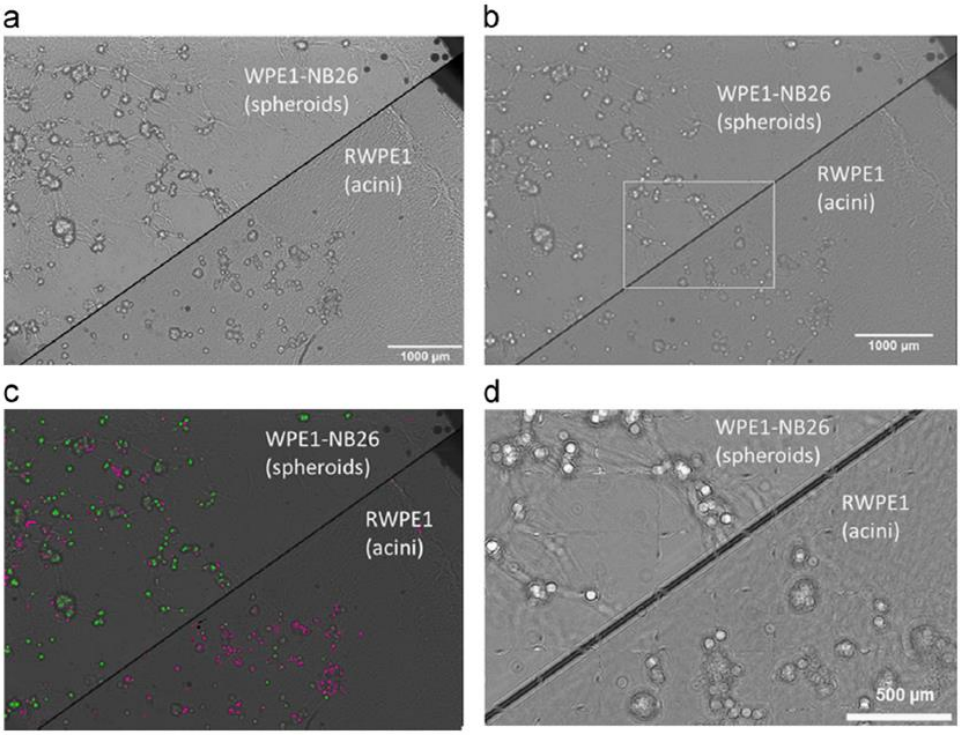

Fig. 3. Holographic reconstruction of acini with lumen versus spheroids. (a) The 24 mm^2 lensfree acquisition of two chambers of an 8-well Labtek® slide containing WPE1-NB26 (top half) and RWPE1 (bottom half) 3D cell cultures. (b) Reconstructed amplitude lensfree images. The white rectangle in (b) is expanded in (d). (c) Local maxima and gray-level thresholding of the reconstructed amplitude lensfree images show the detection of acini with lumen (in purple) and spheroids (in green). (For interpretation of the references to color in this figure legend, the reader is referred to the web version of this article.)

two-fold difference in the number of spheroids between the control and TGF beta-1 experiments.

4. Discussion

The optical observation of biological objects and tissues is traditionally performed using conventional light microscopes and immunofluorescence. However, the quantitative measurement of cellular responses in 3D over periods of time has been hampered (Yue et al., 2012). Therefore, there is a need for alternative microscopy techniques such as label-free, miniaturized and immobilized platforms enabling the study of 3D biological architectures. The lensfree system that we present in this study is a tool to observe epithelial 3D architectures. It does not allow the reconstruction of large 3D features because we did not implement tomography methods (Isikman et al., 2012). Instead, it allows the observation of light propagating through the 3D objects. To correlate these observations with 3D cell structures, we introduced several metrics. Part of our method is the use of appropriate metrics to discriminate spheroids from acini.

We showed that when a lensing effect is observed (Fig. 2), mainly with spheroids, the gray-level threshold could be used to discriminate spheroids from acini. These observations have been confirmed by standard fluorescence techniques. A similar lensing effect acquired by lensfree imaging has been already described (Allier et al., 2010). However, in further experiments, this criterion was not sufficiently discriminating. It is not robust enough to take into account the variations observed in 3D culture experiments arising from the composition and physical properties of the ECM layer that lead to changes in the distance between the object embedded in the ECM and the sensor. Therefore, the gray-level analysis can be used only when the acini are very similar, for example, as micropatterns in standardized 3D cultures (Rodriguez-Fraticelli et al., 2012).

Under more variable conditions, the Zernike transform is preferred to gray-level thresholding. This method is based on the mapping of an image onto a set of polynomials that are perpendicular to each other (see Supporting information S-2). The Zernike moments have been successfully used for the recognition of patterns including the analysis of mammograms (Tahmasbi et al., 2011). The high computational complexity of Zernike moments has often hampered its suitability for real-time applications. Here, we successfully performed discrimination on the basis of only one Zernike moment, i.e., applying simple thresholding, which drastically reduced the computational task. We achieved discrimination between the two populations of acini with two-sigma significance (Fig. S-1). This result is underestimated as it is calculated assuming that all the RWPE1 and WPE1-NB26 cells form acini and spheroids, respectively, which is not the case. Practically, 60–80% of a standard 3D culture of non-malignant epithelial cells forms polarized structures (refs in Yue et al., 2012). Furthermore, we verified that the discrimination is not related to another variable. By measuring the maximum gray level, the mean gray level, the diameter, the kurtosis and the sphericity on different lensfree holograms ($N=120$), we could not find any difference larger than one-sigma between the two populations of acini. This result means that in this experiment, the Zernike transform allowed the identification of different features of the acini with lumen and the spheroids in the lensfree holograms.

A third means of analysis was based on the assumption that the acini can be described as 2D objects whose transmission can be analyzed by holographic reconstruction. Hence, by applying a threshold to the reconstructed amplitude, we successfully estimated the number of acini and spheroids in a culture of RWPE1 and WPE-NB26 cells (Fig. 3).

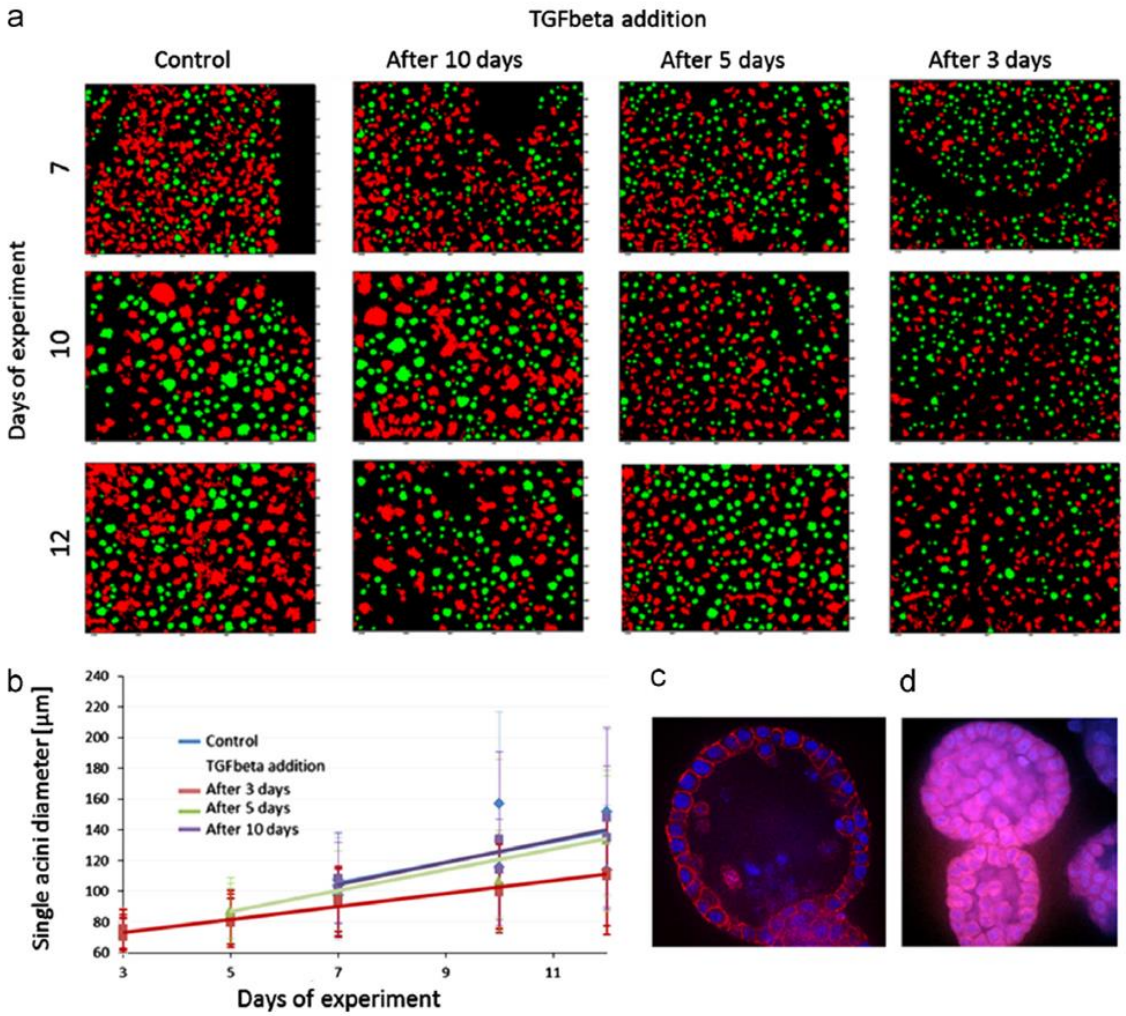

Fig. 4. Influence of TGF beta-1 addition on the acini size and the multiacinar structures. (a) The 24 mm^2 lensfree acquisitions of RWPE1 3D cell cultures 3, 5 and 10 days after TGF beta-1 (3 ng/mL) or no TGF beta-1 addition as a control. Every picture shows the single acini in green and multiacinar structures in red. (b) The mean diameter of each acinus measured from 35 lensfree acquisitions, measured over-time and grouped according to the day of TGF beta-1 addition. The error bars correspond to standard deviations of the diameter measured within one lensfree acquisition ($N=150$). (c, d) RWPE1 cells in 3D culture stained with Hoechst (blue) and phalloidin (red) under control conditions (c) and after 3 days of TGF treatment (d) following 8 days of culture in Matrigel. Notice the reduced diameters of the acini and the presence of cortical actin upon TGF treatment. (For interpretation of the references to color in this figure legend, the reader is referred to the web version of this article.)

The main limitation of those metrics is that the choice for the best metric is experiment-dependent owing to the variability in the optical properties of the acini. There are hidden variables that are inaccessible with our lensfree imaging, e.g., the 3D geometry of the acini, the number of cells, refractivity, absorption and diffusion coefficients, presence and size of the lumen. This caveat explains why we consider these metrics a toolset to be systematically applied to each experiment. If the experiment is performed within a multi-well slide with all necessary control measurements, our approach allows qualitative observations and the counting of the different 3D geometries. At this stage this methodology does not allow the analysis of the properties of every single acinus, to quantify for instance the degree and stage of malignancy. This will be a point of focus for future work.

As a demonstration of our lensfree approach, we have studied the influence of TGF beta-1 (transforming growth factor beta-1) on different acini in 3D cell cultures, and we have monitored over time the polarity status, the acini size and the process of acini merging. TGF beta regulates homeostasis and suppresses tumor progression but little is known about how TGF beta treatment influences the formation of acini in 3D cultures of normal prostate epithelial cells. Our measurements showed that the diameter of each acinus decreased upon TGF beta-1 addition, especially when TGF beta-1 was added at a very early stage of growth (3 days). This in vitro inhibitory growth effect is consistent with the prevention of lumen formation that we observed using two separate metrics (Fig. 5). In contrast, the observed decrease in the number of merging acini was not expected, suggesting that TGF beta-1 could limit signaling between the acini. In control experiments, even at low cell seeding density, the acini were able to migrate and merge with one another. To further monitor their polarity, the ratio between the acini and the spheroids was determined based on the previously obtained gray-level signatures [acini (dark pattern) versus spheroids (bright pattern)]. Unexpectedly, a decrease in the proportion of acini was also observed in the cell populations treated with TGF beta after 10 days in culture, when cells were already well differentiated into acini, which suggests that TGF beta treatment can perturb acinar structure and revert the phenotype. The effect of TGF beta on lumen formation could be mediated by mechanotransduction, given the consistent presence of cortical actin following TGF beta treatment (Fig. 4c–d). Such organization of sub-cortical rings is

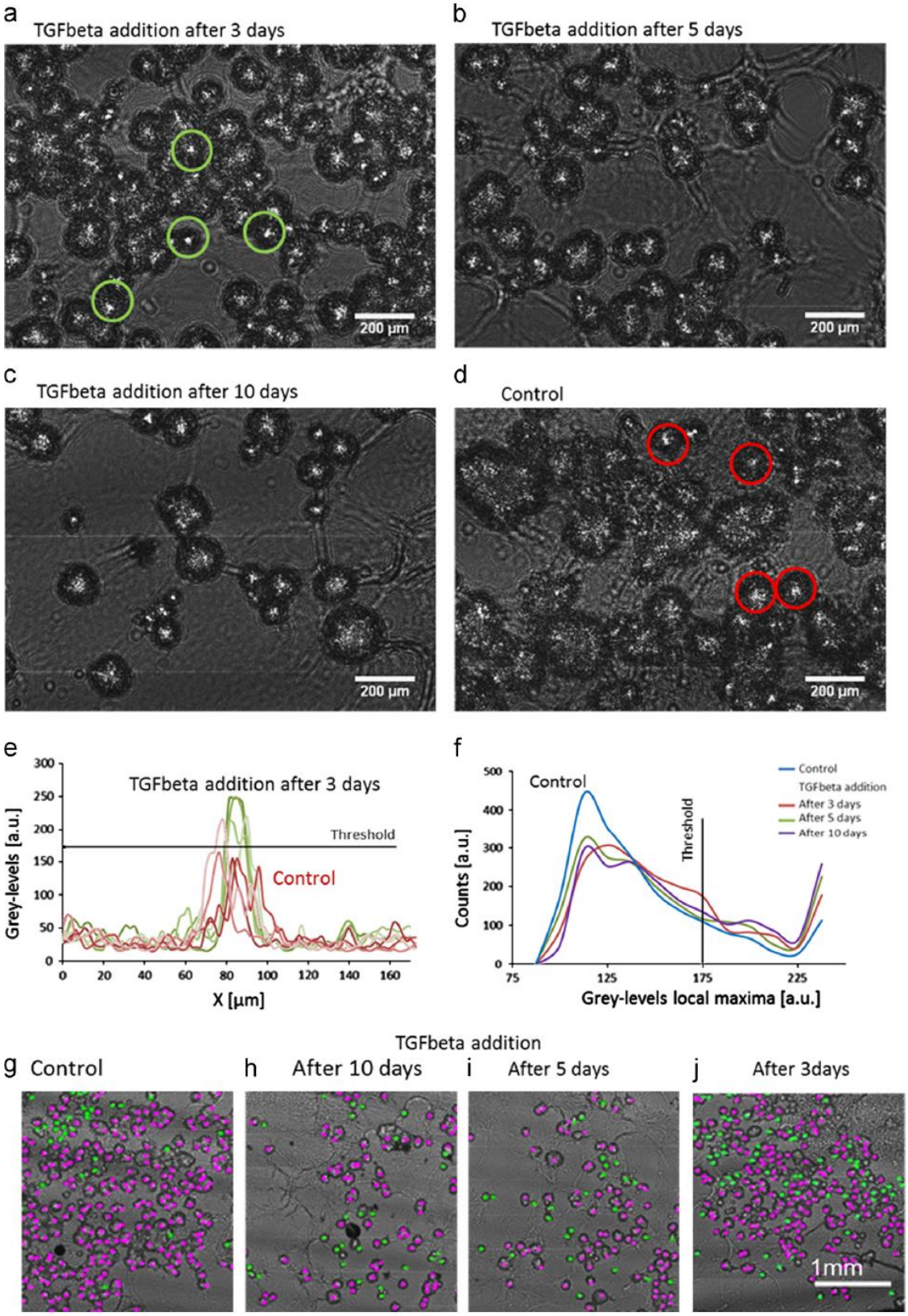

Fig. 5. The influence of TGF beta-1 addition on the number of spheroids. Cropped regions of 24 mm^2 lensfree acquisitions of the RWPE1 3D cell culture on day 12 of the experiment with TGF beta-1 (3 ng/mL) having been added after 3 (a), 5 (b) and 10 days (c) and with no TGF beta-1 treatment serving as a control (d). Note that acini hologram patterns with strong lensing effects are present in the acquisition, showing a very bright spot at the center of each pattern. Intensity profiles of such patterns, with green circles in (a) plotted in green in (e). For comparison, the control acini pattern intensity profiles [red in (d)] are plotted in red in (e). Local maxima distributions measured on four 24 mm^2 lensfree acquisitions (75 Gy-levels noise tolerance, ImageJ) are plotted as a function of the day on which TGF beta-1 had been added. (g, h, i, j) Cropped regions of 24 mm^2 lensfree acquisitions of RWPE1 3D cell cultures on day 12 of experiment as a function of the day on which TGF beta-1 had been added. Lensfree holograms of strongly lensing acini are marked as green points after manual counting (cell counter, ImageJ). Single acini and multiacinar structure are marked as purple points. (For interpretation of the references to color in this figure legend, the reader is referred to the web version of this article.)

known to be associated with cell tension that could mediate TGF beta activation (Giacomini et al., 2012). Interestingly, the cortical actin was still present after 9 days of treatment, indicating the long-term effects of TGF beta.

When combined with 3D culture and the appropriate metrics, our lensfree system allows the discrimination of polarized assemblies (acini) from non-polarized architectures (spheroids). As the maintenance of polarity is critical for the function of epithelial cells, our system provides a relevant tool to decipher biological processes in development and morphogenesis in a more physiological context than in traditional 2D cultures. Biomedical and drug screening applications are detailed in Supplementary information S-3.

5. Conclusions

This study demonstrates for the first time that lensfree imaging is a new methodology able to analyze distinct 3D cellular objects and discriminate acini from spheroids. It could be extensively used for studying cell–cell and cell–environment interactions by modulating the biochemical and mechanical stimuli within the ECM. We believe that this technique will be a powerful method for the future large field analysis of multiple soluble effects, including fundamental and pharmacological research in carcinogenesis.

Acknowledgments

The work at CEA-Leti was supported by the Carnot Institutes Network.

Appendix A. Supporting information

Supplementary data associated with this article can be found in the online version at http://dx.doi.org/10.1016/j.bios.2013.05.001.

References

Allier, C.P., Hiernard, G., Poher, V., Dinten, J.M., 2010. Biomedical Optics Express 1 (3), 762–770.
Bae, E., Ying, D., Kramer, D., Patsekin, V., Rajwa, B., Holdman, C., Sturgis, J., Davisson, V.J., Robinson, P., 2012. Journal of Biological Engineering 6 (1), 12.
Banada, P.P., Guo, S., Bayraktar, B., Bae, E., Rajwa, B., Robinson, J.P., Hirleman, E.D., Bhunia, A.K., 2007. Biosensors and Bioelectronics 22 (8), 1664–1671.
Baum, C., Dullmann., J., Li, Z., Fehse, B., Meyer, J., Williams, D.A., von Kalle, C., 2003. Blood 101 (6), 2099–2114.
Bello-DeOcampo, D., Kleinman, H.K., Webber, M.M., 2001. Mutation Research 480–481, 209–217.
Bishara, W., Sikora, U., Mudanyali, O., Su, T-W., Yaglidere, O., et al., 2011. Lab on a Chip 11 (7), 1276–1279.
Bryant, D.M., Mostov, K.E., 2008. Nature Reviews Molecular Cell Biology 9 (11), 887–901.
Debnath, J., Brugge, J.S., 2005. Nature Reviews Cancer 5 (9), 675–688.
Fienup, J.R., 1982. Applied Optics 21 (15), 2758–2769.
Giacomini, M.M., Travis, M.A., Kudo, M., Sheppard, D., 2012. Experimental Cell Research 318, 716–722.
Greenbaum, A., Luo, W., Su, T.W., Göröcs, Z., Xue, L., Isikman, S.O., Coskun, A.F., Mudanyali, O., Ozcan, A., 2012. Nature Methods 9, 889–895.
Hebner, C., Weaver, V.M., Debnath, J., 2008. Annual Review of Pathology 3, 313–339.
Isikman, S.O., Bishara, W., Mavandadi, S., Yu, F.W., Feng, S., Lau, R., Ozcan, A., et al., 2011. Proceedings of the National Academy of Sciences of USA 108 (18), 7296–7301.
Isikman, S.O., Bishara, W., Mudanyali, O., Sencan, I., Ting-Wei, Su., Tseng, D.K., 2012. IEEE Journal of Selected Topics in Quantum Electronics 18 (3), 1059–1072.
Lee, G.Y., Kenny, P.A, Lee, E.H., Bissell, M.J., 2007. Nature Methods 4 (4), 359–365.
Mailleux, A.A., Overholtzer, M., Brugge, J.S., 2008. Cell Cycle 7 (1), 57–62.
Moscelli, N., Van den Driesche, S., Witarski, W., Pastorekova, S., Vellekoop, M.J., 2011. Sensors and Actuators A: Physical 172 (1), 175–180.
Mudanyali, O., Bishara, W., Ozcan, A., 2011. Optics Express 19 (18), 17378–17389.
Mudanyali, O, McLeod, E, Luo, W, et al., 2013. Nature Photonics 7, 247–254.
O'Brien, L.E., Zegers, M.M.P., Mostov, K.E., 2002. Nature Reviews 3, 531–537.
Ozcan, A., Demirci, U., 2008. Lab on Chips 8 (1), 98–106.
Pampaloni, F., Reynaud, E.G., Stelzer, E.H., 2007. Nature Reviews Molecular Cell Biology 8 (10), 839–845.
Pearson, J.F., Hughes, S., Chambers, K., Lang, S.H., 2009. Cell Death and Differentiation 16 (3), 475–482.
Rodriguez-Fraticelli, A.E., Auzan, M., Alonso, M.A., Bornens, M., Martin-Belmonte, F., 2012. Journal of Cell Biology 198 (6), 1011–1023.
Seo, S., Su, T.W., Tseng, D.K., Erlinger, A., Ozcan, A., 2009. Lab on Chips 9 (6), 777–787.
Soulez, F., Denis, L., Fournier, C., Thiebaut, E., Goepfert, C., 2007. Journal of the Optical Society of America A: Optics, Image and Vision 24 (4), 1164–1171.
Su, T.W., Xue, L., Ozcan, A., 2012. Proceedings of the National Academy of Sciences of USA 109 (40), 16018–16022.
Tahmasbi, A., Saki, F., Shoukouhi, S.B., 2011. Computers in Biology and Medicine 41, 726–735.
Weidling, J., Isikman, S.O., Greenbaum, A., Ozcan, A., Botvinick, E., 2012. Journal of Biomedical Optics 17 (12) 126018.
Yue, S., Cardenas-Mora, J.M., Chaboub, L.S., Lelièvre, S.A., Cheng, J-X., 2012. Biophysical Journal 102, 1215–1223.
Zegers, M.M., O'Brien, L.E., Yu, W., Datta, A., Mostov, K.E., 2003. Trends in Cell Biology 13 (4), 169–176.
Zheng, G., Lee, S.A., Antebi, Y., Elowitz, M.B., Yang, C., 2011. Proceedings of the National Academy of Sciences of USA 108 (41), 16889–16894.

Supplementary material S-1

Table 1: List of the different CMOS sensors.

CMOS Sensor	Chip dimensions		Pixel pitch	Dynamic	Color
1/ Aptina MT9P031	5.7x4.2= 23.9 mm^2	2592x1944 pixels	2.2 µm	12 bits	Bayer RGB
2/ Mightex BCN-B050-U	5.7x4.2= 23.9 mm^2	2592x1944 pixels	2.2 µm	8 bits	mono.
3/ VFU-J003-MH-C	6.1x4.6= 28 mm^2	3664x2748 pixels	1.67 µm	8 bits	mono.

Supplementary material S-2

1. *Holographic reconstruction*

To investigate the complete signature within the raw image, we implemented a holographic reconstruction scheme based on the back-projection method detailed in [22][23]. Assuming Fraunhofer diffraction, the hologram pattern recorded at the detector plane at a distance z from the sample can be described using the Fresnel function $h(z)$. This function describes the propagation of the light scattered by the object through free space, where λ denotes the wavelength of light and (x, y, z) the spatial variables:

$$h_z = \frac{1}{j\lambda z} e^{j2\pi\frac{z}{\lambda}} \exp(j\pi \frac{x^2+y^2}{\lambda z}) \tag{1}$$

The diffracting object can be described by its complex transmitted amplitude t, which transforms into the light amplitude A after propagation to the detector plane:

$$t = (1-a)$$

$$A = t * h_z = (1-a) * h_z = 1 * h_z - a * h_z = e^{j2\pi\frac{z}{\lambda}} - a * h_z \tag{2}$$

The intensity I of the incident field is then recorded by the sensor:

$$I = A.A^* = 1 - e^{j2\pi\frac{z}{\lambda}}.a^* * h_z^* - e^{-j2\pi\frac{z}{\lambda}}.a * h_z + (a * h_z).(a^* * h_z^*) \tag{3}$$

From Equation (3), calculating the convolution between I and h_{-z} gives

$$I * h_{-z} \approx e^{j2\pi\frac{-z}{\lambda}} \left(1 - a - e^{j2\pi\frac{2z}{\lambda}}.a^* * h_{-2z}\right) \tag{4}$$

In this equation, a denotes the reconstructed object complex value.

2. *Zernike decomposition*

Zernike moments Z_{nm} of the image $f(x,y)$ are calculated for different values of n and m :

$$Z_{nm} = \frac{n+1}{\pi} \iint_{x^2+y^2 \le 1} f(x,y)[V_{nm}(r,\theta)]^* dxdy = \frac{n+1}{\pi} \int_0^1 \int_0^{2\pi} f(x,y)[V_{nm}(r,\theta)]^* rdrd\theta \tag{5}$$

Z_{mn} is the projection of the image function f onto the Zernike polynomial $V_{nm}(r,\theta)$ with

- $n \in N, m \in \mathbf{Z}$, $|m| \le n$, $n - |m|$ is an even number;

- $\left[V_{nm}(r,\theta)\right]^*$ is the conjugate of the complex Zernike polynomial $V_{nm}(r,\theta)$ of order n and repetition m: $V_{nm}(r,\theta) = R_{nm}(r)e^{im\theta}$ (6)

- $$R_{nm}(r) = \sum_{s=0}^{\frac{n-|m|}{2}} \frac{(-1)^s (n-s)!}{s!\left[\frac{(n+|m|)}{2}-s\right]!\left[\frac{(n-|m|)}{2}-s\right]!} r^{n-2s} \quad (7)$$

If we consider a rotation of the image $f(x,y)$ through an angle a, a new image $f'(x,y)$ is obtained, with $f'(r,\theta) = f(r,\theta-\alpha)$. The projection Z'_{mn} of the rotated image $f'(x,y)$ onto V_{nm} is $Z'_{mn} = Z_{mn}e^{-im\alpha}$. As a consequence, $|Z'_{mn}| = |Z_{mn}|$; the magnitudes of Zernike moments can be used as features that are invariant towards rotations. That result explains why only $|Z_{mn}|$ is necessary for our investigations. For a given value of n, m varies from $-n$ to $+n$ with a +2 increment:

(0,0)
(1,-1)(1,1)
(2,-2)(2,0)(2,2)
(3,-3)(3,-1)(3,1)(3,3)
(4,-4)(4,-2)(4,0)(4,2)(4,4)
(5,-5)(5,-3)(5,-1)(5,1)(5,3)(5,5)
(6,-6)(6,-4)(6,-2)(6,0)(6,2)(6,4)(6,6)
etc.

However, only values for positive m are computed because $|Z_{n,m}| = |Z_{n,-m}|$:

(0,0)
(1,1)
(2,0)(2,2)
(3,1)(3,3)
(4,0)(4,2)(4,4)
(5,1)(5,3)(5,5)
(6,0)(6,2)(6,4)(6,6)
etc.

In the end, for e.g., n varying from 0 to 20, 120 $|Z_{mn}|$ coefficients can be calculated. These 120 features are the data to be extracted from scattering images.

Figure S-1

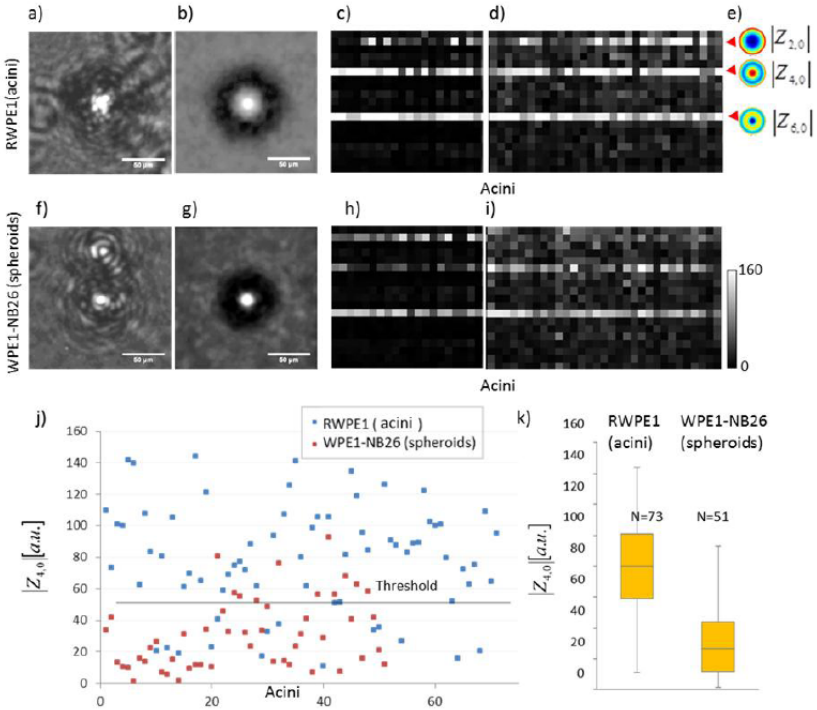

Zernike transform of lensfree imaging, acini with lumen versus spheroids.

(a) Lensfree holographic diffraction pattern of acini with lumen (RWPE-1 cells) exclusively from this experiment that is the average of 20 patterns (scale bar 50 µm). (b) Lensfree holographic diffraction pattern of spheroids (WPE1-NB26 cells) typical of this experiment that is the average of 20 patterns (scale bar 50 µm). (c, d, h, i) 2D map of 19 Zernike moments (from bottom to top: $|Z_{1,1}|$ to ||; see supporting information) as a function of 50 acini. (c, d) and (h, i) depict the moments calculated for the acini with lumen (RWPE-1) versus spheroids (WPE1-NB26). The largest difference between the two populations of acini is obtained from the calculation of the $|Z_{2,0}|$, $|Z_{4,0}|$, $|Z_{6,0}|$, Zernike moments (e). (c, d, h, i) Four different chambers of an 8-well Labtek® slide showing that the results are reproducible. (k) Plot of the $|Z_{4,0}|$ calculated for 21 WPE1-NB26 acini (in red) and 73 RWPE-1 acini (in blue). (j) Box plot showing the distribution of the calculated $|Z_{4,0}|$ Zernike moment. Each box encloses the middle 50% of the distribution, with the horizontal line marking the median and the diamond marker the average. The vertical lines and whiskers mark the minimum and maximum values of the distribution.

Supplementary information S-3

Biomedical and drug screening applications of a lensless biosensor

Being able to directly image such 3D architectures is of great interest because they mimic the specific cellular organization within an assembly of cells that is found in real tissue architecture. Given that spheroids are highly associated with a tumorigenic phenotype characterized by the loss of acinar polarity, our system could be used to screen cancer drugs based on the ratio of spheroids to acini. Moreover, such systems that enable the rapid imaging and measurement of polarity changes would greatly facilitate screening for environmental factors that affect epithelial homeostasis. Interestingly, tumor spheroids are often considered good models that recapitulate features of cancer because they are characterized by hypoxic and necrotic regions. Therefore, spheroids are used in pharmaceutical labs in in vitro 3D spheroid-based assays for measuring tumor growth and evaluating anticancer drugs. Functional assays for the evaluation of tumor progression are mostly based on assays of spheroid migration and their ability to invade connective tissue (Vinci et al, 2012). However, those assays do not consider the status of polarity that remains a critical readout to assess, for example, epithelial tissue integrity and homeostasis. Our technique can be potentially used as a screening method to identify risk factors for prostate cancer or other cancers of glandular tissues and to screen new drugs to prevent or revert polarity loss. Combined with 3D cell culture, lensfree imaging provides a tool to rapidly assess the epithelial polarity of living cells because it permits the measuring of dynamic biological responses over time. Moreover, there are plans to parallelize this system to make it compatible for high-throughput preclinical studies and suitable for dynamic, automated and quantitative imaging and analysis. It would therefore be a powerful tool to follow cancer progression, including changes in the size, shape and polarity of 3D structures and to evaluate drugs that increase acini-forming ability while decreasing invasiveness.

Vinci, M., Gowan, S., Boxall, F., Patterson, L., Zimmermann, M., Court, W., Lomas, C., Mendiola, M., Hardisson, D., Eccles, S.A. et al. 2012. B.M.C. Biol. 10, 29.

7.3 Hypothesis: Nidogen promotes branching-like morphogenesis and interacini communication as observed by lens free methods

7.3.1 Context

Along with acini, tubules are forming blocks of glandular tissues. Tubulogenesis development is a complex process in which tubules can arise from cells in many different starting conditions and configurations. Furthermore, local changes in growth factors concentration can induce branching process. Mechanisms of tubologenesis remain poorly understood and sit at the crossroads of developmental and cell biology (Chapter 2.3.4). In order to better understand epithelial tubulogenesis several advances are required. Development of new cell culture models that closely recapitulate key developmental processes is important to reveal new tubulogenic factors, including introduction of new markers diverse for cell types. Furthermore, understanding complexity and identification of intermediate stages of the development requires robust systems for live imaging.

Non-malignant prostate epithelial cells (RWPE1) were used to show that alteration in environment reflected in nidogen (entactin) concentration, leads to branching-like morphogenesis without additional growth factor stimulation. We employed lens-free time-lapsee microscopy to observe the sprouting-like process modeling EMT in 3D culture. The large field of view of our imaging system revealed the coexistence of various phenotypes and allowed us to observe the cooperation between cells that collectively changed their environment. We observed distinct cell phenotypes including path-finders, path-generators and spies travelling back and forth, from one 3D structure to another. To the best of our knowledge we are the first to observe such collective cell co-operation in 3D culture. Our observations provide new insights on how cells and grown structures coordinate in a 3D environment and how information is transmitted in both directions between them.

7.3.2 Result 1 - Branching-like process is governed by microenvironmental changes

In our model system of 3D cell culture on Matrigel we observed that prostatic acini cooperatively establish a branching-like phenotype through long-range interactions upon alterations in ECM composition. Traditional 3D cell culture on Matrigel can be performed according to two protocols – embedded and *top-coat* (Chapter 1). In embedded protocol cells are mixed with prepolymerized Matrigel thus during growth they are fully surrounded by Matrigel. *Top-coat* protocol relies on seeding cells on polymerized layer of Matrigel and adding diluted Matrigel 10% (v/v) into culture medium ("top-coat"). As has been presented in Chapter 4 RWPE1 cells without top-coat layer had a branching-like invasive phenotype. In order to verify if the change in phenotype is not cell-line dependent we seeded WPE1-NB26 (prostatic invasive cell line) in *no top-coat* conditions. Invasive WPE1-NB26 cells followed similar branching-like organization as compared to non-malignant RWPE1 (Figure 7-5C) with the difference that WPE1-NB26 cells within the branch were highly elongated as compared to well-organized RWPE1 (Figure 7-5 panel α and β). A high proliferation and cell migration has been observed as compared to surprisingly non –active behavior in standard conditions (Figure 7-5). Average area of spheroid after 5 days was 1432 μm^2 for control (*top-coat*) and 7287 μm^2 for *no top-coat* conditions. We observed that initially created networks by WPE1-NB26 observed after 3 days (Figure 7-5A) disappeared after 6 days which indicates self-seeding mechanisms since the number of total spheroids decreased in parallel with significant increase in the spheroid area at the same time (Figure 7-5B). Moreover,

We further asked if the observed branching-like process exhibits properties characteristic for EMT, which are *i)* changes in morphology, *ii)* functional changes associated with the conversion of stationary cells into motile cells that invade through the ECM and iii) changes in differentiation markers (expression of vimentin). *No top-coat* conditions cause high cellular motility which is reflected by branching-like process. As a result chains of cells inter-connect acini (Figure7-6A) to form a tree-like structure. Furthermore, migrating cells transform into more elongated, mesenchymal shape, expressing vimentin (mesenchymal marker) (Figure 7-6B panel β). Immunostaining for beta-catenin or E-cadherin did not show any staining on forming cellular branches and golgi apparatus was randomly positioned. We verified that the migrative cells invade Matrigel. Z-stack microscopy showed that cells leaving 3D structures form branches within the Matrigel and invade up to 100 μm in depth (Figure 7-6C). By superposition of the Z-stack images we observed that branches are formed throughout the Matrigel volume (Figure 7-6D and 7-6E).

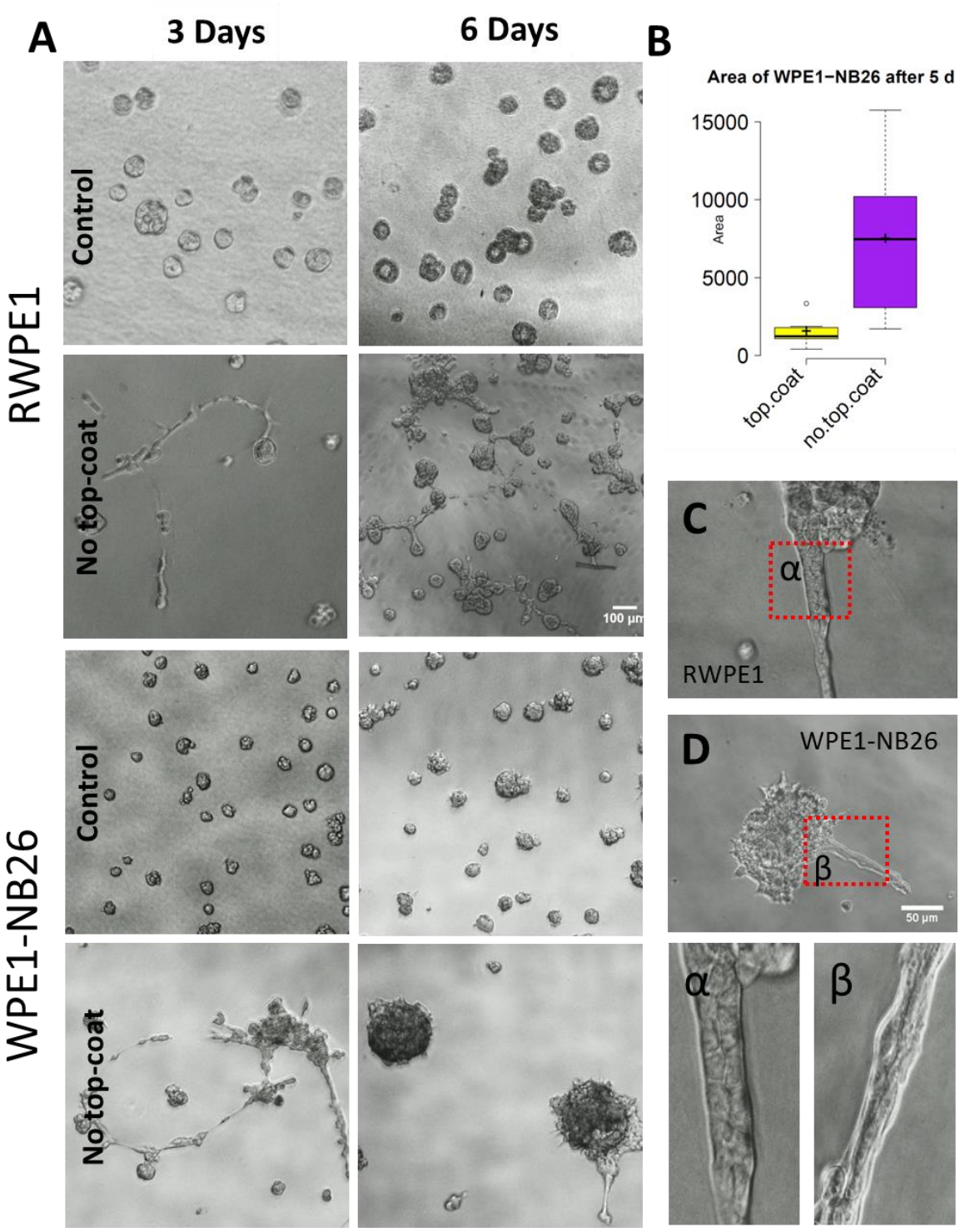

Figure 7-5 Effect of *no top-coat* in 3D cell culture of RWPE1 and WPE1-NB26. A) Phase contrast images present cellular organization after 3 and after 6 days of culture. Control conditions contain 10% Matrigel top-coat. **B)** Box-plot comparing area of WPE1-NB26 spheroids after 6 days in top-coat and no top-coat conditions. **C)** and **D)** show the cellular organization within the branches with zoom presented in panel α and β. Scale for all images in A is 100 µm and for C and D, 50 µm.

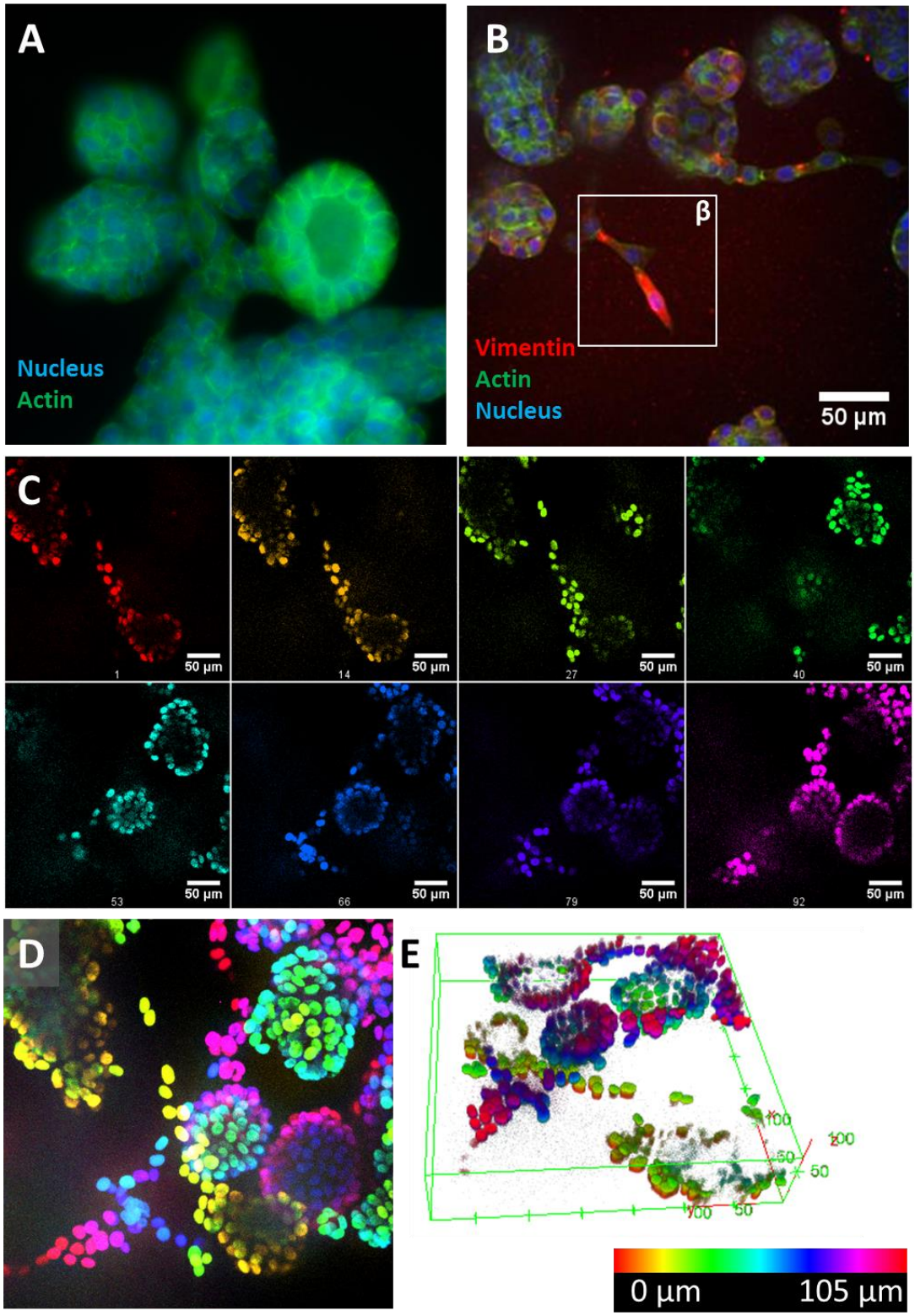

Figure 7-6 Organization of RWPE1 cells in 3D in no top-coat conditions. A) Staining for nuclei and actin reveals the tree-like organization with 3D structures containing lumen. **B)** Motile cells change their form into more mesenchymal-like expressing vimentin marker. **C)** Chosen sections of Z-stack (step size 1 µm) show the presence of cells on different levels of Matrigel volume. False colors represent the depth over 105 µm. **D)** Superposition of all Z-sections shows branches overlapping and crossing. **E)** 3D representation of cells organization within the Matrigel. Scale bar B) and C) 50 µm.

In order to better understand the microenvironmental changes that underlie branching process, we refer to our previous results with Matrigel beads. We observed that formed Matrigel beads undergo slow dissolution reflected by change in size (Chapter 5, Figure 5-8) but only in absence of 1% Matrigel in culture medium. Since cell-ECM signaling is important in development and morphogenesis (Fata *et al.*, 2004), we asked whether dissolution is homogeneous or only some components of Matrigel are transferred into culture medium. To verify if the dissolution is homogenous, Matrigel layers were incubated in PBS (Ca^{2+}, Mg^{2+}) during 6 days. Concentration of proteins was measured by UV/Vis spectroscopy means (NanoDrop) and shown that already after 24 hours protein concentration was ~0,3-0,5 mg/ml (in dependence of the amount of Matrigel polymerized inside the well) and reached ~0,8 mg/ml after 6 days (Figure 7-7A). We further used an agarose gel protein separation technique to check whether all components diffuse homogenously out from Matrigel beads. A protein solution in PBS (supernatant) has been compared with pure Matrigel. Separated proteins were stained with Coomassie blue stain (Figure 7-7B). For comparison, concentrations of both Matrigel and supernatant were adjusted equal by determining initial concentration using BCA kit (see Materials and Methods, Chapter 9.2.3). Matrigel presented an additional band (around 170kDa) as compared to supernatant. This indicates that this component of Matrigel concentrates inside beads while others slowly get into solution. We have identified by Mass Spectrometry technique (collaboration with CEA/iRTSV/BGE/Edyp platform) that the protein that stays in Matrigel and is not detectable in supernatant is nidogen (also known as entactin) (one of the four major components of Matrigel).

We hypothesize therefore, that nidogen plays an important role in ECM-cell signaling and in branching morphogenesis.

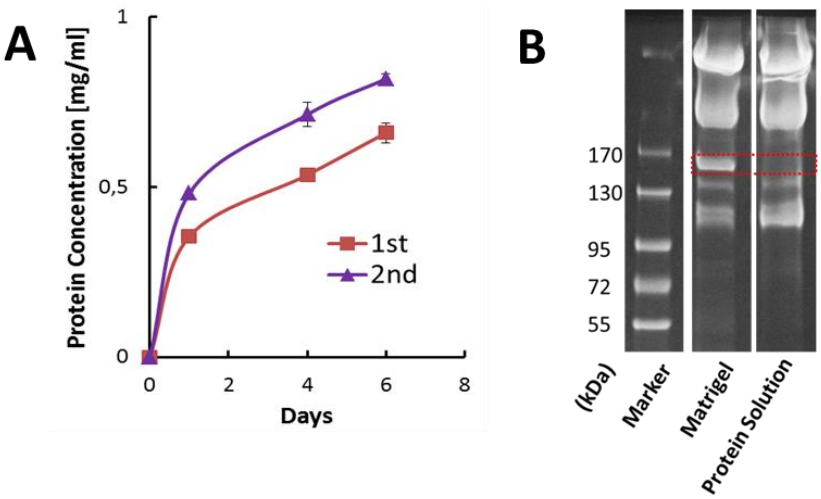

Figure 7-7 Instability of Matrigel. A) Polymerized Matrigel was kept in PBS. At different time points protein concentration has been measured. 1st is the well that contained less Matrigel as compared to 2nd. B) Agarose gel with separated proteins from Matrigel and Protein Solution (supernatant obtained during first 48 hours of incubation in PBS). Proteins well stained with Coomassie blue.

7.3.3 Result 2 – TGF-β1 inhibits branching-like process

We have further asked how these environmental changes induce branching-like process. Since the only change between *top-coat* and *no top-coat* occurs in the environment, we suspected that integrin signaling could be altered. We used RNAi approach to decrease expression of β1-integrin. To obtain high transfection efficiency we transfected cells in 2D for 72 hours and further transferred them into 3D culture. As a negative control we used siAllStar. Small phenotypic changes in 2D culture were observed, which reflected in bigger population of more elongated cells (not shown). While siβ1-integrin-treated cells were proliferating in 2D culture, after transfer on Matrigel, majority has died or poorly developed amorphous 3D structures (Figure 7-8A). We have compared expression of beta-catenin in 2D culture of a control and transfected cells. Observed change in the phenotype upon transfection did not affect β-catenin expression (Figure 7-8 right panel). On the other hand, Rac1 which in cancer drives cell motility by formation of lamellipodia (Parri and Chiarugi, 2010) has relatively increased in siβ1-integrin-treated cells which correlates well with the observed change in cellular shape.

Because si-β1-integrin treatment did not provide any phenotype in 3D culture we have used a TGFβ1 treatment. TGFβ1 has an inhibitory effect on RWPE1 cells as we observed in Chapter 7.2. RWPE1 cells were seeded in *top-coat* and *no top-coat* conditions and treated at the very beginning of the 3D culture with 3 ng/ml TGFβ1. As expected, *top-coat* protocol induced acinar morphogenesis while *no-top-coat* promoted branching-like process (Figure 7-8B). Treatment with TGFβ1 prevented entirely formation of branches. However, structures grown under TGFβ1 culture resulted in a less organized 3D morphology, both in *top-coat* and *no top-coat conditions.* Interestingly, expression of β-catenin remained unchanged in *no top-coat* as compared to *top-coat* conditions (Figure 7-8B). β-catenin is an important protein correlated with formation of adherent-junctions, whose loss can be associated with EMT. After treatment with TGFβ1 we observed decrease in β-catenin expression. Because β1-integrin signaling is involved in the ECM-cell interaction we have further looked into the expression of β1-integrin, FAK, and Rac1 (Figure 7-8B). In these preliminary studies, we have observed an increase of the expression of β1-integrin in *no top-coat* conditions. On the other hand, FAK (focal adhesion kinease) has maintained on the similar level in all conditions while Rac1 (Ras-related C3 botulinum toxin substrate 1) increased significantly in *no top-coat* +TGFβ1 conditions.

Further studies on particular integrin heterodimers are required to better understand the role of ECM composition changes on epithelial phenotype and cell-ECM signaling.

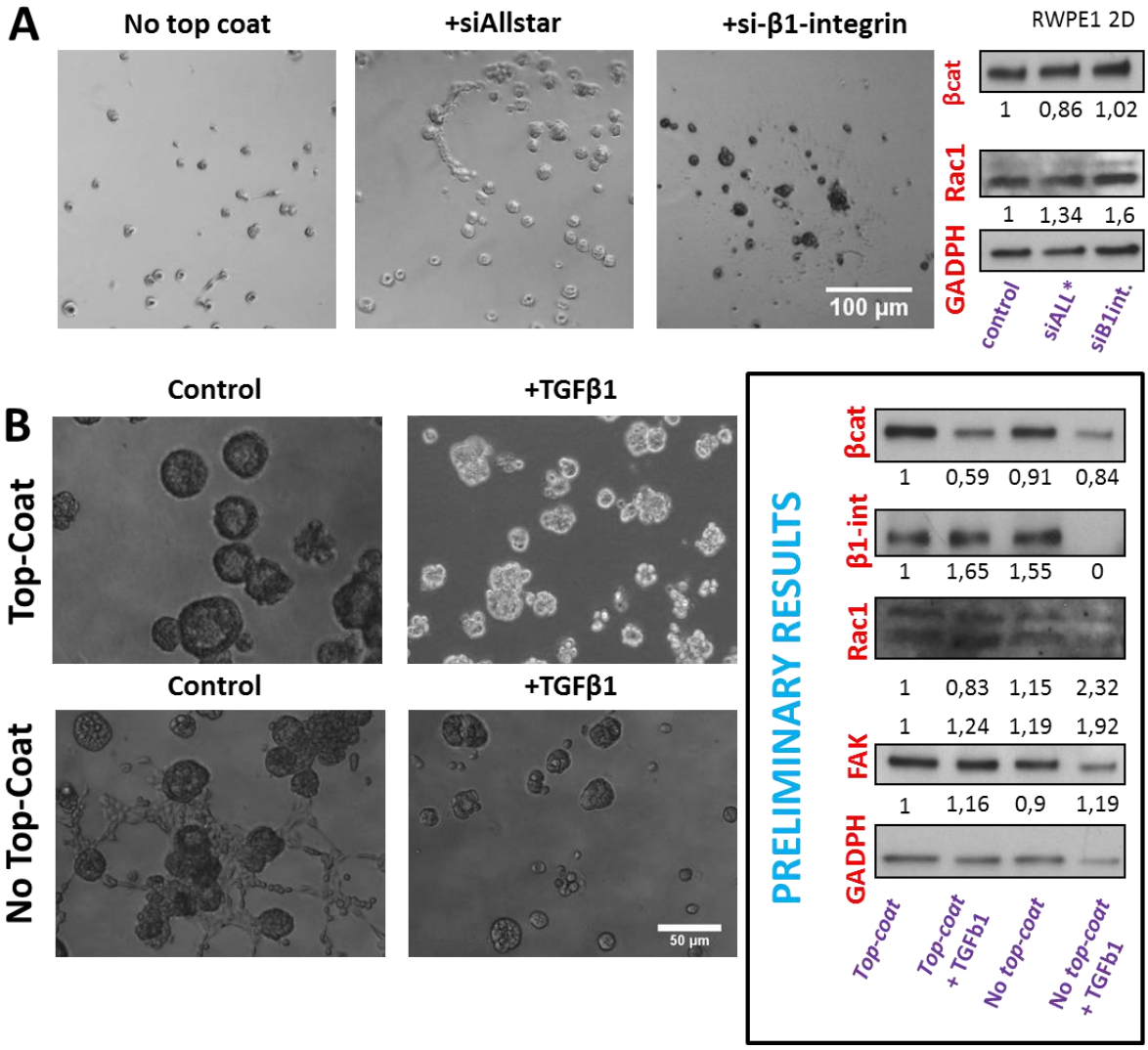

Figure 7-8 ECM-cell interaction in 3D *top-coat* and *no top-coat* conditions. A) Microphotographs of 3D culture transfection experiment to decrease β1-integrin signaling in *no top-coat conditions*. Right panel: expression of β-catenin and Rac1 protein with GADPH loading-control for *no top-coat,* siAllStar and β1-integrin transfected cells. **B)** Effect of TGFβ1 treatment on 3D cell culture in *top-coat* and *no top-coat* conditions. Right panel: comparison of protein expression between *top-coat* and *no top-coat* conditions, and with or without TGFβ1. Number below indicate the relative density including correction for loading of proteins. Scale A) 100 µm, B) 50 µm.

7.3.4 Result 3 - Self-seeding in branching morphogenesis?

Since we have discovered a way to induce branching-like process we have further asked how dynamic these process is and how the network of branches in 3D culture is established.

It has been proposed and preliminarily observed that cells during morphogenesis and healing have assigned distinctive roles in the process (Gov, 2007), as has been shown experimentaly for instance on wound-healing assays (Fenteany *et al.*, 2000; Poujade *et al.*, 2007). These roles include leaders (path-generators) who are the cells in the front of the collective migration and are characterized by the elongated form, and followers that use the paths generated by the leaders. However, technological limitations (described in Chapter 2.4) and restricted number of cellular models hampered observations of *in vitro* 3D morphogenesis.

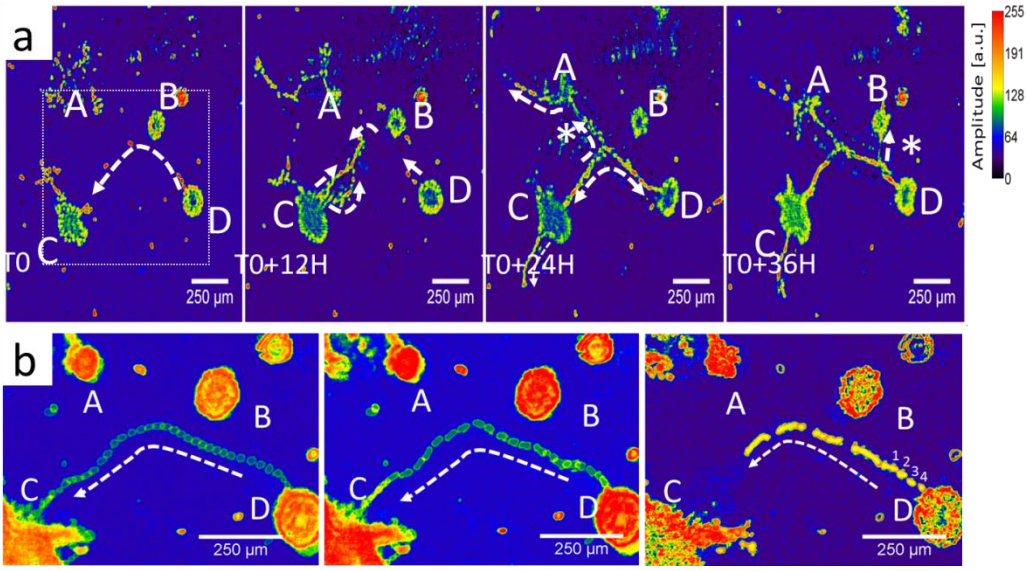

Figure 7-9 **(a)** 36H time-lapsee imaging shows the construction of a network between four acini A, B, C and D that are enclosed in a surface of 0.6mm^2. The network is first initiated by the ejection of a single cell from acini D (80 µm in diameter). The trajectory of this cell goes close to acini B and then reaches acini C in a journey of 17 hours (track of 750 µm, distance/route=0.81). A cell or a batch of two is again ejected from acini D and reaches acini C taking the exact same path as described in **(b)** It is followed by a collective cell migration (4 cells) between acini D and C, along again the same path. The average speed measured in (b, c and d) increase slightly, respectively 0.9, 1.1 and 1.3 µm/min with a standard deviation of 0.2 µm/min. This path further serves as the grounding for the construction of a network between the four acini. Two sub-branches (*) allow connection to acini A and B. The network is completed at T0+24H and remains stable

To overcome these limitations, we used a lens-free video microscopy characterized by the large field of view (25 mm^2) which allows monitoring dynamic processes between many 3D structures at the same time. Thus detection and observation of rare events within the cell culture is possible. By using lens-free approach we observed that the population of non-malignant epithelial cells assigns different roles including path-generators and followers during branching-like morphogenesis (Figure 7-9A). By the cooperation between migrative

cells, complex communities are developed. We observed release of single leader cells (path-generators) from stably growing structures (often containing lumen) that find their way between two distinct acini. The establishment of the branch, therefore, proceeds first by the path establishment and subsequently by collective cell migration (Figure 7-9B). We measured that the first leader cell migrates and generates a 920 µm non-linear track in the Matrigel in approximately 11 hours. Once leader cells establish a path, ejection of follower cells from structure *D* to structure *A* occurred along the same non-linear path. Cell tracking experiments and velocity measurements (Figure 7-9B,) showed that the single cell migration velocities significantly increased from 0.9 µm/min to 1.3 µm/min, between the first to the last cell traveling along the same migration track.

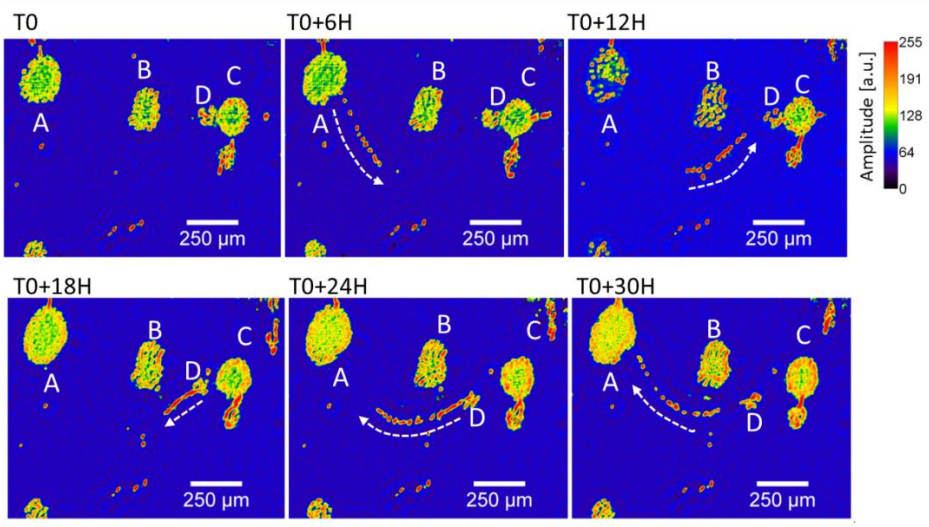

Figure 7-10 30H time-lapsee imaging shows the collective migration of a batch of ~15 cells between two acini (*A* and *C*), bypassing a third acini B. The track is as long as 990 µm and the cell migration last about 13 hours (1.26 µm/min). Migrating cells reach acini *C* but do not attach to form a stable network. Instead they use previously established path to return with a newly recruited structure *D* (~80 µm diameter)to the initial structure *A*.

Furthermore, with the advantage of our imaging system, we observed the multi-directional migration in branching-like morphogenesis in which cells use back and forth migration to seed distant sites and return to the original structure (Figure 7-10). Interestingly, these findings (Figure 7-10) also show that this back and forth migration promotes accelerated growth because the initial acinus-like structure (*A*) gradually increases in size as cells return. Structure *A* increased in size from T0 to T0+30 hours while a group of cells (*D*) are taken from the transmitter-structure *C* and sent back to *A*. The mechanism for self-seeding in cancer is generally accepted (Comen and Norton, 2012). We have observed a similar mechanism during branching-like morphogenesis in 3D culture of prostatic non-malignant cells. In here, self-seeding mechanism aimed to accelerate initial structures (*A*) growth under the experimental

conditions of this study. Observation of seeding during branching-like process is visible also in Figure 7-9B, where structure that accepted collectively migrating cells permanently increased in size while the sending structure reduced its size.

Furthermore, observed back and forth migration process may bypass acini that are much closer to the original tumor suggesting a complex mechanism of the migration and communication. For example, Figure 7-9B shows that acinus *D* connects to acinus *C* and bypasses *B.* Furthermore, Figure 7-10 shows that acinus A did not connect with the nearest acinus *B* but targeted the acinus the most far away (structure *C*). These observations suggest that cells may use mechanisms other than mechanical ones (via collagen fibers for instance) to initiate seeding. These alternate mechanisms may potentially involve chemical signaling inside the ECM and diffusible repulsive and/or attractive factors secreted by the cells. Our observations are consistent with the finding that primary tumors may use chemical signals to send out aggressive tumor cells as "spies" explore environments (Ben-Jacob *et al.*, 2012).

7.3.5 Result 4 - Cell migration but not cell proliferation establishes branches between structures

Surprisingly, cells coordinate seeding over a very long distance (> mm), and faster than previously described (900 µm in 14 hours (65 µm/h)) (Guo *et al.*, 2012). The trajectories of 18 different migration tracks during seeding were measured (Figure 7-11). The distance traveled varies between 200 and 1450 µm, with an average distance traveled of approximately 600 µm, and the average speed calculated over 436 positions was 0.9 ± 0.4 µm/min. We defined the seeding index as a ratio of the distance between the start and end points of the actual trajectory. Using this definition, we measured a high seeding index of 0.78 ± 0,16, and the seeding index was higher than 0.9 when the distance traveled was less than 350 µm (Figure 7-11A). With the short distance seeding cells travel along a straight path until they encounter another object e.g., an acinus or a cell aggregate. Beyond 350 µm, we observed that the trajectories changed from this initial straight path and were altered in response to the presence of other objects in its surrounding environment, at distances up to 400 µm away. Surprisingly, for eight trajectories of this type, we observed that the directional changes occurred at angles close to 90° (Figure 7-11B). These observations have led to the proposed model, which is discussed in a later section.

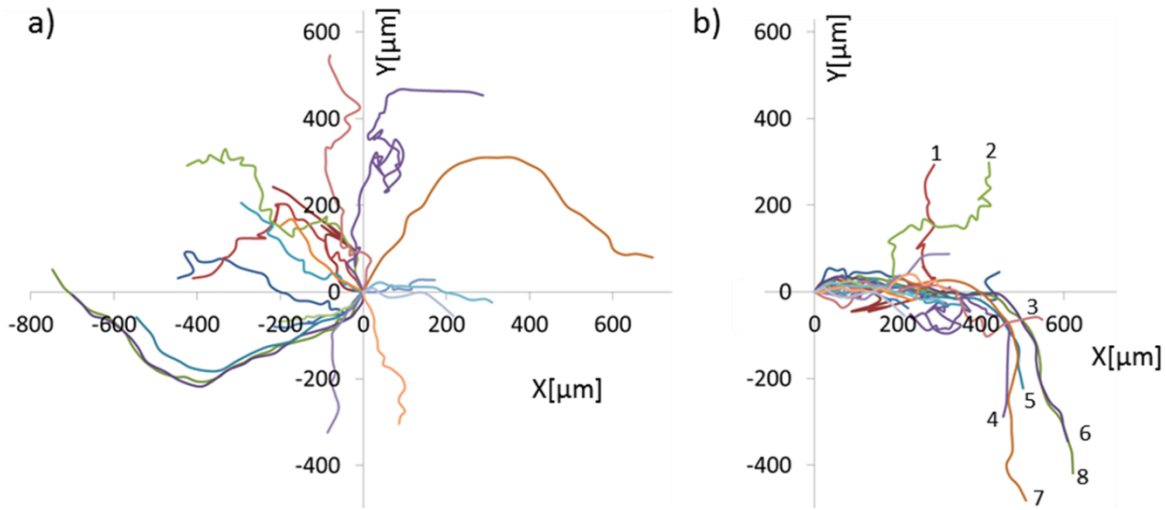

Figure 7-11 **(a)** Graph depicts the trajectories of 18 different branching connecting acini to acini or acini to cell aggregates. Trajectories are measured by following the tip of the branching position relative with the first position as origin. Over 436 positions, we have calculated an average speed of 0.9±0.4 µm. We can define the connection efficiency as the percentage ratio between the effective distance and the travelled distance. We measure a pretty high efficiency of 78±16% and larger than 90% if the travelled distance is below 350 µm. **(b)** The graph shows trajectories rotated so that initial direction taken in the first 100 µm matches with the X axis. This representation shows that branching takes at first a straight direction till it encounters another object, e.g. an acini or a cell aggregate. If not the trajectory can be modified (see labels 1 to 8) by the presence of another object in its surrounding, at distances up to 400 µm. It means that when branching connection occurs between different objects, it is straightforward: this no random walk, there is obviously something at work.

7.3.6 Result 5 - Chemo-attraction and -repulsion as a model for spatial orientation of formed branches

We further asked if control over observed interactions between 3D structures can be correlated with the model of chemoattraction. In order to verify this hypothesis, we used a simple 2D model (Figure 7-12) in which the chemical signal is calculated based on the diffusion process, and the cell velocity is assumed to be proportional to the concentration gradient of the chemical signal (Serini *et al.*, 2003):

Eq. 4 $$\frac{dC}{dt} = D\Delta C$$

Eq. 5 $$\vec{v} = k\nabla C = k\left(\frac{dC}{dx}\vec{\imath} + \frac{dC}{dy}\vec{\jmath}\right)$$

,where C(x, y) is the chemical signal concentration, (x, y) are spatial variables, D is the coefficient of diffusion and k is a speed coefficient that relates the speed to the chemical concentration. Fitting parameter are the variables D and k, and the initial condition C0(x, y). C0(x, y) matches the acini map, a weighing factor is given to each acini, i.e., positive and negatives values that correspond to attraction and repulsion, respectively. The computation of

this model allows us to match the observed track (Figure 7-12). It shows that the observed phenomena could be attributed to chemotactism, but further experiments are necessary to demonstrate this possibility.

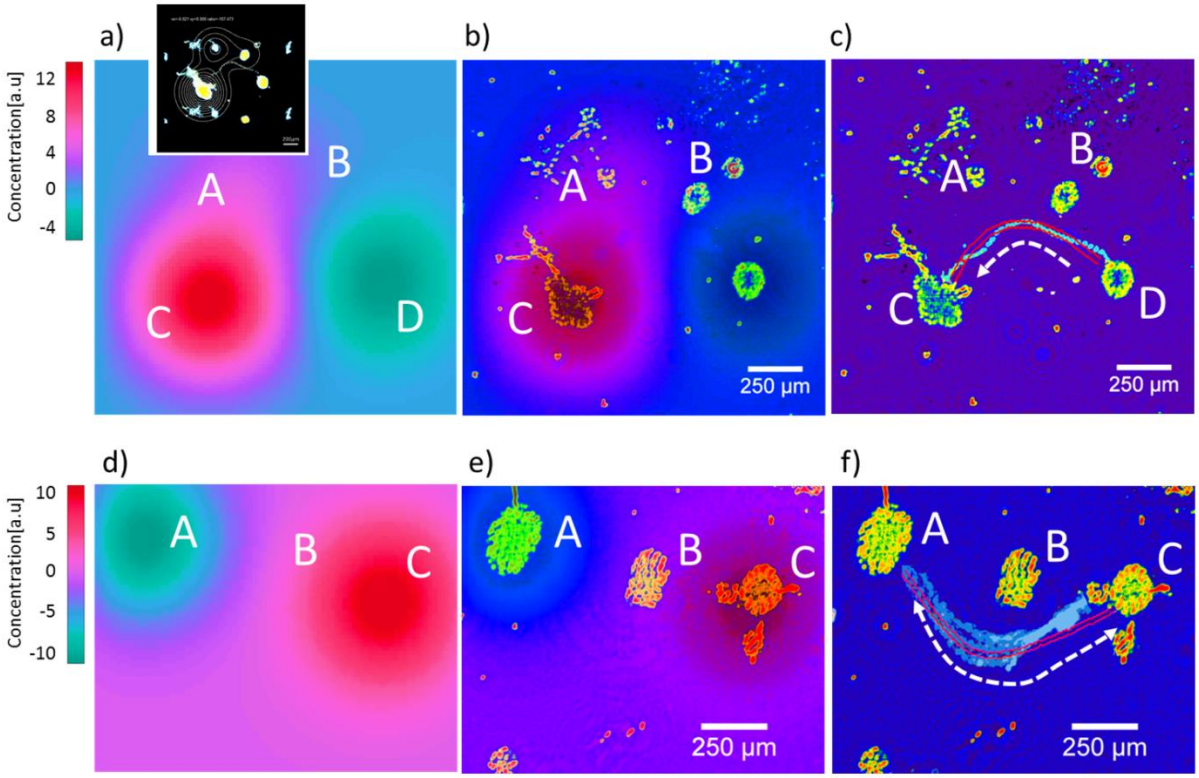

Figure 7-12 Cell trajectory calculated as the path following the gradient of the chemo-attraction map. (a, d) Chemical signal concentration computed from Eq. (1) to model the observation of cell migration as depicted in respectively Fig. 2 and 3. Positive and negative values correspond respectively to attractive and repulsive signaling. **(b, e)** represent the chemical concentration overlaid with the holographic reconstruction as taken from Figure 7-9 and 7-10 respectively. In **(a)** we have considered acini A and C as attractive, B as neutral and D as repulsive. **(c)** Shows the simulated cell trajectory (red) starting from acini D following the gradient of the concentration (Eq. (2)). In **(d)** we have considered acini A as repulsive, B as neutral and C as attractive. **(f)** Shows the simulated cell trajectory (red), starting from acini A, following the gradient of the concentration. In the two cases the simulated trajectory matches well the observed cell trajectories (cyan).

7.3.7 Result 6 - Mechanical remodeling of ECM occurs during branching-like morphogenesis

Recent studies in 3D cell culture showed, that branching morphogenesis is governed not only by soluble signals sent by surrounding tissues but also by mechanical signaling (Shi *et al.*, 2014). It has been observed that MCF10A-Ras-transformed acini disorganize when transferred on top of collagen I gels (Shi *et al.*, 2014). Authors show that cells mechanically align and concentrate fibers in their ECM environment. We used fluorescent nanobeads to verify if acini in *no top-coat* and *top-coat* conditions exert similar forces on Matrigel

environment. Nanobeads were homogenously immobilized within the polymerized Matrigel layer on which cells were seeded (detailed in Materials and protocol, Chapter 9.2). We have observed previously described in literature reorganization of environment by multicellular structures pulling on ECM fibers around (Figure 7-13). Further studies, should provide an answer if the observed migration of cells during branching-like process occurs along these reorganized ECM fibers.

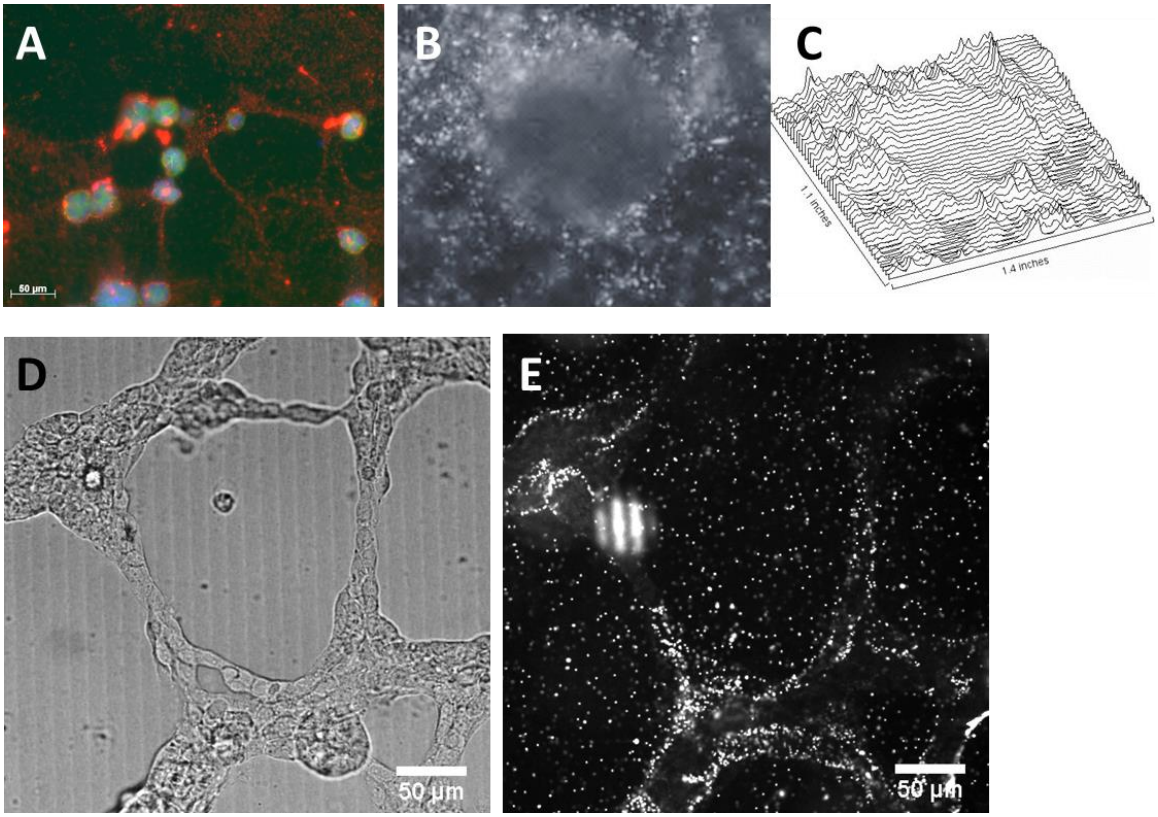

Figure 7-13 Cell-ECM interactions. A) Overview of the ECM reorganization by acini in *top-coat* conditions. Remodeling of the environment is reflected in local concentration of red fluorescent nanobeads. A directional acini' pulling concentrates nanobeads within the Matrigel into a network between structures. **B)** A single structure concentrates ECM around by pulling as visualized by nanobeads. A surface profile of nanobeads concentration confirms the pulling effect (**C**). **D)** Phase contrast image of the branching-like process (*no top-coat*) and a corresponding fluorescent image of nanobeads distribution (**E**). Scale bar 50 µm.

7.3.8 Discussion and future work

It is widely accepted that cell migration and tissue invasion are controlled by external stimuli, such as growth factors and cell–cell interactions. Moreover, distal effectors, including extracellular matrix components, are important factors in regulating sprouting and branching events (Friedl and Gilmour, 2009). We determined conditions upon which RWPE1 prostatic epithelial cells undergo repeatable branching-like morphogenesis in 3D culture on Matrigel. The instability of Matrigel achieved by *no top-coat* conditions causes proteins transfer into solution (culture medium) with the exception of nidogen. As a consequence ratio of particular components of Matrigel undergoes changes. Yet we do not know how exactly these changes influence cells fate to promote branching-like morphogenesis in RWPE1 cells, which in *top-coat* conditions in Matrigel culture form polarized acini. Transformed WPE1-NB26 cells underwent similar process which finally indicated a self-seeding model, which served to increase growth of spheroids.

Under *top-coat* conditions, RWPE1 cells form acini. However, observed alteration of the ECM composition has led to changes which are often associated with tumorigenesis, such as invasion, uncontrolled proliferation, and loss of apico-basal polarity in migrating cells (Debnath and Brugge, 2005; Paszek *et al.*, 2005). In general, ECM stiffening is associated with cancer. *In vitro* experiments showed that Matrigel matrices enriched with collagen-I became more rigid and induced malignant phenotypes (Paszek *et al.*, 2005). However, in parallel to alteration of ECM rigidity, the concentration of binding sites to integrin has increased with increased collagen I (Engler *et al.*, 2004). Here we have shown that instability of Matrigel reflected in its dissolution and lead to the malignant-like phenotype. Due to the time constraint, we did not measure the rigidity of the Matrigel during the dissolution process. However, it has been shown that rigidity of semiflexible polymers is proportional to the square of the protein concentration (Mackintosh *et al.*, 1995). Therefore, we anticipate that observed Matrigel dissolution is associated in the rigidity decrease and thus that the changes in the composition are responsible for the phenotype alteration.

Role of nidogen

The composition of basement membrane varies among the human tissues during tissue development, homeostasis and eventual pathologies. A natural extract from EHS tumor (Matrigel) used widely for 3D cell culture is largely composed of laminin, collagen IV, heparin sulfate, and nidogen (entactin). Cell attachment to ECM occurs mainly through basally located integrin receptors (Alford and Taylor-Papadimitriou, 1996). Gene knockout mice studies showed the importance of ECM-signaling on mammary branching morphogenesis (Chen *et al.*, 2002). Much attention turned into laminin family as important ECM molecules in epithelial morphogenesis (Stahl *et al.*, 1997; Wang *et al.*, 2013). Conversely less is known how nidogen interacts with cells and what is its role in branching morphogenesis.

Nidogen has been identified as ECM component containing cell binding and collagen IV and laminin-1 binding sites (Pujuguet *et al.*, 2000). Our results of mass spectrometry analysis confirm high affinity of nidogen and laminin-γ1 by the presence of the latter within the analyzed gel band. *In vitro* studies showed that nidogen is synthetized and secreted by primary and established mesenchymal and myoepithelial cells but not by epithelial cells (Pujuguet *et al.*, 2000). Furthermore, antibodies that block nidogen-laminin binding site have shown perturbation of kidney and lung morphogenesis (Ekblom *et al.*, 1994) indicating that binding of nidogen with laminin-1 could be required for development. On the other hand nidogen (both isoforms) gene knockout studies in mice showed mild phenotypes (Gersdorff *et al.*, 2007).

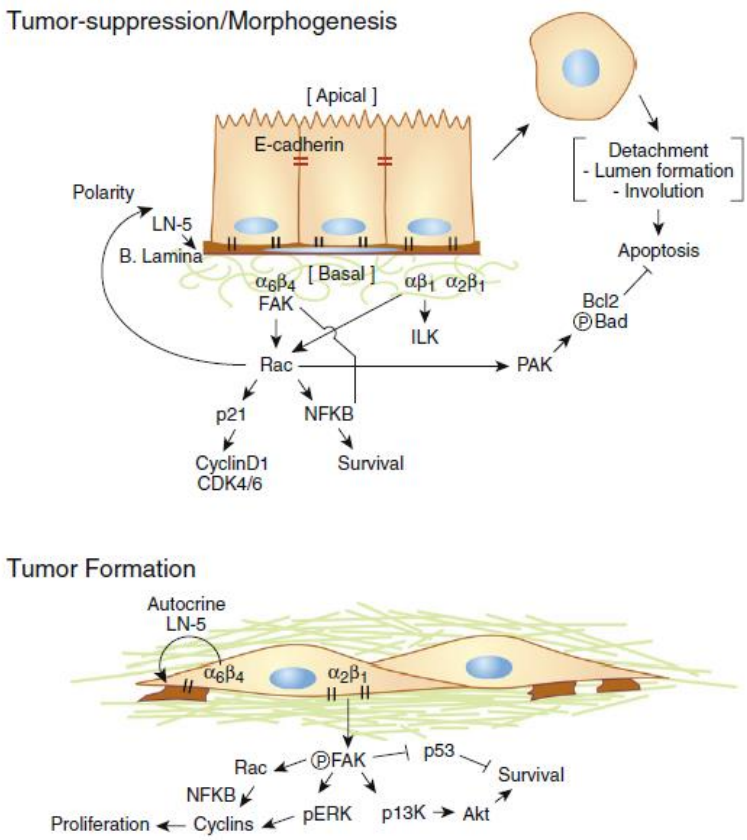

Figure 7-14 Integrin-mediated signaling pathways regulate normal epithelial phenotype and differentiation. Source: (Keely, 2011)

Nidogen is a ligand of α3β1, α6β4 and αVβ3 integrin (Darribere *et al.*, 2000). We have therefore, focused on β1-integrin signaling (a scheme on integrin-ECM signaling is presented in Figure 7-14). The role of certain integrins in branching morphogenesis is highly complex and depends on the model system. For example knockout studies in mice revealed that α3, α6 and β4 integrin subunit are not required for branching morphogenesis (Klinowska *et al.*, 2001) while α2 drastically limits branching (Chen *et al.*, 2002). Contrary, α3 enhances branching in *in vitro* collagen I cultures (Berdichevsky *et al.*, 1994) while inhibitory effect has been observed in Matrigel cultures (Stahl *et al.*, 1997). We observed preliminarily an increase in β1-integrin

expression in *no top-coat* conditions as compared to *top-coat* conditions. However, we did not observe any significant change in the ß-catenin and FAK expression suggesting maintenance of non-malignant phenotype in *no top-coat* conditions. FAK is one of the dominant integrin-mediated signaling events and increased levels have been observed in many breast carcinoma (Owens *et al.*, 1995). Similarly activation of Rac1 and P13K leads to malignants phenotype (Marinkovich, 2007). Moreover, it has been shown that induced malignant sprouting phenotype of MCF10-A on stiff matrices can be inhibited by decreasing Rac1 signaling (Chaudhuri *et al.*, 2014). In our culture conditions levels of Rac1 remained approximately equal as measured semi-quantitatively by western blot technique.

Integrin – TGFß crosstalk

Integrins present a dual role; they serve as tumor suppressors and tumor promoters. Integrin activation of Rac promotes cells progression by regulating G1 via CDK6 and CDK6 (Mettouchi *et al.*, 2001). It has been also shown in epithelial 3D culture of malignant cells, that malignant phenotype could be reversed by using β1-integrin blocking antibodies (prostate (Zhang *et al.*, 2009), breast (Park *et al.*, 2006)). On the other hand, loss of certain integrin subunits (i.e., α6 and α2) is responsible for tumor progression (Knox *et al.*, 1994; Tagliabue *et al.*, 1998).

We have shown that TGF-ß1 treatment on *no top-coat* cultures prevents branching-like morphogenesis. As we previously observed in our lens-free experiments, also *top-coat* cultures had smaller rate of growth and different morphology. We have observed that ß1-integrin expression in *no top-coat* conditions was higher than in standard 3D culture. The inhibitory effect of TGFß1 has been observed in both cultures conditions. We did not observe any ß1-integrin expression in *no-top-coat* conditions but this can be an effect of the low protein concentration in the western blot loading step. Recently various reports indicate that there is an extensive integrin - TGF-ß crosstalk. TGF-ß is able to affect integrin mediated cell migration and adhesion by integrin expression regulation. TGF-ß signaling is involved in development but also in variety diseases including cancer. In most cases TGF-ß stimulates integrins expression however, downregulation of integrin expression has also been observed (mostly laminin receptors) (Margadant and Sonnenberg, 2010). TGF-ß family has an inhibitory effect on branching morphogenesis in mammary gland development in mouse, however, the mechanism has not been presented (Robinson *et al.*, 1991).

Dynamism of branching-like process

To date definition of EMT process assumes unidirectional migration of cells, which in case of metastasis, leave primary tumor to induce metastasis at distant sites. Recently a theory of self-seeding tumor has been proposed and experimentally proved (Kim *et al.*, 2009). Authors implanted differently labeled xenografts at different anatomical sites within the same mouse to

show, that after two months metastatic tumor cells injected at one site were detectable in the second xenograft. Furthermore, the self-seeding process involves chemoattraction of metastatic cells by tumor derived cytokines interleukin 6 and 8. Consistent with this model, a recent paper by Ben–Jacob and colleagues compared the collective behavior of cancer cells to that of bacteria and hypothesized that similarly to the cooperative strategies used by bacteria to survive extreme stress, cells within a tumor act cooperatively to promote metastasis (Ben-Jacob *et al.*, 2012). Indeed, bacteria form a mother colony after inoculation. This colony sends out spying cells to explore the surrounding environment and return to the colony with the gathered information. The colony undergoes complex internal morphogenesis before sending groups of cells out to invade distant territories. Even after the initial migration, the mother colony continues to assist in the navigation of the scouting cells by emitting signals, such as repulsive chemical agents, and the scouting cells continue to send return messages containing valuable information about the microenvironment. This information is generally used to navigate towards the most beneficial location.

With our imaging system that provides large field-of-view we were able to observe and quantify the branching-like process. We observed that among the culture distinct and sometimes rare dynamic phenotypes are present, including cell migration leading to self-seeding or back-and-forth migration resembling spying-like environment sensing. Due to the large field-of-view we were able to observe and quantify long-distance cell migration. Our experimental observations of collective cell migration fit well with the theory of chemotactism which governs and directs dynamic movements of cells. On the other hand, consistently with literature (Shi *et al.*, 2014) we showed that 3D structures reorganize ECM to form a network of fibers that interconnects acini. Yet, we did not verify if ejected migrating cells follow these paths.

Future work

We have shown that the alteration in the 3D microenvironment is sufficient to induce a significant change in the phenotype of non-malignant prostatic epithelial cells. This phenotype change reflected in the transition from a non-migrative stable growth of cells into the phenotype of increased cellular motility. By use of lens-free video microscopy we observed that the cellular migration is not random and leads to establishment of branching network between growing cells. It still remains unknown what is the mechanisms responsible for this phenotypic alteration that is induced simply by the change of the environment composition. In order to better understand observed process, following questions are awaiting to be answered. How and if the change of the matrix composition changes its mechanical properties? Does phenotype change due to alteration of mechanical properties or due to increased concentration of nidogen and direct cell-nidogen interaction? Which integrin receptors are involved in cell adhesion upon these changes?

Numerous further experiments can help to find answers to questions listed above.

- It is important to show that the microenvironmental changes in *no top-coat* conditions induce branching-like process also in another non-malignant epithelial cells (for example MCF10-A). Potential discovery of the method that universally induces migrative phenotype in epithelial cells culture can in future bring new insights on the mechanisms of tubulogenesis or EMT.
- Measurement of the mechanical properties (Young's modulus) of Matrigel in *no top-coat* and *top-coat* conditions by means of AFM nano-indentation. It has been showed that increased ECM stiffness leads to malignant phenotypes (Engler *et al.*, 2004; Paszek *et al.*, 2005) Therefore, it is important to verify the influence of the dissolution on the matrix stiffness. However, logically decreased protein concentration within the gel should lead to more compliant properties.
- In order to indirectly show that nidogen induces phenotypic change reflected in branching-like process, a *top-coat* experiment with nidogen-enriched Matrigel needs to be performed. *Top-coat* conditions will provide conditions for acinar growth but increased concentration of nidogen might promote branching. Otherwise, blocking antibodies can be used.
- Since integrin receptors directly translate signals from the ECM to the cell function, it is important to study their expression in *top-coat* and *no top-coat* conditions. Of particular importance are β1α3, β3αV, and β4α6 as those integrins are recognized to be specific for nidogen. Due to the time constraint western blots were performed only once and therefore, further work is required. Moreover, to better quantify integrin signaling, other techniques should be used (f.e. RTq-PCR).
- Immunofluorescence of FAK can indicate whether FAK is localized in the cytoplasm or by the 3D matrix adhesions where it binds to downstream effectors (Src, Grb2 etc.).
- Long-term (~2 weeks) observation of branching-like process could reveal if formed branches contain lumen and recapitulate polarity.

8. Conclusions and Perspectives

The purpose to develop or use emerging technologies was above all to better understand the molecular determinants of acini morphogenesis and lumen formation. Developmental research is important since cancer, which is characterized by uncontrolled proliferation, migration and cell survival often reactivates and follows pathways of development. However, in general, studying processes *in vivo* is difficult. 3D cell culture models were introduced as an alternative since they recapitulate properties of tissues *in vivo* and at the same time maintain characteristics of cellular reductionist systems. Systems biology approach aims to systematically analyze and determine the phenotypic consequences of genetic perturbations and microenvironmental perturbations. While these approaches have been successfully performed in 2D culture, the limitations inherent to 3D culture impeded application of the high-throughput approaches. To enable efficient screens, following improvements were developed and described in this manuscript: i) high-throughput and high-content analysis of the phenotype (lumen *versus* spheroid, but also proliferative *versus* differentiated cells), ii) homogenous and controlled culture conditions, and iii) powerful imaging systems.

RWPE1 prostatic epithelial cells were used as a model to study acini morphogenesis. After optimization of the protocol for RWPE1 3D culture we have shown that lumen can be formed independently of the polarity of the acini forming cells, which often appears later. Moreover, we observed that existing mechanisms for acini formation (hollowing and cavitation) co-exist in the RWPE1 3D cell model.

We developed two technologies in order to provide **high-content and high-throughput analysis** in 3D culture. First, based on the **microfluidic cell encapsulation** opens possibility to use flow-based analysis methods. We provide a proof-of-concept siRNA transfection protocol which serves to show feasibility of the analytical method. In future applications, we envisage that by using specific markers, for example, vimentin for mesenchymal cells; ki67 for proliferation; or cytokeratins for differentiation, it will be possible to observe changes in phenotype upon genetic alterations. Moreover, the encapsulation method has proved to induce more **homogenous populations of acini** that are formed starting from a single cell, as compared to traditional 3D cell culture. This approach allowed us to observe for the first time, that a single-cell is sufficient and independent of epithelial paracrine signaling, to form an acinus. In the future this droplet microfluidic approach can be used universally for other types of cells which require a natural ECM environment to proliferate.

The second developed method is a **lens-free imaging system**. This approach is complementary to droplet microfluidics, since instead of applying fluorescent markers to describe the phenotype, it provides direct information on the presence or absence of the lumen within 3D structures. We describe a **specific holographic signature** which serves to distinguish between acini with lumen and tumor-like spheroids, i.e., full aberrant masses. By combining 3D culture of prostate cells and a parallelized lens-free imaging system accompanied by holographic 3D image reconstruction, it is now feasible to identify those human genes which play a key role in the formation of differentiated structures (acini). In the laboratory, we took advantage of this technological innovation: we used 96 detectors for parallel lens-free imaging to perform for the first time, automated intermediate-throughput reverse genetics screens in 3D cultures of prostate cells. The aim was to analyze the consequences of the RNAi-mediated down-regulation of both individual kinases and phosphatases in the human genome on the dynamic proportion of fully-differentiated acini *versus* proliferating unorganized tumor-like spheroids. The lens-free method allows fast tracking of the effect of siRNA with an extensive statistical analysis of the percentage of 3D structures (Project 2015-2017, "plan de couplage DSV-DRT", CEA Grant). In the context of the controversial issue of PSA, lens-free imaging can also be extended to biomedical and drug screening applications to evaluate anti-cancer drugs and to discover new predictive biomarkers in cancer.

Furthermore, we have shown that the **large field-of-view of lens-free imaging set-up** enables monitoring of dynamic cellular 3D assemblies. Using this approach, we have shown that **environmental alteration** can lead to distinctive phenotypes in 3D cell culture. Matrigel used as a scaffold for 3D cell culture presents structural instability which leads to changes in environment composition. We present a hypothesis on the potentially interesting role of **nidogen** (entactin), which is one of the major proteins of the ECM but not yet well studied. With the powerful lens-free imaging system we have detected for the first time **self-seeding** between 3D structures. Observed collective cell migration served to establish branches and to physically interconnect structures. In order to understand the origins of this process, we have preliminarily compared expression of proteins involved in the *outside-in* integrin-ECM interaction. The mechanisms and signaling pathways responsible for induction of the observed migration phenotype remain unknown and require further studies (see discussion and future work, Chapter 7.3.8).

In a near future, a read-out based on dynamic branching should be also useful in the study of the invasive properties and metastatic potential of tumor cells and in conducting screening assays for cell migration.

During this thesis, I also took part in other projects aiming to provide controlled environments through the implementation of new 3D scaffolds suitable for prostate cells growth. First, I was a co-author on an article describing the characterizion of cell proliferation

on **micro-carriers in a bench-top microfluidic bioreactor** (Abeille F. et al, *LOC*, 2014). Second, I developed a simple microfluidic approach to **construct circular-shaped microchannels**, coated either with Matrigel or with polyelectrolyte, to mimic a duct-like structure (Dolega ME et al, *PloSOne,* 2014). This was developed in the frame of "Brocoli", a National project (ANR-11-BSV5-009, 2012-2015) aiming to demonstrate that polyelectrolyte membrane was suitable for controlling epithelial cell growth in 3D scaffolds (Picollet-D'hahan N. et al, *Biomaterials*, 2013). These results served to establish the principle of a new European project in the Biomics lab (UroLOC proposal, SEP-210177219, second stage), with the goal of developing a novel diagnostic device for urological cancers that takes a secretomics-based approach. More specifically, the nanostructured polyelectrolyte membrane will be used to create a 3D scaffold for the growth of urothelial cells isolated from urine and will be combined with microfluidic-flow systems for extensive studies of secretions.

In the long term, such 3D cell microsystems (e.g., encapsulation, lens-free microsensors) will potentially allow for drug screening under conditions closer to the *in vivo* reality, thereby in turn reducing drug attrition and optimizing the efficiency/cost ratio in cell-based HT screens. In the same way, such devices could provide new insights into tissue dysfunction associated with specific diseases and consequently may offer more realistic conditions for modeling therapeutic interventions. Finally, microscale 3D tumor tissue constructs may be valuable tools for testing drugs targeting the cancer microenvironment as well as the cancer cells themselves.

These technologies could be extended to any secretory epithelium as well as to large scale screening for drug discovery or toxicology studies in organ-like models.

Limitations of commercial cell lines or primary cells are well known as they do not exactly represent the histology and architecture observed *in vivo* and hence poorly mimic the real physiology of tissues. In this PhD work, we used such models (either non-tumorigenic or cancerous) to show the feasibility of our approach. In addition, we also pointed out the limitations of the commercially available RWPE-1 cell line. Contrary to information described in the literature, in our hands RWPE-1 cells do not secrete PSA (data not shown). In future studies, for example to investigate prostate cell secretions, 3D cell models therefore require further optimization so as to increase their physiological relevance. First, co-cultures of epithelial and stromal cells (fibroblasts, mesenchymal cells…) will be developed (Project "Plan de couplage" CEA, 2015-2017; and UroLOC proposal); second, cells from patients will be incorporated into the experimental protocols since they are likely to represent the secretory environment (UroLOC proposal). As controls, primary cells from healthy subjects, either commercially available or obtained from fresh biopsies, will be utilized. For cancerous models, VCaP cells, available in Biomics lab, will be tested since they highly express the characteristic androgen receptor, the TMPRSS2-ERG fusion that represents family of fused genes found predominantly in prostate cancer.

In conclusion, we proffer that the techniques that I have developed in collaboration with my colleagues in the Biomics lab and Leti Lab will not only advance the studies on prostate cancer that have been initiated by these associated laboratories, but that they will likely be of general application at least to cancers of epithelial origin.

9. Supplementary Data

9.1 Supplementary Results

9.1.1 Optimization of the experimental setup for Matrigel droplet formation

As has been mentioned in the introductory part, the material used for fabrication of microchips is an important parameter. If the aim is to produce water-in-oil droplets in majority cases systems do not need to be specially treated in order to prevent wetting of channels by water phase (dispersed phase). However, when the dispersed phase is a non-polymerized hydrogel whose composition is complex, formation of monodispere droplet can be hampered by wetting phenomenon (Figure 9-1) Numerous methods for channels treatment were reported (Riche *et al.*, 2014) in order to obtain surface more hydrophilic (for oil-in-water emulsions)(Jankowski *et al.*, 2013) or hydrophobic (for water-in-oil emulsions)(Jankowski *et al.*, 2011).

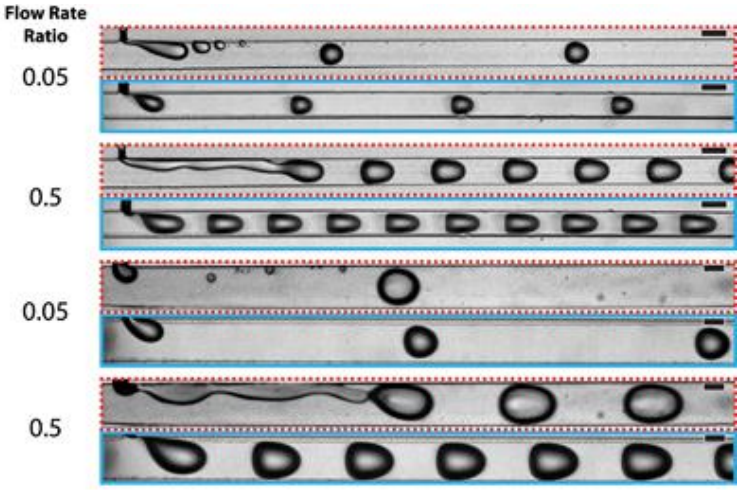

Figure 9-1 Micrographs contrast the droplet formation process in uncoated (red/dashed outline) and fluoropolymer coated (cyan/ solid outline) channels. Source: (Riche *et al.*, 2014)

Microfluidic device fabrication and channels wettability

Among the possibilities (and also availability of the technology in CEA) to fabricate systems in thermoplastic polymers (PC or PMMA) by milling, PDMS was chosen due to its high hydrophobic properties (Morra *et al.*, 1990). Another advantage is that once a master is prepared, PDMS fabrication technique allows preparing tens of systems autonomously contrary to thermoplastic systems which need to be milled separately with a specialized milling-equipment. Due to the limited availability of the specialized equipment for standard soft-

lithography process, masters were prepared from the thermoplastic polymers as fallows (Figure9-2):

1) Desired channels were milled in PMMA material
2) PDMS has been poured over the PMMA surface and allowed to polymerize
3) Removed PDMS layer served as a master after silanization
4) Non-polymerized PDMS has been poured over the silanized PDMS-master and allowed to polymerize
5) After polymerization, PDMS containing channels has been bonded with a glass slide by oxygen plasma surface activation

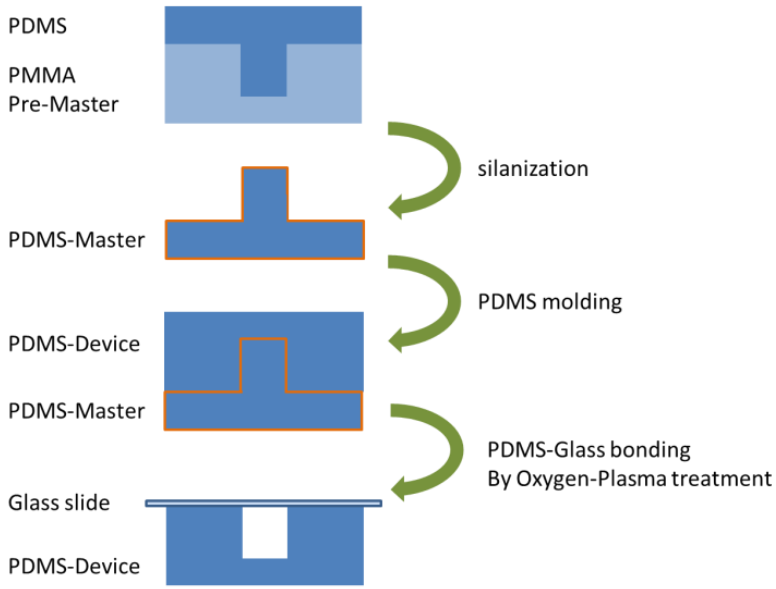

Figure 9-2 Fabrication of PDMS/glass microfluidic devices.

Although, PDMS is naturally a hydrophobic material, after oxygen plasma treatment it loses its appropriate surface properties. A high channel wettability of Matrigel during initial experiments has been observed. Therefore to optimize surface properties, treatment with Aquapel (commercially available treatment for car windows) has been acquired as described in literature(Brouzes *et al.*, 2009). To increase the hydrophobicity of PDMS, freshly prepared devices were treated by fusing Aquapel® into the channels (PPG Industries, USA) followed by baking for 10 minutes in 70˚C and dried with an airgun. Microfluidic chip has been connected to syringe pumps through the elastic tubings. Droplet formation has been observed under microscope. Figure 9-3 presents the experimental bench set-up.

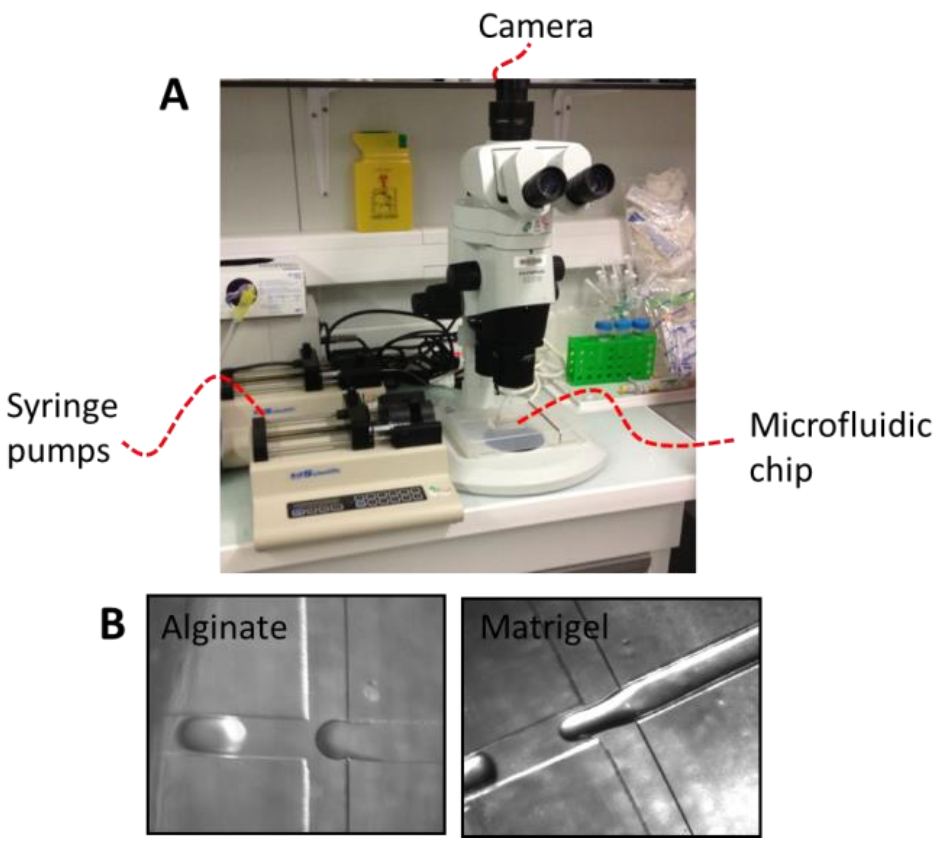

Figure 9-3 **A)** Experimental setup and **B)** first successful Alginate and Matrigel droplets formation in PDMS device with Aquapel surface treatment

Optimization of a microfluidic design

For the initial droplet formation process, the most basic design of flow-focusing (FF) junction was used (Anna *et al.*, 2003). Infusion of liquids and control over flow rates was applied by syringe pumps. Process of droplets formation was observed with a stereomicroscope equipped with a camera. However, droplets formation process is rapid in microscale and the available camera to record images had insufficient fps (frames per second) capabilities. Therefore, design has changed in order to provide the possibility to observe droplets without need to acquire more powerful camera. The problem has been solved by fabricating outlet channel 3x wider so that the flow of the droplets will be slower (Figure 9-4).

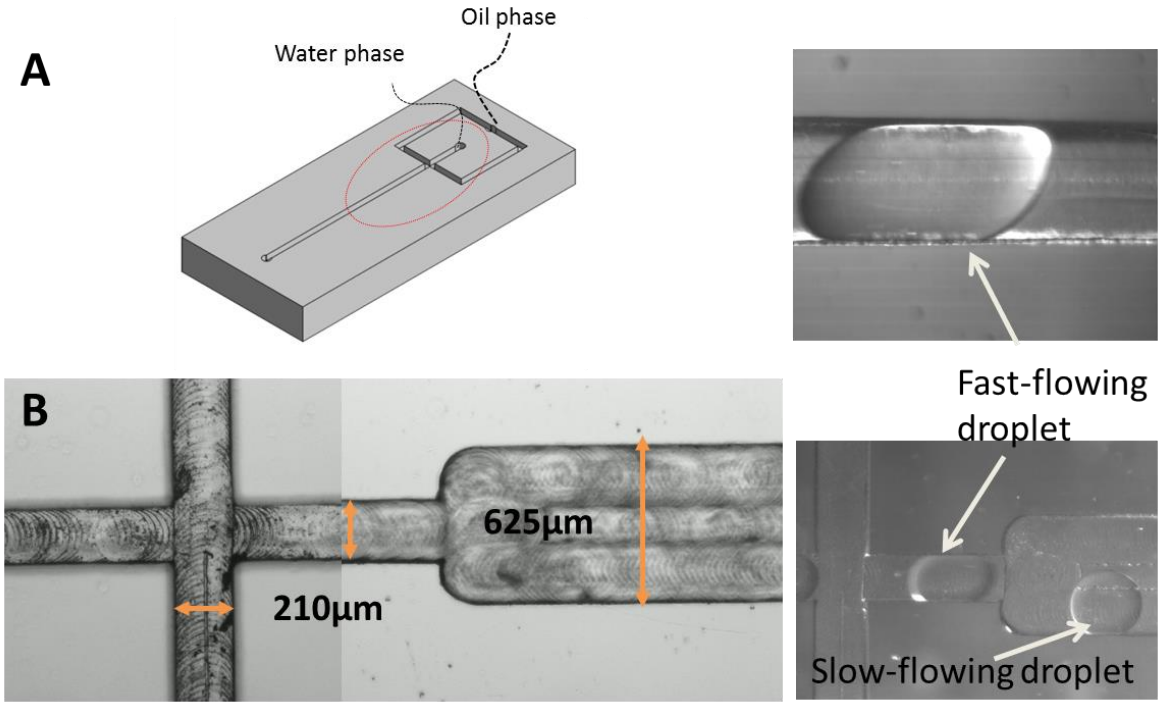

Figure 9-4 Microfluidic system optimization. An outlet of a simple flow-focusing design (**A**) has been fabricated wider in order to enable observation of formed droplets flowing to the outlet (**B**). For visualization, images taken from camera show blurred image of flowing droplet in a standard system (**A**) and slowed-down droplet flow in a modified system (**B**)

Since Matrigel is liquid in 4'C all experiments on Matrigel droplet formation were performed in cold-room. For every experiment, cell-pellet is mixed with Matrigel and infused into syringe that is connected to a microsystem. Infusion of Matrigel with cells is controlled by a syringe pump. In such configuration, for a proper infusion, a single experiment requires at least 500µL of Matrigel infused into a 1 mL syringe. Furthermore, infusing Matrigel from a syringe is impractical and stabilization of droplet formation is long (~15 minutes). In order to limit the time of the experiment, and more importantly time that cells reside in 4°C, a system with direct injection-on-chip has been developed (Figure 9-5). A long serpentine channel serves as a reservoir into which 100 µL Matrigel with cells is directly injected with a P100 µL pipette. Subsequently, Matrigel-injection inlet is plugged, and oil is infused upstream and the rate of flow is controlled by syringe pumps. Oil is used to push the Matrigel phase towards the flow-focusing junction and to indirectly control the rate of flow of Matrigel.

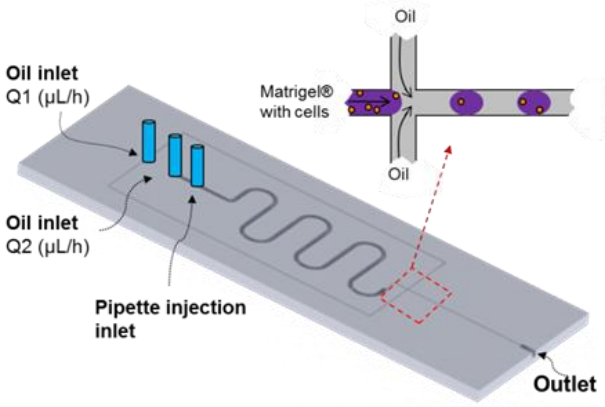

Figure 9-5 Final design of microfluidic device for Matrigel droplet formation

A single experiment takes ~ 1 hour (starting at the moment of cell detachment from the culture flask) relies on:

- Preparation of a cell pellet at an appropriate concentration and subsequent mixing it with the Matrigel
- Infusing the Matrigel (with cells) into flow-focusing device where it breaks into droplets
- Formed droplets exit the device through the outlet channel and are collected in oil into an eppendorf tube
- If emulsion is stable, the tube is put in 37'C in order to polymerize Matrigel droplets into beads[1]
- Beads are transferred from oil into culture media by multiple wash with a pure oil (to decrease the concentration of surfactant around beads) to start 3D cell culture

Preventing Matrigel droplets coalescence

First experiments on formation of droplet in PDMS microfluidic devices showed the importance of the surfactant presence. As has been mentioned above, in microscale surface to volume ratio is high and formed droplets naturally tend to undergo coalescence. In order to stabilize emulsions by decreasing the surface tension it is necessary to use a surfactant. The choice of surfactant goes in pair with the choice of oil and needs to be considered carefully. Surfactant has to be soluble in oil, stabilize emulsion and be biocompatible. Among many commercially available surfactants and oils, the most often used were tested at different configurations to stabilize Matrigel/oil emulsions (Table 9-1).

[1] It is important to note that beads are not capsules, which by definition contain a liquid core

Table 9-1 Chosen tested surfactant/oil conditions for matrigel droplet stabilization and biocompatibility

oil	surfactant	concetration	stability of droplets	division of cell
mineral oil	SPAN 80	1%	-	
		2%	-	
		3%	+/-	NO
mineral oil	Span 20	1%	-	
		2%	-	
		3%	-	
corn oil	lecithin (1)	1%	-	
		2%	-	
		3%	-	
corn oil	lecithin (2)	0,125%	+/-	NO
		0,5%	+	NO
		1%	+	NO
		2%	+	NO
FC 40	PFPE-PEG	1%	-	
		2%	-	
		3%	-	
HFE-7500	PFPE-PEG	1%	-	
		2%	+	YES
		3%	+	YES

(-) No stability; (+/-) partial stability; (+) good stability; lecithin (1) LIPOID (Germany); lecithin (2) WAKO (Japan)

SPAN 80/mineral oil system

A popular mineral oil and SPAN 80 has been broadly used in biological studies, for instance, to encapsulate cells (Chabert and Viovy, 2008), for experiments on protein expression (Dittrich *et al.*, 2005), and molecular exchange experiments(Bai *et al.*, 2010). However, this oil/surfactant system (despite the various concentrations tested) did not provide sufficient stability of droplets reflected by coalescence when droplets were collected in an eppendorf tube. To further minimize the coalescence of droplets just before leaving the channel, a planar outlet tubing connection was designed. As a result droplets were stable in the outlet tubing after they exited the microchip. In order to verify if cells would be able to divide a strategy to polymerize Matrigel droplets inside long tubing, was applied (Figure 9-6A). After polymerization Matrigel beads were pushed out from the tubing and transferred to culture medium. The whole experiment starting from mixing cells with Matrigel to the moment of transfer into culture media took ~1 hour. However, encapsulated cells did not divide during the following days (Figure 4-6B).

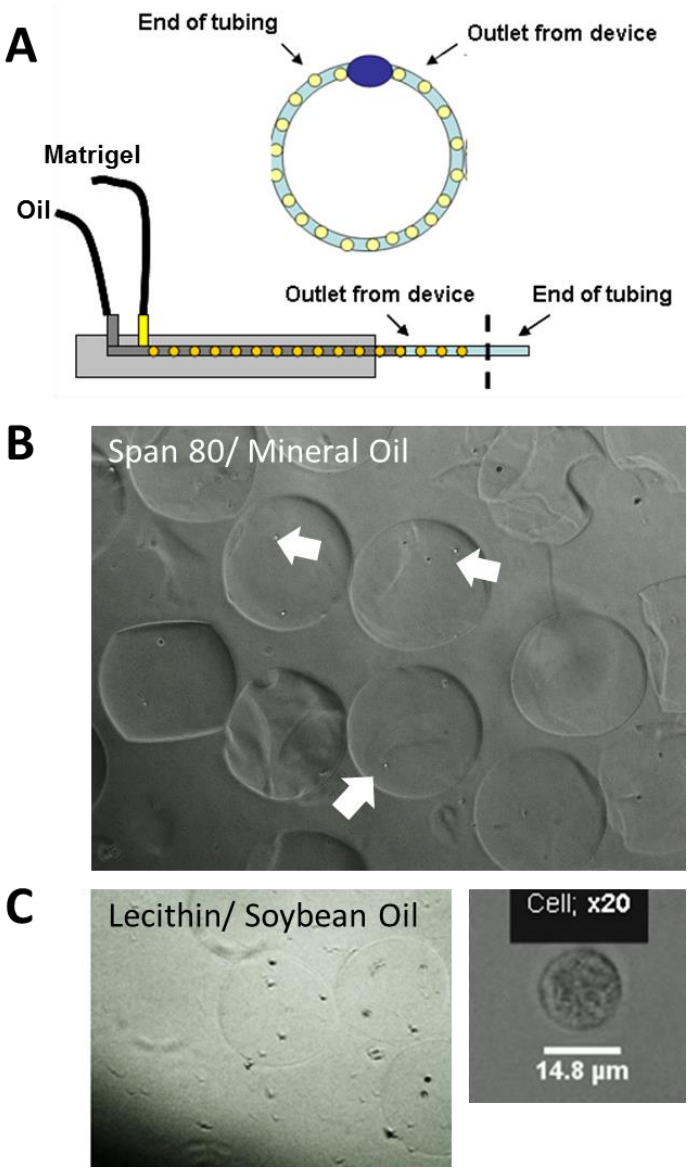

Figure 9-6 A) Schematic illustration of Matrigel droplets polymerization in an outlet tubing. **B)** Phase contrast image of Matrigel beads polymerized in tubing and transferred into culture medium. Arrows indicate beads containing cells. **C) (on the left)** Phase contrast image of Matrigel beads polymerized in an eppendorf tube and transferred to culture medium. **(on the right)** Cells did not divide and had a "porous-like" membrane due to the effect of surfactant.

Lecithin/Soybean oil system

Inspired by the report on microfluidic collagen beads formation for cell encapsulation (Matsunaga *et al.*, 2011), lecithin has been used a surfactant to stabilize Matrigel droplets. Interestingly lecithin obtained from SIGMA did not provide any stability in contrast to one from WAKO (Japan). Lecithin (Wako) in corn oil provided superior stability (for over 24 hours) of Matrigel droplets. However, encapsulated with such system cells never divided (Figure 9-6C) despite the concentration of the surfactant that has been minimized to 0,125% (w/w). A biocompatibility test has been performed in order to verify the effect of surfactant presence on cell viability (Figure 9-7).

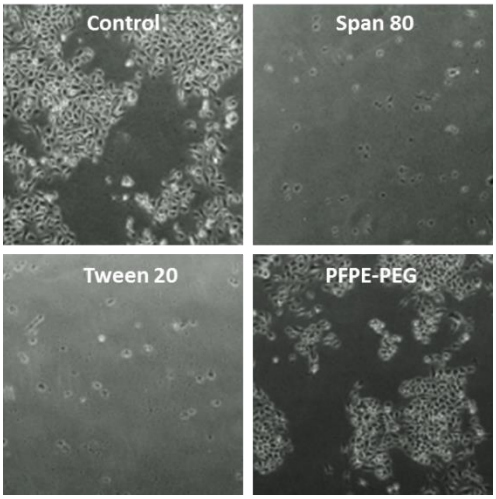

Figure 9-7 Biocompatibility test of chosen surfactants on cell viability in standard 2D culture.

Cell in standard 2D culture were exposed to culture medium containing tested surfactants and the effect on cell viability was observed. Interestingly, both surfactants SPAN 80 and Lecithin used for cell encapsulation were toxic and cells died within 24 hours. This result indicates that epithelial cells are highly fragile to the presence of surfactant.

PFPE-PEG/HFE 7500 oil system

PFPE-PEG has been discovered recently and used to provide high stability of aqueous droplets for high-throughput fluorescent analysis on chip (Brouzes *et al.*, 2009). PFPE-PEG surfactant is biocompatible and cells have proliferated in its presence in culture medium (Figure 9-7). Test on stability of Matrigel droplets during microfluidic process revealed that only HFE 7500 oil prevent coalescence (Table 9-1). After transfer of droplets containing cells into culture medium, cells divided and formed the first 3D culture in Matrigel beads (Figure 9-8).

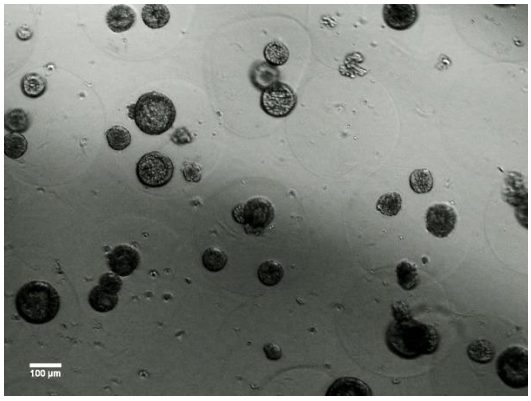

Figure 9-8 Phase contrast image of the first 3D epithelial cell culture in Matrigel beads.

9.1.2 SiRNA transfection on 3D culture

RNA interference (RNAi) has been introduced in 1998 by Fire *et al.* who discovered the ability of double-strand RNA to silence gene expression (Fire *et al.*, 1998). Followed this discovery, a proof-of-concept of synthetic small interfering RNA (siRNA) to knock-down specific gene sequence has been presented in mammalian cells (Elbashir *et al.*, 2001) and in mice (McCaffrey *et al.*, 2002). Since then siRNA received much interest as potential treatment to viral disease (Okumura *et al.*, 2008) and cancer (Kim *et al.*, 2008). SiRNA could be potentially used to treat any disease in the body. However, naked siRNA (without a delivery system) can reach only certain physiological sites such as brain (DiFiglia *et al.*, 2007) or lungs (de Fougerolles and Novobrantseva, 2008). In order to enable siRNA to cross cellular membranes of more native tissues, numerous mechanisms for transfection have been developed (David *et al.*, 2010). *In vitro* siRNA are widely used in standard 2D culture but efficiency of transfection is limited in 3D culture on Matrigel. Since 3D models (as described in the Chapter 2) become more relevant in *in vitro* studies, series of experiment to optimize transfection with a lipofectamine♣ have been performed and will be described below.

siRNA transfection

Lipofectamine RNAiMax (Invitrongen), a lipids-based vector dedicated to siRNA transfection, has been used to introduce siRNA into cells. Invitrogen, subconfluent breast cancer cells overexpressing GFP (MCF10-A-GFP cells) were cultured in maintained in 2D culture then and transfected for 72 hours using Lipofectamine RNAiMAX complexed to a siRNA against GFP (siGFP-22, Qiagen 1022064, and Qiagen negative control siAllStar 1027280) at a final concentration of 20 nmol/L reagent. The transfection kinetic has been optimized using a positive siRNA, siCelldeath, allowing and easy visualization by phase contrast microscopy and fluorescent observation of propidium iodide staining♦ (not shown) of transfected cells who undergo a pro-apoptotic pathway by use of siCelldeath. After 72 hours MCF10A-GFP cells transfected with siGFP had significantly decreased GFP fluorescence as observed by fluorescent microscopy (Figure 9-9A) and by FACS method (Figure 9-9B). As calculated by the data obtained with FACS the mean fluorescence has been quantified in relation to control assigned as a reference. GFP signal in siGFP transfected cells has decreased to 27% and a control of siAll*♥ to 68% (Figure 9-9C).

♣ Lipofectamine is a commercially available agent to increase the efficiency of the siRNA delivery into the cell. In aqueous solutions it forms liposomes which carry trapped siRNA molecules.

♦ Propidium iodide selectively infuses into cells whose membrane started to degrade.

♥ siAllstar is traditionally called “scramble” control which should not have any specific effect on the cell.

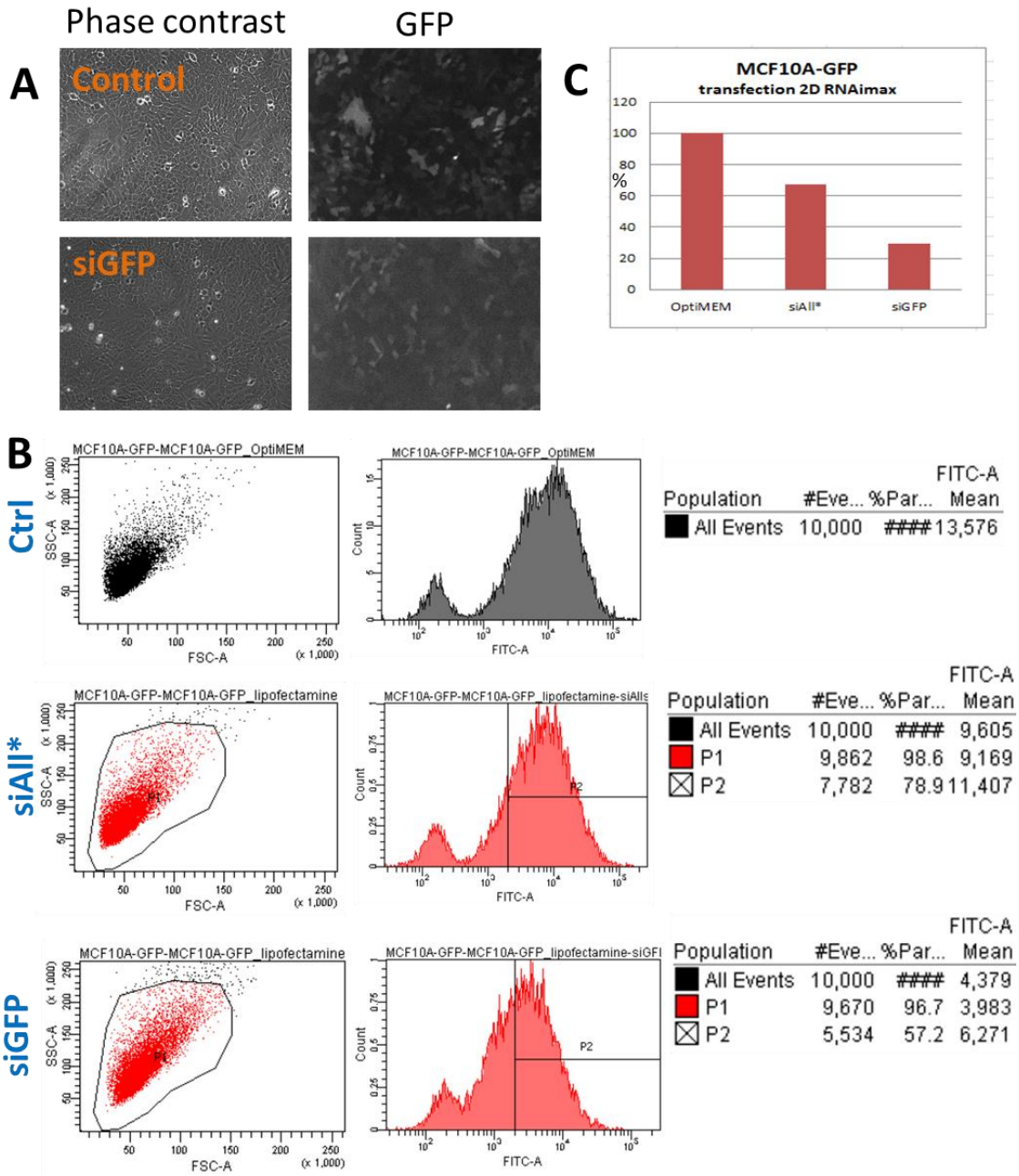

Figure 9-9 Transfection optimization on MCF10-A-GFP cells on 2D culture. A) Comparison between cells transfected with siGFP and a control as observed by phase contrast and fluorescent microscopy. Cells after 72 hours of transfection have equivalent morphology as compared to control. **B)** FACS measurement on FITC channel to quantify the fluorescence intensity. SiAllstar (siAll*) has been used as transfection control. **C)** A bar chart indicates the transfection efficiency by comparison of fluorescence intensity level.

siRNA transfection – in 3Dcell culture

The reason behind the decreased efficiency of lipofectamine-based transfection in 3D Matrigel cell culture is unknown. On the other hand, to the best of my knowledge, there are no dedicated for 3D Matrigel cell culture transfection solutions. In order to verify the efficiency of lipofectamine RNAiMAX-based transfection in 3D, optimizing experiments were performed. The basic problem occurs due to the fact of immobilization of cells in Matrigel in 3D culture and necessity to use microscopy and image analysis to quantify the fluorescent signal (Figure 9-10). First, this limits the number of cells used for analysis and second, it precludes the use of the FACS analysis. To overcome this obstacle a protocol to dissolve Matrigel and release acini in a single cells solution has been developed.

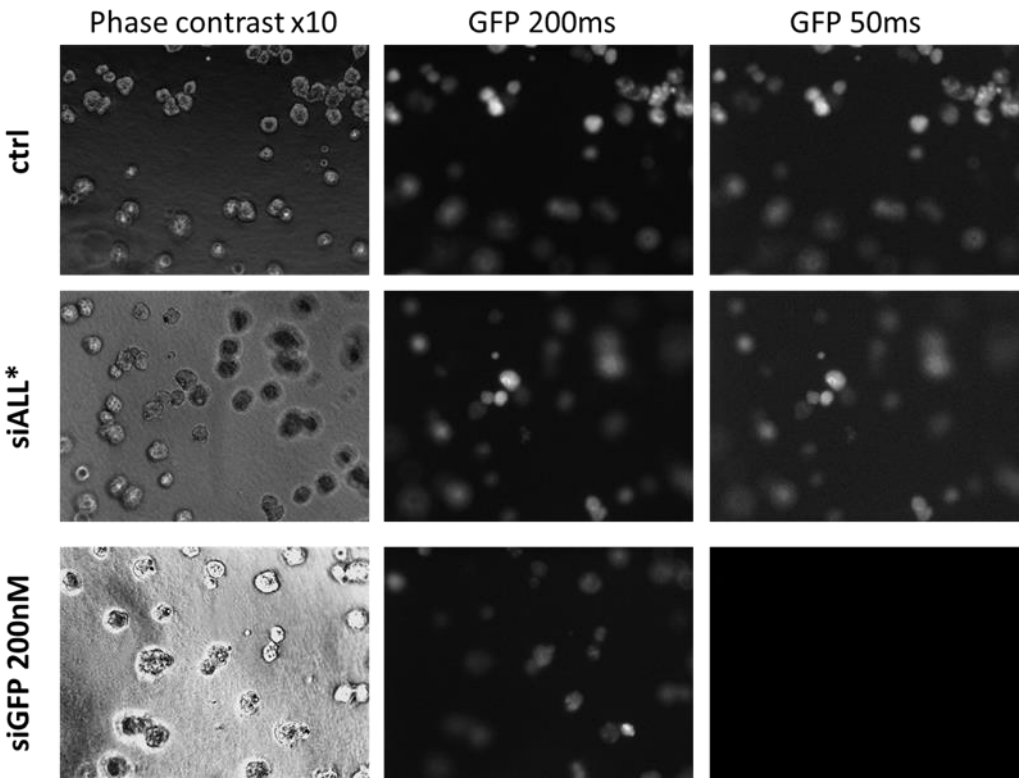

Figure 9-10 Fluorescence observation of GFP in control and siGFP 3D cultures on Matrigel. Different exposure times were used to observe the difference in fluorescence

Matrigel can be digested by Dispase (BD) or can be dissolved more gently without disrupting the cells structure by nonenyzmatic reaction with Cell Recovery Solution (BD). The choice to optimize Cell Recovery has been interesting also for other types of experiments (i.e., Extraction of proteins from cells or immobilization of grown acini into a new ECM).

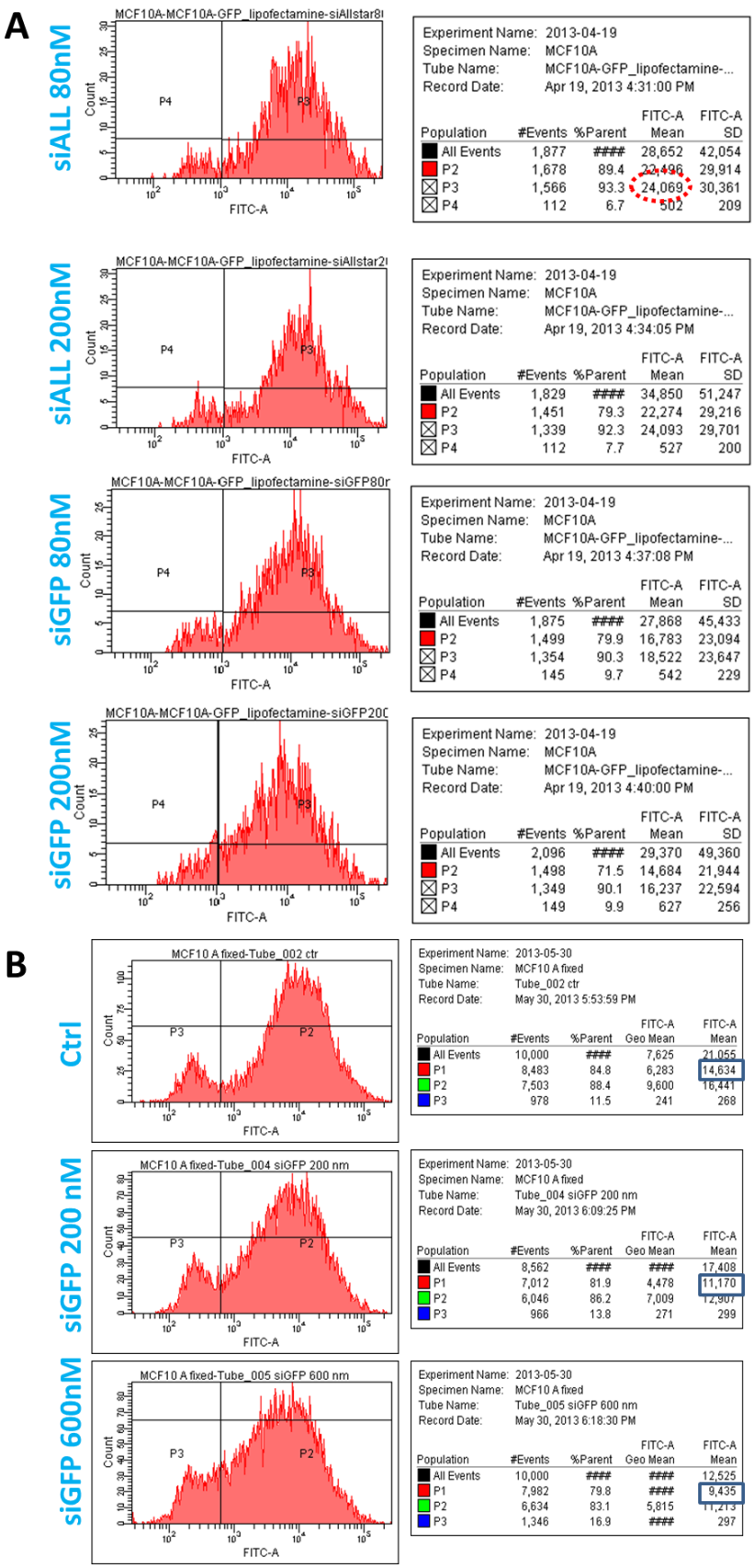

Figure 9-11 FACS analysis over direct transfection (72 hours) on MCF10A-GFP in 3D Matrigel cell culture. A) First experiments on increased concentration of siRNA proved to increase the transfection efficiency. **B)** Further increase in siRNA concentration

Cells were seeded according to the top-coat protocol (Please refer to Materials and Methods) and after 3 days were transfected as described above. After 72 hours, Matrigel is dissolved by Cell Recovery solution (50 minutes on ice; centrifugation of acini at 800 rpm for 5 minutes). In order to have a single cell solution (to enable FACS analysis) acini are disrupted by use of trypsin/EDTA. Cell solution is further fixed with 2% PFA (20 minutes) and undergoes FACS analysis. The number of analyzed cells according to the protocol described above was ~1800 cells (for 2D culture experiments ~10 000 2D culture) (Figure 9-11A). With the increased concentration of siRNA to 80nM and 200nM, the mean fluorescence was 74,1% and 65,3% respectively (summarized in Figure 9-12). The controls of siAllstar were prepared at the same concentration. The amount of lipofectamine RNAiMax used for transfection has been (3 µL / 200µL) as compared to 2D transfection (1 µL / 200 µL).

Since increased concentration increases the transfection efficiency, a concentration of 600 nM was tested (Figure 9-11B). No cellular toxicity was observed. With the further improved protocol single cells solutions were more concentrated and analysis has been performed on ~10 000 events. For clarification, siAllstar controls are not shown. The 600 nM concentration did not further significantly improve the transfection efficiency and fluorescence had decreased of 36% (Figure 9-12).

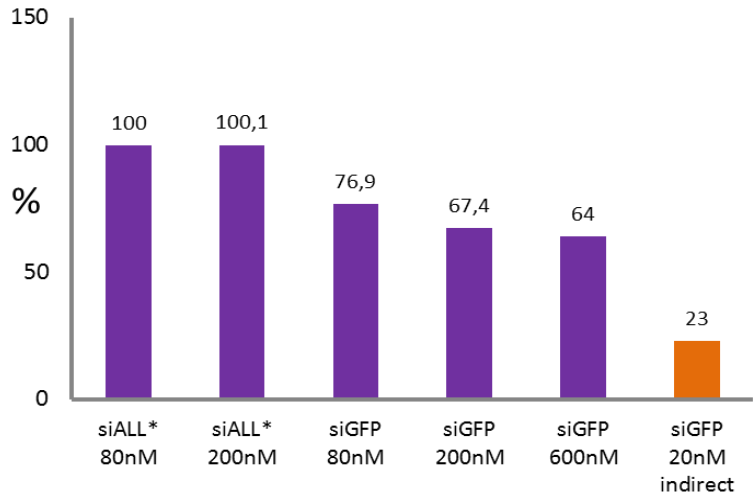

Figure 9-12 Summary on the mean fluorescence of MCF10-A-GFP cells transfected with siAllstar and siGFP in relation to the protocol and concentration of SiRNA. In orange indirect transfection protocol has been used as a positive control. Data express the relative change of GFP fluorescence as compared to control.

In order to provide high transfection efficiency for 3D culture a strategy to transfect cells indirectly has been acquired. Cells were maintained in 2D culture and transfected for 72 hours. Subsequently cells were reseeded in Matrigel and kept in 3D culture for 4 days before FACS analysis. The mean fluorescence of siGFP 20nM treated cells was 23% (orange chart, Figure 9-12).

Direct siRNA transfection on 3D cell culture in beads – preliminary results

As has been mentioned above the reason behind the inefficient transfection in 3D with standard protocol is unknown. A key difference between 2D and 3D cell culture is the presence of Matrigel which can constitute to limited diffusion of reagents in 3D culture. Matrigel cell encapsulation by droplet microfluidics provides a controlled environment. An important property for diffusion of cell culture in beads is the high surface to volume ratio. In these conditions diffusion should proceed more efficiently than through the thick layer of Matrigel. Therefore, MCF10-A-GFP cells were encapsulated in 300 µm in diameter beads and after 4 days in culture transfected with siGFP (400nM) and siAllstar as a control (Figure 9-13).

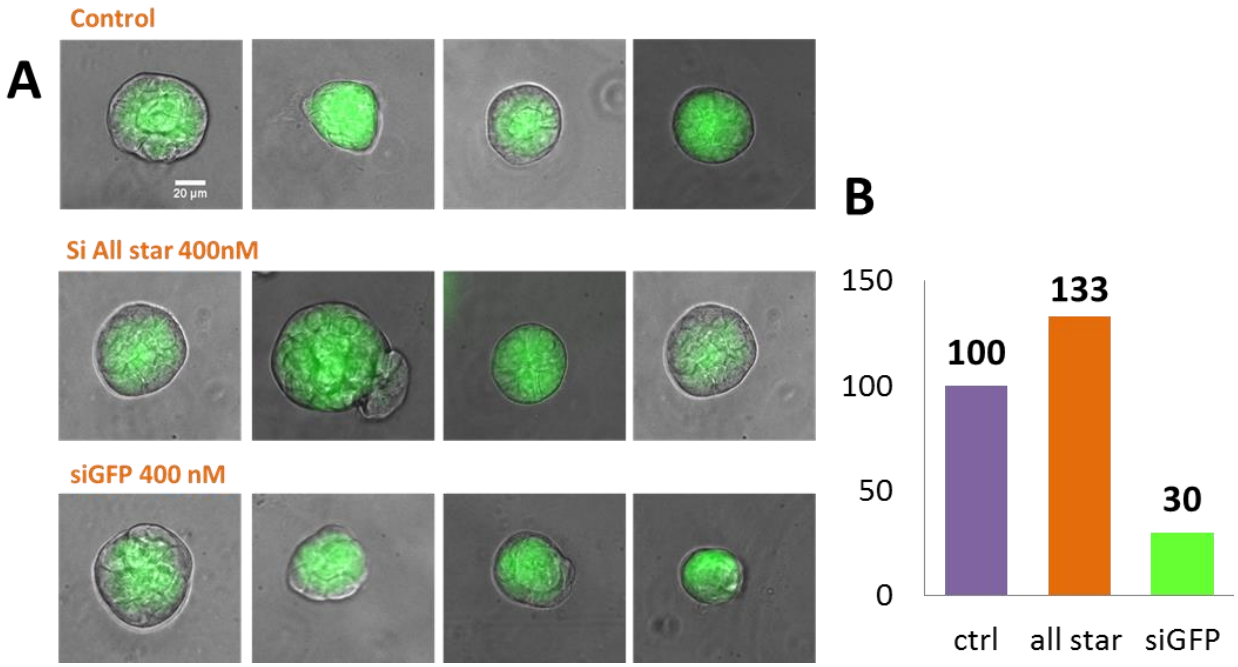

Figure 9-13 Direct transfection of structures grown in beads. A) Phase contrast merged with fluorescent GFP images of MCF10-A-GFP structures grown in beads and transfected with siGFP and siAllstar. Scale bar 20 µm. **B)** A bar chart indicates the fluorescence intensity in relation to the control.

Because of the limited access to the Large Particle FACS the level of fluorescence has been based on image analysis (Figure 9-19). However, the high heterogeneity of fluorescence at a single level (as shown in FACS experiments or fluorescent image of a control in Figure 9-10) and a significantly lower fluorescence of structures analyzed (N=20 per condition) rendered high standard deviation. Images were taken with equivalent settings. Cell fluorescence has been measured by manual selection of the area-of-interest and subsequent measurement of area, integrated density and mean gray value (performed with ImageJ software). The same values were measured for the background around the structures. Transfection efficiency is represented by fluorescence intensity of transfected structures in relation to a level of fluorescence in control. After 4 days in culture control structures had average diameter 71 µm.

Transfected structures with siAllstar had an average diameter of 85 µm while siGFP 79 µm respectively. Transfection with siGFP has decreased the fluorescence of 70% while siAllstar increased over 33% as compared to control (Figure 4-13). An increase in GFP fluorescence has been observed before by collaborators from CEA-Leti who develop Lipid nanoparticles for transfection purposes. However, presented results can serve only as an indication and further optimization experiments need to be performed.

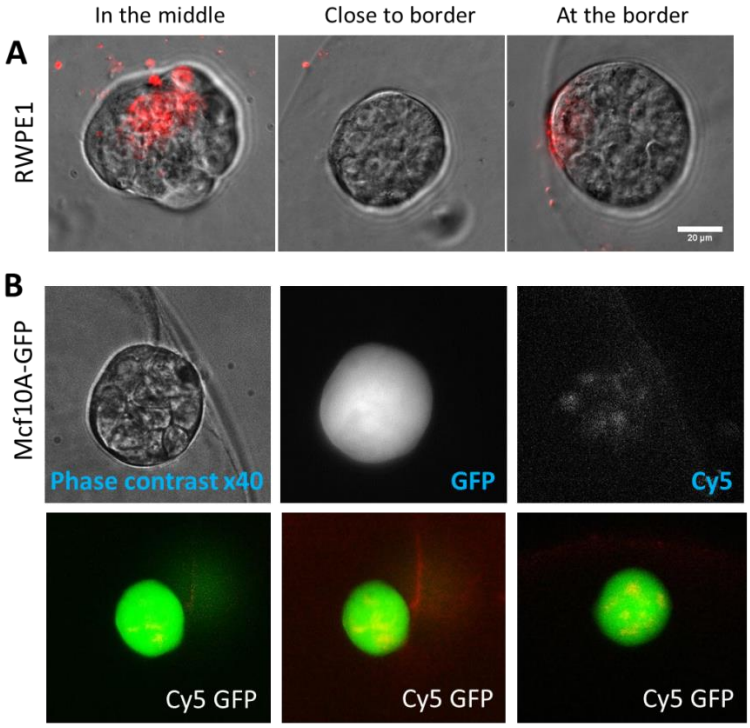

Figure 9-14 Direct transfection on 3D cell culture in beads with siAllstar with fluorophore conjugated. A) RWPE1 cells were transfected with Lipofectamine + siAllstar-Alexa 546 nm for 48 hours. Phase contrast and fluorescent images of Cy3 channels were merged to represent the transfected structures. Scale 20 µm **B)** MCF10-A-GFP cells were transfected with cationic lipid nanoparticles (J.Bruniaux, CEA-Leti) conjugated with DID-fluorophore (channel Cy5). Upper panel presents structure observed by phase contrast, GFP channel, and Cy5 channel respectively. Below, other structures with Cy5 and GFP channels are presented.

In order to confirm that siRNA enters structures embedded in Matrigel beads additional experiments were performed. Lipofectamine + siAllstar-Alexa 546nm complexes were added to the RWPE1 3D cell culture in beads according to the conditions described above. After 48 hours, majority structures that grew by close to the border of the bead had traces of siAllstar-Cy3 incorporation indicating that transfection occurs in beads (Figure 9-14A) at least when structures are close to the bead border. Only some structures that grew in the middle of the bead incorporated the fluorophore.

A similar experiment has been performed with the use of Lipid Nanoparticles containing siAllstar and Cy5 fluorophore. After 48 hours, 85% of structures (N=24) had traces of Cy5 fluorescence (Figure 9-14B).

In conclusion it has been verified that direct transfection on standard 3D culture does not achieve more that 36% of functional efficiency (as measured by decrease in mean fluorescence). Alternatively, a protocol for indirect transfection has been developed and its efficiency leads to a strong decrease in fluorescence over ~70%. However, transfection according to the indirect protocol *i)* limits length of the experiment, because the effect of transfection will decrease in time and *ii)* transfection is limited only for early stages of morphogenesis and cannot serve, for instance, to knock-out genes after acini are formed.

Therefore, it is necessary to perform further test in order to measure the capabilities of direct transfection on acini in Matrigel beads. Experiments with siRNA containing fluorophore suggest the diffusion limitation. As shown, majority of structures contained fluorophore when grew by the border of the beads. A possible solution is to encapsulate cells in smaller beads to decrease the length of diffusion.

9.1.3 Encapsulation in matrigel beads provides control over environment

3D epithelial cells culture lacks the control over environment as has been described in Chapter 2. Application of collagen as a support for 3D culture allows to some extent controlling the rigidity, however, not all cells lines form polarized acini within it. Furthermore, change in rigidity is a consequence of protein concentration alteration and thus collagen fiber density and average size of pores change in parallel (Miroshnikova *et al.*, 2011). Another approach relied on the coating of tunable polyacrylamide with a thin-layer of basement membrane proteins followed by seeding cells on top of it (Butcher *et al.*, 2009). Seeded cells on such composite 2D surfaces with a Matrigel diluted in culture media constantly experienced altered environment in which they proliferated. Compliant matrices resulted in formation of acini-like structures while rigid promoted cellular migration. These experiments proved the importance of mechanical signaling in tissue morphogenesis. However, to date it is difficult to observe how alteration of mechanical properties of the environment influences cells that have already fully developed into acini.

We used our Matrigel encapsulation technique to provide cells with a spherical homogenous environment in which cells form acini. Since the control over Matrigel rigidity is poor we used a second material to control mechanical properties. Polyacrylamide, which presents well tunable rigidity, has been toxic to cells. Furthermore, during polymerization it increases its volume which resulted in the squeezed and deformed Matrigel beads. Therefore for our experiments we have chosen agarose, a biologically inert and mechanically tunable material, which does not provide any cell-adhesion points. Matrigel beads, each containing a single cell, were immobilized in an agarose gel. During the first stage of experiment cells proliferate into acini receiving only signals (both mechanical and chemical) from surrounding Matrigel (Figure 9-15A). If the size of the bead is appropriate (100 - 200 μm) at the late stages of growth acini fills up the volume of the Matrigel (Figure 9-15B and Figure 9-15C). Such situation provides an acinus at a particular stage of growth with chemical signals originating from the cells' deposited basement membrane and mechanical signals from the tunable agarose. Furthermore, since agarose is biologically inert acini growth is constrained by agarose gel. With the possibility to control the size of the formed Matrigel beads during the process of formation, it is amenable to control constraint of growing acini. Within the beads of diameter of 400 μm, acini (with average diameter of ~120 μm) will never fill up the whole volume of the Matrigel beads. However, when beads size becomes of comparable size to the diameter of acini, grown structures experience the environmental constraint. We encapsulated MCF10A-GFP cells in 150 μm beads which were subsequently immobilized in an agarose gel. After 12 days in culture cell have proliferated and formed double layer acini which highly resemble the cellular

organization in the breast epithelial tissue (Figure 9-15D). *In vivo* acini are composed of a layer of basal cells (elongated) which surround layer of luminal cells (described in chapter 2.1).

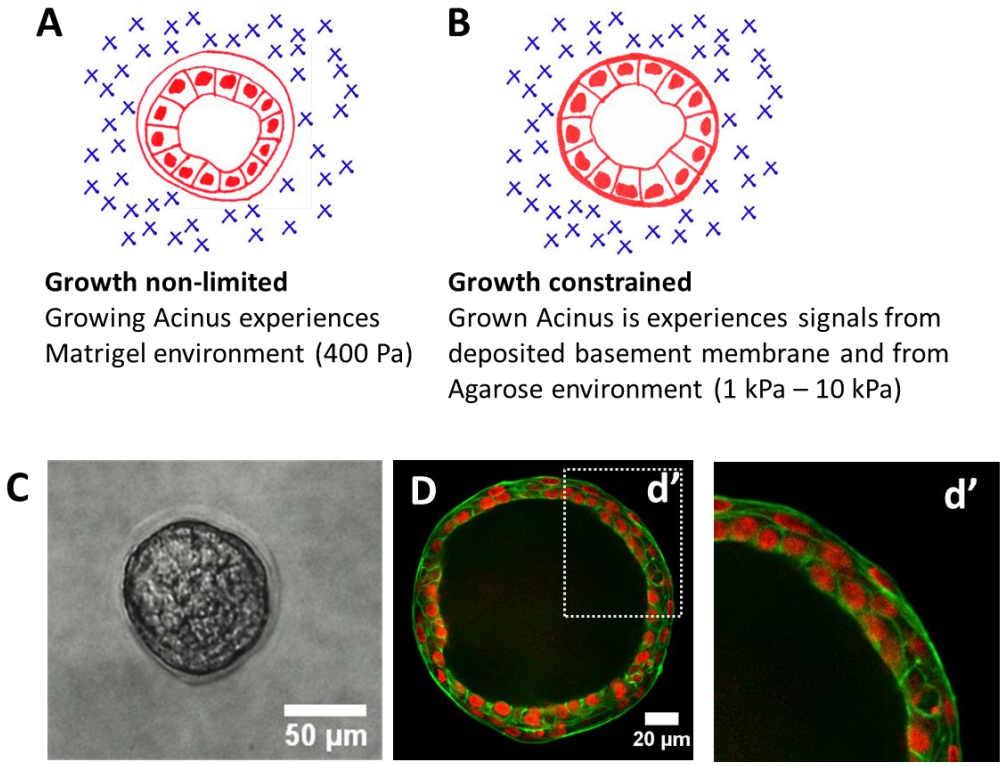

Figure 9-15 Control over environment in 3D cell culture in beads. A) and **B)** schematic representation of acini growth in Matrigel bead (red) surrounded by agarose gel (blue). Initially cells grow in Matrigel (**A**) but after they reach available matrigel volume (**B**) structures are constrained by agarose of tunable rigidity. **C)** phase contrast image of RWPE1 structure at day 6 grown in ~100 µm Matrigel bead immobilized in 3% agarose gel. **D)** Fluorescent image of MCF10A structure encapsulated in 150 µm Matrigel beads and immobilized in 3% agarose gel. Nuclei were stained with Hoechst (red) and actin was stained with Phalloidine (green). **d')** presents a zoom over a double-layer cell organization. Scale bar: C) 50 µm and D) 20 µm.

The mechanism of double-layer acini formation in Matrigel beads is unknown and further experiments need to be performed. It is possible that used agarose (that does not provide adhesion) forced such cellular organization. It still remains unclear whether these acini were formed through the clonal division that resulted in an acinus formation or by initial spreading of cells on the border of the beads and subsequent proliferation. It is also remaining to verify if cells have differentiated into basal and luminal cells by immunostaining with characteristic markers (i.e., cytokeratin markers specific for luminal cells).

9.2 Materials and protocols

9.2.1 Cell culture and immunofluorescence

2D cell culture

RWPE1 cells were both maintained in KSFM (Life Technologies, Carlsbad, CA, ref.17005-075) supplemented with 5ng/mL epidermal growth factor (EGF) and 50 mg/mL bovine pituitary extract. The cells were maintained in culture until approximately 70% confluence. For passaging, cells were washed with Dulbecco's Ca2+/Mg-free PBS (D-PBS, Life Technologies, ref. 14190) and incubated with 1mL trypsin–EDTA (Lonza, Basel, CH, ref.CC-5012,0.25mg/mL) for approximately 7min. The trypsin was neutralized with 2 mL trypsin-neutralizing solution (Lonza, ref.CC-5002), and cells were recovered by centrifugation and counted using a Scepter 2.0 Hand held Automated Cell Counter (Millipore, Billerica, MA, ref. PHCC20060).

Micropatterns

Micropatterned glass chips were obtained from CYTOO. Each mini-chip is composed of cell-adhesion points that are of a disc-shape of 700 μm^2 each and are pre-activated to be coated with the protein of choice (CYTOO, ref. 11-001-00-12). Protocol form CYTOO has been used to perform cell culture on micropattern. Briefly, for coating, each chip was immerged in 2 mL of Dulbecco's Ca2+/Mg-free PBS (D-PBS, Life Technologies, ref. 14190). Chips were incubated with a protein solution of 20 µg/mL of Matrigel for 2 hours at RT or overnight at 4˚C. After, multiple careful washes with PBS (total volume of washes 20 mL) were performed in order not to dry the surface of the chip. Just before cell seeding, PBS is removed and cells in culture media (10000 cells / mL) are poured over the surface of the chip. In order, to let the cells adhere, plate is left stable for 1 hour at room temperature and then incubated further for 3-4 hours in 37˚C. A *top-coat* layer containing 10% Matrigel is poured gently to overlay cells.

3D cell culture

For the acinar morphogenesis assay, the RWPE1 cells were cultured in 3D with KSFM (LifeTechnologies, ref.17005-075) supplemented with 50 ng/mL EGF and 2% fetal bovine serum (FBS). The 3D culture was grown in Matrigel (BD Biosciences, San Jose, CA, ref.356231) according to the top-coat protocol or embedded assay.

a) Top-coat protocol

Matrigel was thawed overnight and poured into 4-well (160 mL of Matrigel, 500 mL of culture media) or 8-wellLabtek (90 mL of Matrigel, 250 mL of culture media) plates on ice. For polymerization, Matrigel was incubated for 30 min at 37˚C. Cells were seeded in half the final volume and allowed to adhere for approximately 45 minutes. The *top-coat* layer containing 8% Matrigel was slowly poured over the attached cells. The

culture media was changed every other day. 3D assays were routinely cultured in a humidified atmosphere with 5% CO_2 at 37˚C.

b) Embedded protocol

Matrigel was thawed overnight on ice and poured as a pre-coat layer into 4-well (50 mL of Matrigel) or 8-wellLabtek (30 mL of Matrigel) plates on ice. For polymerization of the pre-coat layer plates were incubated for 30 minutes in 37˚C. Appropriate number of cells (0,5 x 10^6 cells/mL) is pelleted by centrifugation. Cells are resuspended with 100 µL of Matrigel (for 4-well Labtek) or 200 µL of Matrigel (for 8-well Labtek) and mixed gently by aspirating and dispensing Matrigel within an eppendorf tube on ice. Subsequently, Matrigel-cells mix is poured into Labtek and allowed to polymerize for 30 minutes in 37˚C and culture medium is added (200 µL for 4-well Labtek and 500 µL for 8-well Labtek). The culture media was changed every day to ensure high viability of cells. 3D assays were routinely cultured in a humidified atmosphere with 5% CO_2 at 37˚C.

Immunofluorescence

Performance of antibody has been verified on 2D culture in order to establish immunostaining in 3D culture. First, cells were fixed with 4% paraformaldehyde (freshly prepared in PBS) for 20 minutes at room temperature. After fixation cells can be stored in PBS at 4˚C up to one week before performing further steps. For 8-well slides 250 µL volumes were used for all stages of the staining. Followed fixation, cells are permeabilized with 0,5% Triton X-100 (freshly prepared in PBS; Sigma-Aldrich, ref. T8787) for 10 minutes at room temperature. Nonspecific sites were blocked with 10% goat serum (CELLect, MP, ref. 2939249) in a working buffer (Tris buffer saline, Tween 20 0,05%, Bovine Serum Albumin 0,1%) for 1-1,5 hour at room temperature. Subsequently, first antibody (dilutions of antibodies used for immunofluorescent staining are presented in table 9-2) in working buffer with 5% goat serum were incubated for at least 1 hour at room temperature or overnight at 4˚C. After, one quick wash and 4 washes for 15 minutes each were performed with working buffer. A second fluorescent antibody (Jackson, anti-mouse ref. 115-005-166, anti-rabbit 111-225-003 and anti-rat 112-485-062) was incubated for 40 minutes along with phalloidin (dilution 1:300, Sigma-Aldrich, ref. P1951). After, one quick wash and 4 washes for 15 minutes each were performed with working buffer. Nuclei were counterstained with Hoechst (Life Technologies, ref. H-1399) at a 1:7000 dilution. Glass cover slides were mounted on the glass slides with a Dako Fluorescent Mounting Medium kit (Dako, DK, ref. S3023) and stored at 4˚C before imaging.

Fluorescent microscopy

Time-lapsee acquisitions were taken with an inverted microscope (Axiovert 200M; Carl Zeiss, Inc.). The temperature, CO_2, and humidity control were performed using a Box and Brick system (Life Imaging Services). Multiple positions were recorded using an XY motorized stage (Marzhauser). Images were acquired through a 10x magnification phase contrast objective (Plan Neofluar, Ph1, NA= 0.3, Zeiss). The system was driven by Metamorph software (Universal Imaging Corporation).

Observation of 3D objects required use of confocal microscopy. For preliminary acquisition the AxioImager Z1 Zeiss microscope with a 20x objective equipped with the straight Apotome module for z-stack acquisitions was used. It gives a lower quality images however it has been widely accessible in the laboratory. The system was driven by AxioImager software (Carl Zeiss, Inc.).

For high-quality images confocal acquisition was performed on an Eclipse TI-E Nikon inverted microscope equipped with a CSUX1-A1 Yokogawa confocal head and an Evolve EMCCD camera (Ropert Scientific—Princeton Instrument). A CFI Plan APO VC oil × 60/1.4 objective or a CFI Plan Fluor oil × 40/1.3 objective (Nikon) was used. The system was driven by Metamorph software (Universal Imaging Corporation).

Table 9-2 Antibodies used for immunostaining of epithelial cells in 2D and 3D cell culture. In red, antibodies that did not work, in orange antibodies were not specific or signal was weak, and in green antibodies and concentrations that provided satisfactory results.

Antibody	Staining of	Ref	Dilution A	Dilution B	Comment
GM130	Golgi/ apical	BD 610823	1/500	1/250	non specific
Giantin	Golgi/ apical	Abcam ab24586	1/500	1/250	
Centrosome	Apical	gift from M.Therry	1/20,		
E-cadherin	cell-cell junctions	Abcam ab1416	1/200	1/100	
β - catenin	cell-cell junctions	BD 610153	1/200		
E - cadherin	cell-cell junctions	BD 610181	1/200	1/100	non specific
ZO1	cell-cell junctions	Invitrogen 61-7300	1/100	1/50	weak signal
N-cadherin	cell-cell junctions	BD 610920	1/500		no signal
laminin-5	basal membrane	Millipore MAB19562X	1/200		
β 4 integrin	basal membrane	Millipore MAB1964	1/200	1/100	
β 1 integrin	basal membrane	Abcam ab30394	1/100	1/50	
β 1 integrin	basal membrane	BD 610468	1/150	1/100	no signal
Ki67	proliferation	Invitrogen 18-0191Z	1/150	1/100	
Caspase 3	apoptose	Millipore AB3623	1/250		
Vimentin	mesenchymal marker	Sigma V5255	1/200		
Vimentin	mesenchymal marker	gift from J. Baudier	1/200	1/100	no signal

9.2.2 Methods in microfluidics

Microfluidic device fabrication

We prepared a positive master by milling the network of channels in PMMA 4 mm thick plates. The negative masters were made by molding PDMS (Sylgard 184, Dow Corning, USA) onto the PMMA chips and subsequently silanizing them with vapors of tridecafluoro-1, 1, 2, 2-tetrahydrooctyl)-1-trichlorosilane (UCT, USA). Negative masters served for molding of the positive PDMS replicas, which were subsequently bonded to glass slides or slabs of PDMS by exposure to oxygen plasma for 45 seconds followed by backing for 40 minutes in 70˚C. To increase the hydrophobicity of PDMS, we treated freshly prepared devices by fusing Aquapel® into the channels (PPG Industries, USA) followed by baking for 10 minutes in 70˚C and dried with an airgun.

We used flat sharp needles (G18, OD 1.27 mm, ID 0.84 mm) to punch holes for the direct connection of polyethylene tubing (OD 1.22 mm, ID 0.76 mm, Becton Dickinson) between the microfluidic chip and syringe pumps (KD Scientific) (syringes, various diameter BD; needles G18, OD 1.27 mm, ID 0.84 mm, Dominique Dutcher, France) that were used to generate the flow.

Preparation of monodisperse Matrigel beads

To prepare monodisperse Matrigel beads of controlled size, we used a microfluidic chip with flow focusing (FF) geometry (Fig 1). Channels have square cross sections with a reservoir of 1 mm height and width and a volume of ~100 μL. We used different sizes of channels (100, 200, and 300 μm) depending on the required size of the beads. All experiments were performed in the cold room at 4˚C to prevent polymerization of Matrigel inside the microfluidic channels. We used perfluorinated oil HFE-7500 (3M) with 2% w/v PFPE-PEG surfactant (kindly given by Prof. Garstecki) as a continuous phase and Matrigel (BD) premixed with cells as a dispersed phase. Flow inside the channel was induced and controlled by syringe pumps. Matrigel was directly injected by pipette into a reservoir channel and pushed into the FF junction by HFE-7500 oil. Droplets were collected into an eppendorf microtube for 15 minutes on average and subsequently incubated at 37˚C for 20 minutes to promote Matrigel droplets polymerization onto beads. Transfer of beads from oil into culture media was achieved by multiple washings (~6 washes) with pure HFE-7500 to eliminate surfactant. The addition of 1 mL of culture media into the tube allowed the transferring of beads to perform further tests.

We imaged the formation of Matrigel droplets in perfluorinated oil using a stereomicroscope (Olympus SZX16) equipped with an uEYE (Edmund Optics) camera. Microparticles were imaged after transfer from oil into culture media with an inverted microscope (Olympus KX41). To quantify the relationship between flow rate and the size of

formed drops we measured the size of at least 30 polymerized Matrigel beads with ImageJ. Similarly, we verified the bead stability by measuring the size of the beads over 20 days.

3D cell culture in beads

Cells were trypsinized and counted. A chosen number of cells were transferred into separate microtubes and centrifuged to form a pellet. After removal of supernatant, cells were put on ice and well mixed with pure Matrigel. The prepared solution was transferred to the cold room and injected into the microfluidic device with a 200 µm pipette tip. Droplets with cells were collected after polymerization and transferred into culture media by subsequent washes with pure HFE7500 to dilute the surfactant and thus facilitate the transfer. Beads were maintained in KSFM (Life Technologies, ref. 17005-075) supplemented with 50 ng/mL EGF, 2% fetal bovine serum (FBS), and 1% dissolved Matrigel in multiwell plate or Labtek. Beads were fixed and stained using the same reagents as for standard 3D culture described above. Beads were kept in solution and incubated with reagents and were centrifuged gently (0.8 rpm for 4 minutes) to change reagents or perform washes. At the end, beads were centrifuged and the pellet was resuspended in Mounting Medium (Dako), mounted on the microscopic glass slide and a 50 µL sample drop was covered with a glass cover slip. Samples were observed as previously described for standard 3D culture.

For single cell isolation, we estimated the concentration of beads by performing multiple dilutions. Afterwards, we dispensed beads into a 384 well-plate with a pipette (100 µL of culture medium in total). After 6 days, encapsulated cells were fixed by the direct addition of PFA into the culture medium (final concentration 2%) for 30 minutes. For the immunostaining described hereinbefore, beads were aspirated and transferred to an eppendorf tube.

Relative homogeneity of 3D culture in beads was verified by measuring the diameter of 30 structures prepared in triplicate compared with those prepared in a *top-coat* culture. We simultaneously measured the growth rate of structures for each protocol. By applying the F test we reject (at significance level 0.05) the null hypothesis and conclude that the variances are not equal.

Biocompatibility of tested surfactants and anti-coalescence properties

We tested the anti-coalescence properties of various surfactants and their biocompatibility by measuring the stability of the Matrigel/oil emulsion. Briefly, surfactant dissolved in the oil phase at various concentrations and Matrigel were fused into the microfluidic device to form droplets. The stability of droplets in the outlet channel or outlet tubing was investigated. We defined a surfactant to be efficient if the collected droplets of Matrigel were stable in oil for at least 30 minutes. When satisfactory emulsion stability was achieved, we determined the surfactant's biocompatibility by adding the surfactant (if possible)

into culture media, and/or we performed the cell encapsulation in the microfluidic device and observed cell viability and proliferation.

Encapsulation of a single cell per bead

To estimate the concentration of cells in Matrigel solution in order to encapsulate a single cell per droplet, we used the Poisson equation. For cells randomly dispersed among the Matrigel, the fraction of microdroplets containing n cells (P) is described by Poisson distribution as show in equation (1).

Eq. 6 $$P(n, \bar{n}) = \frac{\bar{n}^n e^{-\bar{n}}}{n!}$$

where $\bar{n}$ is the average number of cells per microdroplet. Equation (2) defines $\bar{n}$ as

Eq. 7 $$\bar{n} = \rho V$$

Where ρ is the concentration of cells in Matrigel (number of cells per mL) and V is the volume of the microdroplet in (mL).

Cryosectioning of beads with cells

Cells were fixed with 2% PFA for 1 h, washed and maintained in 10% sucrose for 2 hours and subsequently washed and maintained in 20% sucrose overnight. Beads were transferred to a plastic reservoir and covered with Tissue Tek OCT (Sakura) in an isopropanol/dry ice bath. Solidified samples were brought to the cryotome (Leica CM3000) and sectioned into 10 µm layers. Cut layers were deposited onto poly-L-lysine coated glass slides (Sigma) and the region of interest was delineated using a DAKO pen, after which we performed immunostaining as described before.

Cell viability after encapsulation

To determine the influence of low temperature (4˚C) at which the process of encapsulation takes place on cell viability, we determined the percent of cells that undergo apoptosis under following conditions: i) just after encapsulation (Qoil 1600 µL/h, QMatrigel 400 µL/h) ii) just after encapsulation with high-throughput (HT) formation of droplets (Qoil 10 mL/h, QMatrigel 1 mL/h), and iii) 24 hours after encapsulation. A live/dead viability assay was performed using Calcein AM (Molecular probes, C3099) and Propidium Iodide (Molecular Probes, V13245) according to the manufacturer's protocols. Briefly, beads with cells were transferred into culture media, dispensed into a multi well plate and subsequently kept for 3 hours at 37˚C in an incubator. Reagents were added directly to the culture media and live/dead cells were enumerated after 30 minutes of incubation by means of florescent microscopy. Total of 50 cells per each conditions were analyzed.

siRNA transfection and large-particle FACS analysis

Subconfluent MCF10-A cells were maintained in 2D culture and transfected for 72 hours with siRNA (siGFP, Qiagen 1022064, and Qiagen siAllstar 1027280) at a final concentration of 20 nmol/L using Lipofectamine RNAiMAX reagent (Invitrogen). To verify the efficiency of transfection, we used siCellDeath and observed cellular death with phase contrast microscopy. Subsequently, we verified the efficiency of siGFP transfection in relation to control siAllStar by measuring the mean fluorescence. Cells were detached by trypsin-EDTA and counted for subsequent encapsulation (as described before). We prepared microbeads containing a single cell that, upon incubation and proliferation, formed spherical structures within the first 5 days in culture. As a control, we prepared blank beads and treated them in the same manner. Beads were maintained in the MCF10-A culture medium supplemented with 1% Matrigel to provide higher stability and prevent aggregation. After 5 days, 3D structures were fixed by PFA (at final concentration of 2%) for 30 minutes, washed and maintained in PBS (Ca^{2+}, Mg^{2+}) containing 1% Matrigel until Large Particle FACS analysis. Copas FACS (COPAS Select, Union Biometrica Inc.) was used because it is able to analyze objects from 100 µm to 500 µm in size. We used a 250 µm device to obtain beads of 300 µm that were further filtered (pore size 400 µm) to remove any possible bead aggregates. With large particle FACS, we observed fluorescence originating from cells inside the beads. For each sample, we detected ~500 beads with fluorescent signal over 3000 total event detected in 5 minutes.

9.2.3 Methods in branching-like morphogenesis

No top-coat protocol

For the branching-like morphogenesis assay, the RWPE1 cells were cultured in 3D with KSFM (LifeTechnologies, ref.17005-075) supplemented with 50 ng/mL EGF and 2% fetal bovine serum (FBS). The 3D culture was grown in Matrigel (BD Biosciences, San Jose, CA, ref.356231). Matrigel was thawed overnight and poured into 4-well (160 mL of Matrigel, 500 mL of culture media) or 8-wellLabtek (90 mL of Matrigel, 250 mL of culture media) plates on ice. For polymerization, Matrigel was incubated for 30 min at 37˚C. Cells were seeded in 250 µL (8-well Labtek) or 500 µL (4 well Labtek). The culture media was changed every other day. 3D assays were routinely cultured in a humidified atmosphere with 5% CO_2 at 37˚C.

Treatment with TGFβ-1

The Recombinant human transforming growth factor β -1 (TGFβ-1) (R&D systems) was added to the culture medium at the final concentration of 3 ng/mL at the very beginning of the cell culture.

siRNA transfection

Subconfluent MCF10-A cells were maintained in 2D culture and transfected for 72 hours with siRNA (siBeta1-integrin, Qiagen S10300573, and Qiagen siAllstar 1027280) at a final concentration of 20 nmol/L using Lipofectamine RNAiMAX reagent (Invitrogen). To verify the efficiency of transfection, we used siCellDeath and observed cellular death with phase contrast microscopy. Cells were detached by trypsin-EDTA and counted for subsequent 3D culture *no top-coat* assay (as described before).

Measurement of Matrigel dissolution

Matrigel has been poured into 8 well Labtek wells as has been described above. To verify if the concentration of proteins depends on the quantity of Matrigel in the well, we prepared 3 well with 80 µL of Matrigel, and 3 wells with 150µL of Matrigel per well. Instead of culture media, a 250 µL per well of PBS (Ca^{2+}, Mg^{2+}) was added. After appropriate incubation time, 10 µL were aspirated and used for further analysis. In order to estimate the protein concentration we used a Nano Drop Spectrometer.

Protein Separation and Western blot

RWPE1 cells grown according to the top-coat or no top-coat protocol were washed three times with phosphate-buffered saline (PBS). A Cell Recovery Solution (CB-40253, Corning) has been used to dissolve Matrigel. Briefly, ice-colg 400 µL of Cell Recovery Solution has been added to each 8-well LabTek plate. After 2 minutes of incubation, Matrigel culture were scrapped with the P1000 tips, transferred into 2 mL eppendorf and incubated on ice for 40 minutes or until Matrigel has dissolved. Solutions were centrifuged and resting pellet (cells) has been treated

with RIPA with protease inhibitor for 10 minutes on ice. Subsequently solutions were centrifuged at full speed for 20 minutes at 4'C. Supernatant was collected, and the protein concentration was determined by using a protein BCA kit (Pierce, 23225). Western blotting was performed with a Life Technology SDS-PAGE Electrophoresis System. 15-µg protein samples were resuspended and heat denaturized in a reduced sample buffer, and then electrophoresed/separated on NuPAGE® 4-12% gradient Bis-Tris precast polyacrylamide gels (Life Technologies) with MES running buffer. The gel were blotted to nitrocellulose membrane; and sequentially probed with primary antibodies against ß1-integrin (BD, 610468), beta-catenin (BD, 610153), FAK (BD, F15020), Rac1 (BD, 610650) and peroxidase-conjugated goat anti-mouse secondary antibodies. The blots were analyzed by autoradiography using enhanced chemiluminescence solution (ECL Plus, General Electric Healthcare, Milwaukee, WI)

Mass Spectrometry (performed by MS platform in CEA)

- **Protein digestion**

  The gel bands were manually excised and cut in pieces before being washed by 6 successive incubations of 15 min in 25 mM NH_4HCO_3 and in 25mM NH_4HCO_3 containing 50% (v/v) acetonitrile. Gel pieces were then dehydrated with 100 % acetonitrile and incubated for 45 min at 53°C with 10 mM DTT in 25mM NH_4HCO_3 and for 35 min in the dark with 55 mM iodoacétamide in 25mM NH_4HCO_3. Alkylation was stopped by adding 10 mM DTT in 25mM NH_4HCO_3 and mixing for 10 min. Gel pieces were then washed again by incubation in 25 mM NH_4HCO_3 before dehydration with 100% acetonitrile. Modified trypsin (Promega, sequencing grade) in 25 mM NH_4HCO_3 was added to the dehydrated gel pieces for an overnight incubation at 37°C. Peptides were then extracted from gel pieces in three 15 min sequential extraction steps in 30 µL of 50% acetonitrile, 30 µL of 5% formic acid and finally 30µL of 100% acetonitrile. The pooled supernatants were then dried under vacuum.

- **Nano-LC-MS/MS analyses.**

  The dried extracted peptides were resuspended in 5% acetonitrile and 0.1% trifluoroacetic acid and analysed by online nanoLC-MS/MS (Ultimate 3000, Dionex and LTQ-Orbitrap Velos pro, Thermo Fischer Scientific). Peptides were sampled on a 300 µm x 5 mm PepMap C18 precolumn and separated on a 75 µm x 250 mm C18 column (PepMap, Dionex). The nanoLC method consisted in a 15-minutes gradient ranging from 5% to 45% acetronitrile in 0.1% formic acid at a flow rate of 300 nL/min. MS and MS/MS data were acquired using Xcalibur (Thermo Fischer Scientific). Spray voltage and heated capillary were respectively set at 1.4 kV and 200°C. Survey full-scan MS spectra (m/z = 400–1600) were acquired in the Orbitrap with a resolution of 60,000 after accumulation of 10^6 ions (maximum filling time: 500 ms). The twenty most intense

ions from the preview survey scan delivered by the Orbitrap were fragmented by collision induced dissociation (collision energy 35%) in the LTQ after accumulation of 10^4 ions (maximum filling time: 100 ms).

- **Bioinformatics analyses.**

  Data were processed automatically using Mascot Daemon software (version 2.3.2, Matrix Science). Concomitant searches against Mus musculus and classical contaminant protein sequence databases and the corresponding reversed databases were performed using Mascot (version 2.4). ESI-TRAP was chosen as the instrument, trypsin/P as the enzyme and 2 missed cleavage allowed. Precursor and fragment mass error tolerances were set respectively at 10 ppm and 0.6 Da. Peptide modifications allowed during the search were: carbamidomethyl (C, fixes) acetyl (N-ter, variable) and oxidation (M, variable). The IRMa software (Dupierris *et al.*, Bioinformatics, 2009, 25:1980-1, version 1.31.1) was used to filter the results: conservation of rank 1 peptides, query homology threshold $p < 0.01$, single match per query and 2 unique peptides per protein match.

Lens-free real-time imaging

Our lens-free imaging device, which has been previously described (Chapter 7.2), features an Aptina CMOS sensor (MT9P031 RGB, 25 mm^2, 5 M pixels, 2.2 µm pixel pitch). Illumination consisted of 525 nm LED butt-coupled to a 150 µm pinhole. A Labtek plate is placed on the protective cap of the CMOS sensor, the acini are approximately 1 mm above the CMOS sensor and 5 cm below the LED. To maintain the sensor temperature at approximately 37°C, it is switched off during two consecutive acquisitions, and a fan is used to extract the heat from the sensor box. This setup allows us to record the lens-free hologram that results from the interference between the partially coherent incident light and the light scattered by the cells and/or the acini. Next, holographic reconstruction was performed to reconstruct the image of the cell culture from the lens-free hologram. This type of holographic reconstruction is based on the previously described phase retrieval algorithm (Fienup, 1982; Meijering *et al.*, 2012). This method allows us to decipher the overall shape of each cell and acini and identify their precise location in the X-Y plane from the holographic pattern. No refinements were applied to reconstruct the acini. After the holographic reconstruction, the tracking of cell migration was performed using image sequences, and the velocity was calculated using ImageJ MTrackJ (Meijering *et al.*, 2012).

Image J plug-ins and macros

For the preparation of Figure 7-6 following Image J setting were used:

- Macro for 3D LUT – author: Kota Miura (EMBL, Heidelberg)
- Pluging Volume Viewer – author: Kai Uwe Barthel (Internationale Medieninformatik, HTW, Berlin)

10. References

Affolter, M., S. Bellusci, N. Itoh, B. Shilo, J.P. Thiery, and Z. Werb. 2003. Tube or not tube: Remodeling epithelial tissues by branching morphogenesis. *Developmental Cell*. 4:11-18.

Alberts, B., A. Johnson, J. Lewis, M. Raff, K. Roberts, and P. Walter. 2002. Molecular Biology of the Cell. Garland Science.

Alessandri, K., B.R. Sarangi, V.V. Gurchenkov, B. Sinha, T.R. Kiessling, L. Fetler, F. Rico, S. Scheuring, C. Lamaze, A. Simon, S. Geraldo, D. Vignjevic, H. Domejean, L. Rolland, A. Funfak, J. Bibette, N. Bremond, and P. Nassoy. 2013. Cellular capsules as a tool for multicellular spheroid production and for investigating the mechanics of tumor progression in vitro. *Proceedings of the National Academy of Sciences of the United States of America*. 110:14843-14848.

Alford, D., and J. Taylor-Papadimitriou. 1996. Cell Adhesion Molecules in the Normal and Cancerous Mammary Gland. *Journal of Mammary Gland Biology and Neoplasia*. 1:207-218.

Anna, S.L., N. Bontoux, and H.A. Stone. 2003. Formation of dispersions using "flow focusing" in microchannels. *Applied Physics Letters*. 82:364-366.

Aumailley, M., and B. Gayraud. 1998. Structure and biological activity of the extracellular matrix. *Journal of Molecular Medicine-Jmm*. 76:253-265.

Bai, Y., X. He, D. Liu, S.N. Patil, D. Bratton, A. Huebner, F. Hollfelder, C. Abell, and W.T.S. Huck. 2010. A double droplet trap system for studying mass transport across a droplet-droplet interface. *Lab on a Chip*. 10:1281-1285.

Balakrishnan, B., and R. Banerjee. 2011. Biopolymer-Based Hydrogels for Cartilage Tissue Engineering. *Chemical Reviews*. 111:4453-4474.

Barcelloshoff, M.H., J. Aggeler, T.G. Ram, and M.J. Bissell. 1989. FUNCTIONAL-DIFFERENTIATION AND ALVEOLAR MORPHOGENESIS OF PRIMARY MAMMARY CULTURES ON RECONSTITUTED BASEMENT-MEMBRANE. *Development*. 105:223-&.

Baret, J.-C., O.J. Miller, V. Taly, M. Ryckelynck, A. El-Harrak, L. Frenz, C. Rick, M.L. Samuels, J.B. Hutchison, J.J. Agresti, D.R. Link, D.A. Weitz, and A.D. Griffiths. 2009. Fluorescence-activated droplet sorting (FADS): efficient microfluidic cell sorting based on enzymatic activity. *Lab on a Chip*. 9:1850-1858.

Batorsky, A., J.H. Liao, A.W. Lund, G.E. Plopper, and J.P. Stegemann. 2005. Encapsulation of adult human mesenchymal stem cells within collagen-agarose microenvironments. *Biotechnology and Bioengineering*. 92:492-500.

Bello, D., M.M. Webber, H.K. Kleinman, D.D. Wartinger, and J.S. Rhim. 1997. Androgen responsive adult human prostatic epithelial cell lines immortalized by human papillomavirus 18. *Carcinogenesis*. 18:1215-1223.

Bello-Deocampo, D., H.K. Kleinman, N.D. Deocampo, and M.M. Webber. 2001. Laminin-1 and alpha 6 beta 1 integrin regulate acinar morphogenesis of normal and malignant human prostate epithelial cells. *Prostate*. 46:142-153.

Ben-Jacob, E., D.S. Coffey, and H. Levine. 2012. Bacterial survival strategies suggest rethinking cancer cooperativity. *Trends in Microbiology*. 20:403-410.

Berdichevsky, F., D. Alford, B. Dsouza, and J. Taylorpapadimitriou. 1994. BRANCHING MORPHOGENESIS OF HUMAN MAMMARY EPITHELIAL-CELLS IN COLLAGEN GELS. *Journal of Cell Science*. 107:3557-3568.

Bilder, D., M. Li, and N. Perrimon. 2000. Cooperative regulation of cell polarity and growth by Drosophila tumor suppressors. *Science*. 289:113-116.

Bilder, D., M. Schober, and N. Perrimon. 2003. Integrated activity of PDZ protein complexes regulates epithelial polarity. *Nature Cell Biology*. 5:53-58.

Bishara, W., T.W. Su, A.F. Coskun, and A. Ozcan. 2010. Lensfree on-chip microscopy over a wide field-of-view using pixel super-resolution. *Optics Express*. 18:11181-11191.

Bolender, D.L., and R.R. Markwald. 1979. Epithelial-mesenchymal transformation in chick atrioventricular cushion morphogenesis. *Scanning electron microscopy*:313-321.

Brinkmann, A.O., L.J. Blok, P.E. de Ruiter, P. Doesburg, K. Steketee, C.A. Berrevoets, and J. Trapman. 1999. Mechanisms of androgen receptor activation and function. *Journal of Steroid Biochemistry and Molecular Biology*. 69:307-313.

Brouzes, E., M. Medkova, N. Savenelli, D. Marran, M. Twardowski, J.B. Hutchison, J.M. Rothberg, D.R. Link, N. Perrimon, and M.L. Samuels. 2009. Droplet microfluidic technology for single-cell high-throughput screening. *Proceedings of the National Academy of Sciences of the United States of America*. 106:14195-14200.

Brownfield, D.G., G. Venugopalan, A. Lo, H. Mori, K. Tanner, D.A. Fletcher, and M.J. Bissell. 2013. Patterned Collagen Fibers Orient Branching Mammary Epithelium through Distinct Signaling Modules. *Current Biology*. 23:703-709.

Bryant, D.M., and K.E. Mostov. 2008. From cells to organs: building polarized tissue. *Nature Reviews Molecular Cell Biology*. 9:887-901.

Butcher, D.T., T. Alliston, and V.M. Weaver. 2009. A tense situation: forcing tumour progression. *Nature Reviews Cancer*. 9:108-122.

Cai, C., J. Thorne, and L. Grabel. 2008. Hedgehog serves as a mitogen and survival factor during embryonic stem cell neurogenesis. *Stem Cells*. 26:1097-1108.

Campbell, I.D., and M.J. Humphries. 2011. Integrin Structure, Activation, and Interactions. *Cold Spring Harbor Perspectives in Biology*. 3.

Catalona, W.J., D.S. Smith, T.L. Ratliff, K.M. Dodds, D.E. Coplen, J.J.J. Yuan, J.A. Petros, and G.L. Andriole. 1991. MEASUREMENT OF PROSTATE-SPECIFIC ANTIGEN IN SERUM AS A SCREENING-TEST FOR PROSTATE-CANCER. *New England Journal of Medicine*. 324:1156-1161.

Celli, J.P., I. Rizvi, A.R. Blanden, I. Massodi, M.D. Glidden, B.W. Pogue, and T. Hasan. 2014. An imaging-based platform for high-content, quantitative evaluation of therapeutic response in 3D tumour models. *Scientific Reports*. 4.

Chabert, M., and J.-L. Viovy. 2008. Microfluidic high-throughput encapsulation and hydrodynamic self-sorting of single cells. *Proceedings of the National Academy of Sciences of the United States of America*. 105:3191-3196.

Chang, T.M.S. 1964. SEMIPERMEABLE MICROCAPSULES. *Science*. 146:524-&.

Chaudhury, M.K., and G.M. Whitesides. 1991. DIRECT MEASUREMENT OF INTERFACIAL INTERACTIONS BETWEEN SEMISPHERICAL LENSES AND FLAT SHEETS OF POLY(DIMETHYLSILOXANE) AND THEIR CHEMICAL DERIVATIVES. *Langmuir*. 7:1013-1025.

Chen, J.C., T.G. Diacovo, D.G. Grenache, S.A. Santoro, and M.M. Zutter. 2002. The alpha(2) integrin subunit-deficient mouse - A multifaceted phenotype including defects of

branching morphogenesis and hemostasis. *American Journal of Pathology*. 161:337-344.

Chen, S.-Y.C., P.J. Hung, and P.J. Lee. 2011. Microfluidic array for three-dimensional perfusion culture of human mammary epithelial cells. *Biomedical Microdevices*. 13:753-758.

Chiu, D.T., R.M. Lorenz, and G.D.M. Jeffries. 2009. Droplets for Ultrasmall-Volume Analysis. *Analytical Chemistry*. 81:5111-5118.

Christiansen, J.J., and A.K. Rajasekaran. 2006. Reassessing epithelial to mesenchymal transition as a prerequisite for carcinoma invasion and metastasis. *Cancer Research*. 66:8319-8326.

Chung, L.W.K. 1995. THE ROLE OF STROMAL-EPITHELIAL INTERACTION IN NORMAL AND MALIGNANT GROWTH. *Cancer Surveys*. 23:33-42.

Comen, E., and L. Norton. 2012. Self-seeding in cancer. *Recent results in cancer research. Fortschritte der Krebsforschung. Progres dans les recherches sur le cancer*. 195:13-23.

Coppe, J.-P., C.K. Patil, F. Rodier, Y. Sun, D.P. Munoz, J. Goldstein, P.S. Nelson, P.-Y. Desprez, and J. Campisi. 2008. Senescence-Associated Secretory Phenotypes Reveal Cell-Nonautonomous Functions of Oncogenic RAS and the p53 Tumor Suppressor. *Plos Biology*. 6:2853-2868.

Coskun, A.F., I. Sencan, T.W. Su, and A. Ozcan. 2010. Lensless wide-field fluorescent imaging on a chip using compressive decoding of sparse objects. *Optics Express*. 18:10510-10523.

Cramer, C., P. Fischer, and E.J. Windhab. 2004. Drop formation in a co-flowing ambient fluid. *Chemical Engineering Science*. 59:3045-3058.

Cui, X.Q., L.M. Lee, X. Heng, W.W. Zhong, P.W. Sternberg, D. Psaltis, and C.H. Yang. 2008. Lensless high-resolution on-chip optofluidic microscopes for Caenorhabditis elegans and cell imaging. *Proceedings of the National Academy of Sciences of the United States of America*. 105:10670-10675.

Cukierman, E., R. Pankov, D.R. Stevens, and K.M. Yamada. 2001. Taking cell-matrix adhesions to the third dimension. *Science*. 294:1708-1712.

Cukierman, E., R. Pankov, and K.M. Yamada. 2002. Cell interactions with three-dimensional matrices. *Current Opinion in Cell Biology*. 14:633-639.

Cunha, G.R. 1973. The role of androgens in the epithelio-mesenchymal interactions involved in prostatic morphogenesis in embryonic mice. *Anat Rec*. 175:87-96.

Cygan, Z.T., J.T. Cabral, K.L. Beers, and E.J. Amis. 2005. Microfluidic platform for the generation of organic-phase microreactors. *Langmuir*. 21:3629-3634.

Czyz, J., and A.M. Wobus. 2001. Embryonic stem cell differentiation: The role of extracellular factors. *Differentiation*. 68:167-174.

Dafforn, A., P. Chen, G. Deng, M. Herrler, D. Iglehart, S. Koritala, S. Lato, S. Pillarisetty, R. Purohit, M. Wang, S. Wang, and N. Kurn. 2004. Linear mRNA amplification from as little as 5 ng total RNA for global gene expression analysis. *Biotechniques*. 37:854-857.

Darribere, T., M. Skalski, H. Cousin, A. Gaultier, C. Montmory, and D. Alfandari. 2000. Integrins: Regulators of embryogenesis. *Biology of the Cell*. 92:5-25.

Datta, A., D.M. Bryant, and K.E. Mostov. 2011. Molecular Regulation of Lumen Morphogenesis. *Current Biology*. 21:R126-R136.

David, S., B. Pitard, J.-P. Benoit, and C. Passirani. 2010. Non-viral nanosystems for systemic siRNA delivery. *Pharmacological Research*. 62:100-114.

Davies, J.A. 1996. Mesenchyme to epithelium transition during development of the mammalian kidney tubule. *Acta Anatomica*. 156:187-201.

Davis, G.E., and C.W. Camarillo. 1996. An alpha 2 beta 1 integrin-dependent pinocytic mechanism involving intracellular vacuole formation and coalescence regulates capillary lumen and tube formation in three-dimensional collagen matrix. *Experimental Cell Research*. 224:39-51.

de Fougerolles, A., and T. Novobrantseva. 2008. siRNA and the lung: research tool or therapeutic drug? *Current Opinion in Pharmacology*. 8:280-285.

Debnath, J., and J.S. Brugge. 2005. Modelling glandular epithelial cancers in three-dimensional cultures. *Nature Reviews Cancer*. 5:675-688.

Debnath, J., K.R. Mills, N.L. Collins, M.J. Reginato, S.K. Muthuswamy, and J.S. Brugge. 2002. The role of apoptosis in creating and maintaining luminal space with normal and oncogene-expressing mammary acini. *Cell*. 111:29-40.

Debnath, J., S.K. Muthuswamy, and J.S. Brugge. 2003. Morphogenesis and oncogenesis of MCF-10A mammary epithelial acini grown in three-dimensional basement membrane cultures. *Methods*. 30:256-268.

Denis, L., C. Fournier, T. Fournel, and C. Ducottet. 2008. Numerical suppression of the twin image in in-line holography of a volume of micro-objects. *Measurement Science & Technology*. 19.

DiFiglia, M., M. Sena-Esteves, K. Chase, E. Sapp, E. Pfister, M. Sass, J. Yoder, P. Reeves, R.K. Pandey, K.G. Rajeev, M. Manoharan, D.W.Y. Sah, P.D. Zamore, and N. Aronin. 2007. Therapeutic silencing of mutant huntingtin with siRNA attenuates striatal and cortical neuropathology and behavioral deficits. *Proceedings of the National Academy of Sciences of the United States of America*. 104:17204-17209.

Dittrich, P.S., M. Jahnz, and P. Schwille. 2005. A new embedded process for compartmentalized cell-free protein expression and on-line detection in microfluidic devices. *Chembiochem*. 6:811-+.

Duband, J.L., and J.P. Thiery. 1987. DISTRIBUTION OF LAMININ AND COLLAGENS DURING AVIAN NEURAL CREST DEVELOPMENT. *Development*. 101:461-478.

Duffy, D.C., J.C. McDonald, O.J.A. Schueller, and G.M. Whitesides. 1998. Rapid prototyping of microfluidic systems in poly(dimethylsiloxane). *Analytical Chemistry*. 70:4974-4984.

Eisenberger, M.A., B.A. Blumenstein, E.D. Crawford, G. Miller, D.G. McLeod, P.J. Loehrer, G. Wilding, K. Sears, D.J. Culkin, I.M. Thompson, A.J. Bueschen, and B.A. Lowe. 1998. Bilateral orchiectomy with or without flutamide for metastatic prostate cancer. *New England Journal of Medicine*. 339:1036-1042.

Ekblom, P., M. Ekblom, L. Fecker, G. Klein, H.Y. Zhang, Y. Kadoya, M.L. Chu, U. Mayer, and R. Timpl. 1994. ROLE OF MESENCHYMAL NIDOGEN FOR EPITHELIAL MORPHOGENESIS IN-VITRO. *Development*. 120:2003-2014.

Elbashir, S.M., J. Harborth, W. Lendeckel, A. Yalcin, K. Weber, and T. Tuschl. 2001. Duplexes of 21-nucleotide RNAs mediate RNA interference in cultured mammalian cells. *Nature*. 411:494-498.

Engler, A., L. Bacakova, C. Newman, A. Hategan, M. Griffin, and D. Discher. 2004. Substrate compliance versus ligand density in cell on gel responses. *Biophysical Journal*. 86:617-628.

Eun, Y.-J., A.S. Utada, M.F. Copeland, S. Takeuchi, and D.B. Weibel. 2011. Encapsulating Bacteria in Agarose Microparticles Using Microfluidics for High-Throughput Cell Analysis and Isolation. *Acs Chemical Biology*. 6:260-266.

Fata, J.E., Z. Werb, and M.J. Bissell. 2004. Regulation of mammary gland branching morphogenesis by the extracellular matrix and its remodeling enzymes. *Breast Cancer Research*. 6:1-11.

Feldman, B.J., and D. Feldman. 2001. The development of androgen-independent prostate cancer. *Nature Reviews Cancer*. 1:34-45.

Fenteany, G., P.A. Janmey, and T.P. Stossel. 2000. Signaling pathways and cell mechanics involved in wound closure by epithelial cell sheets. *Current Biology*. 10:831-838.

Fienup, J.R. 1982. PHASE RETRIEVAL ALGORITHMS - A COMPARISON. *Applied Optics*. 21:2758-2769.

Fire, A., S.Q. Xu, M.K. Montgomery, S.A. Kostas, S.E. Driver, and C.C. Mello. 1998. Potent and specific genetic interference by double-stranded RNA in Caenorhabditis elegans. *Nature*. 391:806-811.

Frank, S.B., and C.K. Miranti. 2013. Disruption of prostate epithelial differentiation pathways and prostate cancer development. *Frontiers in oncology*. 3:273-273.

Friedl, P., and D. Gilmour. 2009. Collective cell migration in morphogenesis, regeneration and cancer. *Nature Reviews Molecular Cell Biology*. 10:445-457.

Friedl, P., Y. Hegerfeldt, and M. Tusch. 2004. Collective cell migration in morphogenesis and cancer. *International Journal of Developmental Biology*. 48:441-449.

Frisch, S.M., and H. Francis. 1994. DISRUPTION OF EPITHELIAL CELL-MATRIX INTERACTIONS INDUCES APOPTOSIS. *Journal of Cell Biology*. 124:619-626.

Garcia-Sucerquia, J., W.B. Xu, M.H. Jericho, and H.J. Kreuzer. 2006. Immersion digital in-line holographic microscopy. *Optics Letters*. 31:1211-1213.

Garstecki, P., M.J. Fuerstman, H.A. Stone, and G.M. Whitesides. 2006. Formation of droplets and bubbles in a microfluidic T-junction - scaling and mechanism of break-up. *Lab on a Chip*. 6:437-446.

Garstecki, P., I. Gitlin, W. DiLuzio, G.M. Whitesides, E. Kumacheva, and H.A. Stone. 2004. Formation of monodisperse bubbles in a microfluidic flow-focusing device. *Applied Physics Letters*. 85:2649-2651.

Gersdorff, N., S. Otto, M. Roediger, J. Kruegel, and N. Miosge. 2007. The absence of one or both nidogens does not alter basement membrane composition in adult murine kidney. *Histology and Histopathology*. 22:1077-1084.

Giselbrecht, S., T. Gietzelt, E. Gottwald, C. Trautmann, R. Truckenmueller, K.F. Weibezahn, and A. Welle. 2006. 3D tissue culture substrates produced by microthermoforming of pre-processed polymer films. *Biomedical Microdevices*. 8:191-199.

Gov, N.S. 2007. Collective cell migration patterns: Follow the leader. *Proceedings of the National Academy of Sciences of the United States of America*. 104:15970-15971.

Greenburg, G., and E.D. Hay. 1982. EPITHELIA SUSPENDED IN COLLAGEN GELS CAN LOSE POLARITY AND EXPRESS CHARACTERISTICS OF MIGRATING MESENCHYMAL CELLS. *Journal of Cell Biology*. 95:333-339.

Greenburg, G., and E.D. Hay. 1986. CYTODIFFERENTIATION AND TISSUE PHENOTYPE CHANGE DURING TRANSFORMATION OF EMBRYONIC LENS EPITHELIUM TO MESENCHYME-LIKE CELLS-INVITRO. *Developmental Biology*. 115:363-379.

Greenlee, R.T., T. Murray, S. Bolden, and P.A. Wingo. 2000. Cancer statistics, 2000. *Ca-a Cancer Journal for Clinicians*. 50:7-33.

Gunawan, R.C., J. Silvestre, H.R. Gaskins, P.J.A. Kenis, and D.E. Leckband. 2006. Cell migration and polarity on microfabricated gradients of extracellular matrix proteins. *Langmuir*. 22:4250-4258.

Guo, C.-L., M. Ouyang, J.-Y. Yu, J. Maslov, A. Price, and C.-Y. Shen. 2012. Long-range mechanical force enables self-assembly of epithelial tubular patterns. *Proceedings of the National Academy of Sciences of the United States of America*. 109:5576-5582.

Gustafsson, E., and R. Fassler. 2000. Insights into extracellular matrix functions from mutant mouse models. *Experimental Cell Research*. 261:52-68.

Harma, V., J. Virtanen, R. Makela, A. Happonen, J.P. Mpindi, M. Knuuttila, P. Kohonen, J. Lotjonen, O. Kallioniemi, and M. Nees. 2010. A Comprehensive Panel of Three-Dimensional Models for Studies of Prostate Cancer Growth, Invasion and Drug Responses. *Plos One*. 5.

Hayashi, N., Y. Sugimura, J. Kawamura, A.A. Donjacour, and G.R. Cunha. 1991. MORPHOLOGICAL AND FUNCTIONAL-HETEROGENEITY IN THE RAT PROSTATIC GLAND. *Biology of Reproduction*. 45:308-321.

Hayward, S.W., L.S. Baskin, P.C. Haughney, A.R. Cunha, B.A. Foster, R. Dahiya, G.S. Prins, and G.R. Cunha. 1996a. Epithelial development in the rat ventral prostate, anterior prostate and seminal vesicle. *Acta Anatomica*. 155:81-93.

Hayward, S.W., L.S. Baskin, P.C. Haughney, B.A. Foster, A.R. Cunha, R. Dahiya, G.S. Prins, and G.R. Cunha. 1996b. Stromal development in the ventral prostate, anterior prostate and seminal vesicle of the rat. *Acta Anatomica*. 155:94-103.

Hebner, C., V.M. Weaver, and J. Debnath. 2008. Modeling morphogenesis and oncogenesis in three-dimensional breast epithelial cultures. *Annual Review of Pathology-Mechanisms of Disease*. 3:313-339.

Hogan, B.L.M., and P.A. Kolodziej. 2002. Molecular mechanisms of tubulogenesis. *Nature Reviews Genetics*. 3:513-523.

Holtze, C., A.C. Rowat, J.J. Agresti, J.B. Hutchison, F.E. Angile, C.H.J. Schmitz, S. Koster, H. Duan, K.J. Humphry, R.A. Scanga, J.S. Johnson, D. Pisignano, and D.A. Weitz. 2008. Biocompatible surfactants for water-in-fluorocarbon emulsions. *Lab on a Chip*. 8:1632-1639.

Horoszewicz, J.S., S.S. Leong, E. Kawinski, J.P. Karr, H. Rosenthal, T.M. Chu, E.A. Mirand, and G.P. Murphy. 1983. LNCaP model of human prostatic carcinoma. *Cancer Res*. 43:1809-1818.

Hsiung, S.-K., C.-H. Lee, J.-L. Lin, and G.-B. Lee. 2007. Active micro-mixers utilizing moving wall structures activated pneumatically by buried side chambers. *Journal of Micromechanics and Microengineering*. 17:129-138.

Hubbell, J.A. 2004. Biomaterials science and high-throughput screening. *Nature Biotechnology*. 22:828-829.

Huebner, A., S. Sharma, M. Srisa-Art, F. Hollfelder, J.B. Edel, and A.J. deMello. 2008. Microdroplets: A sea of applications? *Lab on a Chip*. 8:1244-1254.

Huggins, C. 1967. Endocrine-induced regression of cancers. *Cancer Res*. 27:1925-1930.

Hughes, C.S., L.M. Postovit, and G.A. Lajoie. 2010. Matrigel: A complex protein mixture required for optimal growth of cell culture. *Proteomics*. 10:1886-1890.

Humphreys, R.C., M. Krajewska, S. Krnacik, R. Jaeger, H. Weiher, S. Krajewski, J.C. Reed, and J.M. Rosen. 1996. Apoptosis in the terminal endbud of the murine mammary gland: A mechanism of ductal morphogenesis. *Development*. 122:4013-4022.

Jakiela, S., P.M. Korczyk, S. Makulska, O. Cybulski, and P. Garstecki. 2012. Discontinuous Transition in a Laminar Fluid Flow: A Change of Flow Topology inside a Droplet Moving in a Micron-Size Channel. *Physical Review Letters*. 108.

Jankowski, P., D. Ogonczyk, L. Derzsi, W. Lisowski, and P. Garstecki. 2013. Hydrophilic polycarbonate chips for generation of oil-in-water (O/W) and water-in-oil-in-water (W/O/W) emulsions. *Microfluidics and Nanofluidics*. 14:767-774.

Jankowski, P., D. Ogonczyk, A. Kosinski, W. Lisowski, and P. Garstecki. 2011. Hydrophobic modification of polycarbonate for reproducible and stable formation of biocompatible microparticles. *Lab on a Chip*. 11:748-752.

Ji, H., D. Sander, A. Haas, and P.A. Abshire. 2007. Contact imaging: Simulation and experiment. *Ieee Transactions on Circuits and Systems I-Regular Papers*. 54:1698-1710.

Joensson, H.N., and H.A. Svahn. 2012. Droplet Microfluidics-A Tool for Single-Cell Analysis. *Angewandte Chemie-International Edition*. 51:12176-12192.

Jun, Y., M.J. Kim, Y.H. Hwang, E.A. Jeon, A.R. Kang, S.-H. Lee, and D.Y. Lee. 2013. Microfluidics-generated pancreatic islet microfibers for enhanced immunoprotection. *Biomaterials*. 34:8122-8130.

Kaighn, M.E., K.S. Narayan, Y. Ohnuki, J.F. Lechner, and L.W. Jones. 1979. ESTABLISHMENT AND CHARACTERIZATION OF A HUMAN PROSTATIC-CARCINOMA CELL-LINE (PC-3). *Investigative Urology*. 17:16-23.

Kamei, M., W.B. Saunders, K.J. Bayless, L. Dye, G.E. Davis, and B.M. Weinstein. 2006. Endothelial tubes assemble from intracellular vacuoles in vivo. *Nature*. 442:453-456.

Katoh, M., T. Matsui, H. Okumura, M. Nakajima, M. Nishimura, S. Naito, C. Tateno, K. Yoshizato, and T. Yokoi. 2005. Expression of human phase II enzymes in chimeric mice with humanized liver. *Drug Metabolism and Disposition*. 33:1333-1340.

Keely, P.J. 2011. Mechanisms by Which the Extracellular Matrix and Integrin Signaling Act to Regulate the Switch Between Tumor Suppression and Tumor Promotion. *Journal of Mammary Gland Biology and Neoplasia*. 16:205-219.

Khademhosseini, A., R. Langer, J. Borenstein, and J.P. Vacanti. 2006. Microscale technologies for tissue engineering and biology. *Proceedings of the National Academy of Sciences of the United States of America*. 103:2480-2487.

Kim, C., S. Chung, Y.E. Kim, K.S. Lee, S.H. Lee, K.W. Oh, and J.Y. Kang. 2011. Generation of core-shell microcapsules with three-dimensional focusing device for efficient formation of cell spheroid. *Lab on a Chip*. 11:246-252.

Kim, M.-Y., T. Oskarsson, S. Acharyya, D.X. Nguyen, X.H.F. Zhang, L. Norton, and J. Massague. 2009. Tumor Self-Seeding by Circulating Cancer Cells. *Cell*. 139:1315-1326.

Kim, S.H., J.H. Jeong, S.H. Lee, S.W. Kim, and T.G. Park. 2008. Local and systemic delivery of VEGF siRNA using polyelectrolyte complex micelles for effective treatment of cancer. *Journal of Controlled Release*. 129:107-116.

Kirshner, J., C.J. Chen, P.F. Liu, J. Huang, and J.E. Shively. 2003. CEACAM1-4S, a cell-cell adhesion molecule, mediates apoptosis and reverts mammary carcinoma cells to a normal morphogenic phenotype in a 3D culture. *Proceedings of the National Academy of Sciences of the United States of America*. 100:521-526.

Kleinman, H.K., R.J. Klebe, and G.R. Martin. 1981. ROLE OF COLLAGENOUS MATRICES IN THE ADHESION AND GROWTH OF CELLS. *Journal of Cell Biology*. 88:473-485.

Kleinman, H.K., and G.R. Martin. 2005. Matrigel: Basement membrane matrix with biological activity. *Seminars in Cancer Biology*. 15:378-386.

Klinowska, T.C.M., C.M. Alexander, E. Georges-Labouesse, R. Van der Neut, J.A. Kreidberg, C.J.P. Jones, A. Sonnenberg, and C.H. Streuli. 2001. Epithelial development and differentiation in the mammary gland is not dependent on alpha 3 or alpha 6 integrin subunits. *Developmental Biology*. 233:449-467.

Knox, J.D., A.E. Cress, V. Clark, L. Manriquez, K.S. Affinito, B.L. Dalkin, and R.B. Nagle. 1994. DIFFERENTIAL EXPRESSION OF EXTRACELLULAR-MATRIX MOLECULES AND THE ALPHA(6)-INTEGRINS IN THE NORMAL AND NEOPLASTIC PROSTATE. *American Journal of Pathology*. 145:167-174.

Kobel, S., and M.P. Lutolf. 2011. Biomaterials meet microfluidics: building the next generation of artificial niches. *Current Opinion in Biotechnology*. 22:690-697.

Korczyk, P.M., O. Cybulski, S. Makulska, and P. Garstecki. 2011. Effects of unsteadiness of the rates of flow on the dynamics of formation of droplets in microfluidic systems. *Lab on a Chip*. 11:173-175.

Kuperwasser, C., T. Chavarria, M. Wu, G. Magrane, J.W. Gray, L. Carey, A. Richardson, and R.A. Weinberg. 2004. Reconstruction of functionally normal and malignant human breast tissues in mice. *Proceedings of the National Academy of Sciences of the United States of America*. 101:4966-4971.

Labrie, F., A. Dupont, R. Suburu, L. Cusan, M. Tremblay, J.L. Gomez, J. Emond, T.A. Stamey, and P.H. Lange. 1992. SERUM PROSTATE SPECIFIC ANTIGEN AS PRE-SCREENING TEST FOR PROSTATE-CANCER. *Journal of Urology*. 147:846-852.

Lasnitzki, I., and T. Mizuno. 1977. Induction of the rat prostate gland by androgens in organ culture. *J Endocrinol*. 74:47-55.

Lecuit, T., and E. Wieschaus. 2002. Junctions as organizing centers in epithelial cells? A fly perspective. *Traffic*. 3:92-97.

Lee, G.Y., P.A. Kenny, E.H. Lee, and M.J. Bissell. 2007. Three-dimensional culture models of normal and malignant breast epithelial cells. *Nature Methods*. 4:359-365.

Lee, M.-Y., R.A. Kumar, S.M. Sukumaran, M.G. Hogg, D.S. Clark, and J.S. Dordick. 2008. Three-dimensional cellular microarray for high-throughput toxicology assays. *Proceedings of the National Academy of Sciences of the United States of America*. 105:59-63.

Lee, S.A., R. Leitao, G.A. Zheng, S. Yang, A. Rodriguez, and C.H. Yang. 2011. Color Capable Sub-Pixel Resolving Optofluidic Microscope and Its Application to Blood Cell Imaging for Malaria Diagnosis. *Plos One*. 6.

Leung, C.T., and J.S. Brugge. 2012. Outgrowth of single oncogene-expressing cells from suppressive epithelial environments. *Nature*. 482:410-U160.

Levee, M.G., G.M. Lee, S.H. Paek, and B.O. Palsson. 1994. MICROENCAPSULATED HUMAN BONE-MARROW CULTURES - A POTENTIAL CULTURE SYSTEM FOR THE CLONAL OUTGROWTH OF HEMATOPOIETIC PROGENITOR CELLS. *Biotechnology and Bioengineering*. 43:734-739.

Lilja, H., J. Oldbring, G. Rannevik, and C.B. Laurell. 1987. SEMINAL VESICLE-SECRETED PROTEINS AND THEIR REACTIONS DURING GELATION AND LIQUEFACTION OF HUMAN-SEMEN. *Journal of Clinical Investigation*. 80:281-285.

Lipschutz, J.H., B.A. Foster, and G.R. Cunha. 1997. Differentiation of rat neonatal ventral prostates grown in a serum-free organ culture system. *Prostate*. 32:35-42.

Lowsley, O.S. 1912. The development of the human prostate gland with reference to the development of other structures at the neck of the urinary bladder. *American Journal of Anatomy*. 13:299-349.

Lubarsky, B., and M.A. Krasnow. 2003. Tube morphogenesis: Making and shaping biological tubes. *Cell*. 112:19-28.

Lutolf, M.P., and J.A. Hubbell. 2005. Synthetic biomaterials as instructive extracellular microenvironments for morphogenesis in tissue engineering. *Nature Biotechnology*. 23:47-55.

Maan, A.A., R. Boom, and K. Schroen. 2013. Preparation of monodispersed oil-in-water emulsions through semi-metal microfluidic EDGE systems. *Microfluidics and Nanofluidics*. 14:775-784.

Mackintosh, F.C., J. Kas, and P.A. Janmey. 1995. ELASTICITY OF SEMIFLEXIBLE BIOPOLYMER NETWORKS. *Physical Review Letters*. 75:4425-4428.

Magklara, A., A. Scorilas, C. Stephan, G.O. Kristiansen, S. Hauptmann, K. Jung, and E.P. Diamandis. 2000. Decreased concentrations of prostate-specific antigen and human glandular kallikrein 2 in malignant versus nonmalignant prostatic tissue. *Urology*. 56:527-532.

Mailleux, A.A., M. Overholtzer, and J.S. Brugge. 2008. Lumen formation during mammary epithelial morphogenesis - Insights from in vitro and in vivo models. *Cell Cycle*. 7:57-62.

Margadant, C., and A. Sonnenberg. 2010. Integrin-TGF-beta crosstalk in fibrosis, cancer and wound healing. *Embo Reports*. 11:97-105.

Marinkovich, M.P. 2007. Laminin 332 in squamous-cell carcinoma. *Nature Reviews Cancer*. 7:370-380.

Martin, K., T. Henkel, V. Baier, A. Grodrian, T. Schon, M. Roth, J.M. Kohler, and J. Metze. 2003. Generation of larger numbers of separated microbial populations by cultivation in segmented-flow microdevices. *Lab on a Chip*. 3:202-207.

Martin-Belmonte, F., A. Gassama, A. Datta, W. Yu, U. Rescher, V. Gerke, and K. Mostov. 2007. PTEN-mediated apical segregation of phosphoinositides controls epithelial morphogenesis through Cdc42. *Cell*. 128:383-397.

Martin-Belmonte, F., W. Yu, A.E. Rodriguez-Fraticelli, A. Ewald, Z. Werb, M.A. Alonso, and K. Mostov. 2008. Cell-polarity dynamics controls the mechanism of lumen formation in epithelial morphogenesis. *Current Biology*. 18:507-513.

Martynova, L., L.E. Locascio, M. Gaitan, G.W. Kramer, R.G. Christensen, and W.A. MacCrehan. 1997. Fabrication of plastic microfluid channels by imprinting methods. *Analytical Chemistry*. 69:4783-4789.

Matsunaga, Y.T., Y. Morimoto, and S. Takeuchi. 2011. Molding Cell Beads for Rapid Construction of Macroscopic 3D Tissue Architecture. *Advanced Materials*. 23:H90-H94.

Mazutis, L., A.F. Araghi, O.J. Miller, J.-C. Baret, L. Frenz, A. Janoshazi, V. Taly, B.J. Miller, J.B. Hutchison, D. Link, A.D. Griffiths, and M. Ryckelynck. 2009. Droplet-Based Microfluidic Systems for High-Throughput Single DNA Molecule Isothermal Amplification and Analysis. *Analytical Chemistry*. 81:4813-4821.

Mazutis, L., J. Gilbert, W.L. Ung, D.A. Weitz, A.D. Griffiths, and J.A. Heyman. 2013. Single-cell analysis and sorting using droplet-based microfluidics. *Nature Protocols*. 8:870-891.

McCaffrey, A.P., L. Meuse, T.T.T. Pham, D.S. Conklin, G.J. Hannon, and M.A. Kay. 2002. Gene expression - RNA interference in adult mice. *Nature*. 418:38-39.

McCormick, R.M., R.J. Nelson, M.G. AlonsoAmigo, J. Benvegnu, and H.H. Hooper. 1997. Microchannel electrophoretic separations of DNA in injection-molded plastic substrates. *Analytical Chemistry*. 69:2626-2630.

McGuigan, A.P., and M.V. Sefton. 2007. Design criteria for a modular tissue-engineered construct. *Tissue Engineering*. 13:1079-1089.

McKenna, N.J., R.B. Lanz, and B.W. O'Malley. 1999. Nuclear receptor coregulators: Cellular and molecular biology. *Endocrine Reviews*. 20:321-344.

Meijering, E., O. Dzyubachyk, and I. Smal. 2012. METHODS FOR CELL AND PARTICLE TRACKING. *Imaging and Spectroscopic Analysis of Living Cells: Optical and Spectroscopic Techniques*. 504:183-200.

Mettouchi, A., S. Klein, W.J. Guo, M. Lopez-Lago, E. Lemichez, J.K. Westwick, and F.G. Giancotti. 2001. Integrin-specific activation of Rac controls progression through the G(1) phase of the cell cycle. *Molecular Cell*. 8:115-127.

Miller, B.A., S.M. Scoppa, and E.J. Feuer. 2006. Racial/ethnic patterns in lifetime and age-conditional risk estimates for selected cancers. *Cancer*. 106:670-682.

Miroshnikova, Y.A., D.M. Jorgens, L. Spirio, M. Auer, A.L. Sarang-Sieminski, and V.M. Weaver. 2011. Engineering strategies to recapitulate epithelial morphogenesis within synthetic three-dimensional extracellular matrix with tunable mechanical properties. *Physical Biology*. 8.

Morra, M., E. Occhiello, R. Marola, F. Garbassi, P. Humphrey, and D. Johnson. 1990. ON THE AGING OF OXYGEN PLASMA-TREATED POLYDIMETHYLSILOXANE SURFACES. *Journal of Colloid and Interface Science*. 137:11-24.

Moyer, V.A. 2012. Screening for prostate cancer: U.S. Preventive Services Task Force recommendation statement. *Ann Intern Med*. 157:120-134.

Mudanyali, O., W. Bishara, and A. Ozcan. 2011. Lensfree super-resolution holographic microscopy using wetting films on a chip. *Optics Express*. 19:17378-17389.

Mudanyali, O., E. McLeod, W. Luo, A. Greenbaum, A.F. Coskun, Y. Hennequin, C.P. Allier, and A. Ozcan. 2013. Wide-field optical detection of nanoparticles using on-chip microscopy and self-assembled nanolenses. *Nature Photonics*. 7:247-254.

Mudanyali, O., D. Tseng, C. Oh, S.O. Isikman, I. Sencan, W. Bishara, C. Oztoprak, S.K. Seo, B. Khademhosseini, and A. Ozcan. 2010. Compact, light-weight and cost-effective microscope based on lensless incoherent holography for telemedicine applications. *Lab on a Chip*. 10:1417-1428.

Naoghare, P.K., H.T. Kwon, and J.M. Song. 2007. An automated method for in vitro anticancer drug efficacy monitoring based on cell viability measurement using a portable photodiode array chip. *Lab on a Chip*. 7:1202-1205.

Nelson, C.M., and M.J. Bissell. 2006. Of extracellular matrix, scaffolds, and signaling: Tissue architecture regulates development, homeostasis, and cancer. *Annual Review of Cell and Developmental Biology*. 22:287-309.

Nie, Z., M. Seo, S. Xu, P.C. Lewis, M. Mok, E. Kumacheva, G.M. Whitesides, P. Garstecki, and H.A. Stone. 2008. Emulsification in a microfluidic flow-focusing device: effect of the viscosities of the liquids. *Microfluidics and Nanofluidics*. 5:585-594.

Nisisako, T., T. Torii, T. Takahashi, and Y. Takizawa. 2006. Synthesis of monodisperse bicolored janus particles with electrical anisotropy using a microfluidic co-flow system. *Advanced Materials*. 18:1152-+.

O'Brien, L.E., M.M.P. Zegers, and K.E. Mostov. 2002. Opinion - Building epithelial architecture: insights from three-dimensional culture models. *Nature Reviews Molecular Cell Biology*. 3:531-537.

Okumura, A., P.M. Pitha, and R.N. Harty. 2008. ISG15 inhibit Ebola VP40VLP budding in an L-domain-dependent manner by blocking Nedd4 ligase activity. *Proceedings of the National Academy of Sciences of the United States of America*. 105:3974-3979.

Orive, G., R.M. Hernandez, A.R. Gascon, R. Calafiore, T.M.S. Chang, P. de Vos, G. Hortelano, D. Hunkeler, I. Lacik, and J.L. Pedraz. 2004. History, challenges and perspectives of cell microencapsulation. *Trends in Biotechnology*. 22:87-92.

Orkin, R.W., P. Gehron, E.B. McGoodwin, G.R. Martin, T. Valentine, and R. Swarm. 1977. MURINE TUMOR PRODUCING A MATRIX OF BASEMENT-MEMBRANE. *Journal of Experimental Medicine*. 145:204-220.

Owens, L.V., L.H. Xu, R.J. Craven, G.A. Dent, T.M. Weiner, L. Kornberg, E.T. Liu, and W.G. Cance. 1995. OVEREXPRESSION OF THE FOCAL ADHESION KINASE (P125(FAK)) IN INVASIVE HUMAN TUMORS. *Cancer Research*. 55:2752-2755.

Ozcan, A., and U. Demirci. 2008. Ultra wide-field lens-free monitoring of cells on-chip. *Lab on a Chip*. 8:98-106.

Park, C.C., H. Zhang, M. Paravicini, J.W. Gray, F. Baehner, C.J. Park, and M.J. Bissell. 2006. beta(1) integrin inhibitory antibody induces apoptosis of breast cancer cells, inhibits growth, and distinguishes malignant from normal phenotype in three dimensional cultures and in vivo. *Cancer Research*. 66:1526-1535.

Park, S.C., M.K. Park, and M.G. Kang. 2003. Super-resolution image reconstruction: A technical overview. *Ieee Signal Processing Magazine*. 20:21-36.

Parri, M., and P. Chiarugi. 2010. Rac and Rho GTPases in cancer cell motility control. *Cell Communication and Signaling*. 8.

Parry, G., B. Cullen, C.S. Kaetzel, R. Kramer, and L. Moss. 1987. REGULATION OF DIFFERENTIATION AND POLARIZED SECRETION IN MAMMARY EPITHELIAL-CELLS MAINTAINED IN CULTURE - EXTRACELLULAR-MATRIX AND MEMBRANE POLARITY INFLUENCES. *Journal of Cell Biology*. 105:2043-2051.

Paszek, M.J., N. Zahir, K.R. Johnson, J.N. Lakins, G.I. Rozenberg, A. Gefen, C.A. Reinhart-King, S.S. Margulies, M. Dembo, D. Boettiger, D.A. Hammer, and V.M. Weaver. 2005. Tensional homeostasis and the malignant phenotype. *Cancer Cell*. 8:241-254.

Pearson, G.W., and T. Hunter. 2007. Real-time imaging reveals that noninvasive mammary epithelial acini can contain motile cells. *Journal of Cell Biology*. 179:1555-1567.

Pearson, J.F., S. Hughes, K. Chambers, and S.H. Lang. 2009. Polarized fluid movement and not cell death, creates luminal spaces in adult prostate epithelium. *Cell Death and Differentiation*. 16:475-482.

Petersen, O.W., L. Ronnovjessen, A.R. Howlett, and M.J. Bissell. 1992. INTERACTION WITH BASEMENT-MEMBRANE SERVES TO RAPIDLY DISTINGUISH GROWTH AND DIFFERENTIATION PATTERN OF NORMAL AND MALIGNANT HUMAN BREAST EPITHELIAL-CELLS. *Proceedings of the National Academy of Sciences of the United States of America*. 89:9064-9068.

Picelli, S., O.R. Faridani, A.K. Bjorklund, G. Winberg, S. Sagasser, and R. Sandberg. 2014. Full-length RNA-seq from single cells using Smart-seq2. *Nature Protocols*. 9:171-181.

Pollack, A.L., R.B. Runyan, and K.E. Mostov. 1998. Morphogenetic mechanisms of epithelial tubulogenesis: MDCK cell polarity is transiently rearranged without loss

of cell-cell contact during scatter factor hepatocyte growth factor-induced tubulogenesis. *Developmental Biology*. 204:64-79.

Poncelet, D., and R.J. Neufeld. 1989. SHEAR BREAKAGE OF NYLON MEMBRANE MICROCAPSULES IN A TURBINE REACTOR. *Biotechnology and Bioengineering*. 33:95-103.

Poujade, M., E. Grasland-Mongrain, A. Hertzog, J. Jouanneau, P. Chavrier, B. Ladoux, A. Buguin, and P. Silberzan. 2007. Collective migration of an epithelial monolayer in response to a model wound. *Proceedings of the National Academy of Sciences of the United States of America*. 104:15988-15993.

Pretlow, T.G., T.P. Pretlow, B. Yang, C.S. Kaetzel, C.M. Delmoro, S.M. Kamis, D.R. Bodner, E. Kursh, M.I. Resnick, and E.L. Bradley. 1991. TISSUE CONCENTRATIONS OF PROSTATE-SPECIFIC ANTIGEN IN PROSTATIC-CARCINOMA AND BENIGN PROSTATIC HYPERPLASIA. *International Journal of Cancer*. 49:645-649.

Price, D. 1936. Normal development of the prostate and seminal vesicles of the rat with a study of experimental postnatal modifications. *American Journal of Anatomy*. 60:79-127.

Prins, G.S., and L. Birch. 1995. THE DEVELOPMENTAL PATTERN OF ANDROGEN RECEPTOR EXPRESSION IN RAT PROSTATE LOBES IS ALTERED AFTER NEONATAL EXPOSURE TO ESTROGEN. *Endocrinology*. 136:1303-1314.

Prins, G.S., and O. Putz. 2008. Molecular signaling pathways that regulate prostate gland development. *Differentiation*. 76:641-659.

Prokop, A., Z. Prokop, D. Schaffer, E. Kozlov, J. Wikswo, D. Cliffel, and F. Baudenbacher. 2004. NanoLiterBioReactor: Long-term mammalian cell culture at nanofabricated scale. *Biomedical Microdevices*. 6:325-339.

Pujuguet, P., M. Simian, J. Liaw, R. Timpl, Z. Werb, and M.J. Bissell. 2000. Nidogen-1 regulates laminin-1-dependent mammary-specific gene expression. *Journal of Cell Science*. 113:849-858.

Quigley, C.A., A. Debellis, K.B. Marschke, M.K. Elawady, E.M. Wilson, and F.S. French. 1995. ANDROGEN RECEPTOR DEFECTS - HISTORICAL, CLINICAL, AND MOLECULAR PERSPECTIVES. *Endocrine Reviews*. 16:271-321.

Rabanel, J.-M., X. Banquy, H. Zouaoui, M. Mokhtar, and P. Hildgen. 2009. Progress Technology in Microencapsulation Methods for Cell Therapy. *Biotechnology Progress*. 25:946-963.

Rangarajan, A., S.J. Hong, A. Gifford, and R.A. Weinberg. 2004. Species- and cell type-specific requirements for cellular transformation. *Cancer Cell*. 6:171-183.

Riche, C.T., C. Zhang, M. Gupta, and N. Malmstadt. 2014. Fluoropolymer surface coatings to control droplets in microfluidic devices. *Lab on a Chip*. 14:1834-1841.

Robinson, S.D., G.B. Silberstein, A.B. Roberts, K.C. Flanders, and C.W. Daniel. 1991. REGULATED EXPRESSION AND GROWTH INHIBITORY EFFECTS OF TRANSFORMING GROWTH-FACTOR-BETA ISOFORMS IN MOUSE MAMMARY-GLAND DEVELOPMENT. *Development*. 113:867-&.

Rodriguez-Fraticelli, A.E., M. Auzan, M.A. Alonso, M. Bornens, and F. Martin-Belmonte. 2012. Cell confinement controls centrosome positioning and lumen initiation during epithelial morphogenesis. *Journal of Cell Biology*. 198:1011-1023.

Scherer, A., A. Krause, J.R. Walker, S.E. Sutton, D. Seron, F. Raulf, and M.P. Cooke. 2003. Optimized protocol for linear RNA amplification and application to gene expression profiling of human renal biopsies. *Biotechniques*. 34:546-+.

Schwinger, C., S. Koch, U. Jahnz, P. Wittlich, N.G. Rainov, and J. Kressler. 2002. High throughput encapsulation of murine fibroblasts in alginate using the JetCutter technology. *Journal of Microencapsulation*. 19:273-280.

Seewaldt, V.L., K. Mrozek, R. Sigle, E.C. Dietze, K. Heine, D.M. Hockenbery, K.B. Hobbs, and L.E. Caldwell. 2001. Suppression of p53 function in normal human mammary epithelial cells increases sensitivity to extracellular matrix-induced apoptosis. *Journal of Cell Biology*. 155:471-486.

Seo, S., S.O. Isikman, I. Sencan, O. Mudanyali, T.W. Su, W. Bishara, A. Erlinger, and A. Ozcan. 2010. High-Throughput Lens-Free Blood Analysis on a Chip. *Analytical Chemistry*. 82:4621-4627.

Serini, G., D. Ambrosi, E. Giraudo, A. Gamba, L. Preziosi, and F. Bussolino. 2003. Modeling the early stages of vascular network assembly. *Embo Journal*. 22:1771-1779.

Shi, Q., R.P. Ghosh, H. Engelke, C.H. Rycroft, L. Cassereau, J.A. Sethian, V.M. Weaver, and J.T. Liphardt. 2014. Rapid disorganization of mechanically interacting systems of mammary acini. *Proceedings of the National Academy of Sciences of the United States of America*. 111:658-663.

Silberstein, G.B., and C.W. Daniel. 1982. GLYCOSAMINOGLYCANS IN THE BASAL LAMINA AND EXTRACELLULAR-MATRIX OF THE DEVELOPING MOUSE MAMMARY DUCT. *Developmental Biology*. 90:215-222.

Silberstein, G.B., P. Strickland, S. Coleman, and C.W. Daniel. 1990. EPITHELIUM-DEPENDENT EXTRACELLULAR-MATRIX SYNTHESIS IN TRANSFORMING GROWTH FACTOR-BETA-1 GROWTH-INHIBITED MOUSE MAMMARY-GLAND. *Journal of Cell Biology*. 110:2209-2219.

Singh, R.R., J.E. Kim, Y. Davuluri, E. Drakos, J.H. Cho-Vega, H.M. Amin, and F. Vega. 2010. Hedgehog signaling pathway is activated in diffuse large B-cell lymphoma and contributes to tumor cell survival and proliferation. *Leukemia*. 24:1025-1036.

Sivaraman, A., J.K. Leach, S. Townsend, T. Iida, B.J. Hogan, D.B. Stolz, R. Fry, L.D. Samson, S.R. Tannenbaum, and L.G. Griffith. 2005. A microscale in vitro physiological model of the liver: Predictive screens for drug metabolism and enzyme induction. *Current Drug Metabolism*. 6:569-591.

Slaughter, B.V., S.S. Khurshid, O.Z. Fisher, A. Khademhosseini, and N.A. Peppas. 2009. Hydrogels in Regenerative Medicine. *Advanced Materials*. 21:3307-3329.

Song, H., D.L. Chen, and R.F. Ismagilov. 2006. Reactions in droplets in microflulidic channels. *Angewandte Chemie-International Edition*. 45:7336-7356.

Song, H., and R.F. Ismagilov. 2003. Millisecond kinetics on a microfluidic chip using nanoliters of reagents. *Journal of the American Chemical Society*. 125:14613-14619.

Stahl, S., S. Weitzman, and J.C.R. Jones. 1997. The role of laminin-5 and its receptors in mammary epithelial cell branching morphogenesis. *Journal of Cell Science*. 110:55-63.

Stone, K.R., D.D. Mickey, H. Wunderli, G.H. Mickey, and D.F. Paulson. 1978. Isolation of a human prostate carcinoma cell line (DU 145). *Int J Cancer*. 21:274-281.

Streuli, C. 1999. Extracellular matrix remodelling and cellular differentiation. *Current Opinion in Cell Biology*. 11:634-640.

Su, T.W., A. Erlinger, D. Tseng, and A. Ozcan. 2010. Compact and Light-Weight Automated Semen Analysis Platform Using Lensfree on-Chip Microscopy. *Analytical Chemistry*. 82:8307-8312.

Su, T.W., S. Seo, A. Erlinger, and A. Ozean. 2009. High-Throughput Lensfree Imaging and Characterization of a Heterogeneous Cell Solution On a Chip. *Biotechnology and Bioengineering*. 102:856-868.

Sugimura, Y., G.R. Cunha, and A.A. Donjacour. 1986. MORPHOGENESIS OF DUCTAL NETWORKS IN THE MOUSE PROSTATE. *Biology of Reproduction*. 34:961-971.

Suuronen, E.J., H. Sheardown, K.D. Newman, C.R. McLaughlin, and M. Griffith. 2005. Building in vitro models of organs. *International Review of Cytology - a Survey of Cell Biology, Vol 244*. 244:137-173.

Tagliabue, E., C. Ghirelli, P. Squicciarini, P. Aiello, M.I. Colnaghi, and S. Menard. 1998. Prognostic value of alpha 6 beta 4 integrin expression in breast carcinomas is affected by laminin production from tumor cells. *Clinical Cancer Research*. 4:407-410.

Takeuchi, S., P. Garstecki, D.B. Weibel, and G.M. Whitesides. 2005. An axisymmetric flow-focusing microfluidic device. *Advanced Materials*. 17:1067-+.

Tan, Y.C., V. Cristini, and A.P. Lee. 2006. Monodispersed microfluidic droplet generation by shear focusing microfluidic device. *Sensors and Actuators B-Chemical*. 114:350-356.

Tanner, K., H. Mori, R. Mroue, A. Bruni-Cardoso, and M.J. Bissell. 2012. Coherent angular motion in the establishment of multicellular architecture of glandular tissues. *Proceedings of the National Academy of Sciences of the United States of America*. 109:1973-1978.

Tepass, U. 2012. The Apical Polarity Protein Network in Drosophila Epithelial Cells: Regulation of Polarity, Junctions, Morphogenesis, Cell Growth, and Survival. *Annual Review of Cell and Developmental Biology, Vol 28*. 28:655-685.

Thery, M. 2010. Micropatterning as a tool to decipher cell morphogenesis and functions. *Journal of Cell Science*. 123:4201-4213.

Thorsen, T., R.W. Roberts, F.H. Arnold, and S.R. Quake. 2001. Dynamic pattern formation in a vesicle-generating microfluidic device. *Physical Review Letters*. 86:4163-4166.

Tian, X.L., S.Y. Wang, Z. Zhang, and D.C. Lv. 2012. Rat Bone Marrow-Derived Schwann-Like Cells Differentiated by the Optimal Inducers Combination on Microfluidic Chip and Their Functional Performance. *Plos One*. 7.

Tice, J.D., A.D. Lyon, and R.F. Ismagilov. 2004. Effects of viscosity on droplet formation and mixing in microfluidic channels. *Analytica Chimica Acta*. 507:73-77.

Timms, B.G., T.J. Mohs, and L.J.A. Didio. 1994. DUCTAL BUDDING AND BRANCHING PATTERNS IN THE DEVELOPING PROSTATE. *Journal of Urology*. 151:1427-1432.

Timpl, R., H. Wiedemann, V. Vandelden, H. Furthmayr, and K. Kuhn. 1981. A NETWORK MODEL FOR THE ORGANIZATION OF TYPE-IV COLLAGEN MOLECULES IN BASEMENT-MEMBRANES. *European Journal of Biochemistry*. 120:203-211.

Tsao, C.-W., and D.L. DeVoe. 2009. Bonding of thermoplastic polymer microfluidics. *Microfluidics and Nanofluidics*. 6:1-16.

Tyson, D.R., J.C. Inokuchi, T. Tsunoda, A. Lau, and D.K. Ornstein. 2007. Culture requirements of prostatic epithelial cell lines for acinar morphogenesis and lumen formation InVitro: Role of extracellular calcium. *Prostate*. 67:1601-1613.

Utada, A.S., E. Lorenceau, D.R. Link, P.D. Kaplan, H.A. Stone, and D.A. Weitz. 2005. Monodisperse double emulsions generated from a microcapillary device. *Science*. 308:537-541.

van Bokhoven, A., M. Varella-Garcia, C. Korch, W.U. Johannes, E.E. Smith, H.L. Miller, S.K. Nordeen, G.J. Miller, and M.S. Lucia. 2003. Molecular characterization of human prostate carcinoma cell lines. *Prostate*. 57:205-225.

Velasco, D., E. Tumarkin, and E. Kumacheva. 2012. Microfluidic Encapsulation of Cells in Polymer Microgels. *Small*. 8:1633-1642.

Viebahn, C., B. Mayer, and A. Miething. 1995. Morphology of incipient mesoderm formation in the rabbit embryo: A light- and retrospective electron-microscopic study. *Acta Anatomica*. 154:99-110.

Viktorinova, I., and C. Dahmann. 2013. Microtubule Polarity Predicts Direction of Egg Chamber Rotation in Drosophila. *Current Biology*. 23:1472-1477.

Vukicevic, S., H.K. Kleinman, F.P. Luyten, A.B. Roberts, N.S. Roche, and A.H. Reddi. 1992. IDENTIFICATION OF MULTIPLE ACTIVE GROWTH-FACTORS IN BASEMENT-MEMBRANE MATRIGEL SUGGESTS CAUTION IN INTERPRETATION OF CELLULAR-ACTIVITY RELATED TO EXTRACELLULAR-MATRIX COMPONENTS. *Experimental Cell Research*. 202:1-8.

Wang, A.Z., G.K. Ojakian, and W.J. Nelson. 1990. STEPS IN THE MORPHOGENESIS OF A POLARIZED EPITHELIUM .2. DISASSEMBLY AND ASSEMBLY OF PLASMA-MEMBRANE DOMAINS DURING REVERSAL OF EPITHELIAL-CELL POLARITY IN MULTICELLULAR EPITHELIAL (MDCK) CYSTS. *Journal of Cell Science*. 95:153-165.

Wang, H., S. Lacoche, L. Huang, B. Xue, and S.K. Muthuswamy. 2013. Rotational motion during three-dimensional morphogenesis of mammary epithelial acini relates to laminin matrix assembly. *Proceedings of the National Academy of Sciences of the United States of America*. 110:163-168.

Wang, H.P., W.S. Lin, B. Popko, and I.L. Campbell. 2004. Inducible production of interferon-gamma in the developing brain causes cerebellar dysplasia with activation of the Sonic hedgehog pathway. *Molecular and Cellular Neuroscience*. 27:489-496.

Webber, M.M., D. Bello, H.K. Kleinman, and M.P. Hoffman. 1997. Acinar differentiation by non-malignant immortalized human prostatic epithelial cells and its loss by malignant cells. *Carcinogenesis*. 18:1225-1231.

Weibel, D.B., W.R. DiLuzio, and G.M. Whitesides. 2007. Microfabrication meets microbiology. *Nature Reviews Microbiology*. 5:209-218.

Whitesides, G.M. 2006. The origins and the future of microfluidics. *Nature*. 442:368-373.

Wicha, M.S., L.A. Liotta, B.K. Vonderhaar, and W.R. Kidwell. 1980. EFFECTS OF INHIBITION OF BASEMENT-MEMBRANE COLLAGEN DEPOSITION ON RAT MAMMARY-GLAND DEVELOPMENT. *Developmental Biology*. 80:253-266.

Williams, D.F. 2009. On the nature of biomaterials. *Biomaterials*. 30:5897-5909.

Xia, Y.N., and G.M. Whitesides. 1998. Soft lithography. *Annual Review of Materials Science*. 28:153-184.

Xu, W.B., M.H. Jericho, I.A. Meinertzhagen, and H.J. Kreuzer. 2001. Digital in-line holography for biological applications. *Proceedings of the National Academy of Sciences of the United States of America*. 98:11301-11305.

Yap, A.S., W.M. Brieher, and B.M. Gumbiner. 1997. Molecular and functional analysis of cadherin-based adherens junctions. *Annual Review of Cell and Developmental Biology*. 13:119-146.

Yu, H., J.K. Mouw, and V.M. Weaver. 2011. Forcing form and function: biomechanical regulation of tumor evolution. *Trends in Cell Biology*. 21:47-56.

Yu, W., L.E. O'Brien, F. Wang, H. Bourne, K.E. Mostov, and M.M.P. Zegers. 2003. Hepatocyte growth factor switches orientation of polarity and mode of movement during morphogenesis of multicellular epithelial structures. *Molecular Biology of the Cell*. 14:748-763.

Yurchenco, P.D., and Y.S. Cheng. 1993. SELF-ASSEMBLY AND CALCIUM-BINDING SITES IN LAMININ - A 3-ARM INTERACTION-MODEL. *Journal of Biological Chemistry*. 268:17286-17299.

Yurchenco, P.D., and G.C. Ruben. 1988. TYPE-IV COLLAGEN LATERAL ASSOCIATIONS IN THE EHS TUMOR MATRIX - COMPARISON WITH AMNIOTIC AND INVITRO NETWORKS. *American Journal of Pathology*. 132:278-291.

Zegers, M.M.P., L.E. O'Brien, W. Yu, A. Datta, and K.E. Mostov. 2003. Epithelial polarity and tubulogenesis in vitro. *Trends in Cell Biology*. 13:169-176.

Zhang, X., M.V. Fournier, J.L. Ware, M.J. Bissell, A. Yacoub, and Z.E. Zehner. 2009. Inhibition of vimentin or beta(1) integrin revert morphology of prostate tumor cells grown in laminin-rich extracellular matrix gels and reduces tumor growth in vivo. *Molecular Cancer Therapeutics*. 8:499-508.

Zheng, B., and R.F. Ismagilov. 2005. A microfluidic approach for screening submicroliter volumes against multiple reagents by using preformed arrays of nanoliter plugs in a three-phase liquid/liquid/gas flow. *Angewandte Chemie-International Edition*. 44:2520-2523.

Zheng, G.A., S.A. Lee, Y. Antebi, M.B. Elowitz, and C.H. Yang. 2011. The ePetri dish, an on-chip cell imaging platform based on subpixel perspective sweeping microscopy (SPSM). *Proceedings of the National Academy of Sciences of the United States of America*. 108:16889-16894.

Zimmermann, H., F. Ehrhart, D. Zimmermann, K. Mueller, A. Katsen-Globa, M. Behringer, P.J. Feilen, P. Gessner, G. Zimmermann, S.G. Shirley, M.M. Weber, J. Metze, and U. Zimmermann. 2007. Hydrogel-based encapsulation of biological, functional tissue: fundamentals, technologies and applications. *Applied Physics a-Materials Science & Processing*. 89:909-922.